

THE DESIGN, TESTING AND ANALYSIS
OF A BIOFUEL MICRO-TRIGENERATION
SYSTEM

Thesis by
Hongdong Yu

Doctor of Philosophy



Sir Joseph Swan Centre for
Energy Research
Newcastle upon Tyne
United Kingdom

October 2012

Abstract

Trigeneration and the use of biofuels are two research topics which are important in trying to help relieve global energy shortage and bring about a reduction in greenhouse gas emissions. Trigeneration produces electricity, cooling, and heating simultaneously using a single fuel source and can operate at a high efficiency rate. The use of biofuel provides a renewable and carbon neutral substitution for fossil fuels.

This research thesis describes the development of a biofuel micro-trigeneration (BMT) system using raw vegetable oils and explores the feasibility of meeting the total energy demand of a typical household. The system was designed and constructed using a 6.5kW single cylinder diesel generator as the prime mover, two heat exchangers for recovering waste heat from the engine coolant and exhaust gas, and an absorption refrigerator driven by exhaust gas heat.

Four raw vegetable oils: sunflower, rapeseed, jatropha and croton oils were preheated to 90°C and used in the study. The system performance using the vegetable oils was compared to that of the gas oil. Experiments were carried out to determine the fuel properties of the oils, including viscosity, density, higher heating value and fatty acid components. Power generation, combined heat & power and trigeneration tests were also carried out. The experimental results reveal that the BMT system performed with a high efficiency of 65% for trigeneration at full load, and CO₂ emissions was reduced by around 60% compared to single power generation mode. The exergy efficiency was also increased by approximately 5 points.

An engine model was developed using DIESEL-RK software to study the engine performance and emissions using different fuel types. Optimizations were performed to improve the engine performance and emissions. A trigeneration system model was also developed using Dymola software and was used to predict the dynamic performance of the system parameters. These models and simulation studies were validated against experimental results and matched well with the experimental results; hence can be used to explore wider system design and performance considerations. Both the experimental and theoretical studies have proved the feasibility of the BMT system to meet the overall energy demand of a household user.

Acknowledgements

I gratefully acknowledge the support received through the Engineering and Physical Sciences Research Council (EPSRC) under the project ‘Biofuel Micro-Trigeneration with Cryogenic Energy Storage’.

I would like to express my deepest gratitude first and foremost to my supervisors, Professor Tony Roskilly and Dr Yaodong Wang, for their constant encouragement, guidance and support throughout my PhD study. Without their consistent and illuminating instruction, this thesis would not have reached its present form.

I would like to express my heartfelt gratitude to colleagues and staff for their help and support; including Dr Dawei Wu, Mr Paul Watson, Mr Ian Milne, Mr Stephen Crosby, Dr Anh Phan, Mr Graham Baker, Prof Adam Harvey, Dr Richard Mikalsen, Mr Leigh Ingle, Mrs Lisa Smeaton and Ms Michelle Wagner.

I also owe my sincere gratitude to friends who provided their help and time during the course of this thesis. Last but not least, my gratitude also extends to my family, especially my wife and daughter, who have been assisting, supporting and caring for me all of my life.

Contents

Chapter 1. Introduction	1
1.1 Research Background	1
1.2 Aims and Objectives	2
1.3 Methodology	3
1.3.1 Investigation of domestic energy consumption	3
1.3.2 Biofuel properties investigation	3
1.3.3 Computational modelling and simulation	3
1.3.4 Experimental investigation of the BMT system	3
1.4 Contribution to existing research	4
Chapter 2. Literature Review	6
2.1 Introduction	6
2.2 Domestic energy demand and consumption in the UK	7
2.3 Micro-trigeneration	10
2.3.1 Trigeneration Classification and Typical Applications	10
2.3.2 Micro-trigeneration Technologies	11
2.3.3 Existing work on micro-trigeneration	20
2.4 Vegetable oils	24
2.4.1 Physicochemical property	24
2.4.2 Existing works on vegetable oil	27
2.5 Summary	30
2.5.1 Summary of domestic energy demand and consumption	30
2.5.2 Summary of micro-trigeneration	30
2.5.3 Summary of vegetable oil research	31
Chapter 3. Experimental Apparatus, Instrumentation and Test Plan	32
3.1 Introduction	32
3.2 Experimental setup	33
3.2.1 Biofuel property test facilities	33
3.2.2 Biofuel micro-trigeneration system	36
3.3 Data acquisition	42
3.3.1 PLC and control software	42
3.3.2 Data logger	44

3.3.3	Power quality analyser	47
3.3.4	Fuel flow meter and balance	48
3.3.5	Exhaust gas analyser	49
3.4	Test plan and procedure	51
3.4.1	Test plan	51
3.4.2	Test procedure	52
3.5	Error Analyses	53
3.5.1	Rules of uncertainty calculation	54
3.5.2	Uncertainty of the experimental results	56
Chapter 4.	Experimental Results and Discussions	64
4.1	Introduction	64
4.2	Physicochemical properties of vegetable oils	64
4.2.1	Viscosity	64
4.2.2	Density	66
4.2.3	Heating value	67
4.2.4	Compositions of the vegetable oils	68
4.3	Trigeneration	72
4.3.1	Generator performance and emissions	72
4.3.2	Waste heat recovery by heat exchanger	79
4.3.3	Absorption refrigeration	83
4.3.4	Cogeneration and trigeneration performance	96
4.3.5	Exergy analysis	99
4.4	Conclusions and discussions	103
Chapter 5.	Modelling and Simulation	105
5.1	Introduction	105
5.2	Engine modelling and investigation strategy	105
5.2.1	DIESEL-RK software and engine model	105
5.2.2	Estimation of fuel properties	108
5.2.3	Investigation strategy	112
5.3	Engine simulation and prediction	113
5.3.1	Validation of the engine model	113
5.3.2	Engine performance and emissions predictions	116

5.3.3	Engine performance optimisation	121
5.4	Biofuel micro-trigeneration modelling	127
5.4.1	Introduction to Dymola and Modelica	127
5.4.2	BMT model and mathematic principles	128
5.5	BMT simulation and prediction	142
5.6	Conclusions and discussions	146
Chapter 6.	Conclusions and Recommendations	148
6.1	Conclusions	148
6.2	Recommendations for future work	150
6.2.1	Diesel generator	150
6.2.2	Heat exchanger and refrigerator	151
6.2.3	BMT system	151
6.2.4	Simulation and optimisation	151
References	153
Appendices	167
A.	Specifications of Apparatus and Instruments	167
B.	Details of experimental results	179

List of papers

1. Hongdong Yu, Jonathan Heslop, Rikard Mikalsen, Yaodong Wang, Anthony P. Roskilly. *Optimising the operation of a large two-stroke marine engine for slow steaming*. Low Carbon Shipping Conference. 2012. Newcastle, UK.
2. Dawei Wu, Hongdong Yu, Adam Harvey, Anthony P. Roskilly. *Micro trigeneration system driven with preheated croton megalocarpus oil - a performance and particulate emission study*. Applied Energy (under review, September 2012).
3. X.P. Chen, Y.D. Wang, H.D. Yu, D.W. Wu, Yapeng, Li, A.P. Roskilly. *A domestic CHP system with hybrid electrical energy storage*. Energy and Building (Accepted).
4. Dawei Wu, Anthony P. Roskilly, Hongdong Yu. *Croton megalocarpus oil fired micro trigeneration prototype for remote and self-contained applications: experimental assessment of its performance and gaseous and particulate emissions*. Interface Focus - Journal of Royal Society (Accepted, August 2012).
5. Yaodong Wang, Ye Huang, Elijah Chiremba, Anthony P. Roskilly, Neil Hewitt, Yulong Ding, Dawei Wu, Hongdong Yu, , Xiangping Chen, Yapeng LI, Jincheng Huang, Ruzhu Wang, Jingyi Wu, Chunqing Tan. *An investigation of a household size trigeneration running with hydrogen*. Applied Energy, **Vol 88, 6** (2011): 2176-2182.
6. Jincheng Huang, Yaodong Wang, Shuangding Li, Anthony P. Roskilly, Hongdong Yu, Huifen Li. *Experimental investigation on the performance and emissions of a diesel engine fuelled with ethanol–diesel blends*. Applied Thermal Engineering, **Vol. 29, 11-12** (2009): 2484-2490.
7. Dawei Wu, Hongdong Yu, Adam Harvey, Anthony P. Roskilly. *Micro trigeneration system driven with preheated croton oil – a performance and particulate emission study*. The 4th International Conference on Applied Energy ICAE 2012. Jul 5-8, 2012. Suzhou, China.
8. X.P. Chen, Y.D. Wang, D.W. Wu, H.D. Yu, Yapeng Li, A.P. Roskilly, *Investigation of a combined CHP with energy storage system*. International Conference on Applied Energy, ICAE 2012. Jul 5-8, 2012. Suzhou, China.
9. Dawei Wu, Tony Roskilly, Yaodong Wang, Hongdong Yu. *Optimal Design and Emission Scenario Analysis of Biofuel Trigeneration for UK Residential Houses*. 9th

International Conference on Sustainable Energy Technologies. August 2010. Shanghai, China.

10. D.W.Wu, A.P.Roskilly, R.Z.Wang, J.Y.Wu, Y.D.Wang, H.D.Yu. *The use of Pinch Analysis in the designing of a distributed trigeneration application*. Heat Powered Cycles Conference. 7- 9 September 2009. TU Berlin, Germany.
11. Yaodong Wang, Ye Huang, Anthony P. Roskilly, Neil Hewitt, Yulong Ding, Constantinos Charalambous, Dawei Wu, Hongdong Yu, Xiangping Chen, Fu-Yun Zhao, Jincheng Huang, Ruzhu Wang, Jingyi Wu, Zaizhong Xia, Chunqing Tan, A study of a diesel genset based trigeneration running with raw jatropha oil. Heat Powered Cycles Conference 2009. 7- 9 September 2009. TU Berlin, Germany.

List of Figures

2.1	UK domestic energy consumption by end use in 2009.....	8
2.2	Total power consumption of a single house within 2 years.....	8
2.3	Trends in the daily and 30-day rolling average heat and power demands for a single house from January to December	9
2.4	Basic schematic diagram of absorption refrigeration.....	17
2.5	Basic schematic and thermodynamic diagram of adsorption refrigeration.....	18
2.6	Schematic diagram of a micro-trigeneration system	22
3.1	Viscosity test system.....	33
3.2	Higher heating value test system.....	34
3.3	HR-200 analytical balance.....	34
3.4	HP 5890 Gas Chromatograph.....	35
3.5	Biodiesel conversion.....	36
3.6	Yanmar YTG6.5S diesel generator.....	37
3.7	Biofuel micro-trigeneration system.....	37
3.8	Fuel supply system.....	38
3.9	Instruments of fuel supply system.....	38
3.10	Schematic diagram of coolant heat recovery system.....	39
3.11	Schematic diagram of exhaust heat recovery system.....	41
3.12	Waste heat recovery system.....	41
3.13	Dometic RM 7655L refrigerator.....	42
3.14	Schematic diagram of the SCADA system.....	43
3.15	Control box.....	43
3.16	Screen shot of the panel PC and control software.....	43
3.17	Schematic diagram of the data logger and the connected sensors.....	44
3.18	Fluke 435 power quality analyser and FlukeView software.....	48
3.19	FC2210 fuel flow meter and PCB 1000-1 balance.....	49
3.20	MEXA-1600D exhaust gas analyser.....	50
3.21	IC-LT 1/2 " turbine flow meter and 101 totalizer.....	50

3.22	Flowline DF10MFG Pitot flow meter and IMV30-T totalizer.....	51
4.1	Variation of viscosities as a function of temperature.....	66
4.2	Reaction equation of transesterification.....	68
4.3	Chromatogram of croton biodiesel.....	69
4.4	Constituents of fatty acids in the vegetable oils.....	71
4.5	Electric power of the oils for different loads.....	72
4.6	Fuel consumption of the oils for different loads.....	73
4.7	BSFC of the oils for different loads	73
4.8	BSEC of the oils for different loads	74
4.9	Electrical efficiencies of the oils for different loads.....	74
4.10	Exhaust gas temperatures of the oils for different loads.....	75
4.11	CO ₂ emissions of the oils for different loads.....	76
4.12	O ₂ contents in the exhaust gas of the oils for different loads.....	76
4.13	CO emissions of the oils for different loads.....	77
4.14	NO _x emissions of the oils for different loads.....	78
4.15	HC emissions of the oils for different loads.....	79
4.16	Recovered exhaust gas heat for cogeneration.....	80
4.17	Recovered exhaust gas heat for trigeneration.....	80
4.18	Recovered coolant heat for cogeneration.....	82
4.19	Recovered coolant heat for trigeneration	82
4.20	Total recovered heat for cogeneration	83
4.21	Total recovered heat for trigeneration.....	83
4.22	Heating power and operation temperature of the refrigerator at full load scale.....	84
4.23	Comparison of electric powers at different load scales.....	85
4.24	Comparison of heater temperatures at different load scales.....	86
4.25	Comparison of evaporator temperatures at different load scales.....	86
4.26	Comparison of freezer and food chiller temperatures at different load scales.....	87
4.27	Comparison of heat input with different exhaust gases and loads.....	90
4.28	Comparison of heater temperatures with different exhaust gases and loads.....	90

4.29	Comparison of evaporator temperatures with different exhaust gases and loads....	91
4.30	Comparison of freezer temperatures with different exhaust gases and load.....	92
4.31	Comparison of food chiller temperatures with different exhaust gases and loads...	92
4.32	BSFC for cogeneration.....	96
4.33	BSFC for trigeneration.....	96
4.34	BSEC for cogeneration.....	97
4.35	BSEC for trigeneration.....	97
4.36	CO ₂ emissions for cogeneration.....	98
4.37	CO ₂ emissions for trigeneration.....	98
4.38	Overall efficiency for cogeneration.....	99
4.39	Overall efficiency for trigeneration.....	99
4.40	Exergy of recovered exhaust gas heat for cogeneration.....	100
4.41	Exergy of recovered coolant heat for cogeneration.....	101
4.42	Exergy of recovered exhaust gas heat for trigeneration.....	101
4.43	Exergy of recovered coolant heat for trigeneration.....	101
4.44	Exergy of cooling energy for trigeneration.....	102
4.45	Overall exergy efficiencies for cogeneration.....	102
4.46	Overall exergy efficiencies for trigeneration.....	103
5.1	Characteristic zones of diesel spray.....	107
5.2	Comparison of tested and simulated engine power.....	113
5.3	Comparison of tested and simulated BSFC.....	114
5.4	Deviation of engine power and BSFC.....	114
5.5	Comparison of tested and simulated CO ₂ emissions.....	115
5.6	Comparison of tested and simulated NO _x emissions.....	115
5.7	Deviation of CO ₂ and NO _x emissions.....	115
5.8	Preheating temperature dependent engine power.....	116
5.9	Preheating temperature dependent BSFC.....	116
5.10	Comparison of combustion pressures at full load with different preheating temperatures.....	117
5.11	Comparison of combustion temperatures at full load with different preheating temperatures.....	117

5.12	Preheating temperature dependent engine power efficiency.....	118
5.13	Preheating temperature dependent CO ₂ emission.....	119
5.14	Preheating temperature dependent NO _x emission.....	119
5.15	Preheating temperature dependent Bosch smoke.....	120
5.16	Preheating temperature dependent PM emission.....	120
5.17	Injection timing dependence in engine power optimisation.....	122
5.18	Injection timing dependence in SFC optimisation.....	122
5.19	Compression ratio dependence in engine power optimisation.....	123
5.20	Compression ratio dependence in SFC optimisation.....	123
5.21	Swirl ratio dependence in engine power optimisation.....	124
5.22	Swirl ratio dependence in SFC optimisation.....	124
5.23	Intake valve opening dependence in engine power optimisation.....	125
5.24	Intake valve opening dependence in SFC optimisation.....	125
5.25	Injection duration dependence in engine power optimisation.....	126
5.26	Injection duration dependence in SFC optimisation.....	126
5.27	Electrical load.....	129
5.28	Trigeneration model.....	130
5.29	dieselGenerator module.....	130
5.30	coolantEnergy module.....	132
5.31	cHX module.....	133
5.32	Parameter setting of module cHX.....	133
5.33	Schematic diagram of diffusion absorption system.....	137
5.34	Energy distributions with gas oil and croton oil.....	142
5.35	Recovered heat energy with gas oil and croton oil.....	143
5.36	Cooling energy with gas oil and croton oil.....	144
5.37	COP with gas oil and croton oil.....	144
5.38	Power and electrical efficiencies with gas oil and croton oil.....	145
5.39	Trigeneration efficiencies with gas oil and croton oil.....	146

List of Tables

2.1	Technical characteristics of the prime movers in micro-trigeneration.....	15
2.2	Comparison of adsorption working pairs.....	19
2.3	Comparison of physicochemical properties of vegetable oils to diesel.....	25
3.1	Arrangement of the sensors on the diesel generator	45
3.2	Arrangement of the thermocouples on the absorption refrigerator.....	47
3.3	Status of exhaust valves for different tests.....	52
3.4	Engine rig test plans.....	52
3.5	Uncertainties of measurements on diesel generator.....	57
3.6	Uncertainties of measurements on the absorption refrigerator.....	58
3.7	Uncertainties of other measurements.....	61
4.1	Viscosities of the oils.....	65
4.2	Densities of the oils.....	66
4.3	Heating values of the oils.....	68
4.4	GC traces data of croton biodiesel.....	69
4.5	Proportions of the constituents in croton biodiesel and croton oil.....	70
4.6	Elementary compositions of the vegetable oils.....	71
4.7	Effects of refrigeration at different load scales driven by electricity.....	87
4.8	Effects of refrigeration with different heating sources and loads.....	94
4.8	Effects of refrigeration with different heating sources and loads (Renewal).....	95
5.1	Physicochemical property of croton oil and diesel fuel.....	111
5.2	Critical pressures and critical temperatures of fatty acids.....	111
5.3	Comparison of the electrical power and the engine power.....	112
5.4	Engine performance and emissions after optimisation.....	127
5.5	Summary of equations for simulating absorption refrigeration.....	137
5.6	Exponents and coefficients for x''	139
5.7	Exponents and coefficients for h_l	140
5.8	Exponents and coefficients for h_g	140

5.9	Exponents and coefficients for $T(p, x')$	141
5.10	Exponents and coefficients for calculating $T(p, x'')$	141

Nomenclature

Symbols

b_i	Evaporation constants
c_p	specific heat at constant pressure, kJ/kgK
d_c	Drop diameter, mm
d_{32}	Sauter Mean Diameter, mm
E_e	Electric power, kW
E_V	Volumetric energy, MJ/m ³
E_X	Exergy, kW
G	Thermal conductance, kJ/K
H_U	Lower heating value, MJ/kg
h	Latent heat, MJ/kg or Enthalpy, kJ/kg
$k_{i,f}$	Forward reaction rate, cm ³ / (mol·s)
M	Molar mass, kg/ mol
m	Mass, kg
\dot{m}	Mass flow rate, kg/s
Pe	Engine power, kW
P_{max}	Peak combustion pressure, bar
p_c	Critical pressure, bar
p_s	Saturated vapour pressure, bar
Q	Thermal energy, kW
Q_c	Cooling power, kW
Q_h	Heating power, kW
T	Temperature, °C
T_C	Critical temperature, °C

T_{exh}	Exhaust temperature, °C
T_{max}	Peak combustion temperature, °C
t_e	Evaporation time, s
V	Volume, m ³
X	Molar fraction
x	Mass fraction

Greek letters

γ	Surface tension, N/m
Δ	Absolute uncertainty
Δh	Difference of specific enthalpy, kJ/kg
ε	Relative uncertainty or Effectiveness
η	Dynamic viscosity, mPa.s;
η_e	Electrical efficiency, %
η_p	Engine power efficiency, %
η_{TG}	Trigeneration efficiency, %
ρ	Density, kg/m ³
ν	Kinematic viscosity, mm ² s ⁻¹ ;

Subscripts

A	Absorber
ADD	Additive combination
AR	Absorption refrigerator
a	air
C	Condenser

DAR	Difference of parameters between the inlet and outlet of refrigerator
DEXH	Difference of parameters between the inlet and outlet of exhaust heat exchanger
DG	Diesel generator
E	Evaporator
EB	Engine block
EX	Exhaust gas
EXH	Exhaust heat exchanger
f	Fuel
fa	Fatty acid
G	Generator
GH	Gas heat exchanger
H	Hot side
HW	HIPS wall
in	Input
L	Liquid or Cold side
LC	Loss heat of coolant
LM	lumped mass
M	Molar
R	Rectifier
r	Random error
RC	recovered coolant energy
RE	recovered exhaust gas energy
RSS	Root-sum-square combination
SH	Solution heat exchanger

s	System error
V	Vapour
W	Water

Chapter 1. Introduction

1.1 Research Background

The global economy is currently driven by an ever increasing demand in fossil fuel consumption. According to the predictions of International Energy Outlook 2011 [1], global market energy consumption will increase by 53% between 2008 and 2035. Among the available energy sources, fossil fuels are still the most dominant energy source worldwide and account for over 80% of the total prime energy supply, in which 33% are contributed by liquid fuels [2].

However, energy supplied from fossil fuels has already been recognized as unsustainable since the energy crisis in the 1970s [3-5]. Based on the current conventional prime energy consumption rate, British Petroleum predicted that major fossil sources, i.e. crude oil, natural gas and coal, would be depleted within 46, 59 and 118 years respectively [3]. Similar simulation results have also indicated the depletion of global crude oil and natural gas reserves [4, 6, 7].

Global warming is another issue caused by fossil fuel combustion, mainly due to the increase in emissions of greenhouse gases (GHG), such as carbon dioxide (CO₂) and methane. Between 1980 and 2008, global fossil fuels consumption led to CO₂ emissions increasing by 63%, from 18.5 billion metric tonnes (BMTs) per annum to 30.2 BMTs per annum, and this figure is predicted to reach 43.2 BMTs by 2035 [1, 8]. As a result, polar ice cap melting, sea levels rising, climate change, water shortages and land desertification have increased in intensity.

Realizing the serious situation of environment deterioration, great efforts have been made to find feasible sustainable development solutions. International conventions, such as Agenda 21 and the Kyoto Protocol, have been approved by a vast majority of countries to help maintain GHG emissions to an acceptable level [9, 10]. Consequently, the European Union has set a target to cut 80-95% of emissions compared to the 1990 level by 2050 [11]. The UK figure is set at 80% reduction by the year 2050 [12].

Many legislations and policies have been adopted in the UK with respect to energy demand and towards cutting CO₂ emission. Some of these policies were for electricity generation or the utilisation of heat from renewable energy[12-16]; especially the Microgeneration Strategy[15] and the Low Carbon Buildings Programme[16]. The aim was to improve the domestic energy efficiency with the use of popularised efforts on decentralised generation technologies, with respect to household energy consumption accounting for about one third of the UK energy supply [17]. Accordingly, the UK government proposed to meet 30-40% of the domestic electricity needs through micro-generation by 2050, hence this should reduce the annual household carbon emissions by 15%.

Micro-trigeneration is a new emerging technology, integrating micro-cogeneration with waste heat driven cooling/refrigeration technologies. It operates in high efficiency modes and is projected to meet all the energy demand, namely, electricity, heating and cooling energy for household users, helping relieve the burden of the energy supply[18-22].

Biofuel is considered as substitute energy for fossil fuel, characterised by renewable and carbon neutral, and has been studied intensively during the past decades [23-28]. The combination of these two promising solutions will provide great benefits in energy saving and GHG reduction.

1.2 Aims and Objectives

As the major part of the Engineering and Physical Sciences Research Council (EPSRC) funded project ‘Biofuel Micro-Trigeneration with Cryogenic Energy Storage’ (BMT-CES), this research work was to develop an advanced micro-trigeneration system fuelled with raw vegetable oils, which will meet the household energy demand with high efficiency, energy savings and low emissions. The specific objectives of the study are:

- a) To design and construct a diesel generator based micro-trigeneration system, thus generate power, heat and cooling energy simultaneously using raw vegetable oils.
- b) To investigate the operational characteristics and emissions of the raw vegetable oils used in the engine compared to diesel fuel.
- c) Trigeneration system modelling and simulation covering the system dynamic performance evaluation, prediction and optimisation.

1.3 Methodology

1.3.1 Investigation of domestic energy consumption

Consideration into the variation of domestic electrical, heating and cooling requirements, a literature investigation and analysis was conducted for the design specification of the BMT system, including the power and heat loads for the diesel generator, waste heat recovery for heating and refrigeration requirements, etc.

1.3.2 Biofuel properties investigation

A number of physicochemical properties of raw vegetable oils, such as viscosity, heat value and cetane number may affect the engines' performance and emissions. Hence, experiments were carried out to study the properties of the vegetable oils and to evaluate the effects of these oils when applied to the BMT system. The test data was used for the validation of engine model and as the input of micro-trigeneration model.

1.3.3 Computational modelling and simulation

To understand the influencing factors relating to the performance of the BMT system, modelling and dynamic simulation was conducted to study the energy, heat flow and thermodynamic processes of the system. The research outcomes were used to address the key factors for the design and experimentation of the micro-trigeneration system.

1.3.4 Experimental investigation of the BMT system

Based on the results of the above work, a BMT system was designed and constructed. Experiments were conducted to evaluate the performance of the BMT system including: power output, fuel consumption, quantity of recovered waste heat and energy efficiency of the diesel generator, heat exchanger, absorption refrigerator, etc. Four types of raw vegetable oils (two edible and two inedible) were tested with the aim of reducing emissions, whilst maintaining the power output from the diesel generator.

The viscosity of raw vegetable oil is higher than that of diesel fuel and may cause negative effects when directly applied in diesel engines, such as injector obstruction and carbon deposition in the combustion chamber, thus it will deteriorate the engine performance and durability. To solve the problem, a fuel preheating unit was designed for heating the fuel tank or fuel lines by electricity and additionally by exhaust gas when engine was operational.

Experiments were carried out to investigate the performance and emissions of the prime mover and the complete trigeneration system. This included measuring power output, fuel consumption, quantity of recovered waste heat and energy efficiency of the diesel generator, heat exchanger, absorption refrigerator, CO₂, CO (carbon monoxide), HC (unburnt hydrocarbons) and NO_x (nitrogen oxides) emissions, etc. An experimental comparison between diesel fuel and the preheated vegetable oils was assessed using different load profiles. An absorption refrigeration unit was used to study the cooling effects driven by exhaust gas heat. A monitoring and control system was developed as well to monitor and control the system operation.

1.4 Contribution to existing research

As a novel technology, micro- trigeneration can provide great benefits in achieving national and European targets of energy saving and carbon reduction. Currently, research achievements of micro-trigeneration have been reported with most based on theoretical studies. Limited examples of micro-trigeneration systems using biofuel have been documented. This research work is collaboration with University of Leeds and University of Ulster in the UK, and three research institutes and universities in China. The research presents the details of theoretical and experimental investigations on the BMT and will contribute to the existing research in the following fields:

- a) To accumulate experience in BMT system design, construction and commissioning.
- b) To improve understanding of the system performance running with vegetable oils, especially for the real operational characteristics.
- c) To provide a virtual platform for system performance simulation, optimisation and prediction.
- d) To strengthen the collaborative research relationships between the UK and China.

- e) To benefit households/companies economically in the long term, thus promote the development of renewable biofuels.

Chapter 2. Literature Review

2.1 Introduction

Energy consumption always accompanies waste heat delivery, usually resulting in waste heat transmitted directly to the environment. In 2008, approximately one third of the global energy by electricity generation was delivered to end users, whilst the rest was lost in some form of waste heat during the conversion process [29].

Cogeneration or combined heat and power (CHP) is a mature and highly efficient technology developed for waste heat recovery, which has been widely applied in industry, commercial environments and large buildings for decades. In recent years, stimulated by the increasing demand of cooling energy and carbon dioxide reduction, trigeneration was developed with the aim of producing cooling, heating and power energy simultaneously by integrating waste heat activated refrigeration, i.e., CCHP. It has presented great merits in energy-saving, economics, reliability and environmentally friendly.

Benefits from the new concept of distributed power supply, trigeneration systems have been developed to a smaller scale with lower power transportation and distribution losses. They are expected to play an important role on downtown, populated areas, office buildings and hospitals, etc.

Biofuel is another research focus for clean and renewable energy. Biofuel refers to the fuel originally from biological substances, in the form of gaseous, liquid, or solid. Early research on biofuels can be traced back to 1900, when Rudolf Diesel ran a diesel engine with peanut oil at The World Fair [30]. In previous decades, biofuel research has been carried out intensively for relieving energy shortage and the reduction of GHG. In 2010, global biofuel production was 105 billion litres, an increase of 17% with regards to 2009 and contributed 2.7% of the fuel consumption for road transportation [31].

The vast majority of biofuels are made up of bioethanol and biodiesel. The former accounts for about 85% of the liquid biofuel production and is produced by sugar crops, starchy crops and cellulosic materials; the latter was mainly converted by transesterification sourced from vegetable oils and animal fats [32]. In 2010, 86 billion litres of ethanol were

produced, in which 90% were from the United States and Brazil, while biodiesel production in the European Union accounts for 53% of the worldwide production. It was estimated that biofuels would meet over 25% of global fuels demand for transportation by 2050 [32].

2.2 Domestic energy demand and consumption in the UK

Energy consumption supports a comprehensive range of human activities, from industry, transportation, financial circles and service trade to daily life. In the UK, 2010 household energy use was 48.871 million tonnes of oil equivalent (MTOE), accounting for 32% of the total final energy consumption [33]. The Department of Energy and Climate Change (DECC) released statistics[34] depicting that in 2008 the average domestic consumption of gas in the UK was 16,971 kWh, and for electricity it was 4,413 kWh (with a low profile of 3,627 kWh for floor area less than 50m² and a high profile of 7,799 kWh for floor area of 200-250m²). This indicated an approximate heat to electricity ratio of 4:1. As the major energy sources, gas and electricity had met 69% and 21% of the domestic energy demand; the remainder were supplied by solid fuel and oil. The consumption of gas was mainly for cooking, space heating and hot water supply, while electricity consumption was largely for lighting, appliance and space heating. The specific energy consumption rates in household, space heating, hot water, cooking, lighting and appliances were 62%, 17%, 18% and 3% of the total energy (Fig. 2.1).

The energy consumption of an individual house varies by the house type, geographical position, electrical appliance type and number, boiler efficiency, occupants' number and occupancy patterns, etc. [35, 36]. Besides, seasons and weather also posed great influence to domestic energy consumption [35, 37-39]. A two-year investigation into the daily power consumption of 72 UK households demonstrated that the domestic electricity demands were mostly lower than 0.5 kW in off-peak hours (21:00 to 6:00) and no more than 8 kW during peak time (Fig. 2.2) [35]. M. Newborough [37] investigated the annual energy consumption of a detached house and found that the gas consumption for heating from April to September was low, usually less than 20kWh per day; this figure increased by four times higher in winter (Fig. 2.3). Meanwhile, the electricity demand fluctuated between 10-40kWh per day, appearing to have an indistinctive seasonal impact. Peacock et al. [38] tested the energy demand of a single dwelling in January, April and August, and discovered

tremendous variation of heat to power ratios of 8.5, 3.7 and 0.6. Newborough and Augood [39] also pointed out that the maximum electrical load was 10-15kW and the average figure was 0.3-1kW per day in each investigated house.

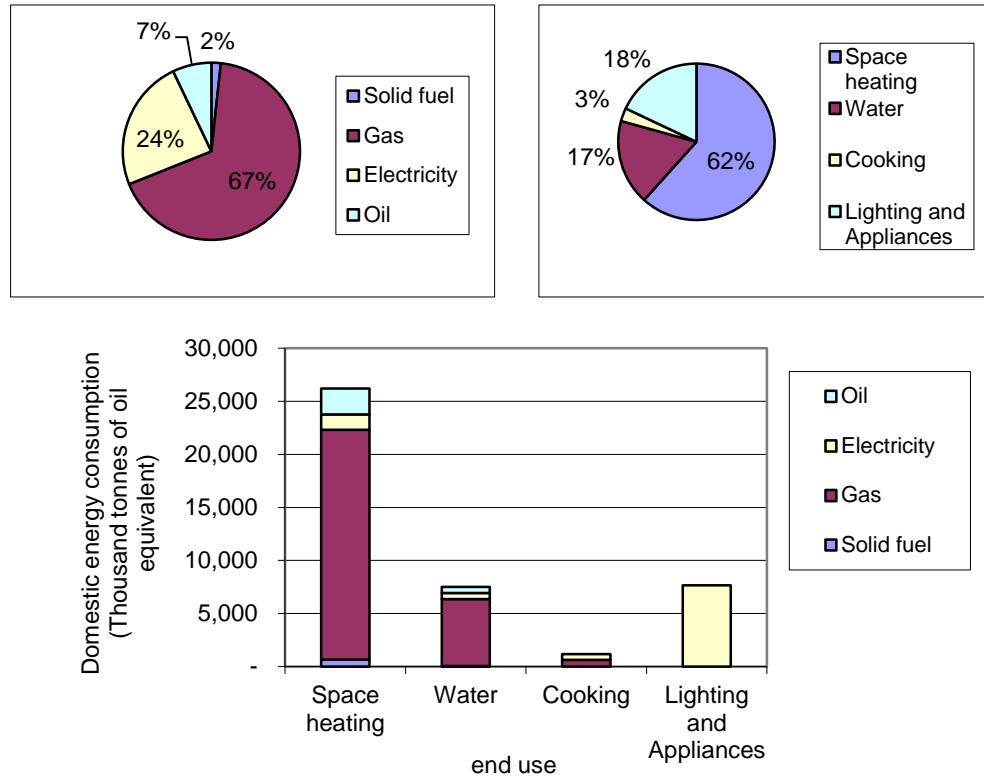


Fig. 2.1 UK domestic energy consumption by end use in 2009 (data sourced from [34])

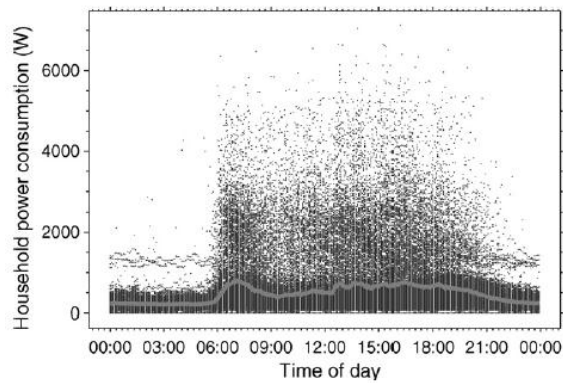


Fig. 2.2 Total power consumption of a single house within 2 years (The grey line shows the average values for each 5 min period) [35]

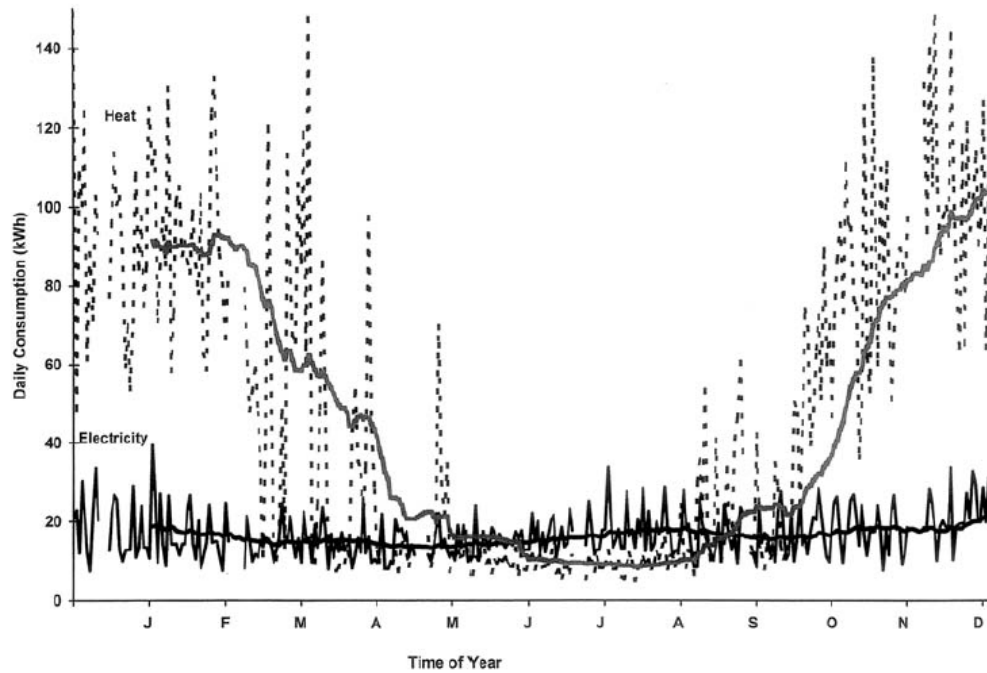


Fig. 2.3 Trends in the daily and 30-day rolling average heat and power demands for a single house from January to December [37]

Wood et al. [40] classified domestic electricity consumption as ‘predictable’, ‘Moderately predictable’ and ‘unpredictable’. Predictable electricity consumption was aroused by constantly switched on electrical appliances, for instance, refrigeration appliances, security lighting, televisions, video camera recorders, broadband modems and burglar alarms; moderately predictable electricity consumption was mainly accounted for by electrical appliances running periodically, such as watching TV and switching lights on/off; while unpredictable electricity consumption was referred to applications like food cooking and clothes/dish-washing [35, 41]. The authors pointed out that lighting (717kWh/Year), fridge-freezer (500kWh/Year) and dishwasher (400kWh/Year) were the top three sources for domestic electricity consumption. Firth et al. [35] also presented a similar classification and listed typical power ratings of different electrical appliances. The investigation results revealed that high electrical power devices, such as kettle, electric shower, washing machine and Electric cooker were the major reasons for the fluctuation of domestic electricity load.

2.3 Micro-trigeneration

2.3.1 Trigeneration Classification and Typical Applications

Due to the close relationship between cogeneration and trigeneration, the classification of a trigeneration system can be borrowed from the former; by means of technology types, prime movers applied or system scales, etc. [20, 42]. Usually, typical centralised industrial power plants are divided into medium or large scale, with electricity output no less than 1 megawatt electricity (MWe). Other non-industrial application units may reach up to 10 MWe, but most are applied to office buildings, hotels and restaurants, ranging from 20 kilowatt electricity (kWe) to 1MWe, which can be classified as small and mini size. The Europe Union has defined a micro cogeneration system with a power output lower than 50 kWe [43], considering the real domestic electricity consumption is usually lower than 15 kWe [35, 37-39], the range of micro-cogeneration can be narrowed down to under 20 kWe electricity output [42, 44-46]. Some researchers also classified a micro system with a power output lower than 15 kWe [47, 48].

Large and medium scale trigeneration systems have been commercially operating over 20 years, mainly powered by reciprocating engines, steam turbines and gas turbines [49, 50]. The first trigeneration plant in Europe was setup and operated in Lisbon (Portugal), serving for the 1998 World Expo [50]. It was driven by a 5 MW natural gas turbine with 28 MW cooling capacity generated from a lithium bromide (LiBr) refrigeration unit and 22 MW heating capacity. The electrical and overall thermal efficiency of this plant was 30% and 82%. A large scale trigeneration plant in the University of Illinois was powered by two 3.8 MW gas reciprocating engines, three 5.4 MW gas engine generators and three 7.0 MW solar turbines, supplying almost all of the campus energy demand [51]. A solar gas turbine trigeneration system combined with an absorption chiller was installed in the Domain Plant of Austin, providing 4.3 MW net electricity and 8,918 kW cooling power [52].

Most trigeneration applications are focused on small and mini scale sectors, whereby each type of prime mover can be found in these ranges to meet the varying demands of office buildings, small enterprises, schools and merchandising businesses. A small trigeneration system was setup in University of Maryland for supplying energy to a building. This system generated 60

kWe of electricity using a gas turbine, and 65 kW cooling power by an absorption chiller with a coefficient of performance (COP) of 0.65. The average electrical efficiency and total efficiency of the system were reported as being 26.9% and 72% [53].

For micro-trigeneration, the reciprocating engine appears to be the most mature and popular prime mover, especially for powering domestic users in a remote region or an isolated island. Other competitive prime movers include the micro turbine, Stirling engine and fuel cell. The details of this technology are discussed in the following sections.

2.3.2 Micro-trigeneration Technologies

Basically, a micro-trigeneration system is much more compact and structurally simple compared to a large system. Nevertheless, they still have the same major units and each performs a unique function: a) Prime mover and generator to transfer chemical energy or another type of energy into electricity; b) Heat exchanger(s) to recover waste heat contained in working medium or coolant; and c) Chiller for space cooling or refrigeration.

2.3.2.1 Prime Movers

A prime mover is the dominate factor to the electrical efficiency and the available waste heat of a trigeneration system. As mentioned above, four competitive prime movers are currently available for micro-trigeneration. The technical features of these prime movers have been well documented and are summarised in Table 2.1.

A. Internal Combustion Engine

The Internal Combustion Engine (ICE) is a well-developed commercial product for auto power, electricity generation and other applications, prevailing in competitive price, low operating and maintenances costs. It is a fuel-flexible power device which can be driven by fossil fuel, gas, biofuel or blended fuels, at the same time retaining similar power output and high energy efficiency. For the purpose of continuous operation, an engine usually runs on liquid fuels; while a gas engine is applied mainly for back up purposes [54, 55]. To

date, a number of 1–4 kW ICE based micro-CHP systems have been installed in the UK, with reported ratings of approximately 30% electrical efficiency and 85% overall efficiency [56].

However, intensive vibration and noise caused by reciprocating and rotational parts of the ICE will deliver an unpleasant experience to domestic users. This results in a higher wear and damage rate and also indicates a relatively short maintenance interval. Another drawback of the ICE is that it has the highest exhaust emission of all the prime movers; in particular the NO_x emission is several times higher than the other prime movers.

B. Stirling Engine

The Stirling engine is a canned cycle external combustion engine which operates by cycling working gas, such as H_2 or He, between the hot portion and the cold portion. In the hot portion, the gas is heated in the heater by means of external combustion and it swells in the expansion chamber to output mechanical energy. After that, the working gas is delivered to the cold portion, where it is compressed in a compression chamber and is cooled down in a cooling chamber for the next circulation [57-60].

Compared to the ICE, the Stirling engine operates with lower noise and less emissions, especially NO_x emission. Besides, it can be driven by solar energy, biomass or even waste heat. The maintenance cost of the Stirling engine is cheaper than that of the ICE. Nevertheless, it also has some drawbacks, such as expensive prime costs and 2-3 times higher heat loss. This engine is usually recommended for domestic backup purposes and rare Stirling engine based trigeneration systems have been reported. However, due to its ideal power to heat ratio, it is still attractive for domestic trigeneration [44, 55-57].

C. Micro turbine

The definition of scale relating to micro-turbines varies greatly within different literature reviews. Pilavachi [61] categorises turbines with a power output rating lower than 150 kWe as micro types; while Alanne et al. [54] defines them as having a 25-250 kWe power output. These turbines usually consist of a single-shaft stringed air compressor, combustion chamber, gas turbine and a generator. They are characterised by their compact

size, small number of moving parts and a high power/weight ratio. Compared to an ICE, the moving parts contained in a micro-turbine are all high speed rotating ones; hence it operates smoothly and with high reliability. Further merits of a micro turbine include multi-fuel capabilities and low emissions, mainly due to the low continuous combustion temperature and pressure in the combustion chamber. Nevertheless, extra components such as a rectifier and transformer are needed for a micro turbine to convert the high frequency electricity into commercial power [55, 61, 62]. Despite the high cost and relatively poor part load performance, micro turbines have shown potential to be used in applications. Worldwide, a number of micro turbines have been commercially operating in North America and Europe, most ranging from 30kW to 100kW [63, 64].

D. Proton Exchange Membrane Fuel Cell

A Fuel cell performs both roles of prime mover and generator to produce power by an electrochemical reaction. The most popular fuel cells are the proton exchange membrane fuel cell (PEMFC), alkaline fuel cells (AFC), phosphoric acid fuel cell (PAFC), molten carbonate fuel cell (MCFC) and solid oxide fuel cell (SOFC), being classified by their electrolyte type. The benefits for applying a fuel cell include [65-68]:

- a) High electrical efficiency and quick response to load changes. The average efficiency of a fuel cell can be up to 45%. This figure is load-independent and only affected in the main by operating temperature, fuel and electrolyte type.
- b) Very low noise. There is no combustion or moving parts in a fuel cell system. The only noise sources are from air pumps and fans operating with a low noise value of between 40-60dBA.
- c) Very low emission. Hydrogen is the major fuel used in a fuel cell; hence the only by-product is water. CO₂, negligible amount of SO₂ and nitrogen may also be emitted when methanol or hydrocarbon gases are used.
- d) High reliability. Without any moving parts, a fuel cell is free of wear and tear and hence more reliable.

A PEMFC was first applied in the 1960s and experienced intensive studies in the 1990s[65]. Due to the use of solid organic polymer electrolyte, it was also characterised by less corrosion and electrolyte management problems with a quick start-up. Like AFC, PEMFC

operates under low temperature conditions of 50-100 °C, distinguishing it from those of PAFC (150-200 °C), MCFC (600-700 °C) and SOFC (600-1000 °C). This result in a reduced system warming-up time is needed; lower cooling efficiency and less recovered heat.

Though each type of fuel cell has specific applications, PEMFC covers almost all fields including space flight, electric vehicles, electronic products, traffic signals, military communications and other portable applications. It has shown strong competitiveness in residential sectors relative to other fuel cells [65, 66].

Due to the expensive cost (3 times that of ICE), PEMFC has potentially been applied on commercial buildings rather than individual houses [65]. Some residential fuel cell cogeneration or trigeneration systems have been reported in demonstrations or trials, ranging from 1 kWe to 10 kWe. In order to meet the off-grid power load, a minimum 5 kWe unit was recommended for household users, and lower power units are usually used as a backup system for off-peak operation [66, 69].

Items	Internal combustion engine	Stirling engine	Micro turbine	PEMFC
Typical capacity (kW)	3-200	1-100	15-250	1–250
Fuel	Natural gas, LPG, distillate oils, liquid fuels, biogas	Natural gas, LPG, liquid or solid fuels, biogas	Natural gas, distillate oils, biogas	Hydrogen, hydrocarbons or methanol
Full load electrical efficiency (%)	25-45	15-35	15-30	30-60
Half load electrical efficiency (%)	23-40	15-30	15-25	30-60
Overall efficiency (%)	65-90	65-85	65–87	70-90
Power to heat ratio	0.8-2.4	1.2-1.7	1.2-1.7	0.8-1.1
Noise(distance of 3 feet) (dBA)	56-105	50-75	57-82	50-60
CO ₂ emissions (g/kWh)	500-650	672	720	430-490*
NO _x emissions(g/kWh)	0.2-10	0.08-0.288	0.1	0.005–0.01
Availability (%)	95	Not available	98	90-95
Average cost investment (\$/kW)	340–1600	1300-2000	800–1300	2500–3500
Operating and maintenances costs (\$/kWh)	0.007-0.015	0.004-0.015	0.002-0.02	0.02-0.04
Life time (h)	5,000-20,000	5,000-8000	20,000-40,000	7,000-21,000

Table 2.1 Technical characteristics of the prime movers in micro-trigeneration [20, 54, 57, 61, 65, 67, 68, 70, 71]

*: Fuelled by hydrocarbons or methanol.

2.3.2.2 Waste Heat Driven Cooling

Cooling capability is a key factor in distinguishing between trigeneration and cogeneration. To date, four major refrigeration technologies are available: vapour compression, ejector cycles, absorption and adsorption [49]. Except for vapour compression which is either powered by electricity or mechanical energy, all the others can be driven by heat energy.

A. Absorption Refrigeration

Absorption refrigeration was invented by Faraday in 1824, when he used ammonia vapour as a refrigerant and silver chloride as an absorbent for cooling energy generation. The first ammonia-water absorption chiller was invented in 1859, approximately 100 years after the invention of the vapour compression chiller [72]. Currently ammonia-water along with LiBr-water have become the most mature working pair for modern absorption refrigeration [73].

In simple terms an absorption refrigerator is mainly composed of a generator, condenser, evaporator and absorber, sometimes equipped with a rectifier and heat exchanger (Fig. 2.4). The basic cycle of absorption refrigeration is described below:

- a) High quality heat Q_H is supplied to the generator, where it contains a binary concentrated solution of refrigerant and absorbent. High pressure refrigerant evaporates and enters into the condenser. The solution then turns into a lean liquid;
- b) After being condensed, the refrigerant releases intermediate heat Q_{II} before moving to the evaporator;
- c) Therein it absorbs low temperature heat Q_L from the reservoir, evaporates again and changes into being a low pressure gas, thus providing a cooling capacity;
- d) Finally, the refrigerant reaches the absorber and is imbibed by the lean solution coming from the generator, meanwhile releasing low-grade heat Q_{I2} to the environment. The concentrated solution is then pumped back to the generator for the next cycle.

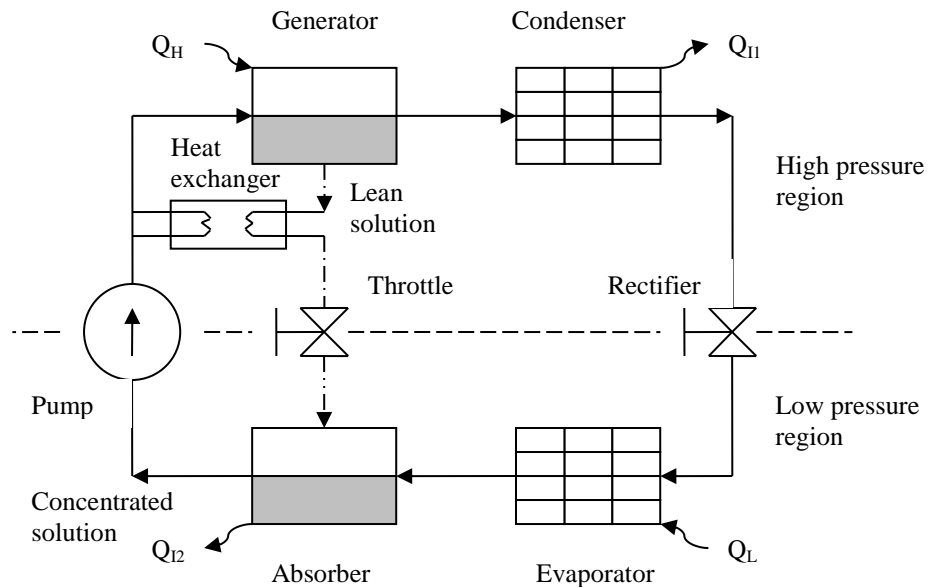


Fig. 2.4 Basic schematic diagram of absorption refrigeration

In this cycle the generator, absorber, pump and rectifier act together as a compressor in the vapour compression refrigeration system. To utilise waste heat in a lean solution, a heat exchanger was engaged for warming up the concentrated solution before it returns to the generator, thus improving the system efficiency. For ammonia-water refrigeration, a rectifier is necessary to remove the water contained in the ammonia vapour. Otherwise it will be deposited in the evaporator and will reduce the refrigeration efficiency. This part is not necessary in a LiBr-water refrigeration system, thanks mainly to the non-volatile property of LiBr. However, limited by the high freezing point of the water refrigerant, LiBr-water refrigeration cannot be applied to freezing demand sectors.

Though characterised by a simple structure and being cost effective, the efficiency of an absorption refrigeration system is fairly low. Single-effect absorption refrigeration only utilises heat energy once in a cycle and performs at low efficiency with COP 0.5-0.7. A multi-effect system performs at a higher efficiency by recovering heat using two or three heat transformers, but mostly with COP less than 1.5 [72]. Usually the higher the heat utilisation level, the better the system efficiency. Nevertheless, this requires higher quality heat sources and the related systems may be more complex and expensive. The installation and maintenance costs for an absorption system are about 140-490 US\$/kW and 4.5-9 US\$/kW/year. LiBr/water double-effect systems appear to be the only commercial product that satisfies both high performance (COP>1.2) and economic costs

[72, 74, 75]. Apart from the current research achievements on absorption refrigeration, more effort is still required to enhance its performance.

B. Adsorption Refrigeration

The principle of adsorption refrigeration was first proposed by Faraday in 1848, but not until the 1920s did studies really focus on this novel technology. An adsorption refrigeration system has simple modular construction and contains only a few moving parts, making it scalable, operate quietly and requires no lubrication and less maintenance. Furthermore, this system can be directly driven by low-grade heat, hence saving energy consumption by up to 90% [20].

A basic adsorption refrigeration system mainly consists of an adsorber, condenser and evaporator. It runs as two processes called desorption and adsorption, which can be ideally broken down into four phases [20, 76], as shown in Fig. 2.5.

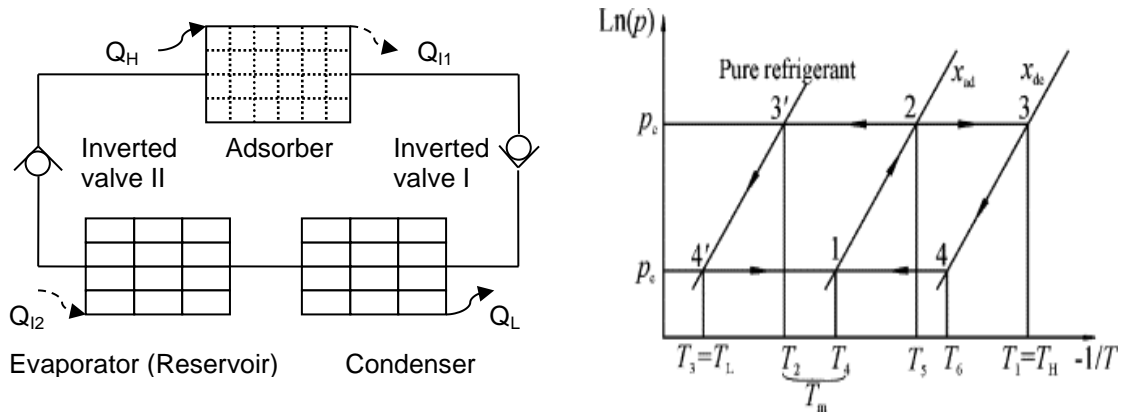


Fig. 2.5 Basic schematic and thermodynamic diagram of adsorption refrigeration

During desorption, the adsorber is heated by high-grade heat Q_H . Adsorbate (refrigerant) overcomes an adsorption force and escapes from the adsorbent surface, resulting in a pressure increase in the adsorber, namely isosteric pressurisation (phase 1-2). The refrigerant vapour then passes through the inverted valve I to reach the condenser. During this time, the pressure in the adsorber is kept stable but the temperature increases continuously. Phase 2-3 is called isobaric desorption. After this stage the refrigerant is condensed and stored in the evaporator (reservoir). The pressure in the adsorber decreases and the inverted valve I is shut closed.

During the adsorption process the adsorption bed is cooled down and releases heat energy Q_{I1} into the surrounding environment. Refrigerant is again adsorbed into the

adsorption bed and the pressure in the absorber decreases. Phase 3-4 is called isasteric depressurisation. Saturated adsorbate vapour from the evaporator pushes open the inverted valve II and enters the adsorber where it is adsorbed. During this period, liquid adsorbate evaporates continuously by absorbing heat Q_{12} from the environment, which then goes to the adsorber. Hence, it retains the pressure balance and is named isobaric adsorption (phase 4-1). Finally, the pressure drops again and the inverted valve II shuts to complete the process.

Accordingly, the cycle 1-2-3'-4'-1 which happens in the condenser and reservoir represents the refrigerant loop, in which phase 2-3' denotes the condensation which occurs in the condenser (isobaric condensation); phase 3'-4' represents refrigerant self-cooling in the reservoir (isasteric cooling) and phase 4'-1 states the evaporating process in the evaporator (isobaric evaporation).

There are two types of adsorption: a) physical adsorption that adsorbents adsorb refrigerants via van de Waals force between molecules and b) chemical adsorption that working pairs react with to form a new compound [77-79]. The major refrigerants for adsorption are water, fluorocarbon, ammonia, alcohol etc. The most common adsorbents are physical activated carbon/carbon fibre, silica gel, zeolite and chemical metal chlorides, salt and metal hydrides/oxides, etc. [80-82]. The properties of some working pairs are listed in Table 2.2.

Working pairs	Refrigerant		Toxicity	Vacuity	Compressive strength	Release temp. (°C)	Driven heat
	Boil (°C)	Latent heat (kJ/kg)					
Zeolite-water	100	2258	No	high	Low	>150	High temp. waste heat
Silica gel-water	100	2258	No	high	Low	100	Solar energy, low temp. waste heat
Charcoal-CH ₃ OH	65	1102	Yes	high	moderate	110	Solar energy, low temp. waste heat
Charcoal Fiber-CH ₃ OH	65	1102	Yes	high	moderate	120	Solar energy, low temp. waste heat
Charcoal Fiber-C ₂ H ₅ OH	79	842	No	moderate	moderate	100	Solar energy, low temp. waste heat
CaCl ₂ -NH ₃	-34	1368	Yes	Low	High	95	Solar energy, low temp. waste heat

Table 2.2 Comparison of adsorption working pairs [81]

Stimulated by the research efforts towards energy saving and environment protection, adsorption refrigeration has achieved many breakthroughs during the previous 2-3 decades. A number of commercial products have already been sold in Japan, USA, France and other countries [76, 83]. In 1986, Nishiyodo Kuchouki Co. Ltd produced a commercial adsorption refrigerator run by silica gel-water. The chiller was driven by hot water at a temperature ranging between 50-90°C, with output chilled water at 3°C and COP up to 0.7. The payback time was estimated to be only 2–3 years [20]. In China, the outcome of a cooperation between Shanghai Jiao Tong University and an industrial company resulted in a series of adsorption chillers ranging from 10 to 100 kW being developed and introduced into the marketplace. Nevertheless, the efficiency of adsorption refrigeration is low, mostly with a COP value of 0.4-0.8 and this tends to be affected by the inlet temperature [84]. Currently, this technology only has a limited share of the marketplace. Additional studies into new working pair development, heat and mass transfer enhancement and the new adsorption cycle have been carried out to improve the refrigeration efficiency [81].

2.3.3 Existing work on micro-trigeneration

According to the current research outcomes, ICEs with a power output lower than 10kW seem to be the favoured prime movers for micro-trigeneration, although other prime movers such as the Stirling engine and fuel cell are available. When the ICE is used as the prime mover, the recoverable waste heat was roughly two times greater than the power output. Either can be recovered by the heat exchanger or heat pump for space heating, or by a waste heat activation system for refrigeration or space cooling [49, 85-88]. Despite many middle and large scale systems having been extensively studied and applied in commercial, institutional and residential sites, limited experience and knowledge has been achieved in micro-trigeneration design, operation, control and optimisation. A number of micro-trigeneration systems have been installed and monitored for experimental studies and demonstration purposes.

Angrisani et Al. [89] coupled a natural gas engine based micro-cogeneration system with a thermal-chemical absorption refrigerator. The system performance for cogeneration and trigeneration were investigated and compared using real operating conditions. When operating in the winter mode and with the supplied electricity at approximately 5.4 kW, the micro-cogeneration was found to save 19% of energy

relative to the conventional system, with the operating cost reduced by up to 30%. Nevertheless, it was also reported to perform inefficiently under the low electric demand condition (about 0.9 kW). While for summer operation mode, the system was found to consume more fuel, emit higher GHG emissions and was classed as uneconomical.

At the University of Nottingham, two micro-trigeneration systems were installed for use in a building's energy supply and for research & teaching. Each was powered by a 5.5 kW single cylinder direct injection diesel generator. The heat energy recovered from the generator, lube oil, coolant and exhaust gas was 12.5 kW. An ejector cooling unit was used for generating cooling energy which claimed to perform better than the absorption cycles. Nevertheless, the overall thermal efficiency of these systems was only around 50% [49].

Lin et al. [85] setup a household sized trigeneration system powered by a 6.0kW direct injection diesel generator. Two heat exchangers and a commercial absorption refrigerator were used for waste heat recovery. The refrigerator was driven either by AC/DC current with 100-105W power input, or by LPG gas with 186W input energy. The total thermal efficiency of the system was 67.3%, three times greater than the power generation; and the CO₂ emission was reduced by two thirds, hence it proved the feasibility of domestic trigeneration.

Wang et al. [86] integrated a biomass downdraft gasifier with a household scale trigeneration system. Feed stocks such as straw, willow and switch grass were gasified into syngas and supplied to a 6 kW direct injection diesel generator. Waste heat was gathered by the heat exchanger and stored in a hot water tank, or for driving an absorption refrigerator. Compared to power generation, the system demonstrated over 2.5 times greater thermal efficiency and four times lower CO₂ emission.

Shanghai Jiao Tong University in China performed experimental studies on a micro-trigeneration system. This system consisted of a 12kW natural gas/LPG-fired diesel generator, a waste heat recovery unit, a 10kW adsorption chiller (for producing cooling energy or hot water through the heat exchanger) and a water cooling tower (Fig. 2.6). The overall system efficiency was greater than 70%, owing mainly to the total 28kW of waste heat recovered from the exhaust gas and engine coolant, where each heat source

contributed almost the same recovered energy. Still, the silica/gel-water adsorption chiller performed a low COP of 0.3-0.4. It was calculated that the payback period time would be 2 to 3 years, providing a great economic advantage [88]. Based on performance data of the above system, Deng et al. [84] performed an exergy cost analysis using the structural theory of thermoeconomics. They concluded that the system equipped with an adsorption chiller with a COP value greater than 0.4, will be more efficient than an electric water chiller with a COP value of 2.51.

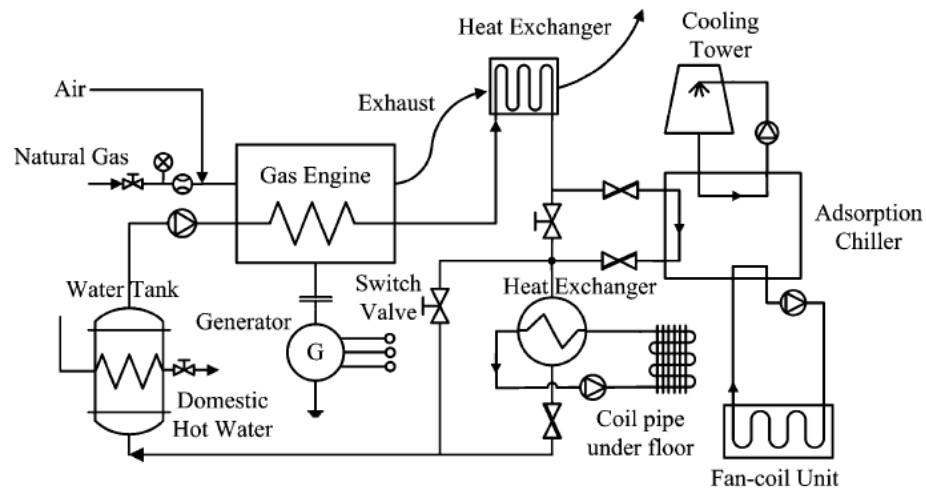


Fig. 2.6 Schematic diagram of a micro-trigeneration system

Miguez et al. [87] and Porteiro et al. [90] designed and constructed a 4kW_e micro-trigeneration system to verify the possibility of supporting the total energy requirements of a single house. Five system running modes were investigated and compared, i.e., stand-by mode, electric generator mode, cogeneration mode, heat pump winter mode and heat pump summer mode. Test results revealed that electric generator mode should always be avoided due to the low energy efficiency. The author also indicated that an extra electricity storage system such as a battery pack would help to improve the independence of a trigeneration system.

Rocha et al. [31] compared the performance and efficiencies of two trigeneration plants, one powered by a 26 kW ICE coupled with an electrical generator, and the other based on a 30 kW micro turbine. Both systems were fuelled with natural gas. The exhaust gas was firstly directed to an ammonia water absorption chiller then to a water heat recovery boiler. Experimental results showed that the ICE system performed with a higher electrical efficiency (27.6%) and lower COP (0.5) relative to the micro turbine

system (22.6% for electrical efficiency and COP of 0.6). Due to the reduced heat losses, the former system presented better primary energy saving (PES) and a lower energy utilisation factor (EUF) compared to the latter.

Moya et al. [91] constructed a trigeneration system based on a 28 kW micro gas turbine, a 17 kW ammonia/water air-cooled absorption chiller and a heat recovery boiler. Tests were performed under different operating conditions. Low ambient temperature and a high turbine load proved to have a positive effect on the system efficiency.

As well as these experimental studies, other theoretical investigations have been carried out mainly focusing on: a) trigeneration performance and emissions using substitute fuels and various prime movers, b) trigeneration tariffs over long term running and, c) system optimisation under different operating conditions.

Kong et al.[57] evaluated a trigeneration system using a 50kW Stirling engine and an absorption chiller. It was claimed that the system would save 33% of the primary energy relative to a power generation system, with an approximate payback period of 2 to 3 years.

Moya et al. [91] developed a model studying the electrical performance of a micro turbine. This proved to be a good match with the experimental results. They also carried out a feasibility analysis of the trigeneration system based on the energy consumption of a large residential building and a medium-sized hotel with thermal energy storage. The results revealed that the payback time for the large residential building was approximately 5.2 years, and for the medium-sized hotel it was 9.6 years. The trigeneration efficiency, equipment scale, reduced annual economic energy savings and the high cost are judged to be the main factors hindering the system application.

Rocha et al. [92] modelled a small-scale trigeneration plant by taking the main components as “black boxes” characterised by their performance parameters. The operating policy of the mode was set automatically using linear optimisation techniques. The influence of additional factors to the economic and energetic savings for end users, such as prime mover efficiencies, maximum power demand, cooling machine performance parameters and costs of fuel were analysed. It depicted that higher figures

for the first three factors provided better savings; while this was achieved by consuming more fuel on the prime movers rather than on the auxiliary boiler.

Wang et al. [93] setup a model of a diesel engine based household size trigeneration system on the ECLIPSE simulation software. The performance and emissions of the system fuelled with hydrogen under power generation, cogeneration and trigeneration modes were studied. It highlighted that hydrogen performed equal to or better than conventional diesel in energetic performance, and nearly zero carbon emissions in terms of life cycle analysis. Also, cogeneration and trigeneration have been proved to prevail in fuel savings and provide a reduction in GHG emissions.

2.4 Vegetable oils

2.4.1 Physicochemical property

Vegetable oils consist mainly of triglyceride basis saturated hydrocarbon, few free fatty acids and other non-grease substances, which are produced commercially through squeezing and extraction from seeds. Compared to diesel, these oils are characterised by a higher viscosity and oxygen component, lower cetane number, lower volatility and less heat energy [94, 95]. Table 2.3 lists the physicochemical properties of some vegetable oils. The differences between the oils and diesel are detailed below:

- a) Viscosity. It is a key measure of the internal friction of a substance resistant to flow, which is affected by temperature, the length of fatty acid chain and the degree of unsaturation [96] [97]. The viscosities of vegetables mostly fall within the range of 30 to 50 cSt (40°C), 9-17 times higher than that of diesel.
- a) Density. Density is the mass of fluid per unit volume. The density of diesel is between 820 kg/m³ to 880 kg/m³, about 90% of the density of vegetable oil. This was due to the low carbon component and 8-11% oxygen concentration in the vegetable oils. Compared to the negligible oxygen content in diesel, it helps to improve combustion and thermal efficiency [83].
- b) Cetane number (CN). This index is for evaluating the ignition quality of fuels. A higher CN represents favourable ignition quality and better combustion efficiency, which also indicates less carbon formation and deposit. Vegetable oils contain mainly fatty acids and very few long-chain normal alkane, which results in low CN (30-40) and poor ignition quality. To improve the firing

ability, methods such as transesterification, blending and preheating are usually adopted.

- c) Heating value. An important measure of energy content and efficiency of fuels. The higher heating values (HHV) of vegetable oils are about 40 MJ/kg, nearly 18% less than that of diesel (roughly 47 MJ/kg). However, owing to the higher density of vegetable oil, the volumetric heat energies of these fuels are only about 8-10% less than that of the diesel.
- d) Flash point. Flash point represents the requirement of the firing temperature. The flash points of various vegetable oils are generally above 200°C, much higher than that of diesel. Further indications reveal they are much safer in terms of fuel handling and storage.
- e) Pour point. This is the representation of low-temperature fluidity. The pour point of most vegetable oils is only above -10°C, thus condensation may occur during the winter period.

Vegetable oils		Viscosity (cSt at 40°C)	Density (kg/m ³)	HHV (MJ/kg)	Cetane number	Flash point (°C)	Pour point(°C)
Edible oils	Corn	34.7-35.4	914-922	39.66	-	259	-12.5
	Cottonseed	33.5-34.7	915-924	40.38	42	251	-13
	Crambe	53.0	902	39.83	-	284	-
	Hazelnut	24.0	910-920	39.33	41-43	230-245	-
	Mustard	31-33.8	913	39.57	-	245	-
	Olive	29.8	918	39.50	-	231	-
	Palm	38.23	910	39.05	42	344	6.0
	Peanut	39.3-39.6	908-919	39.85	36	270	3.0
	Poppy seed	42.4	907	39.73	-	265	-
	Rapeseed	37.3	912	39.52	-	258	-
	Safflower seed	31.3	914	39.79	-	258	-
	H.O.Safflower	41.2	906	39.51	-	275	-
	Sesame	35.5-36.9	913-922	39.63	-	260	-3.0
	Soybean	32.6-40.2	914-926	39.44	37	255	-7.5
	Sunflower seed	34.2	923	39.59	41.8	232	-12.2
Walnut	36.8	912	-	-	251	-	
Inedible oils	Ailanthus	30.2	916	39.44	-	240	-
	Bay laurel	23.2	921	39.30	-	226	-
	Beech	34.6	915	39.59	-	242	-

Beech nut	38.0	912	39.82	-	260	-
Croton	30.37-34.48	904-924	40.3-43.1	45	74	-
Jatropha	35.38-35.47	916-919	38.8	33.7-38.1	186-280	(-6)-2
Karanja	27.84-43.67	911-938	34-41.7	29.9-38.4	205-237	(-3)-6.4
Linseed	27.2	921	39.50	-	247	-
Mahua	34.37	923	-	43.5	260	12
Pongamia	41.85	933	-	37.5	232	
Putranjiva	37.62	918	39.6	31.3	48	-3
Salvadora	44.62	913	-	-	254	36
Spruce	35.6	914	39.57	-	240	-
low-sulphur diesel	2.453	820-880	45.90	47	75	-27

Table 2.3 Comparison of physicochemical properties of vegetable oils to diesel [83, 96-103]

Due to the aforementioned drawbacks, directly applying vegetable oils into the engine may lead to problems. Currently, the one feasible commercial method for using vegetable oils as engine fuel is to convert it into biodiesel by transesterification. From the very beginning of biofuel research, biodiesel was produced mainly from edible vegetable oil [25], so called the first-generation biofuel. Though it possessed the merits of GHG reduction and energy balance, the drawbacks of this fuel are noticeable in terms of: a) Pushed food and animal feeds prices up by 15-25% due to competition with food crops; b) High production costs to implement its operation without government subsidies and; c) Uncertainty of sustainable feedstock supplement [104].

To avoid the negative effects of edible oils, biodiesel conversion turned to inedible oilseed crops, such as jatropha, croton, mahua, etc. These plants have many merits including drought resistant, high levels of oil and protein; require no additional land and low irrigation and fertilisation, etc. Rural areas and undeveloped regions will therefore benefit from the feed stock planting and processing. For instance, the jatropha tree is a tropical plant with over 50 years lifespan, growing in vast regions of India, Thailand, China, Indonesia and Nicaragua etc. This plant provides seeds up to three times per annum [105]. It is estimated that a 5,000 hectare field of jatropha trees will harvest 35,000 tonnes of seeds and could be crushed to 14,000 tonnes of crude oil[106]. The seeds of mahua and karanja were reported to contain oil percentages of 51.5% and 27-39% [102, 107, 108].

To date, almost all of the inedible seeds are picked manually, which represents labour intensive, low efficiency and high cost for biofuel production [109]. Besides, inedible oils consist of toxic ingredients and may pose potential hazards in biofuel applications. Studies show that defatted mahua seed meal still contains a toxic dose of proteins and saponins [108]. Some constituents in karanja oil, such as organic acid (phytates, tannins), furano-flavonoids, protease inhibitors and glabrin, etc., may cause lesion after being ingested [107, 110]. Early studies on birds, mice, goats and chicks fed by karanja, jatropha cake and seeds also show pathological changes in stomachs, heart, lung, livers, pancreas and kidneys [111-117]. No manifestations were observed when the animals were fed extracted oil. This was mainly attributed to the treatment of water or acid/alkali leaching, which had removed almost all of the toxic ingredients from the oil [107, 108].

2.4.2 Existing works on vegetable oil

The great attraction of using vegetable oils as engine fuel is due to their renewable and carbon neutral nature. From the very beginning of biofuel research, efforts were made for directly burning vegetable oil as an engine fuel. However, vegetable oils combust in engines and this may result in reduced thermal efficiency, higher fuel consumption and durability problems.

Hemmerlein et al. [118] investigated the physicochemical properties of rapeseed oil and found that the heating value of the fuel was 7% lower compared to diesel. Accordingly, the engine power decreased and the effective thermal efficiency was about 2% lower. Lower combustion noise and NO_x emission were observed, accounting for the lower cetane number and combustion speed, whereas CO and hydro carbon (HC) emission increased sharply. Labeckas et al. [119] reported a 13% lower heating value for rapeseed oil compared to diesel, and around 12% higher brake specific fuel consumptions (BSFC) for the maximum torque and rated power. The maximum brake thermal efficiency was reported to be almost equal to that of the diesel, with a sharp decrease in smoke emissions. Bari et al. [120] found that an engine run with crude palm oil performed normally in the short term but deteriorated after 500 hours, presenting a power loss up to 20% and increase of BSFC up to 26%. Other problems were found by carrying out an overhaul inspection, including severe carbon deposits in combustion

chamber; piston rings and injection pump wear; cylinder liner scoring mildly; improper injecting of the nozzles and gas leakage through intake and exhaust valves. Haldar et al. [121] investigated an engine performance fuelled with degumming Karanja, Jatropha and Putranjiva oil and their blends with diesel. The best performance of the vegetable oils was observed with injection timing of 45°CA before Top Dead Centre (bTDC) when fuelled by 20%-30% blends, 5°CA earlier than that of diesel. It was also found that a 20% jatropha-diesel blend performed better than diesel both in terms of power output and emissions, except for CO₂ emission.

Methods such as blending, preheating and micro-emulsification are usually adopted to overcome the drawbacks of vegetable oils. Due to the difference in fuel types, experimental designs and test conditions, various research literature results have been reported.

Masjuki et al. [122] tested 10-50% palm oil-diesel blends on an indirect injection diesel engine. Compared to those of diesel, the engine brake-power dropped down for no more than 5%, and the SFC increased with increasing palm oil proportions. The engine emissions improved, especially the HC and polycyclic aromatic hydrocarbons (PAHs) emissions. Wang et al. [123] conducted tests on a diesel generator by palm oil-diesel blends with an interval of 25%. The engine performance was comparable and lower emissions of HC, CO and NO_x were observed with respect to diesel. Hazar and Aydin [124] blended raw rapeseed oil with diesel using 20% and 50% volumetric proportions and preheated the fuel to 100°C to run in the engine. Higher BSFC and lower engine power were reported for the blends in comparison to the diesel, while the exhaust temperatures were almost identical. Lower NO_x emissions were found for the blends at high engine speed whilst lower CO and smoke density were observed.

Kalam and Masjuki [125] used preheated crude palm oil (CPO) at 70°C and palm oil-water (1-3% vol.) emulsions at 65°C in a diesel engine for 100 hours. They observed the lowest HC and CO emissions with preheated CPO among the test fuels and lower nitrogen oxides (NO_x) emission with emulsified fuels. Deposit characteristic analysis showed that the preheated CPO produced a similar volatile fraction, the lowest fraction of fixed carbon and the highest fraction of ash carbon compared to the other fuels. The

authors finally concluded that ‘the preheated CPO was suitable for long term engine operation’.

Almeida et al. [126] tested pure palm oil on a naturally aspirated 70 kW diesel generator. When the fuel was heated to 100°C, its viscosity was very close to diesel, and the engine performance and durability were competitive to those with diesel. The fuel consumption was 10% higher to maintain the same power output. The CO and CO₂ emissions were found to be higher, while NO_x emissions decreased. HC emission was higher during low load but lower during full load conditions. The authors also observed heavy carbon deposit on the cylinder head when the fuel preheated temperature dropped to 50 °C. In order to improve the engine performance, emissions, stability and reliability, the authors proposed some constructive advice, including a higher fuel injection pressure, turbo-charging, lube oil and fuel injection system improvement, etc.

Canakci et al [127] tests preheated crude sunflower oil on an indirect injection engine. The vegetable oil had a similar performance to diesel fuel, but the fuel consumption increased by about 5%. CO₂ and smoke were found to decrease, especially the HC emission which was reduced by 34%. The author concluded that there was no problem running the engine with preheated sunflower oil over the short term.

Agarwal, D and Agarwal, A.K. [128] preheated jatropha oil to 90-100°C to reduce its viscosity close to that of diesel. Engine tests showed that the BSFC and exhaust temperatures for the oil were high in contrast to diesel, with slightly lower thermal efficiency. Higher CO₂, CO, HC and smoke opacity was also observed for the jatropha oil at 100°C, which was close to that of the diesel. The authors declared that jatropha oil could be directly applied to an engine in the short term without any problems. Similar results were reported by Chauhan et al.[129], who used the same oil with a preheated temperature range between 40-100°C. When the oil was heated to 100°C, a slight improvement of HC emissions was found compared to that of diesel.

Yilmaz and Morton [130] investigated three different edible oils, i.e. peanut oil, canola oil and sunflower oil on two engines by preheating these oils to 90°C. In comparison to diesel and unheated vegetable oils, the preheated oils performed with improved power efficiency and reduced HC emissions, while the NO emission was reported to increase.

Pugazhvadivu and Jeyachandran [131] heated waste frying oil (WFO) to 30°C, 75°C and 135°C and compared the performance to that of diesel. The investigation showed that a higher preheating temperature helped to improve the brake specific energy consumption (BSEC) and thermal efficiency, though these figures were still higher than those of diesel. Higher BSEC, thermal efficiency, exhaust temperature and NO_x emissions were reported for the preheated oils compared to diesel, at the same time lower CO and smoke density emissions were found.

Rakopoulos et al. [132, 133] developed a two dimensional, multi-zone model to simulate the fuel spray development, combustion and pollutants formation in direct injection diesel engine running with cottonseed oil and its biodiesel. The nitric monoxide (NO) and soot emissions were calculated and compared to experimental results. The simulation results proved to be reasonable and accurate enough for emission prediction [133].

2.5 Summary

2.5.1 Summary of domestic energy demand and consumption

Domestic energy consumption accounts for nearly one third of the UK energy demand, mainly powered by gas and electricity for space heating, hot water, cooking, lighting and appliances, and the heat to electricity ratio is roughly 4:1. However, household energy consumptions vary from one to another. From a daily point of view, electricity consumption of most houses are lower than 8 kW during peak time and less than 0.5 kW in off-peak hours (around 21:00 to 6:00). From a yearly point of view, gas consumption presented seasonal fluctuation; while electricity consumption was much more stable and appeared to have little indistinctive seasonal impact.

2.5.2 Summary of micro-trigeneration

Micro-trigeneration is a recently developed, decentralised energy supply solution for domestic users. It performs with high thermal efficiency by integrating cogeneration with waste heat activation technologies; hence, the fuel economy and emission rates are improved. Among the available prime movers, ICE with power output lower than 10kw

was the favoured choice for micro-trigeneration. Its characteristics are well-developed performance, fuel-flexible, high efficiency and low maintenance costs etc. The other possibilities for micro-trigeneration systems include micro-turbine, Stirling engine and fuel cell. However, a high price prevents all of these options from wide scale application.

For cooling generation, both absorption and adsorption refrigeration are popular waste heat activation technologies, both of which can be driven by low grade heat.

Absorption refrigeration uses ammonia/water as a working pair and appears to be the favoured type for trigeneration. It is limited by the heat source and the scale of trigeneration, with a typical COP between 0.5-0.7. Due to their low efficiency rates, absorption and adsorption refrigeration are more suitable for a simplified system e.g. domestic applications.

2.5.3 Summary of vegetable oil research

The properties of vegetable oils are different from that of diesel in terms of its high viscosity, low cetane number, low volatility and low heating values, etc. Hence, directly combusting vegetable oils in a diesel engine may lead to higher fuel consumption, lower thermal efficiency and deterioration in the durability of the engine. Except for the method of converting vegetable oils into biodiesel by transesterification, other methods such as blending, preheating and micro-emulsification are technically feasible to overcome the drawbacks. Therefore, the engine performance is rated competitive or better than that of the diesel. A lower NO_x emission was expected by the use of blending and micro-emulsification, whilst higher NO_x emissions will be presented with preheating.

Although significant research work has been carried out on vegetable oil and micro-trigeneration, few reported literatures have focused on both these research fields, especially regarding the application of raw vegetable oil on a micro-trigeneration system. This is the main research area of my PhD thesis.

Chapter 3. Experimental Apparatus, Instrumentation and Test Plan

3.1 Introduction

This chapter introduces the experimental setup of the biofuel property test facilities, biofuel micro-trigeneration system, data acquisition system and test procedures.

Biofuel properties, such as viscosity and heating value, pose great effects to engine performance and emissions. The heating value is a key factor to engine thermal efficiency and fuel consumption; while high viscosity of biofuel deteriorates engine durability. Hence, it is vital to study the physicochemical properties of biofuels before they are applied to the BMT system. The test data is also important to the engine and trigeneration system simulation

In this study, four raw vegetable oils were chosen for the biofuel property and the trigeneration tests, including sunflower oil (SFO) and rapeseed oil (RSO), jatropha oil (JAO) and croton oil (CRO). Gas oil (GO) was also tested for comparison purposes. Sunflower and rapeseed oils are popular cooking oils in Europe; while the jatropha and croton oils are inedible oils mainly sourced from tropic or subtropic areas.

A biofuel micro-trigeneration test rig was constructed to evaluate the performance and emissions running with raw vegetable oils. This system mainly consists of a diesel generator, two heat exchangers and an ammonia-water diffusion absorption refrigerator. The fuel supply system was redesigned for supplying preheated vegetable oils to the generator. The waste heat in the coolant and exhaust gas was recovered by the heat exchangers. Part of the exhaust gas was also supplied to drive the refrigerator.

A Siemens supervisory control and data acquisition (SCADA) system was constructed for the system control and retrieval of the test data. A Fluke power analyser was used to measure the electric output of the trigeneration system. A fuel flow meter and a Horiba emission analyser was used to measure the fuel consumption and gas emissions.

3.2 Experimental setup

3.2.1 Biofuel property test facilities

3.2.1.1 Viscosity test

The Visco 88 portable viscometer was used for determining viscosity. The main parts of the viscometer include a constant speed motor, a torque detection system and a measuring system (coaxial cylinder). The sample to be measured was injected into the gap of the measuring system. A rotational speed (controlled shear rate) was applied by the motor and the resultant torque (resultant shear stress) was measured. The outcome was converted to a viscosity value using a set of measuring system constants. A computer was connected to the viscometer and the Bohlin software installed. This allowed pre-programmed measurements, data processing and a graphic layout of results to be automatically generated. During the test, the measuring system was immersed in a Julabo thermostatic bath for controlling the sample temperature between 20 °C and 120 °C, in steps of 10 °C. The diagram of the test facilities is shown in Fig. 3.1 and the specifications listed in Appendices A.1 and A.2.

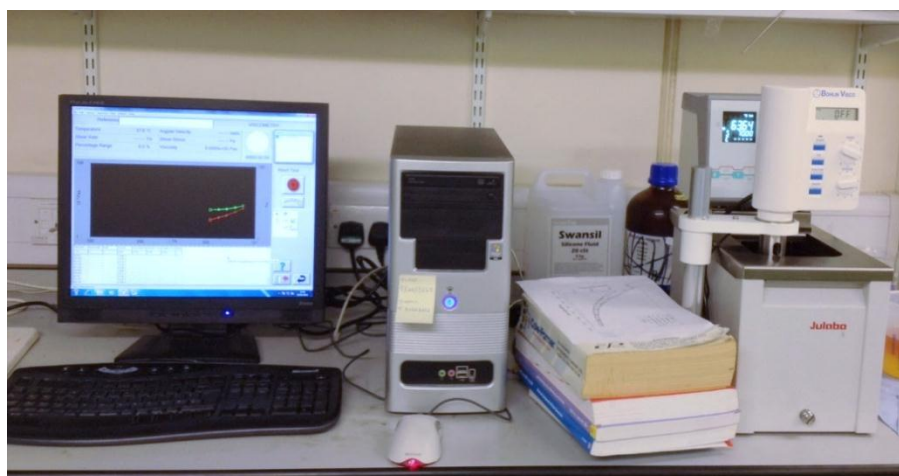


Fig. 3.1 Viscosity test system

3.2.1.2 Higher heating value test

The instrument used for the higher heating value test consists of three components (Fig. 3.2):

- a) CAL2k-ECO calorimeter. This is the key instrument for determining the energy content of a sample, either in solid or liquid phase. The higher heating value was calculated by the input sample mass and the temperature rise of the vessel.

- b) Filling station. This was connected to an oxygen cylinder to charge 3MPa of oxygen into the vessel, enabling the sample to be completely combusted.
- c) Vessel CAL2K-4. This has a combustion chamber where approximately 0.5g of a sample was placed and ignited according to a pre-set burning process. The temperature rise of the vessel was measured by the temperature sensors attached to the vessel wall. The peak temperature was proportional to the calorific value of the sample and was transferred to the calorimeter.

The specification of the calorimeter is listed in Appendix A.3.

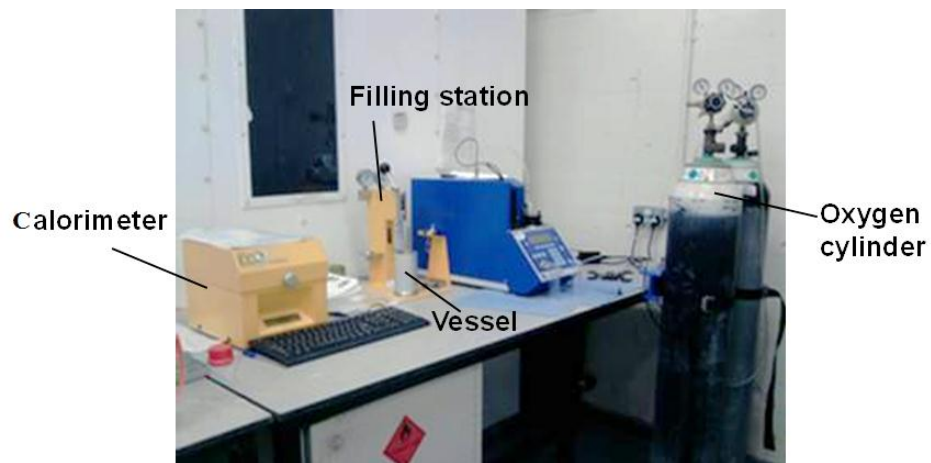


Fig. 3.2 Higher heating value test system

3.2.1.3 Density test

The densities of the fuels were measured by an A&D HR-200 analytical balance with a resolution of 0.0001g. During the test, a test tube was placed onto the balance and the mass displayed on the screen was reset to zero. A 10 ml sample was then dropped into the test tube and the displayed figure was recorded (Fig. 3.3). The tests were repeated three times at the ambient room temperature of 20°C. The specification of the balance is listed in Appendix A.4.



Fig. 3.3 HR-200 analytical balance

3.2.1.4 Fatty acids test

To study the detailed properties of each vegetable oil and for comparison of their differences, experimental tests were carried out using a HP 5890 gas chromatograph (GC), as shown in Fig. 3.4. Due to the high viscosity and low volatility, the vegetable oils cannot be tested on the GC directly and therefore need to be converted into biodiesel first. The equipment uses a CP wax column and Helium gas as a mobile phase for the measurement, with a heating temperature of 250°C. The procedure of transesterification is described as follows[134] and is depicted in Fig. 3.5:

- a) Blend vegetable oil with methanol in a flask with molar ratio of 1:6.
- b) Add potassium hydroxide (KOH) into the blend with a mass proportion of 0.75%-1% to that of the vegetable oil;
- c) Place a magnetic stirrer into the flask and cover it with a film;
- d) Place the flask onto a magnetic stirrer hotplate (Appendix A.5 for the specification); stirring and heating the blend to 60°C;
- e) Stop the reaction after two hours. Uncover the film and drain the liquid into a separating funnel for settle and separation, remove glycerol on the bottom to get biodiesel and methanol blend;
- f) Mix and stir the biodiesel with warm water to wash away residual KOH, methanol and any glycerol, allow settling and separating for two hours and then drain off the water. This procedure is repeated three times.
- g) Drain the biodiesel into a boiling flask and place it onto the hotplate, set the temperature to 100°C and heat for half an hour to get dry and pure biodiesel.

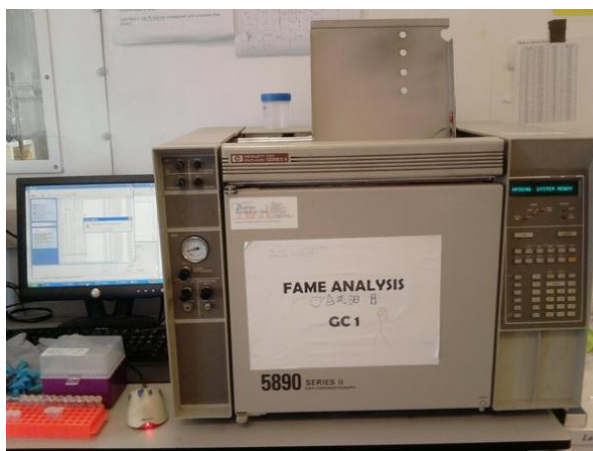


Fig.3.4 HP 5890 Gas Chromatograph



a) Transesterification



b) Separation



c) Sample of biodiesel

Fig.3.5 Biodiesel conversion

3.2.2 Biofuel micro-trigeneration system

3.2.2.1 Diesel engine & generator

A Yanmar YTG6.5S diesel generator (Fig. 3.6) was chosen as the prime mover of the BMT system. It is a naturally-aspirated, four-stroke single cylinder engine, which was originally equipped with a natural convection cooling system and was retrofitted to a pumping cooling system. A single phase alternator was coupled with the engine to generate rated electric power of 6.5 kW. The specification of this genset is listed in Appendix A.6.

The reasons for choosing this engine were mainly based on the preliminary literature investigation as described in Chapter 2 and with the stipulation that:

- a) Peak electricity consumption of most houses was lower than 8 kW.
- b) The concept and design of this trigeneration system was to couple with an electricity storage system to supply 10kW electric power. As the power unit, the prime mover was projected to meet most of the electricity demand.
- c) The cost and availability of this generator is the best among the possible candidate prime movers.
- d) It is a fuel-flexible power device for running with vegetable oil.



Fig. 3.6 Yanmar YTG6.5S diesel generator

For the purpose of biofuel micro-trigeneration, the fuel supply system of the generator was retrofitted for use with vegetable oils. A waste heat recovery system was designed and constructed to recover waste heat from the coolant and exhaust gas. The diagram of the BMT system is shown in Fig. 3.7.



Fig. 3.7 Biofuel micro-trigeneration system

3.2.2.2 Fuel supply system

The diagram of the fuel supply system is shown in Fig. 3.8. This system has a gas oil tank and a vegetable oil tank to supply two types of fuels to the engine. The gas oil was pumped through a fuel pump to a PowerLink FC2210 fuel flow meter (see Appendix A.7), where the fuel consumption was measured. The vegetable oil tank was placed 1.2 meters above the engine to supply gas oil. The fuel oil consumption was determined by a KERN PCB 1000-1 Precision balance (see Appendix A.8). The original tank on the top of the engine was taken off and the fuel pipe was connected to a three way valve, of which the other two ends were connected to a vegetable oil tank and the FC2210 fuel

flow meter for switching between the fuels. Two pre-heaters were wound around the fuel pipe to heat up the vegetable oils before they were injected into the cylinder. The preheating temperature was pre-set and controlled by a temperature/process controller. The specifications of the preheaters and the controller are shown in Appendices A.9 and A.10, and the images of the fuel supply system are shown in Fig. 3.9.

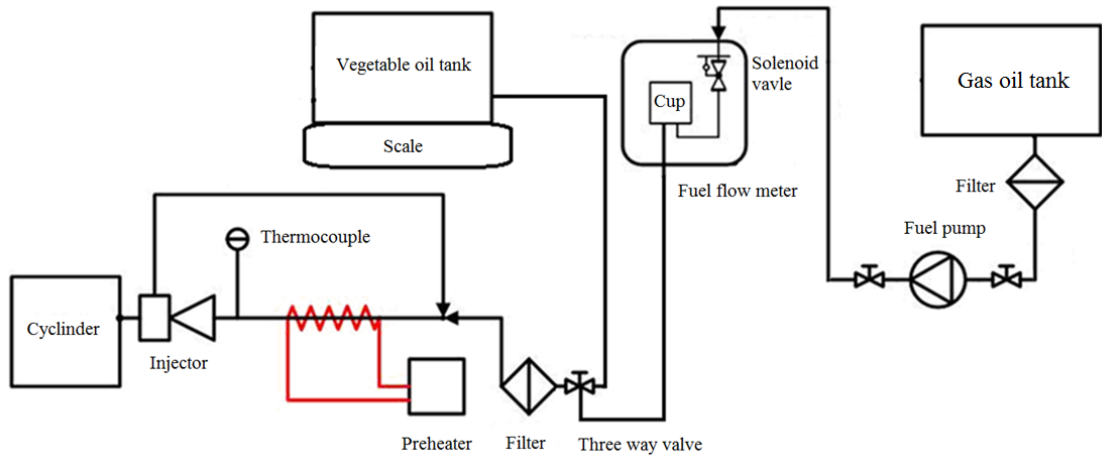


Fig. 3.8 Fuel supply system



a) Fuel pump and filter



b) Flow meter, vegetable oil tank and scale



c) Preheaters

Fig. 3.9 Instruments of fuel supply system

3.2.2.3 Waste heat recovery system

The waste heat recovery system consists of two cycle lines, one is an engine coolant cycle line and the other is a hot water cycle line. Fig. 3.10 and Fig. 3.11 depict the structure of this system.

A coolant pump was used for cycling coolant to a coolant heat exchanger and then back to the engine. A radiator was placed parallel to the heat exchanger for dissipating excess coolant heat. For the hot water cycle, hot water was pumped from the heat dumper to the coolant heat exchanger, where the water absorbs coolant heat and the temperature of the hot water increased. The hot water was then pumped to the exhaust heat exchanger to recover the exhaust heat before it flows back to the heat dumper. A bypass line was constructed for the exhaust heat exchanger to avoid water condensed from the exhaust gas. Three flow meters were used to measure the coolant/water flow rates, as shown in Fig. 3.7. The specifications of the heat exchanger and coolant/water flow meter are shown in Appendices A.11 and A.12.

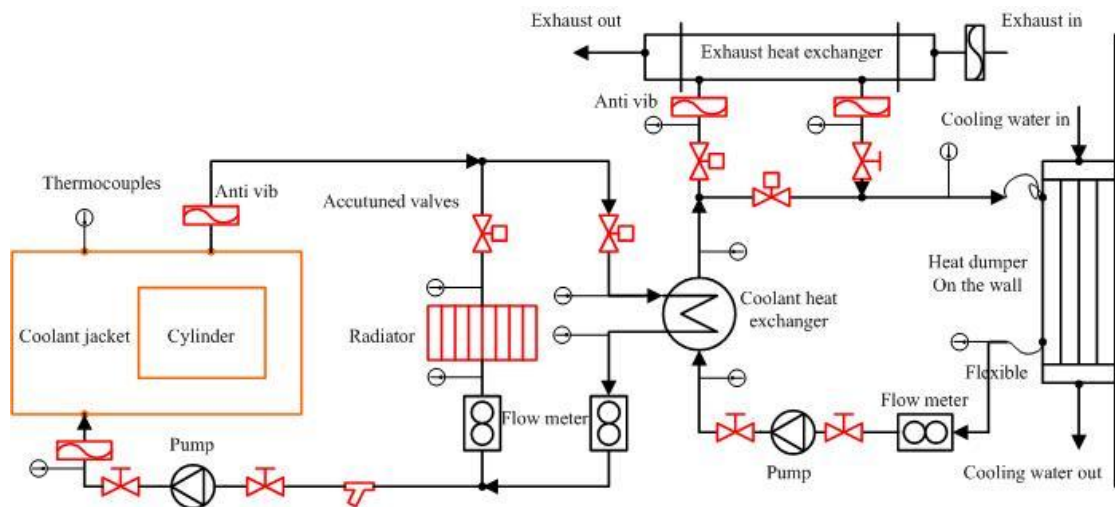


Fig. 3.10 Schematic diagram of coolant heat recovery system

The advantage of the series connection design of the two heat exchangers lies in that the hot water temperature increases twice by passing through the heat exchangers successively, hence it can reach a high level even at a low engine load. Alternatively, the scenario of a parallel connection of the two heat exchangers will result in the inconsistency of the water temperatures at the outlet of the two heat exchangers and this will lead to exergy loss. In this study, the former scenario was chosen for waste heat recovery.

To ensure maximum waste heat is recovered at full load, the hot water flow rate was designed for recovering exhaust heat (double that of the coolant heat). In this scenario, the coolant temperature after the coolant heat exchanger may be too low and this may affect the engine performance and durability. To avoid this situation, five solenoid valves were used to adjust and control the coolant/water flow rate, as shown in Fig. 3.10.

Fig. 3.11 shows the scenario of the exhaust flow line and waste heat recovery. The main exhaust line was the exhaust heat exchanger, where most of the exhaust heat was recovered by water. The second exhaust line was connected to a diffusion absorption refrigerator, in which the exhaust heat was used for driving the refrigerator. An exhaust gas flow meter was installed in the main exhaust line to measure the exhaust flow rate. The third line was a bypass/biofuel preheater line, where exhaust gas can be dispelled directly to the atmosphere. There was a reserved port on this line for a waste heat preheater in the future. Three high temperature proportional valves were used to control exhaust flow in the three lines, hence to switch the system operating mode between power generation (PG), cogeneration (CG) and trigeneration (TG). The specifications of the exhaust heat exchanger and the exhaust flow meter are listed in Appendices A.13-A.14. Images of the waste heat recovery system are shown in Fig. 3.12.

3.2.2.4 Absorption refrigerator

The equipment chosen for the cooling energy generation was a Dometic RM 7655L absorption refrigerator, with an exhaust gas temperature high enough to drive the refrigerator. The efficiency of the refrigerator is higher than that of the adsorption refrigerator. The refrigerator has 150 litres storage capacity, 124 litres for the food chiller and 26 litres for the freezer. It can be driven by either 12V DC power, 230V AC power or gas, which is controlled by an automatic/manual selector. When run by electricity, the rated power consumption was 3.2kWh/24h at ambient temperature of 25°C, and this figure was 380g/24h for gas. The pictures and specification of this refrigerator are shown in Fig. 3.13 and Appendix A.15, respectively.

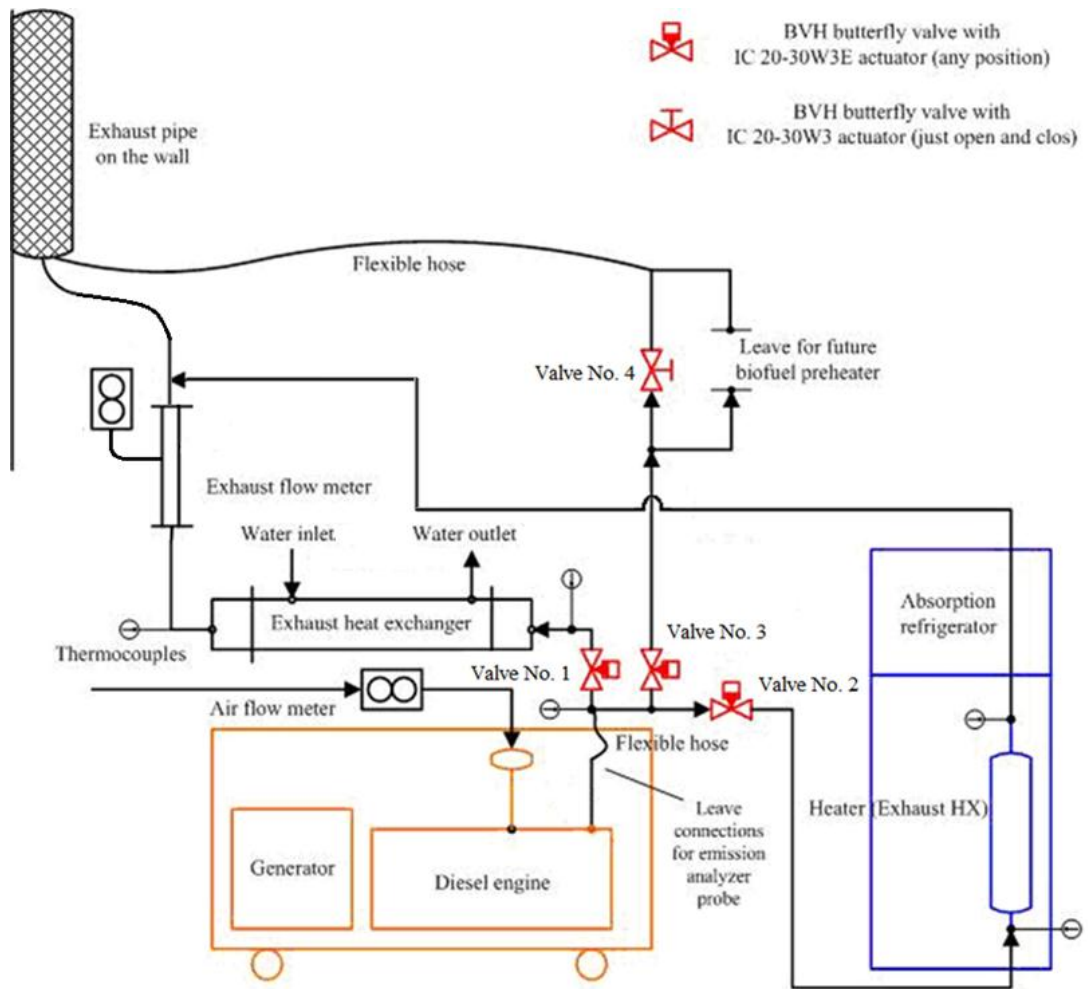


Fig. 3.11 Schematic diagram of exhaust heat recovery system



Fig. 3.12 Waste heat recovery system



a) Front view

b) Back view

c) Inner view

Fig. 3.13 Dometic RM 7655L refrigerator

3.3 Data acquisition

A Siemens SCADA (Supervisory Control and Data Acquisition) system programmed using WinCC software was used for real time monitoring, data logging and system parameter pre-setting. It mainly consists of the following components:

- a) A Siemens SCADA control software programmed using WinCC software;
- b) A Siemens ET 200SP PLC to communicate between the data logger and the control software, and for controlling valves on the diesel generator;
- c) A data logger for recording various measurements from a total of 42 sensors;

A Fluke 435 power quality analyser along with FlukeView software were used to measure and retrieve the electric power output of the diesel generator. The emissions of the engine were measured by a Horiba MEXA-1600 exhaust gas analyser.

3.3.1 PLC and control software

The Siemens ET 200SP is a modular design PLC which allows users to simply construct a wide range of distributed I/O systems (Fig. 3.14). The PLC communicates to the control software via an Ethernet protocol and communicates to the data logger via RS232. The control software was programmed using WinCC installed on a touch screen panel PC. It consists of several visual interfaces offering monitoring of the system operation and access to the database. The PLC actuates four water valves and four exhaust valves through a number of control modules, one digital and three analog.

All of the valves and the PLC were powered by a 24V DC supply. The images of the SCADA system and the user control interface are shown in Fig. 3.15 and Fig. 3.16, respectively.

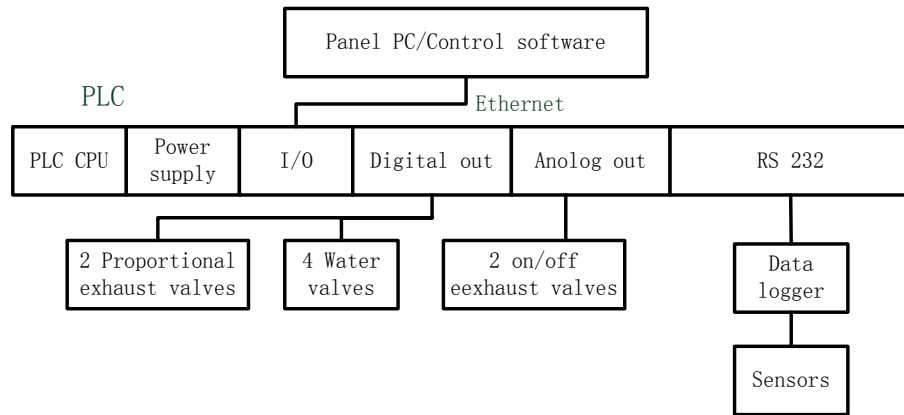


Fig. 3.14 Schematic diagram of the SCADA system



Fig. 3.15 Control box

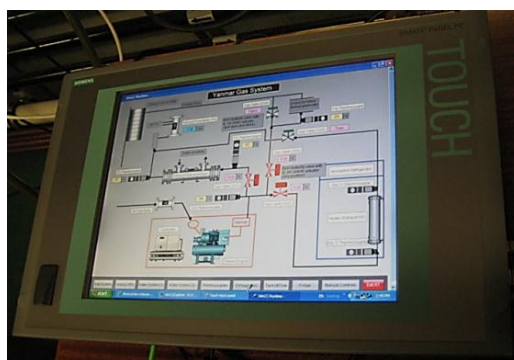


Fig. 3.16 Screen shot of the panel PC and control software

3.3.2 Data logger

A Grant's DataTaker DT85 data logger was used for recording the measurements. This data logger provides up to 48 common analogue inputs and each channel can be configured for different input signals, such as a DC voltage, DC current, resistance, 4-20mA current loop sensors and temperature, etc. Additional signal measurements supported by the DT85 include digital (digital input state, pulse count, phase encoder position), Serial Data Interface -1200 baud (SDI-12), Controller Area Network (CAN) and other serial sensor devices with an RS232/422/485 interface. The DT85 also supplies a regulated 12V DC output to power complex sensors. During the test, the data sampling interval was set to 10 seconds.

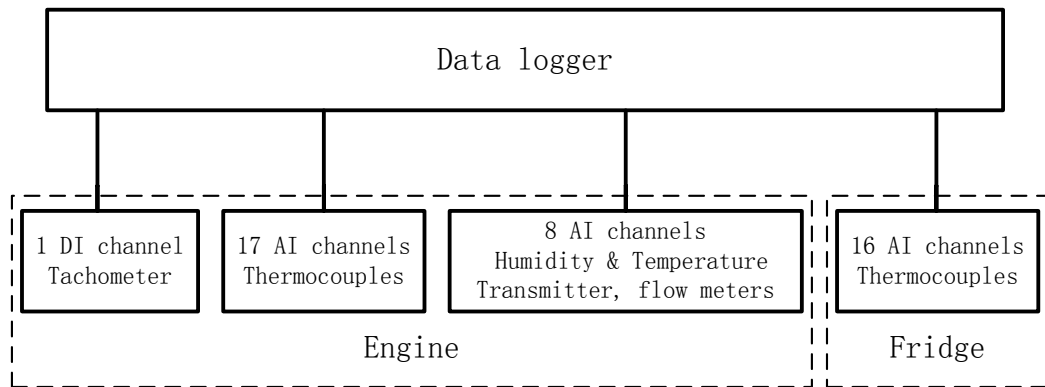


Fig. 3.17 Schematic diagram of the data logger and the connected sensors

Fig. 3.17 and Table 3.1 illustrate the sensors connected to the data logger for the trigeneration tests, these include:

- One digital channel connected to an OMEGA HHT13 tachometer for measuring the engine revolutions. The specification of the tachometer is listed in Appendix A.16.
- Seventeen analog channels for temperature measurements of the diesel generator using K type thermocouples.
- Two analog channels for measuring ambient temperature and humidity using a TC-Direct Humidity & Temperature Sensor & Transmitter; another four channels for measuring the flow rate of the engine coolant (two channels), hot water and exhaust gas.
- Sixteen analog channels for temperature measurements of the diesel generator using K type thermocouples.

The thermocouples used on the trigeneration system were all K type. They operate within a typical temperature range of between 95-1260°C. They are also suitable for cryogenic applications ranging from -200 to 0°C. According to BS EN 60584.2 1993, the output tolerance value of the K type thermocouple is 1.5 °C (Class 1) for the temperature range of -40 °C to 375 °C and 0.004 t for the range of 375 °C to 1000 °C.

Channel Type	No.	Position	Signal	Measurement	Accuracy	Power
Digital	1	Engine block	Pulse	Engine revolution	±0.01%	Battery, DC 3V
Analog	1	Fuel pipe before injector	4-20mA	Temperature	±1.5 °C	-
	2	Exhaust pipe	4-20mA	Temperature	±0.4%T	-
	3	Exhaust heat exchanger gas inlet	4-20mA	Temperature	±0.4%T	-
	4	Exhaust Heater	4-20mA	Temperature	±1.5 °C	-
	5	Exhaust heat exchanger gas outlet	4-20mA	Temperature	±1.5 °C	-
	6	Jacket outlet	4-20mA	Temperature	±1.5 °C	-
	7	Jacket inlet	4-20mA	Temperature	±1.5 °C	-
	8	Radiator inlet	4-20mA	Temperature	±1.5 °C	-
	9	Radiator outlet	4-20mA	Temperature	±1.5 °C	-
	10	Coolant heat exchanger coolant inlet	4-20mA	Temperature	±1.5 °C	-
	11	CHX coolant outlet	4-20mA	Temperature	±1.5 °C	-
	12	Coolant heat exchanger water inlet	4-20mA	Temperature	±1.5 °C	-
	13	Coolant heat	4-20mA	Temperature	±1.5 °C	-

		exchanger water outlet				
14		Exhaust heat exchanger water inlet	4-20mA	Temperature	± 1.5 °C	-
15		Exhaust heat exchanger water outlet	4-20mA	Temperature	± 1.5 °C	-
16		Heat dumper inlet	4-20mA	Temperature	± 1.5 °C	-
17		Heat dumper outlet	4-20mA	Temperature	± 1.5 °C	-
18		Radiator	4-20mA	Flow rate	$\pm 0.1\%$	PSU, DC 24V
19		Coolant flow in Coolant heat exchanger	4-20mA	Flow rate	$\pm 0.1\%$	PSU, DC 24V
20		Water flow in Coolant heat exchanger	4-20mA	Flow rate	$\pm 0.1\%$	PSU, DC 24V
21		Exhaust	4-20mA	Flow rate	<1%	PSU, DC 24V
22		Ambient humidity	4-20mA	Humidity	$\pm 2\%$	-
23		Ambient temperature	4-20mA	Temperature	± 0.2 °C or $\pm 0.15\%$	-

Table 3.1 Arrangement of the sensors on the diesel generator

Sixteen K type thermocouples were used for measuring the refrigerator performance, as listed in Table 3.2. These thermocouples were all attached firmly onto the test surfaces. Thermocouples 1 to 14 were attached onto the surfaces of the refrigerator pipeline. Thermocouples 15 and 16 were placed in the centre of the freezer and food chiller. The positions of the sensors are illustrated in Fig. 3.13.

Channel Type	No.	Position	Signal	Measurement	Accuracy
Analog	1	Heater	4-20mA	Temperature	±1.5 °C
	2	Desorption Outlet	4-20mA	Temperature	±1.5 °C
	3	Rectifier	4-20mA	Temperature	±1.5 °C
	4	Condenser inlet	4-20mA	Temperature	±1.5 °C
	5	Condenser outlet	4-20mA	Temperature	±1.5 °C
	6	Evaporator inlet	4-20mA	Temperature	±1.5 °C
	7	Evaporator mid	4-20mA	Temperature	±1.5 °C
	8	Evaporator bottom	4-20mA	Temperature	±1.5 °C
	9	Absorber inlet	4-20mA	Temperature	±1.5 °C
	10	Absorber outlet	4-20mA	Temperature	±1.5 °C
	11	Solution tank	4-20mA	Temperature	±1.5 °C
	12	Desorption inlet	4-20mA	Temperature	±1.5 °C
	13	Receiver	4-20mA	Temperature	±1.5 °C
	14	Strong solvent	4-20mA	Temperature	±1.5 °C
	15	Freezer	4-20mA	Temperature	±1.5 °C
	16	Food chiller	4-20mA	Temperature	±1.5 °C

Table 3.2 Arrangement of the thermocouples on the absorption refrigerator

3.3.3 Power quality analyser

The Fluke 435 power quality analyser offers an extensive set of measurement capabilities with high accuracy to check the power output of the trigeneration system. During the experiment, the Fluke 435 was set to ‘Power and Energy’ measurement mode. The main readings include voltage (V_{rms}), current (A_{rms}), frequency (Hz) and power (kW). For voltage measurement, a test cable with three connections: live, neutral and earth was connected to the analyser. For current measurement, two current clamps with a selectable measuring scale of 10, 100 and 1000 were clamped to the live and neutral wires of the cable. For test loads of 50%, 75% and 100%, the scale was set to 100, otherwise it was set to 10. The analyser used an optical interface cable to communicate with the FlukeView software installed on a laptop. The test was

monitored and data was retrieved, as shown in Fig. 3.18. The specification of the analyser is listed in Appendix A.17.



Fig. 3.18 Fluke 435 power quality analyser and FlukeView software

3.3.4 Fuel flow meter and balance

As mentioned previously in section 3.2.2, the fuel consumption of the diesel generator was measured by a PowerLink FC2210 fuel flow meter for gas oil or a KERN PCB 1000-1 precision balance for vegetable oils. FC2210 measured the fuel consumption over a specified time period. The time scale can be set from 1 to 200 seconds. By default it was set to 36 seconds for measuring the fuel consumption of the diesel generator. This meter was mounted on the wall, 1.5 meters above the engine fuel inlet port. A solenoid inside of the fuel flow meter was used to control the fuel supply. In the filling state, fuel was supplied to the engine, at the same time it charged a fuel cup. In the weighting state, the solenoid was cut off and the fuel was supplied only by the fuel cup, so that the fuel flow rate was measured. The test result was displayed on the upper screen of the front panel in kg/h. The fuel consumption of vegetable oil was weighted by the KERN PCB 1000-1. The variation of the fuel mass was captured every minute by taking a screen shot, enabling the hourly fuel consumption to be calculated. The picture of the fuel flow meter and the balance are shown in Fig. 3.19.



Fig. 3.19 FC2210 fuel flow meter and PCB 1000-1 balance

3.3.5 Exhaust gas analyser

The HORIBA MEXA-1600D is an exhaust gas measuring system for gasoline and diesel engines. It consists of heat sampling units, analyser modules and operation units.

The analyser modules include:

- a) An AIA-260 module which determines CO and CO₂ by an NDIR (Non Dispersive Infra-Red) analyser.
- b) A FCA-266 module which measures THC by Hot-FID (Flame Ionisation Detection), and NO_x by CLD (Chemiluminescence Detection).
- c) An IMA-262 module that determines O₂ by MPD (Magneto-Pneumatic Detection).

This instrument runs on a Linux operating system for the system operation and measurement. Before each test, the analyser was purged and calibrated by standard gases. Test results were downloaded to a floppy disk for processing. The picture and specifications of the analysers are shown in Fig. 3.20 and appendices A.18. During the test, the data sampling time was set to at least three minutes, with sampling interval of one second.

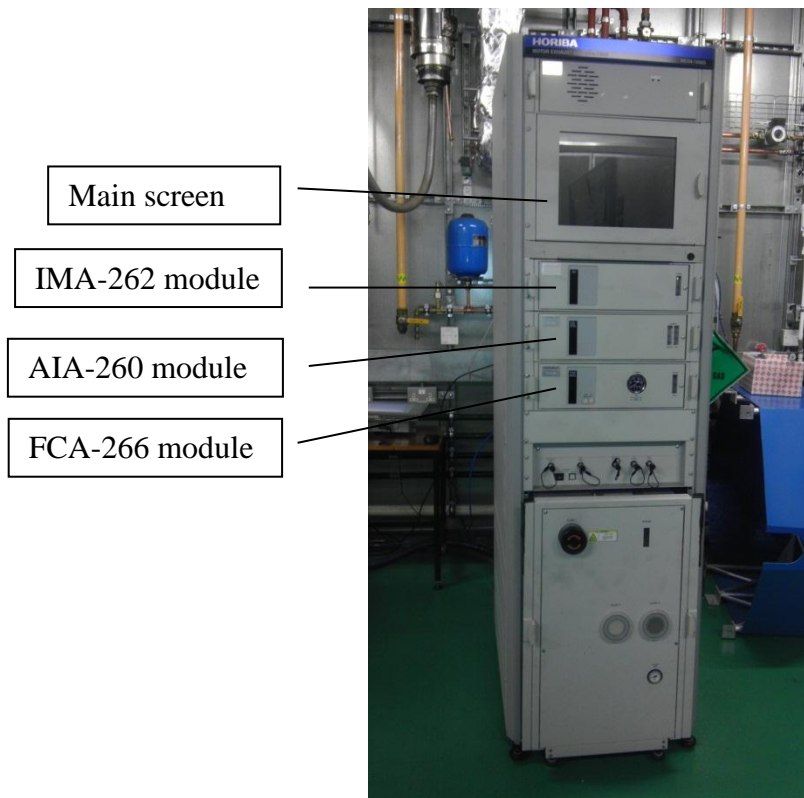


Fig. 3.20 MEXA-1600D exhaust gas analyser

3.3.6 Water and exhaust gas flow meters

Three IC-LT 1/2 " turbine flow meters along with three 101 totalizers are used to measure the coolant/hot water flow rates. The totalizers are powered by 24V DC and the instruments offer high linearity and repeatability of $\pm 0.2\%$ and $\pm 0.1\%$, respectively. The picture of the flow meter and totalizer is illustrated in Fig. 3.15.



Fig. 3.21 IC-LT 1/2" turbine flow meter and 101 totalizer

The exhaust gas flow is measured by a Flowline DF10MFG Pitot flow meter and an IMV30-T totalizer powered by 24V DC. The connection of the exhaust pipe lines is shown in Fig. 3.11. The exhaust flow rate in the exhaust heat exchanger is directly

measured by the exhaust flow meter, while the flow in the absorption refrigerator was provided by calculating the difference in the exhaust flow rates in EXH under cogeneration and trigeneration modes. The image of the exhaust flow and the totalizer are illustrated in Fig. 3.22.

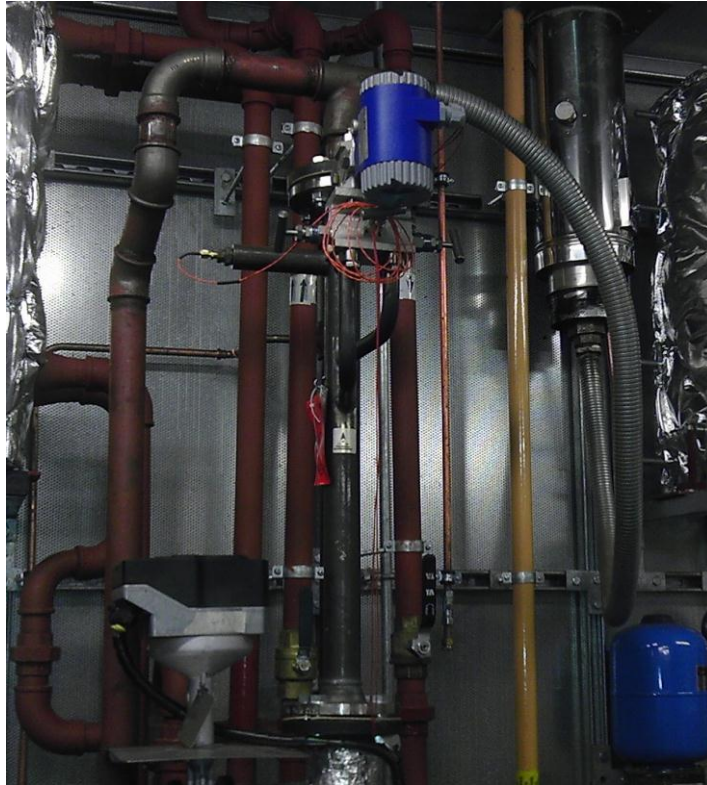


Fig. 3.22 Flowline DF10MFG Pitot flow meter and IMV30-T totalizer

3.4 Test plan and procedure

3.4.1 Test plan

In accordance with the research aims and objectives, a set of test plans were scheduled to use the vegetable oils and gas oil to study the trigeneration performance. The tests are listed below in order of time:

- a) Absorption refrigerator test
- b) Power generation test
- c) Cogeneration test
- d) Trigeneration test

Test a) was run using AC electric power to compare its performance with that of exhaust gas. The test data included the power consumption which was recorded by the power quality analyser and the temperatures listed in Table 3.2.

When performing test b) to d), the positioning of the exhaust valves were changed (see Table 3.3) to direct the exhaust gas flow through different pipe lines. The valve numbers are shown in Fig. 3.8.

Test name	Valve No. 1	Valve No. 2	Valve No. 3	Valve No. 4
Power generation	On	On	Off	Off
Cogeneration	On	Off	Off	Off
Trigeneration	On	On	Off	Off

Table 3.3 Status of exhaust valves for different tests

The test plans for test b) to e) are listed in Table 3.4. These will enable to study of the performance of the generator, heat exchangers, absorption refrigerator and trigeneration. These tests were performed in line with the British Standard: BS EN ISO 8178-4:2007. The test results of the refrigeration were compared to those of the results in test a).

Test name	Fuels	Loads (%)	Test items		
			Electricity generation	Waste heat recovery	Absorption refrigeration
Power generation	CRO, JO, SO, JO, GO	10, 25, 50, 75, 100	Yes	No	No
Cogeneration	CRO, JO, SO, JO, GO	10, 25, 50, 75, 100	Yes	Yes	No
Trigeneration	CRO, JO, SO, JO, GO	10, 25, 50, 75, 100	Yes	Yes	Yes

Table 3.4 Engine rig test plans

3.4.2 Test procedure

The following procedures were applied for each test listed in Table 3.4:

- a) Check connections and safety aspects for all of the test facilities and the trigeneration system.

- b) Switch on all test facilities; enable warm routine up before the engine is started.
- c) Start the diesel generator according to start up procedures. Warm up the engine before applying the engine loads.
- d) For the cogeneration test, apply full load conditions to the engine and wait thirty minutes before recording any measurements. Record the data according to the test plan, whilst checking the results to remove any potential errors. Reduce engine load and repeat the remainder of the tests. For power generation and the trigeneration test, the engine will be required to run for at least two and a half hours to measure the electric power, recovered heat and any cooling effects. Thus, the test for each engine load was a single test covering the whole procedures.
- e) For tests running on vegetable oils, once the tests are complete, turn off the preheater and switch the fuel supply over to gas oil. Run the engine at idle speed for 20 minutes to clean the fuel pipe for the next start up. For tests running with gas oil, run the engine at idle speed for 3 minutes.
- f) Stop the engine, collect all of the test data and then switch off power.

3.5 Error Analyses

“Error” or “uncertainty” is the concept to describe the result of a measurement. When taking experiment, it is impossible to record a measurement of a physical quantity without any error. To discuss error, two terms of "precision" and "accuracy" are commonly used. Precision is the reproducibility of a measurement and reflects the effects of systematic errors; while accuracy is a measure of the closeness to true value, thus reflects both the effects of system errors and random errors.

Systematic errors are the errors of significant difference between mean value of many separate measurements and actual value. Under the same measuring conditions, the absolute values and the symbols of systematic errors of multiple measurements are constant, or vary following a certain law when measuring condition is changed. Systematic error may be caused by zero error, which is due to an imperfect calibration of measurement instruments, or interference of environment with the measurement process, or flaw methods of observation or incorrect measuring technique. A systematic error can be corrected once it is discovered, such as by recalibration to eliminate zero drift.

Random errors are the errors that lead to unpredictable fluctuations or inconsistency to a measurable quantity. Under the same measuring conditions, the absolute values and the symbols of random errors for multiple measurements are variable and unpredictable. This may attribute to some accidental change of experimental conditions, such as temperature variation, noise interference, equipment vibration, etc. Though the random errors of a single measurement cannot be predicted and corrected, or eliminated by improving test method or test equipment, it does follow certain statistics laws by massive repeated measurement. Hence, by processing the data using probability statistics, it is possible to estimate the value and distribution of system errors and to reduce its' effects by taking appropriate measures.

Error analysis is an art of estimating the deviations of measurements, which is necessary procedure for lab report. Actually, it has been discussed in the British Standards (BS ISO TR 5168:1998; PD 6461-3:1995 and BS ISO TR 7066-1:1997) and in the relevant bibliographies. The following discussions are the methods or rules to determine error and uncertainty.

3.5.1 Rules of uncertainty calculation

Assuming x^* is the true value of a quantity, x is the estimate value of x^* , then $|x^* - x|$ is called the absolute uncertainty of x , usually denoted by symbol “ Δ ” and has the same units as the quantity; $|x^* - x|/|x^*|$ is called the relative uncertainty of x , usually denoted by symbol “ ϵ ” and has no units. The Rules of uncertainty calculation are given as:

- a) Addition and Subtraction. The total absolute uncertainty is the sum of each absolute uncertainty.

$$(A \pm \Delta A) + (B \pm \Delta B) = (A + B) \pm (\Delta A + \Delta B) \quad (3-1)$$

$$(A \pm \epsilon A) - (B \pm \epsilon B) = (A - B) \pm (\epsilon A + \epsilon B) \quad (3-2)$$

- b) Multiplication and Division. The total absolute uncertainty is the sum of each relative uncertainty.

$$(A \pm \Delta A) \times (B \pm \Delta B) = (A \times B) \pm (\epsilon A + \epsilon B) \quad (3-3)$$

$$(A \pm \Delta A) / (B \pm \Delta B) = (A / B) \pm (\epsilon A + \epsilon B) \quad (3-4)$$

- c) Raised to a power. Whether it is fractional or not, the rule is simply to multiply the relative uncertainty by the power.

$$(A \pm \varepsilon A)^n = (A^n \pm n \times \varepsilon A) \quad (3-5)$$

- d) General formula. The above propagations of errors are just special cases. A general formula can be used to describe the uncertainty of calculated dependent variable z with two measured variables x and y , which writes:

$$z = f(x, y) \quad (3-6)$$

The systematic uncertainty Δ_s and the random uncertainty Δ_r are given by:

$$\Delta_s = \sqrt{\left(\frac{\partial f}{\partial x} \Delta_{xs}\right)^2 + \left(\frac{\partial f}{\partial y} \Delta_{ys}\right)^2} \quad (3-7)$$

$$\Delta_r = \sqrt{\left(\frac{\partial f}{\partial x} \Delta_{xr}\right)^2 + \left(\frac{\partial f}{\partial y} \Delta_{yr}\right)^2} \quad (3-8)$$

Total uncertainty is the combination of systematic and the random uncertainties, which can be calculated in two ways: the additive or the root-sum-square model of combination.

The additive model gives:

$$\Delta_{ADD} = \Delta_s + 2\Delta_r \quad (3-9)$$

In relative form,

$$\varepsilon_{ADD} = \varepsilon_s + 2\varepsilon_r \quad (3-10)$$

The root-sum-square model gives:

$$\Delta_{RSS} = \sqrt{(\Delta_s)^2 + (2\Delta_r)^2} \quad (3-11)$$

In relative form,

$$\varepsilon_{RSS} = \sqrt{(\varepsilon_s)^2 + (2\varepsilon_r)^2} \quad (3-12)$$

3.5.2 Uncertainty of the experimental results

The uncertainty of the experimental results can be derived by applying the above rules.

The following are the uncertainty calculation samples.

The temperatures listed in Table 3.1, and 3.2 are all measured by Class 1, K type thermocouples. The relative systematic errors of the thermocouples are 0.4%.

A typical value of reading of exhaust gas temperature is 586.68 °C and the random error is 0.85°C. Hence the relative random uncertainty is:

$$\varepsilon_r = 0.85 / (586.68 + 273) = 0.10 \%$$

The total uncertainties ε_{ADD} and ε_{RSS} are given as:

$$\varepsilon_{ADD} = 0.4\% + 2 \times 0.10\% = 0.60\%$$

$$\varepsilon_{RSS} = \sqrt{(0.004)^2 + (2 \times 0.001)^2} = 0.0045 = 0.45\%$$

The results show that the total uncertainties of thermocouple are negligible. Similar calculations can be applied to all the thermocouples and sensors, which are listed in Table 3.5 to Table 3.7.

Position	Measurement	Systematic uncertainty ϵ_s	Random uncertainty ϵ_r	Total uncertainty ϵ_{ADD}	Total uncertainty ϵ_{RSS}
Engine block	Engine revolution	0.01%	0.42%	0.85%	0.84%
Fuel pipe before injector	Temperature	0.4%	0.11%	0.62%	0.46%
Exhaust pipe	Temperature	0.4%	0.10%	0.60%	0.45%
Exhaust heat exchanger gas inlet	Temperature	0.4%	0.09%	0.58%	0.44%
Exhaust Heater	Temperature	0.4%	-	0.40%	0.40%
Exhaust heat exchanger gas outlet	Temperature	0.4%	0.13%	0.66%	0.48%
Jacket outlet	Temperature	0.4%	0.18%	0.76%	0.54%
Jacket inlet	Temperature	0.4%	0.04%	0.48%	0.41%
Radiator inlet	Temperature	0.4%	0.12%	0.64%	0.47%
Radiator outlet	Temperature	0.4%	0.10%	0.60%	0.45%
Coolant heat exchanger coolant inlet	Temperature	0.4%	0.11%	0.62%	0.46%
Coolant heat exchanger coolant outlet	Temperature	0.4%	0.06%	0.52%	0.42%
Coolant heat exchanger water inlet	Temperature	0.4%	0.15%	0.70%	0.50%
Coolant heat exchanger water outlet	Temperature	0.4%	0.09%	0.58%	0.44%
Exhaust heat	Temperature	0.4%	0.07%	0.54%	0.42%

exchanger water inlet					
Exhaust heat exchanger water outlet	Temperature	0.4%	0.08%	0.56%	0.43%
Heat dumper inlet	Temperature	0.4%	0.08%	0.56%	0.43%
Heat dumper outlet	Temperature	0.4%	0.06%	0.52%	0.42%
Radiator	Flow rate	0.1%	-	0.10%	0.10%
Coolant flow in Coolant heat exchanger	Flow rate	0.1%	1.60%	3.30%	3.20%
Water flow in Coolant heat exchanger	Flow rate	0.1%	1.23%	2.56%	2.46%
Exhaust gas	Flow rate	1%	1.68%	4.36%	3.51%
Ambient humidity	Humidity	2%	0.06%	2.12%	2.00%
Ambient temperature	Temperature	0.15%	0.01%	0.17%	0.15%

Table 3.5 Uncertainties of measurements on diesel generator

Position	Measurement	Systematic uncertainty ϵ_s	Random uncertainty ϵ_r	Total uncertainty ϵ_{ADD}	Total uncertainty ϵ_{RSS}
Heater	Temperature	0.4%	0.05%	0.50%	0.41%
Desorption Outlet	Temperature	0.4%	0.04%	0.48%	0.41%
Rectifier	Temperature	0.4%	0.07%	0.54%	0.42%
Condenser inlet	Temperature	0.4%	0.15%	0.70%	0.50%
Condenser	Temperature	0.4%	0.05%	0.50%	0.41%

outlet					
Evaporator inlet	Temperature	0.4%	0.04%	0.48%	0.41%
Evaporator mid	Temperature	0.4%	0.04%	0.48%	0.41%
Evaporator bottom	Temperature	0.4%	0.04%	0.48%	0.41%
Absorber inlet	Temperature	0.4%	0.03%	0.46%	0.40%
Absorber outlet	Temperature	0.4%	0.07%	0.54%	0.42%
Solution tank	Temperature	0.4%	0.04%	0.48%	0.41%
Desorption inlet	Temperature	0.4%	0.03%	0.46%	0.40%
Receiver	Temperature	0.4%	0.12%	0.64%	0.47%
Strong solvent	Temperature	0.4%	0.04%	0.48%	0.41%
Freezer	Temperature	0.4%	0.08%	0.56%	0.43%
Food chiller	Temperature	0.4%	0.13%	0.66%	0.48%

Table 3.6 Uncertainties of measurements on the absorption refrigerator

Another example of uncertainty propagation for heat recovered by coolant heat exchanger is given below by applying the general formula to the measurement. The equation writes:

$$Q = c_p \times \dot{m} \times (T_2 - T_1)$$

$$T = T_2 - T_1$$

Where Q is the recovered heat, Q=4.57kW for the gas oil. c_p is the constant pressure specific heat of water, $c_p=4.2 \text{ J / (kg} \cdot \text{ }^\circ\text{C)}$. \dot{m} is the mass flow rate of water, $\dot{m} = 0.046\text{g/s}$, T_1 is the temperature of the inlet of the heat exchanger, $T_1 = 42.28 \text{ }^\circ\text{C}$. T_2 is

the temperature of the outlet of the heat exchanger, $T_2 = 65.81 \text{ }^\circ\text{C}$. T is the difference of the temperature, $T = 23.53 \text{ }^\circ\text{C}$. The random uncertainty and the systematic uncertainty of Q are given by:

$$\Delta_s = \left[\left(\frac{\partial Q}{\partial \dot{m}} \Delta_{\dot{m}_{ms}} \right)^2 + \left(\frac{\partial Q}{\partial T} \Delta_{Ts} \right)^2 \right]^{\frac{1}{2}}$$

$$\Delta_r = \left[\left(\frac{\partial Q}{\partial \dot{m}} \Delta_{\dot{m}_{mr}} \right)^2 + \left(\frac{\partial Q}{\partial T} \Delta_{Tr} \right)^2 \right]^{\frac{1}{2}}$$

Performing partial differentiations for the various terms in above equations yields:

$$\frac{\partial Q}{\partial \dot{m}} = c_p \times T$$

$$\frac{\partial Q}{\partial T} = c_p \times m$$

Hence the relative uncertainties are given as:

$$\varepsilon_s = \left[\left(\frac{1}{Q} \frac{\partial Q}{\partial \dot{m}} \Delta_{\dot{m}_{ms}} \right)^2 + \left(\frac{1}{Q} \frac{\partial Q}{\partial T} \Delta_{Ts} \right)^2 \right]^{\frac{1}{2}} = \left[\left(\varepsilon_{\dot{m}_{ms}} \right)^2 + \left(\varepsilon_{Ts} \right)^2 \right]^{\frac{1}{2}}$$

$$\varepsilon_r = \left[\left(\frac{1}{Q} \frac{\partial Q}{\partial \dot{m}} \Delta_{\dot{m}_{mr}} \right)^2 + \left(\frac{1}{Q} \frac{\partial Q}{\partial T} \Delta_{Tr} \right)^2 \right]^{\frac{1}{2}} = \left[\left(\varepsilon_{\dot{m}_{mr}} \right)^2 + \left(\varepsilon_{Tr} \right)^2 \right]^{\frac{1}{2}}$$

The relative uncertainties of T can be deduced as follow:

$$\varepsilon_T = \frac{\Delta T_1 + \Delta T_2}{T} = \varepsilon_{T1} \frac{T_1}{T} + \varepsilon_{T2} \frac{T_2}{T}$$

When substitutes the above data and the data in Table 3.5, it gives:

$$\varepsilon_{Ts} = 0.004 \times \frac{(42.28 + 273)}{(23.53 + 273)} + 0.04 \times \frac{(65.81 + 273)}{(23.53 + 273)} = 0.0088 = 0.88\%$$

$$\varepsilon_{Tr} = 0.0015 \times \frac{(42.28 + 273)}{(23.53 + 273)} + 0.009 \times \frac{(65.81 + 273)}{(23.53 + 273)} = 0.0026 = 0.26\%$$

$$\varepsilon_s = \left[(0.001)^2 + (0.0088)^2 \right]^{\frac{1}{2}} = 0.0089 = 0.89\%$$

$$\varepsilon_r = \left[(0.0123)^2 + (0.0026)^2 \right]^{\frac{1}{2}} = 0.0126 = 1.26\%$$

The total uncertainties ε_{ADD} and ε_{RSS} are given as:

$$\varepsilon_{ADD} = 0.89\% + 2 \times 1.26\% = 3.41\%$$

$$\varepsilon_{RSS} = \sqrt{(0.0089)^2 + (2 \times 0.0126)^2} = 0.0267 = 2.67\%$$

Judged from the above error analysis results, it can be concluded that the random uncertainty is the main cause of the errors. Another thing it should be pointed out that to the case of subtraction, when the values of two variables get close, the relative uncertainty will be enlarged and will deteriorate the reliability of test results. Hence it is better to reduce the water flow rate in order to increase the difference of water temperature between the inlet and outlet of the heat exchanger. Other results are shown in the following table. They have revealed that the data presented in this work are reliable.

Measurements	Parameters	Systematic uncertainty	Random uncertainty	Total uncertainty	Total uncertainty
		ε_s	ε_r	ε_{ADD}	ε_{RSS}
Gas oil consumption	Fuel flow rate	0.4%	0.30%	1.0%	0.72%
vegetable oils consumption	Fuel mass	0.01 %	0.26 %		
	Time	0.002%	0.16%		
	Fuel flow rate	0.01 %	0.41 %	0.84 %	0.82 %
Electrical Power	Current	0.1 %	0.09%		
	voltage	0.1 %	0.04%		
	Power	0.14 %	0.10 %	0.34%	0.24%
BSFC of gas oil	Fuel flow rate	0.4%	0.30%		
	Electrical	0.14 %	0.10 %		

	Power				
	BSFC	0.49%	0.36%	1.21%	0.87%
BSFC of vegetable oils	Fuel flow rate	0.01 %	0.41 %		
	Electrical Power	0.14 %	0.10 %		
	BSFC	0.28%	0.46%	1.19	1.95%
Heat recovered by coolant heat exchanger	Water flow rate	0.1%	1.23%		
	Inlet temperature	0.4%	0.15%		
	Outlet temperature	0.4%	0.09%		
	Heat recovered	0.89%	1.26%	3.41%	2.67%
Heat recovered by exhaust heat exchanger	Water flow rate	0.1%	1.23%		
	Inlet temperature	0.4%	0.07%		
	Outlet temperature	0.4%	0.08%		
	Heat recovered	0.89%	1.24%	3.37%	2.64%
Heat input to absorption refrigerator	Exhaust gas flow rate	1%	0.69%		
	Inlet temperature	0.4%	0.05%		
	Outlet temperature	0.4%	0.04%		
	Heat input	1.33%	0.70%	2.73%	1.93%
refrigeration effect of freezer	Evaporator temperature	0.4%	0.04%		
	Freezer temperature	0.4%	0.08%		
	Cooling	0.57%	0.09%	0.74%	0.59%

	energy				
refrigeration effect of food chiller	Evaporator temperature	0.4%	0.04%		
	Food chiller temperature	0.4%	0.13%		
	Cooling energy	0.57	0.75%	2.07%	1.61%
Exhaust emissions measurement	Cooling energy	0.57%	0.14%	0.84%	0.63%
	CO ₂	1.0%	0.82%	2.64%	1.92%
	NO _x	1.0%	1.52%	4.04%	3.20%
	HC	1.0%	1.14%	3.28%	2.49%
Oxygen measurement	oxygen analyser	1.0%	0.14%	1.28%	1.04%
Biofuel properties	Viscosity	-	1.56%	3.12%	3.12%
	Mass of vegetable oils	0.00048%	0.007%		
	Sample volume	0.24%	0.4%		
	Density	0.48%	0.80%	2.08%	1.67%
	HHV	0.1%	0.13%	0.36%	0.28%

Table 3.7 Uncertainties of other measurements

Chapter 4. Experimental Results and Discussions

4.1 Introduction

In this chapter, the physicochemical properties of selected vegetable oils, i.e. croton oil, jatropha oil, rapeseed oil and sunflower oil, were tested and compared to that of gas oil, in terms of viscosity, higher heating value and density. The components of fatty acids of the vegetable oils were analysed. This provided primary information which helped to identify the characteristics of the vegetable oils and their performance on the engine. Experiments were also carried out using the above oils on a micro-trigeneration system running under different operating modes. The diesel generator performance and emissions, the recovered heating and cooling energy and the system efficiency were investigated and reported.

4.2 Physicochemical properties of vegetable oils

4.2.1 Viscosity

Viscosity reflects the resistance of fluid to flow. The kinetic viscosities of the test samples along with the standard deviations at 40°C are shown in Table 4.1, with the referenced data listed. The viscosities of the vegetable oils fell in the range of 25.7 to 31.0 mPa.s, 11 to 13 times higher than that of gas oil. The lowest viscosity among the test samples was observed to be croton oil, and highest was rapeseed oil.

The referenced calculated dynamic viscosities are derived by the following equation:

$$v = \eta / \rho \times 1000 \quad (4-1)$$

Where v is kinematic viscosity in mm^2s^{-1} ; η is dynamic viscosity in mPa.s; ρ is the density of fuel in kg/m^3 . Compared to the referenced calculated figures, the properties of the vegetable oils were slightly lower. The reference viscosities or

densities data used in the calculation were recorded with a lower measuring temperature; hence the results listed in Table 4.1 were slightly higher than the experimental results. In another words, the experimental results are reasonable.

Samples	Tested kinetic viscosity @ 40 °C (mPa.s)	Referenced viscosity @ 40 °C (mm ² /s)	Calculated kinetic viscosity (mPa.s)*	References
Croton oil	25.7 ± 0.4	30.37-34.48	28.06-31.16	[135, 136]
Jatropha oil	30.3 ± 0.4	34.56-35.38	31.14-32.41	[136] [137]
Rapeseed oil	31.0 ± 0.3	37.3@ 38 °C	34.02	[96]
Sunflower oil	27.6 ± 0.4	33.9@ 38 °C	31.05	[96]
Gas oil	2.4 ± 0.6	3.06@ 38 °C**	2.62	[138]

Table 4.1 Viscosities of the oils

*: The values were converted by multiplying the kinetic viscosities to the densities in the references. The densities in Reference [134] were measured at a temperature of 15°C.

** : Data of diesel

The variations of viscosities as a function of temperature are shown in Fig. 4.1, with a temperature range of 20 °C to 120 °C, and the test data is listed in Appendix B.1. The viscosities of gas oil ranging from 20°C to 60 °C were also presented for comparison. When the temperature over 60 °C, the viscosity of gas oil was fairly low and was hard to be measured. The test results reveal that the viscosities of the vegetable oils decrease sharply with the increase of temperature. When heated to 120°C, the viscosity of these oils dropped to approximately 3mPa.s, with a minimum value of 2.2 mPa.s for croton oil and a maximum value of 3.7 mPa.s for rapeseed oil, which were comparable or better than that of the gasoil of 3.0 mPa.s at 30 °C. These results again

proved the feasibility of preheating to minimise the negative effects of high viscosity when applying the vegetable oils to the engine.

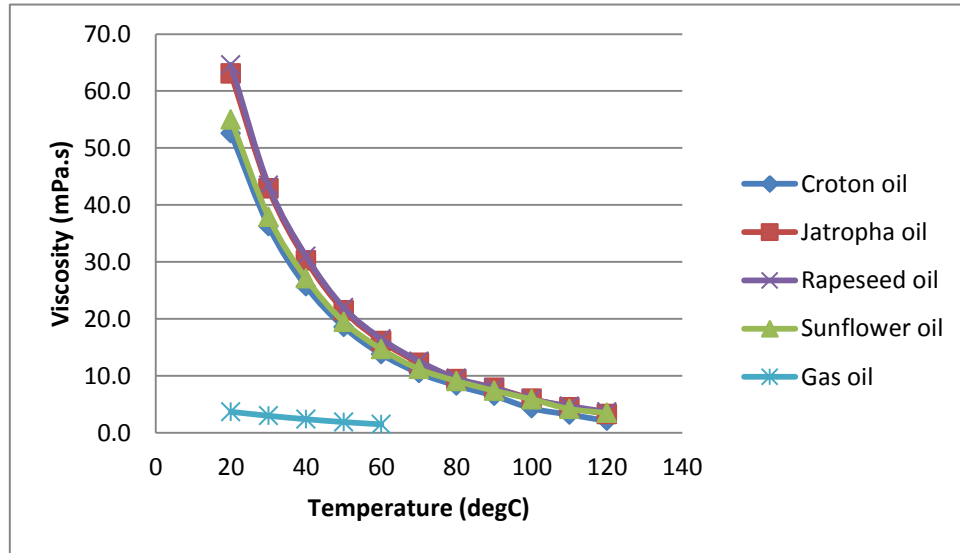


Fig. 4.1 Variation of viscosities as a function of temperature

4.2.2 Density

The density of vegetable oils is affected by factors such as the source of feedstock, extraction methods and oil temperature. In this study, the figures of the raw vegetable oils were all above 900 kg/m^3 (see Table 4.2 and Appendix B.2), within the range of diesel engine fuels of $750\text{-}950 \text{ kg/m}^3$ and were approximately 9-11% higher than that of the gas oil. The density of croton oil competed favourably to that of the results reported by Aliyu [135], while the rest of the data was very close to the densities listed in Table 2.3, hence proving the reliability of the test results.

Samples	Density (kg/m^3)
Croton oil	917.3 ± 1.0
Jatropha oil	903.2 ± 1.7
Rapeseed oil	907.1 ± 0.9
Sunflower oil	914.5 ± 0.6
Gas oil	828.1 ± 0.6

Table 4.2 Densities of the oils

4.2.3 Heating value

Higher heating value and lower heating value (LHV) are the two important parameters to evaluate fuel energy content. The former takes into account the latent heat of water vaporisation, while the latter does not and is usually determined from the former. The test and calculation results of these two figures are listed in Table 4.3 and Appendix B.3. The HHV of the vegetable oils were similar, all lower than 40 MJ/kg and were about 14% less than that of the gas oil.

The value of LHV is given by Eq. 4-2, which is related to HHV by the amount of water vapour and its latent heat of condensation. An empirical cubic function [139] was proposed for calculating the latent heat of water in the temperature range of $-40\text{ }^{\circ}\text{C}$ to $40\text{ }^{\circ}\text{C}$, as shown in Eq.4-3:

$$\text{LHV}=\text{HHV}-h_w \times m_w \quad (4-2)$$

$$h_w=(2500.8-2.36 \times T+0.0016 \times T^2-0.00006 \times T^3)/1000 \quad (4-3)$$

Where h_w is the latent heat of water condensation in MJ/kg. T is the water temperature with a unit of $^{\circ}\text{C}$ and m_w is the mass of water produced as a result of fuel combustion. It can be deduced by the hydrogen components listed in Table 4.6.

Another index of volumetric energy was used to evaluate the energy content by volume, which is usually applied on gaseous fuels:

$$E_v=\text{LHV} \times \rho \quad (4-4)$$

Where E_v is volumetric energy. The calculated results are listed in Table 4.4. Due to the higher densities of the vegetable oils their volumetric energies are only 4.5-6% less than that of the gas oil.

Samples	HHV (MJ/kg)	LHV @ 20°C (MJ/kg)	Volumetric energy (MJ/m ³)
Croton oil	39.60 ± 0.02	37.02	33958.4
Jatropha oil	39.85 ± 0.02	37.22	33617.1
Rapeseed oil	39.71 ± 0.00	37.09	33644.3
Sunflower oil	39.40 ± 0.02	36.81	33331.5
Gas oil	45.74 ± 0.04	42.91	35533.8

Table 4.3 Heating values of the oils

The test results of viscosity, density and HHV also verified the research outcome from Demirbas [96], i.e., the viscosity and HHV of vegetable oils decreased with density.

4.2.4 Compositions of the vegetable oils

Gas chromatography is a popular method to identify the compositions of fatty acid methyl esters (FAMES) in biodiesels. As mentioned in Chapter 3, the vegetable oils were converted into biodiesel for GC tests. After the FAMES were determined, the corresponding fatty acids in the vegetable oils can be deduced by the following chemical equation[140]:

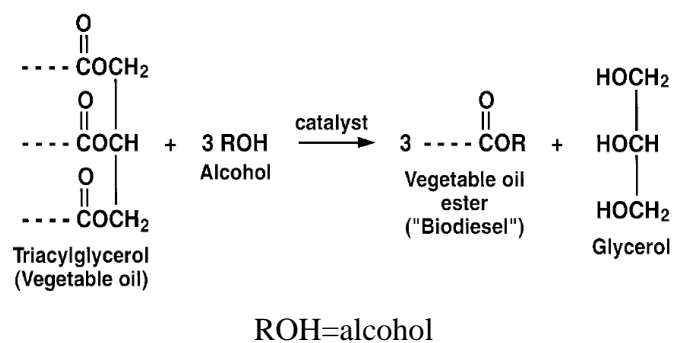


Fig. 4.2 Reaction equation of transesterification

In this study, the alcohol used for transesterification was methanol, namely, ROH = CH₃OH. The test samples were mixed with methyl heptadecanoate (C17 ester), which was used as an internal standard to quantify the other esters. The detailed test

results are shown in Appendices B.4-B.7. As an example, the chromatogram and GC traces data for croton biodiesel are shown in Fig.4-3 and Table 4.4.

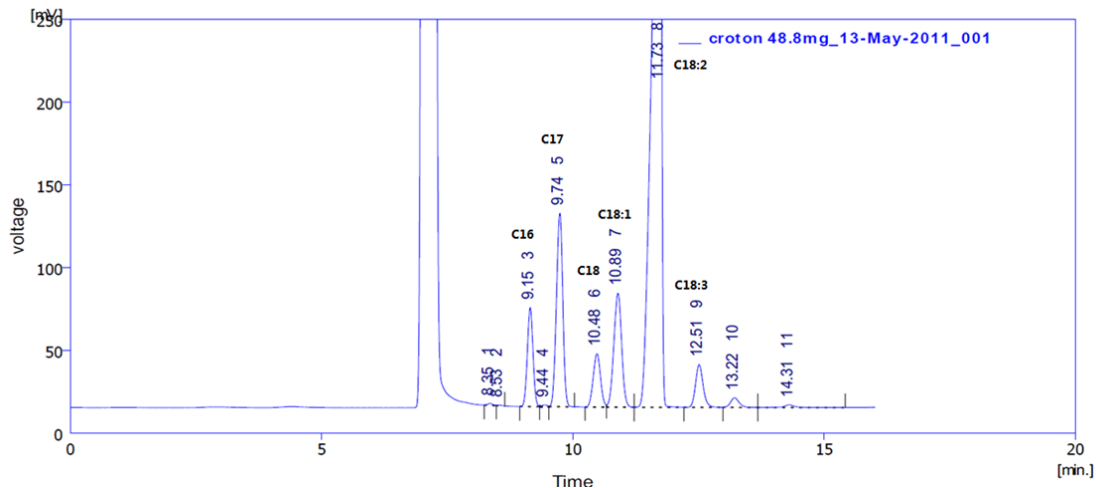


Fig. 4.3 Chromatogram of croton biodiesel

Result Table (croton 48.8mg_13-May-2011_001)

	Reten. Time [min]	Area [mV.s]	Height [mV]	Area [%]	Height [%]	W05 [min]
1	8.353	8.391	1.184	0.1	0.2	0.11
2	8.525	2.887	0.424	0.0	0.1	0.11
3	9.150	468.940	59.877	5.5	7.9	0.12
4	9.442	8.023	1.077	0.1	0.1	0.13
5	9.742	1029.507	117.129	12.0	15.4	0.14
6	10.477	329.087	32.341	3.8	4.2	0.16
7	10.893	748.761	68.997	8.8	9.1	0.17
8	11.730	5591.704	447.809	65.4	58.7	0.20
9	12.508	272.373	25.947	3.2	3.4	0.16
10	13.220	69.594	5.858	0.8	0.8	0.18
11	14.308	25.117	1.599	0.3	0.2	0.19
	Total	8554.382	762.243	100.0	100.0	

Table 4.4 GC traces data of croton biodiesel

The peaks in Fig.4-3 represent the esters of the croton oil, and the figures on the top of each peak are the retention times by order. Amongst the related test data depicted in Table 4.4, peak areas are the mass proportion of the constituents. It is worth pointing out that C17 ester was included in the table with a retention time of 9.742 minutes. This standard accounts for around 12% of the peak area for all of the samples. Hence, the actual proportion of each constituent was required to be

recalculated to remove C17, and the major results are shown in Table 4.5. The proportions of the FAMES in croton biodiesel were almost the same as those of the fatty acids in croton oil, with a deviation value less than 0.1%. This was due to the minor difference in the molecular weights between the FAMES and the fatty acids. Hence, these proportions for the biodiesel were usually considered the same as those of the vegetable oil.

Esters/fatty acids	Proportions in croton biodiesel (wt%)	Proportions in croton oil (wt%)
C16	6.23	6.20
C18	4.37	4.37
C18:1	9.95	9.96
C18:2	74.31	74.33
C18:3	3.62	3.62

Table 4.5 Proportions of the constituents in croton biodiesel and croton oil

Accordingly, the main constituents of the vegetable oils were calculated and compared in Fig.4-4. It revealed that palmitic acid (C16), octadecanoic acid (C18), oleinic acid (C18:1), linoleic acid (C18:2) and linolenic acid (C18:3) were the dominant constituents in the vegetable oils, which accounted for over 98% of the overall weight of the oils. Croton and sunflower oils contained much more linolenic acid than the other oils; while Jatropha oil contained the highest proportion of palmitic acid and octadecanoic acid. Normally, fatty acid with a high carbon number will have a high density and this may explain the test results of the density value.

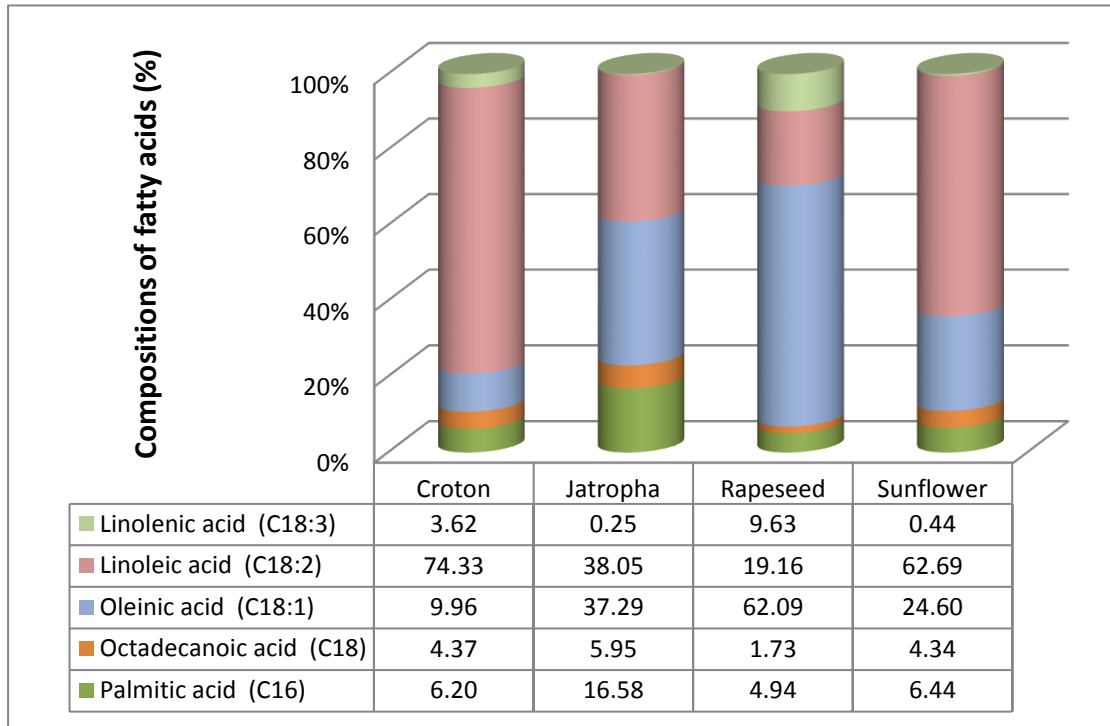


Fig.4.4 Constituents of fatty acids in the vegetable oils

Based on the GC test data, the elementary compositions of the vegetable oils were calculated (Table 4.6). Compared to gas oil, the vegetable oils contained rich oxygen (around 11.5%) which was slightly different to the other oils. However, they have less carbon and hydrogen composition, especially the carbon proportions which were about 9% lower than that of the gas oil, This indicates less oxygen was required when these fuels combust in a diesel engine.

Samples	Carbon (wt%)	Hydrogen (wt%)	Oxygen (wt%)
Croton oil	76.9	11.6	11.5
Jatropha oil	76.5	11.9	11.6
Rapeseed oil	76.7	11.9	11.4
Sunflower oil	76.8	11.7	11.5
Gas oil[141]	86.3	12.8	0

Table 4.6 Elementary compositions of the vegetable oils

4.3 Trigeneration

4.3.1 Generator performance and emissions

4.3.1.1 Generator performance

The generator performance using the four preheated vegetable oils (90°C) is depicted in Fig. 4.5 to Fig. 4.10 and compared to the gas oil. The reference electrical powers for the loads of 10%, 25%, 50%, 75% and 100% are 0.65kW, 1.625kW, 3.25kW, 4.875kW and 6.5kW, respectively. Fig. 4.5 shows the experimental results for different electrical powers with a deviation less than 1.2%, accurate enough for comparison with other data.

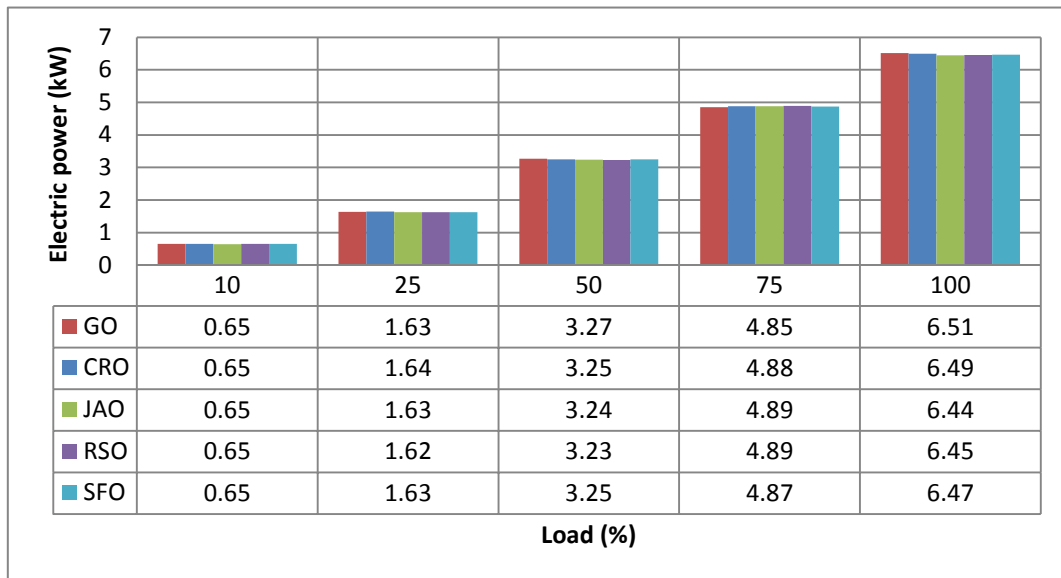


Fig. 4.5 Electric power of the oils for different loads

The fuel consumption (FC) and BSFC of the oils is shown in Fig. 4.6 and Fig. 4.7. They reveal that both values for the four vegetable oils were similar, 18-22% higher than that of the gas oil. The reason was mainly due to less heat energy contained in the vegetable oils and therefore more fuel was needed to retain the same power output. Among the possible vegetable oils, no significant difference was found between the edible oils and the inedible ones, both in terms of FC and BSFC.

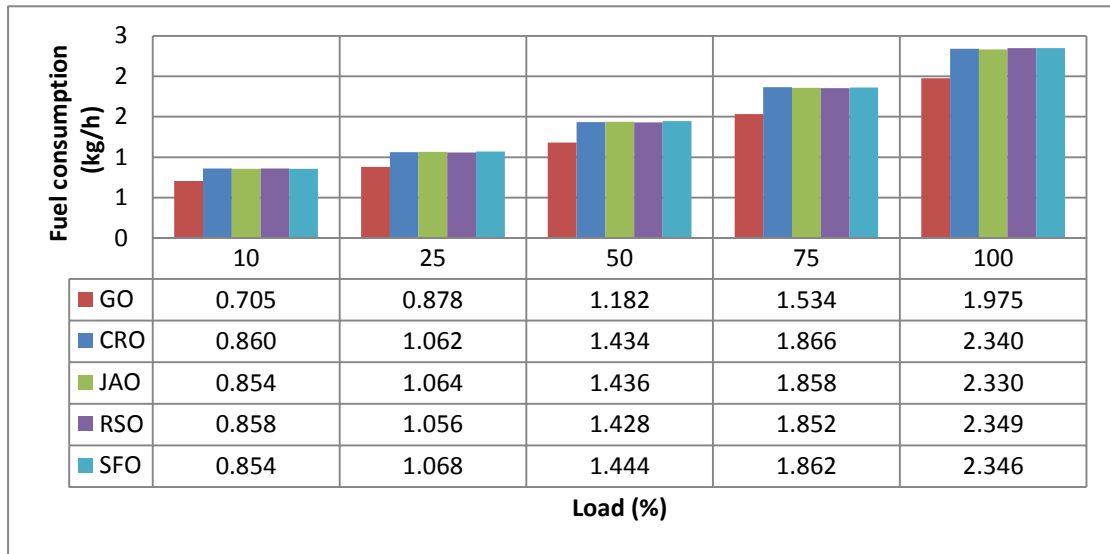


Fig. 4.6 Fuel consumption of the oils for different loads

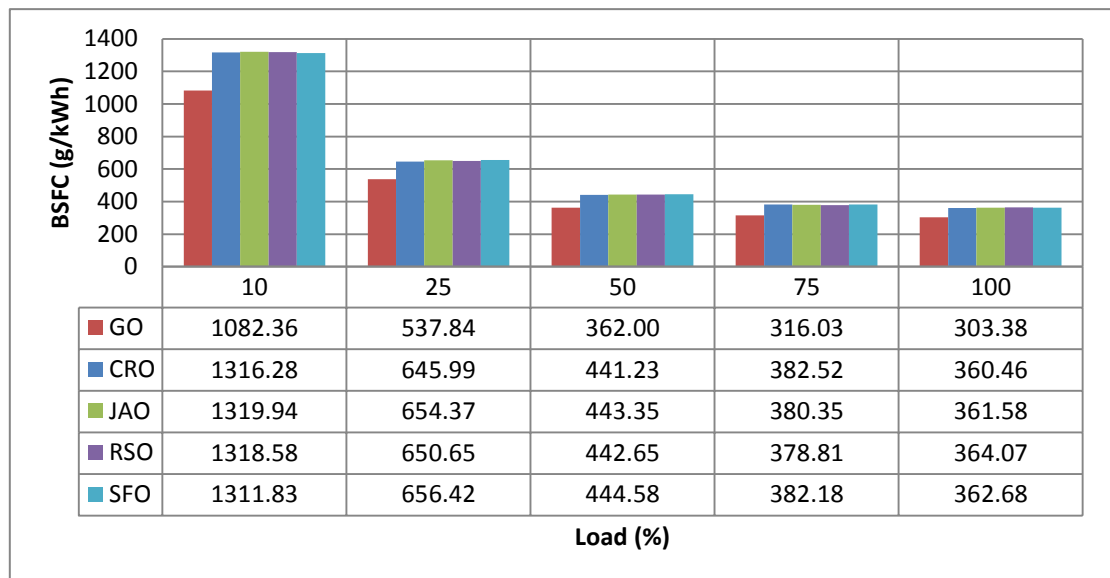


Fig. 4.7 BSFC of the oils for different loads

Brake specific energy consumption is an index for comparing the energy utilisation of the fuels with the different heating value. It is defined by divided fuel energy, that is, fuel consumption times the low heating value of the fuel, by the output energy. The results in Fig. 4.8 show that the BSEC of the vegetable oils was 5% higher on average to that of the gas oil. At full load, this figure was only approximately 3% higher and may be attributed to the higher fuel injection pressure and cylinder temperature, thus improved combustion. These results indicate that the combustion efficiency of the vegetable oils is similar to that of the gas oil.

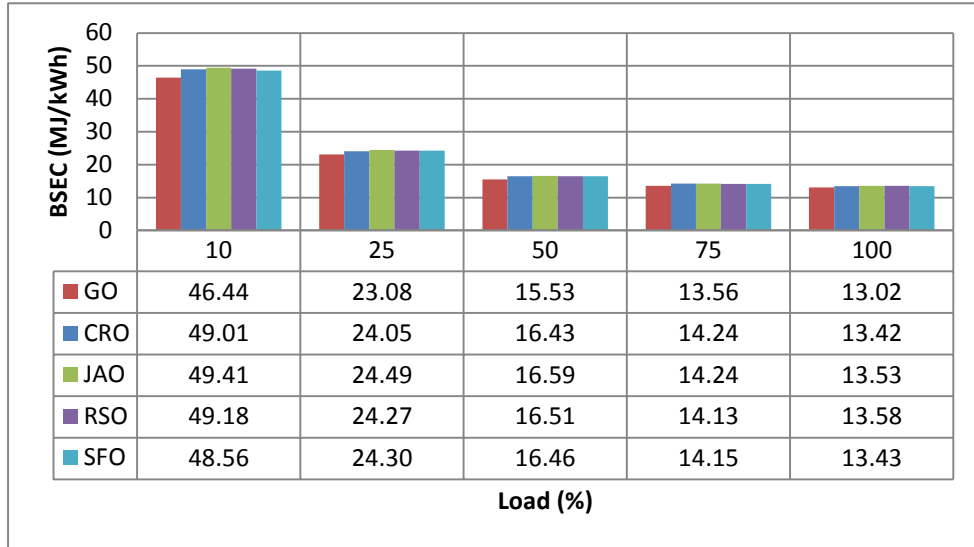


Fig. 4.8 BSEC of the oils for different loads

Fig. 4.9 compares the electrical efficiency of the oils with increasing engine loads. The highest efficiencies were discovered at full load, 27.65% for the gas oil and nearly 27% for the vegetable oils. At 50% load, the efficiency of the generator was still higher than 21%. However, this efficiency value decreased dramatically to about 7% with 10% load. The electrical efficiencies for the vegetable oils were almost identical and approximately 1 point less than those of the gas oil except at 10% load, where the deviations were less than 0.5%. This may be attributed to the rich oxygen content in the oils chain and relative air-fuel ratio compared to that of the gas oil, thus helping improve the combustion.

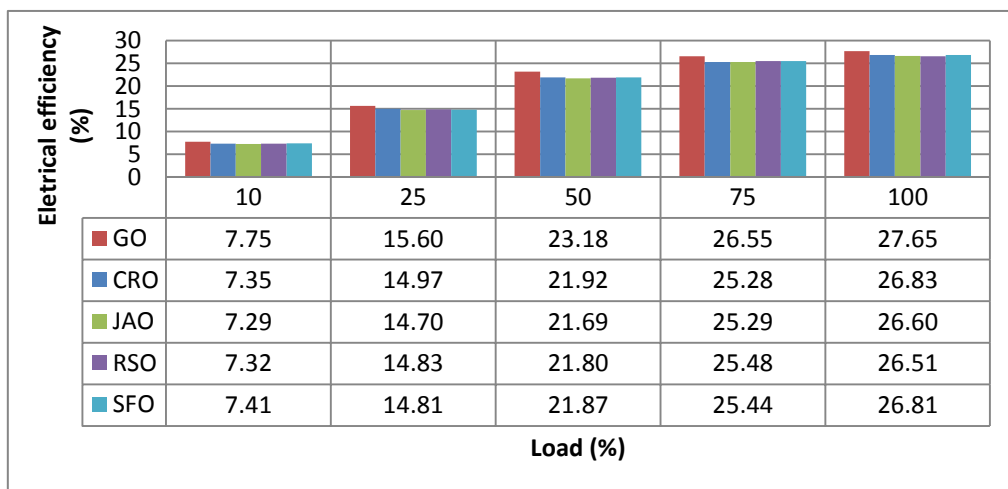


Fig. 4.9 Electrical efficiencies of the oils for different loads

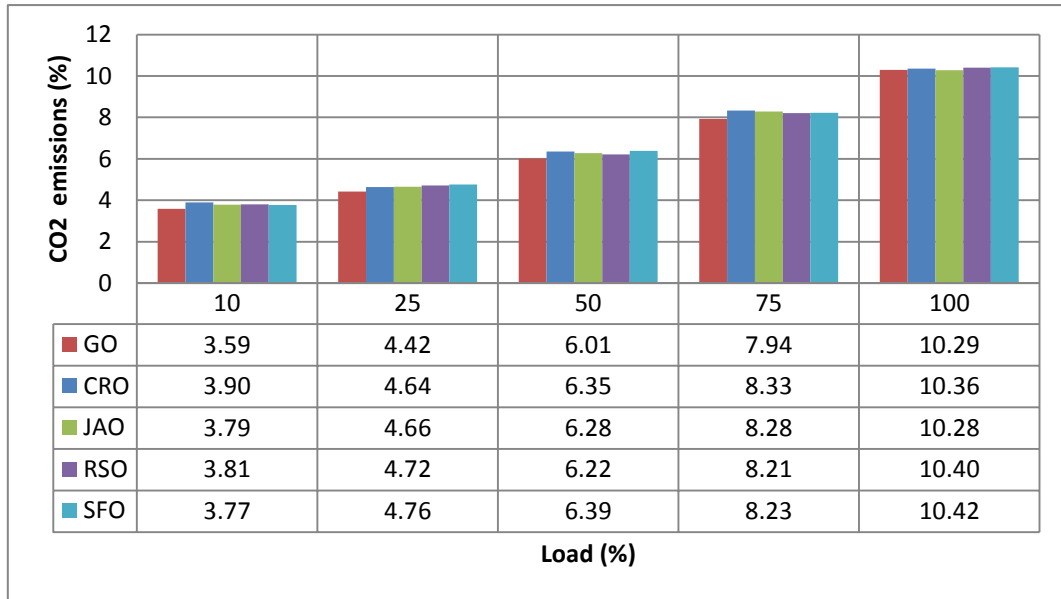


Fig. 4.11 CO₂ emissions of the oils for different loads

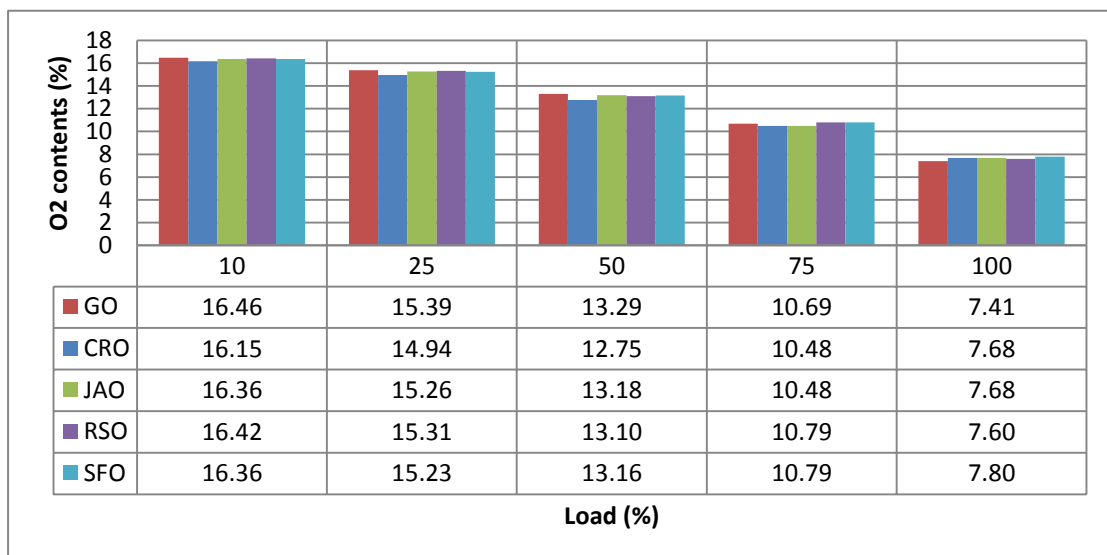


Fig. 4.12 O₂ contents in the exhaust gas of the oils for different loads

The CO emissions of the oils are shown in Fig. 4.13. Carbon monoxide forms with a situation involving a low fuel flame temperature and the incomplete progression to carbon dioxide. This occurs especially on the boundary of the cylinder wall and cylinder liner, where the flame front is cooled down and extinguished. Another important factor for CO formation is insufficient oxygen that prevents the final reaction to CO₂. This is usually attributed to too much fuel being injected into the cylinder.

The CO emissions in Fig. 4.13 appear to be related to the O₂ emissions. At loads ranging from 10% to 75%, the CO emissions for vegetable oils were on average over 30% higher in comparison to the gas oil. Nevertheless, at full load, slightly lower CO was achieved except for use with the rapeseed oil. The reason for the change of the trend was due to the drastically increased CO emissions for the gas oil, ranging from 282.28ppm to 529.71ppm. High viscosity, poor fuel atomisation and a low in-cylinder temperature may be the main reasons for CO formation at low and mid-loads for the vegetable oils. A richer air-fuel mixture of the gas oil seems to be the contributing factor for more CO production at full load.

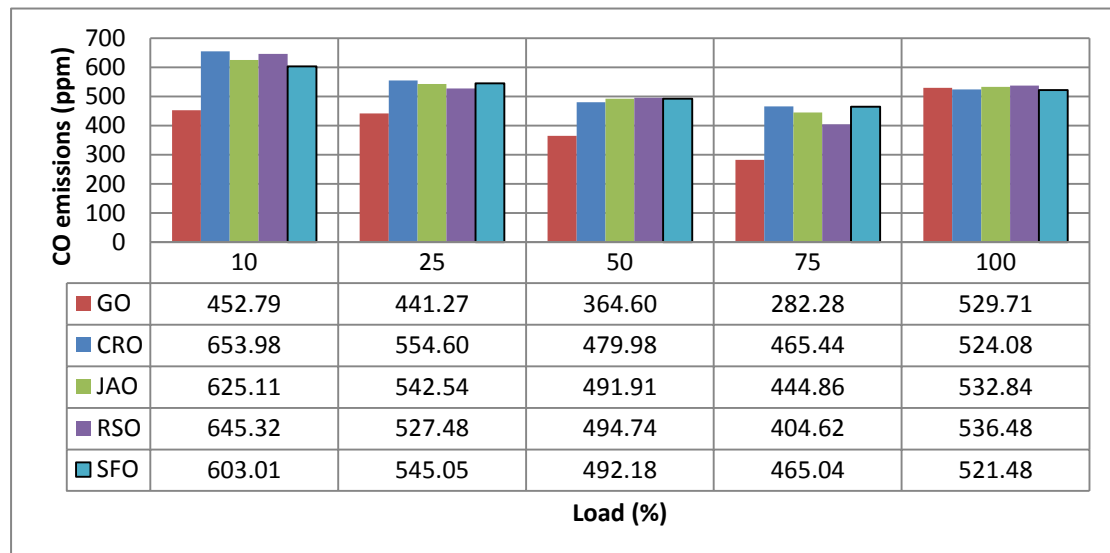


Fig. 4.13 CO emissions of the oils for different loads

The comparison of NO_x emissions is shown in Fig. 4.14. NO_x emission is strongly related to combustion chamber factors such as peak combustion temperature, combustion duration and oxygen concentration in the burning zone. It can be seen in the diagram that the NO_x emissions increased with the engine loads. Lower NO_x emissions were found with the vegetable oils at low and mid-loads compared to the gas oil; note a 16-25% decrease was achieved with 10% load. At 75% load, the NO_x emissions for edible oils were still 3% less, while those figures for the inedible ones were 5% higher than the gas oil. At full load, the NO_x emissions of the vegetable oils

were higher than that of the gas oil, in which rapeseed oil has a comparable emission rate to the gas oil. The maximum value was found using croton oil, 5.35% higher than the gas oil.

The reason for the NO_x emissions of the vegetable oils may be attributed to the co-effects of the aforementioned factors. Due to the higher viscosities, the droplet size of the vegetable oils is deemed to be larger with regards to the gas oil. At low and mid-loads, this may result in longer combustion duration, a lower peak combustion temperature, severe late burning and a higher exhaust gas temperature i.e. the latter has been proved by Fig. 4.10. At high and full loads, more fuels were injected and the in-cylinder temperature increased, helping improve the fuel-air mixture formation and rich oxygen in the vegetable oils. All these factors contributed to the higher NO_x emissions. However, to measure the combustion temperature within the cylinder was out of the scope of this study and may only be verified by simulation.

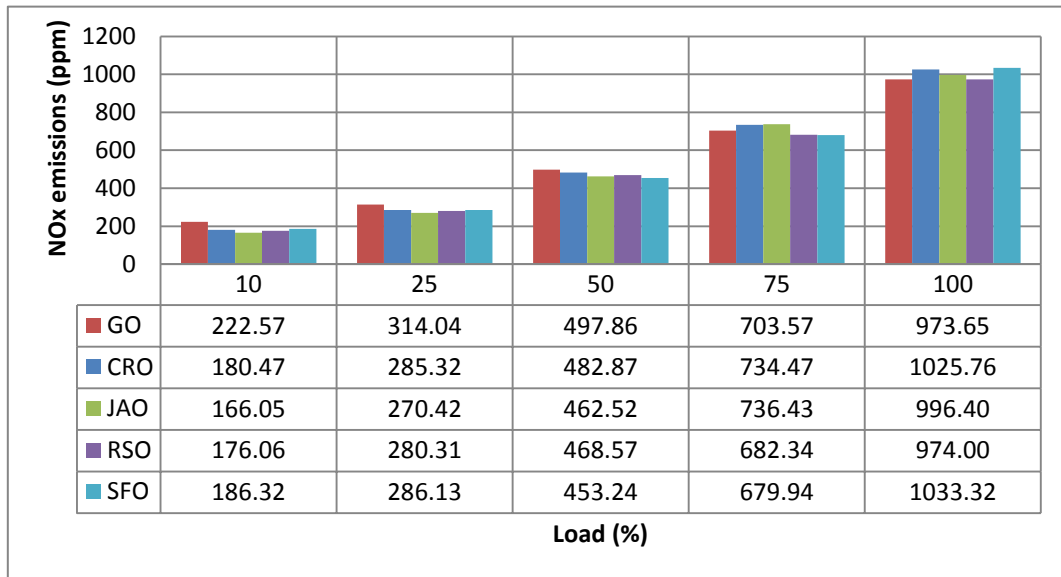


Fig. 4.14 NO_x emissions of the oils for different loads

Unburned hydrocarbons is another reaction product of incomplete combustion, mainly caused by a rich fuel air ratio, misfiring, incomplete combustion of lube oil and flame

quenching near the cylinder walls and in crevice regions. A further cause is that HC is absorbed by the oil film around the cylinder and later released into the exhaust gas.

It can be seen in Fig. 4.15 that the HC emissions increased with decreasing loads. The vegetable oils produced higher HC emissions relative to the gas oil at mid- and high loads. When the engine load dropped from 25% to 10%, the HC emission for gas oil increased by 16% from 361.43ppm to 418.25ppm. Hence, less HC emissions were observed for the vegetable oils, with a maximum of 13% reduction by sunflower oil compared to gas oil. Besides, the edible oils exhibited less HC emissions relative to the inedible ones, except when operating at full load. This may be explained by rich oxygen content in the combustion zone and a reasonable air- fuel ratio for the vegetable oils at low loads.

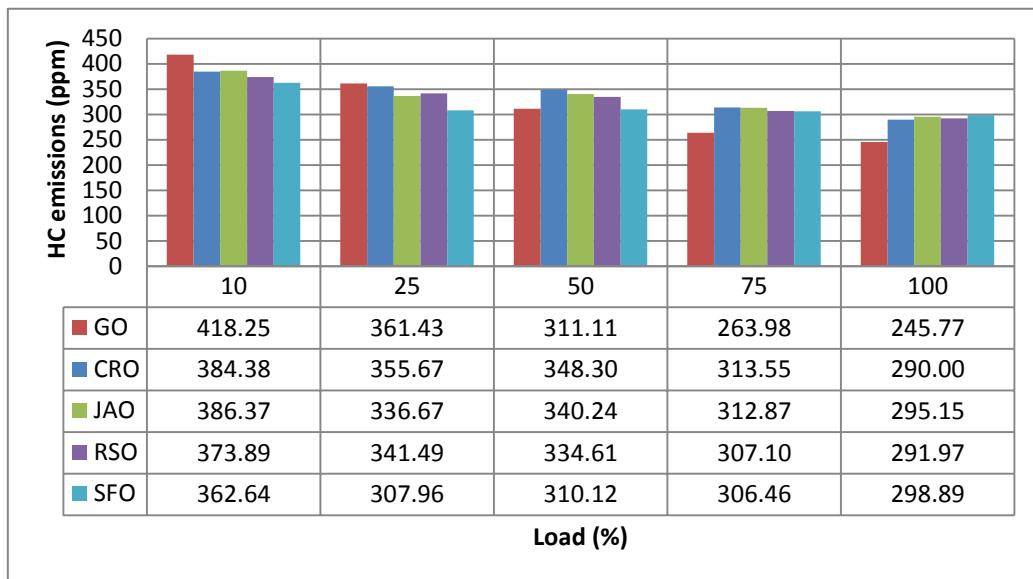


Fig. 4.15 HC emissions of the oils for different loads

4.3.2 Waste heat recovery by heat exchanger

The waste heat recovered by the two heat exchangers, i.e., coolant heat exchanger and exhaust gas heat exchanger, were studied and the results are shown in Fig. 4.16 to Fig. 4.21.

Fig. 4.16 and Fig. 4.17 illustrate the recovered exhaust gas heat for cogeneration and trigeneration, respectively. The values of recovered heat energy at full load under CG mode were approximately 4.7-4.9kW and are over three times higher than that of the 10% load. These figures for trigeneration are about 0.3-0.6kW less than those of the cogeneration, while this gap reduced with decreasing loads. This was due to the fact that part of the exhaust gas was supplied to drive the refrigerator and a proportion of heat was lost along the pipe line. The recovered heats for the gas oil at all loads were almost the lowest amongst the fuels, 0.1-0.2kW less than the vegetable oils.

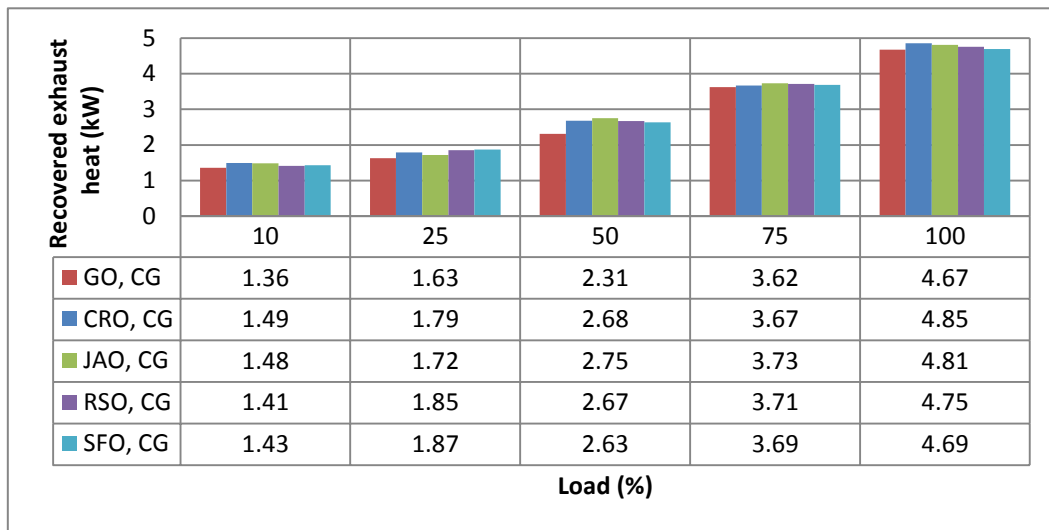


Fig. 4.16 Recovered exhaust gas heat for cogeneration

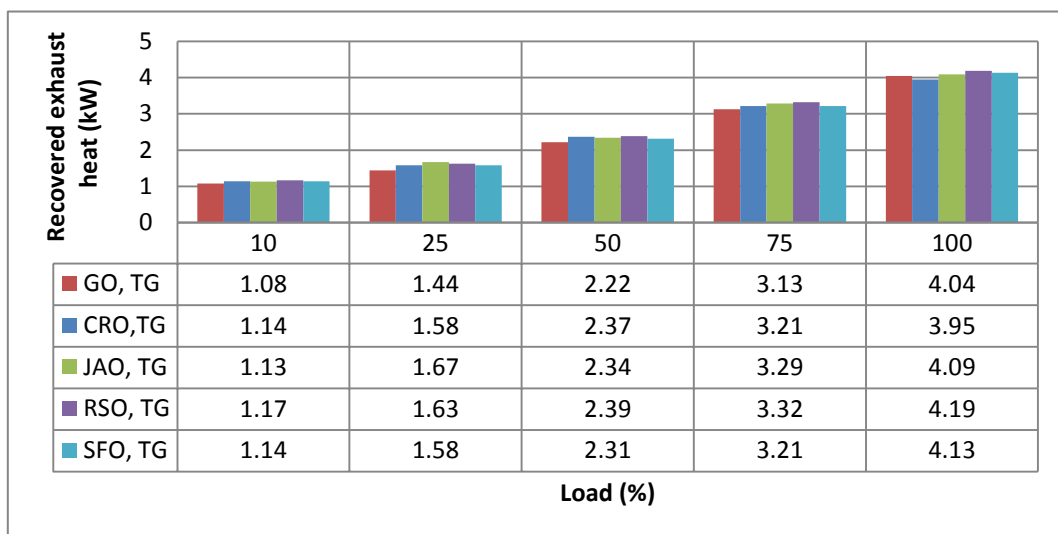


Fig. 4.17 Recovered exhaust gas heat for trigeneration

Fig. 4.18 and Fig. 4.19 show the recovered coolant heat for cogeneration and trigeneration. For each single fuel, no distinct difference was found between the two operating modes. Approximately 0.1-0.5kW more coolant heat was recovered with the vegetable oils relative to the gas oils, and this value increased with the engine load. This was due to a large amount of fuel being consumed for the vegetable oils and part of the heat energy was dissipated to the coolant, while the rest was disseminated in the form of exhaust gas heat. Hence, the available coolant heat and exhaust gas heat increased.

Relating to gas oil, the recovered exhaust gas heats at 75% and 100% full load under CG mode were higher than the recovered coolant heats. However, due to the decrease in exhaust gas temperature with the decreasing load, at mid- and low load, the recovered exhaust gas heat reduced drastically and was less than that of the coolant heat.

For the vegetable oils, the recovered coolant heats were always higher than those of the recovered exhaust gas heat at all loads. One of the reasons was higher fuel consumption, which resulted in more being transferred to the coolant during fuel combustion. Another important reason was that the exhaust gas temperature at the outlet of the heat exchanger was still high (over 180°C for full load), indicating part of the heat was still available but unrecovered. This can be solved by an increase in the water flow rate. Nevertheless, as the two heat exchangers were connected in line (as shown in Fig.3-7), this means more heat can be recovered from the coolant and it may result in a low coolant temperature. Hence, it will pose a negative effect on the engine.

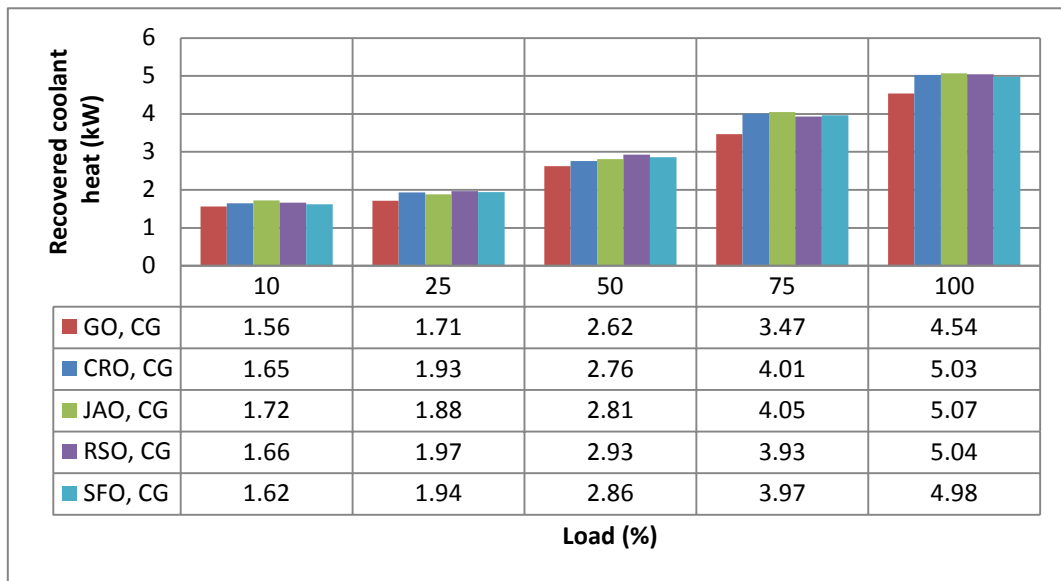


Fig. 4.18 Recovered coolant heat for cogeneration

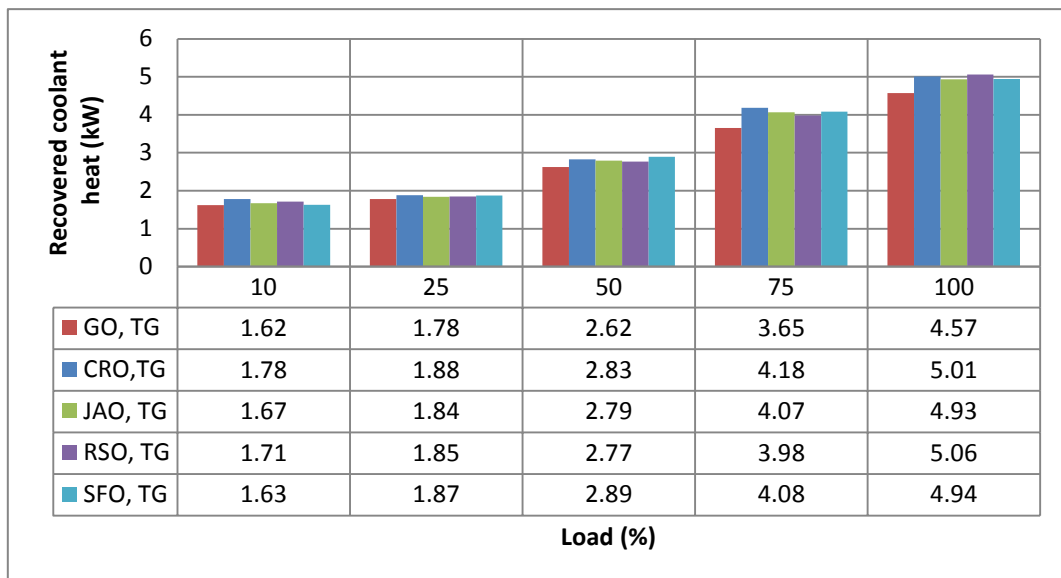


Fig. 4.19 Recovered coolant heat for trigeneration

Fig. 4.20 and Fig. 4.21 illustrate the total recovered heat for cogeneration and trigeneration. There are two characteristics that agree with the trends shown above: a) The recovered heat energy for the vegetable oils was higher than that of the gas oil and; b) The recovered heat energy for trigeneration was less than that of the cogeneration. The figure for full load varied between -10% to -7% for different oils.

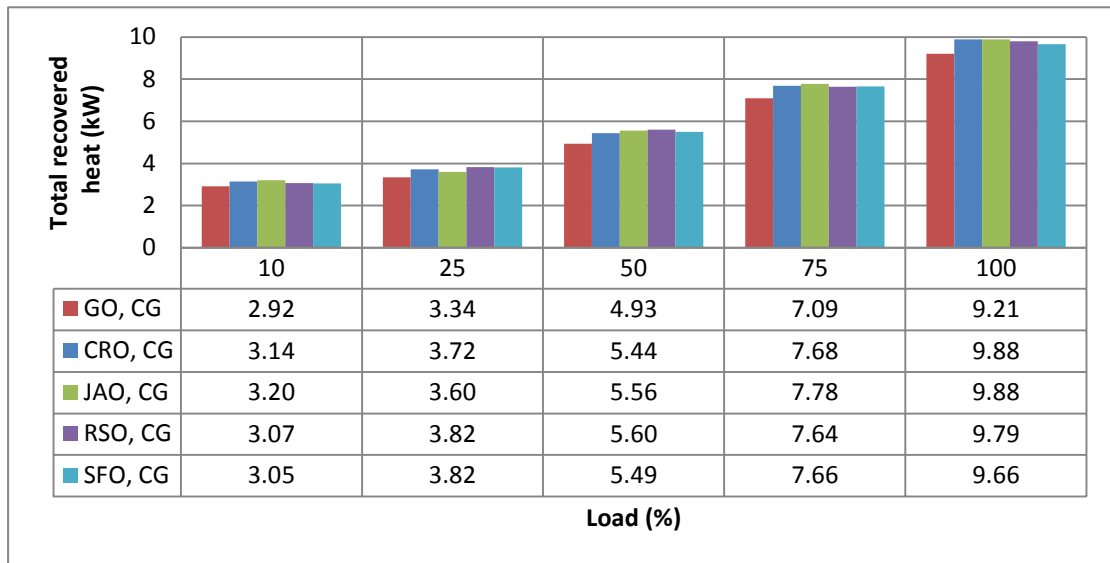


Fig. 4.20 Total recovered heat for cogeneration

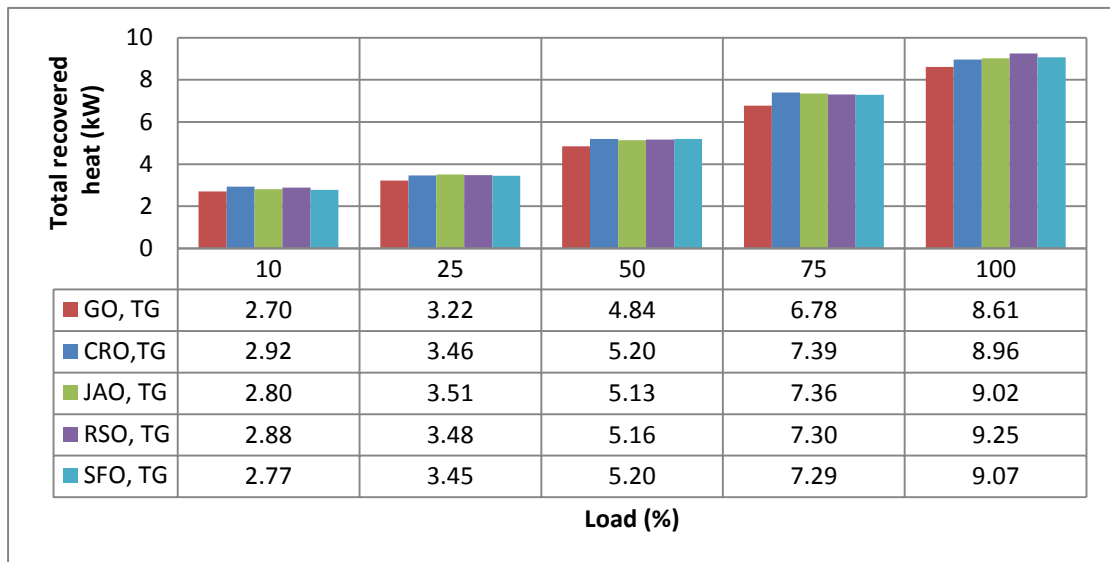


Fig. 4.21 Total recovered heat for trigeneration

4.3.3 Absorption refrigeration

4.3.3.1 Refrigerator performance driven by electricity

A preliminary investigation was carried out using alternating current to drive the diffusion absorption refrigerator. The cooling temperature was adjusted by turning the temperature regulator in the main refrigerator compartment. The positions of the

temperature regulator were set to 50%, 75% and 100% of the full scale value. The test results are depicted below.

Fig. 4.22 shows the heating power and working temperature of the refrigerator at full load scale. A clear control strategy of the electrical heater is illustrated, based on simple on-off control. A temperature sensor was installed in the food chiller to provide a reference signal. The power supply for the refrigerator cuts off when the temperature drops to a certain set-point and switches back on again after rising to a higher threshold level. At the start, the heater ramped up to the peak temperature of 206°C and then stabilised at around 186°C. It took approximately half an hour before the refrigerator cooled down. The electrical power supplied to the heater was approximately 181W. For full load scale operation, the initial power supply to the heater lasted for four and half hours before cut off. It resumed after 15 minutes and lasted for a further 47 minutes before the next cut off occurred. The temperatures of the evaporator, freezer and food chiller fluctuated as a result, with the lowest cooling temperature of -31°C for the evaporator.

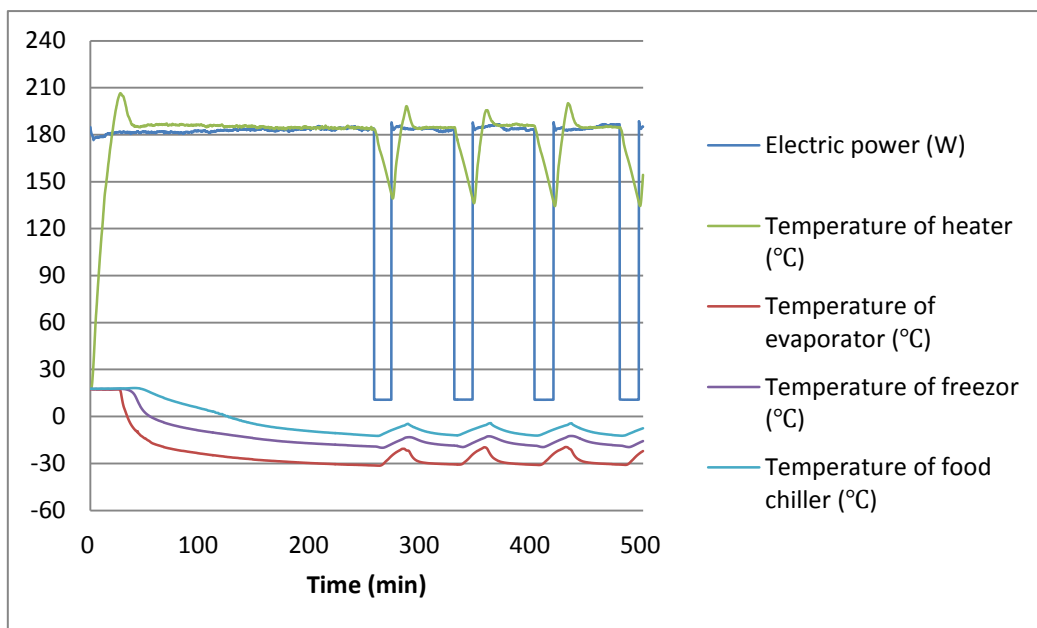


Fig. 4.22 Heating power and operation temperature of the refrigerator at full load scale

The comparisons of the refrigerator performance are shown in Fig. 4.23 to Fig.4-26 and Table 4.7. The heating power and temperature for a part load scale operation were almost identical to those of the full scale, whilst the heating time reduced and the heating interval increased. The heating interval for 75% scale was similar to that of the 100% scale, but the time interval doubled when the load scale reduced to 50%. With the decreasing scales, the time of the heating cycle ramped down from 57 minutes to 38 minutes. Accordingly, the lowest cooling temperature increased from -31.4°C to -26.5°C, though the start times of the cooling phase were almost the same, ranging from 24 to 27 minutes. It was noted that even running with the same heating power for the first three hours, the cooling temperature in the evaporator, freezer and food chiller for the part scales was slightly higher compared to that of the full scale. It is presumed that it is being mainly affected by the ambient temperature or the initial temperature of the refrigerator; hence, it affects the cooling effect.

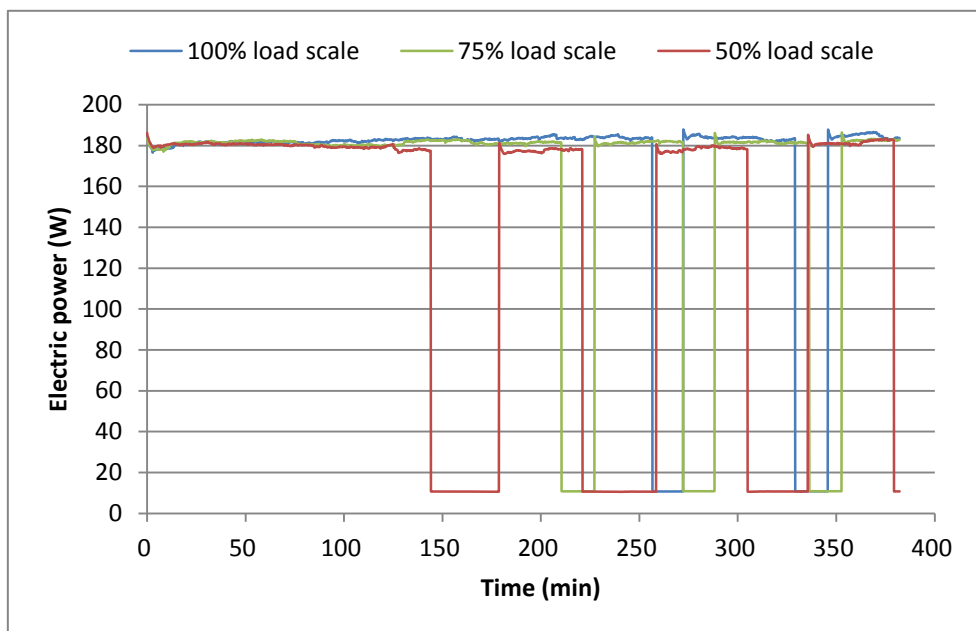


Fig. 4.23 Comparison of electric powers at different load scales

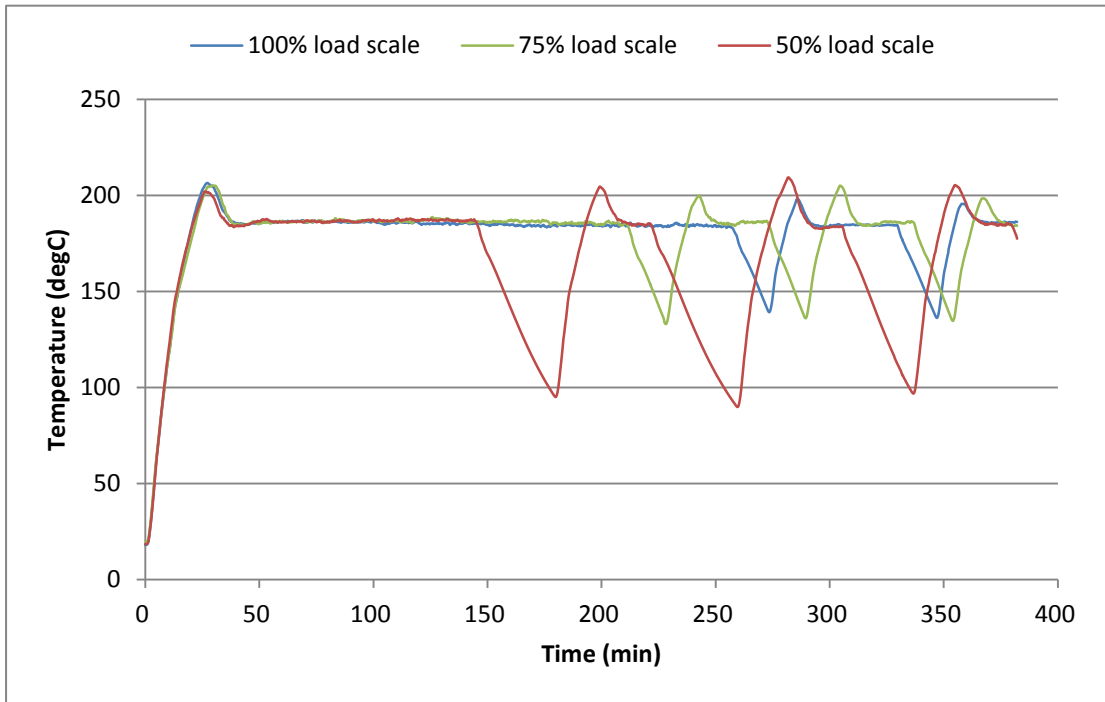


Fig. 4.24 Comparison of heater temperatures at different load scales

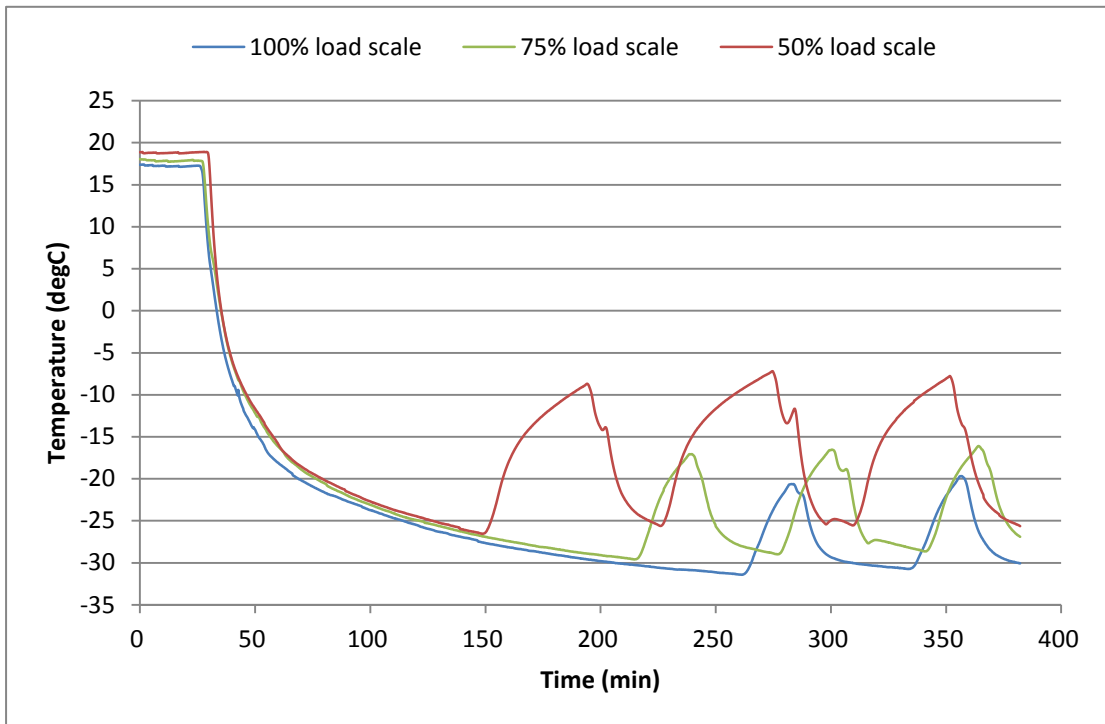


Fig. 4.25 Comparison of evaporator temperatures at different load scales

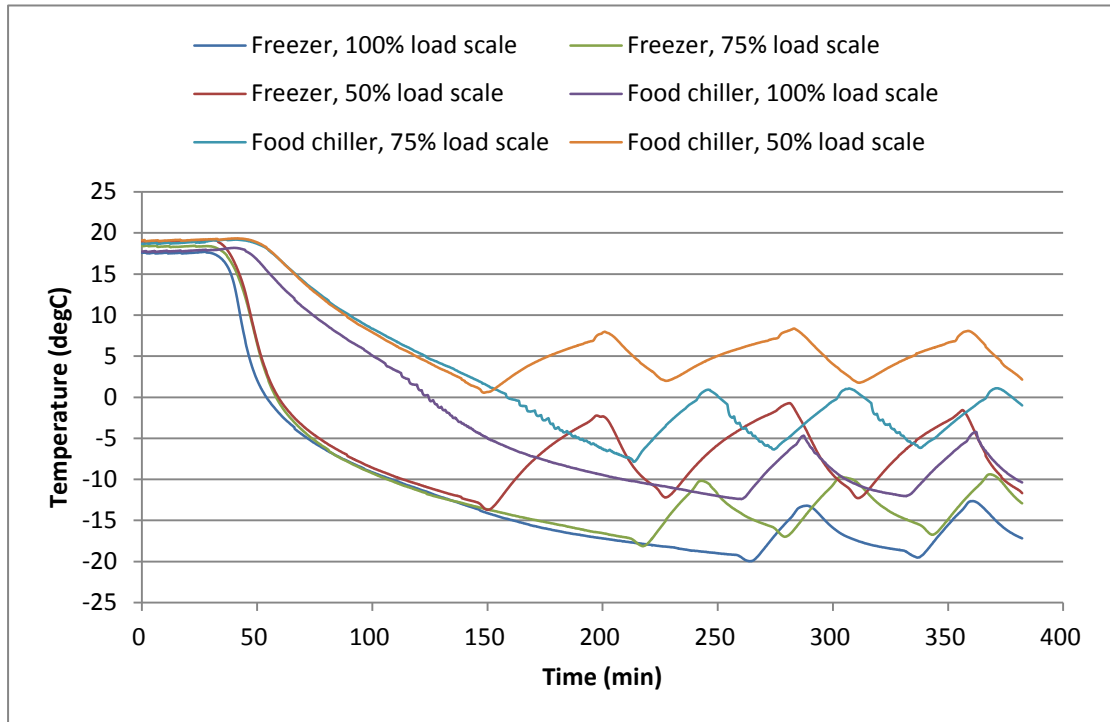


Fig. 4.26 Comparison of freezer and food chiller temperatures at different load scales

Test items	Load scales (%)		
	50	75	100
Ambient temperature (°C)	20.3	19.8	19.3
Heating temperature (°C)	186.8	186.4	186.2
Heating time (min)	38	45	57
Heating interval (min)	35	16	15
Lowest temperature in evaporator (°C)	-26.5	-29.5	-31.4
Lowest temperature in freezer (°C)	-7.4	-12.6	-16.3
Lowest temperature in food chiller (°C)	0.5	-7.9	-12.4
Heating power (W)	180.9	181.6	181.4
Cooling power (W)	13.8	13.0	15.4
COP	0.076	0.072	0.085

Table 4.7 Effects of refrigeration at different load scales driven by electricity

The cooling powers of the refrigerator in Table 4.7 are determined by the experimental data and the following assumptions:

- a) The cooling energy generated by the evaporator is transferred to the attached inner wall of the refrigerator by conduction, and then flows to the air via natural heat convection and conduction.
- b) The wall is assumed to be made from high impact polystyrene (HIPS), which is the most popular plastic for making the inner container of a refrigerator.
- c) At the very beginning of the cooling, except for the rear HIPS wall, the temperature difference between the air and HIPS walls is considered negligible and so no heat transfer occurs. The heat transfer from the rear HIPS wall to the other wall, as well as the cooling energy loss of the evaporator from the rear thermal insulation layer to the surrounding environment will not be taken into account.

Hence, the cooling power is calculated by the following equations:

$$Q_c = Q_{cHW} + Q_{ca} \quad (4-1)$$

$$Q_{cHW} = c_{pHW} \times m_{HW} \times d(T_{HW}) \quad (4-2)$$

$$Q_{ca} = c_{pa} \times m_a \times d(T_a) \quad (4-3)$$

$$m_{HW} = \rho_{HW} \times H_{HW} \times W_{HW} \times D_{HW} \quad (4-4)$$

$$m_a = \rho_a \times \sum V_{ai} \quad (4-5)$$

Where Q_c , c_p , m , ρ and T are the cooling power, specific heat at constant pressure, mass, density and temperature. Subscripts HW and a are related to the HIPS wall and air in the refrigerator. For this calculation, $c_{pw}=1.4 \text{ kJ/kgK}$ [142], $c_{pa}=1.005 \text{E-3 kJ/kgK}$ [142], $\rho_w=1.04 \text{kg/m}^3$ [143]. H_{HW} , W_{HW} and D_{HW} are the height, width and depth of the HIPS wall. V_a is the volume of air in the freezer and food chiller.

The coefficient of performance is therefore calculated by Eq.4-6:

$$\text{COP} = Q_c / Q_h \quad (4-6)$$

Where Q_h is the heating power. This calculation only takes into account the ‘useful’ cooling energy for the freezer and food chiller instead of the ‘generated’ cooling energy, including which parts of the energy is dissipated into the surrounding atmosphere. Thus, the values of cooling power and COP may be low compared to that in literature reports.

The COP results listed in Table 4.7 are the dynamic average of three calculated values. It reveals that around 13-15W of cooling power were generated, with the COP ranging from 0.072 to 0.085. The full load scale operation indicated the best results, while the other two were very similar. The variations in these results were believed to be affected by the initial temperature of the refrigerator. A higher initial temperature means slower temperature decreases using the same heating power. Another important factor was that the accuracy of the calculated result was influenced by the measured temperature field of the refrigerator. The more sensors applied in the measurements will result in more accurate data for the analysis.

4.3.3.2 Refrigerator performance driven by exhaust heat

For biofuel micro-trigeneration, exhaust gas heat was used to drive the refrigerator. The test results are listed in Table 4.8. The dynamic performance is illustrated in Fig. 4.27 to Fig. 4.30 and compared to the refrigerator performance driven by electricity.

Fig. 4.27 and Fig. 4.28 compare the heat input and temperature of the heater with exhaust gases for different fuels. The heat power input with gas oil was 8-10W less than that of the vegetable oil at all loads. This was mainly due to the low exhaust gas temperatures (listed in Fig. 4.10) and exhaust gas flow rates when using gas oil. Hence, the heating temperatures with the gas oil were also low. It is noted that the heating temperatures were only around half the value of the exhaust gas temperatures, meaning large amounts of heat energy was lost in the exhaust pipeline, even though the pipe had been well insulated. This also indicates extra heat transmission is

required if the refrigerator is to run at the furthest position from the diesel generator with exhaust gas.

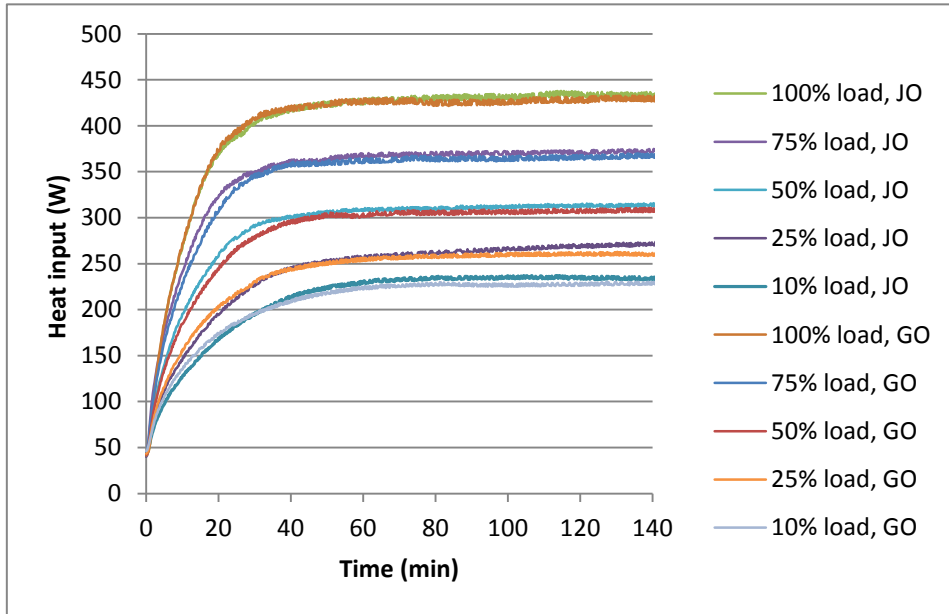


Fig. 4.27 Comparison of heat input with different exhaust gases and loads

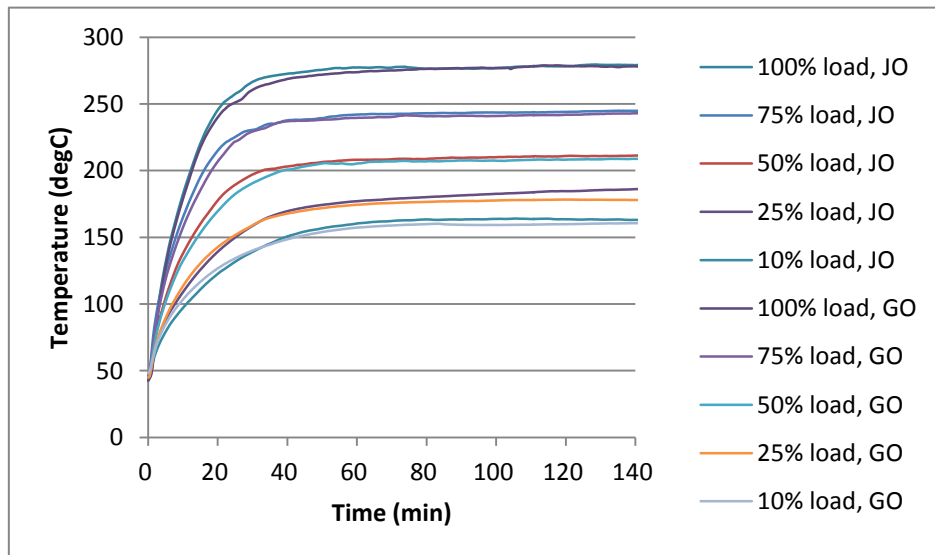


Fig. 4.28 Comparison of heater temperatures with different exhaust gases and loads

Fig. 4.29 compares the temperatures of an evaporator with different exhaust gases and loads. At full load, the start time for cooling of the fuels was approximately 25 minutes, almost the same time as it took when driven by electricity, and this figure

was over 50 minutes for 50% load. With the decreasing loads, a longer time was needed for generating the cooling effects with the exhaust gas of the gas oil. As a result, when run for two hours, lower cooling temperatures were found with the exhaust gas of vegetable oil, due to more heat input and a higher heating temperature. However, when the engine operated at loads of 10% and 25%, no cooling effects were observed and the evaporator temperatures remained almost flat. Table 4.8 shows the test results for the engine loads ranging from 50% to 100%.

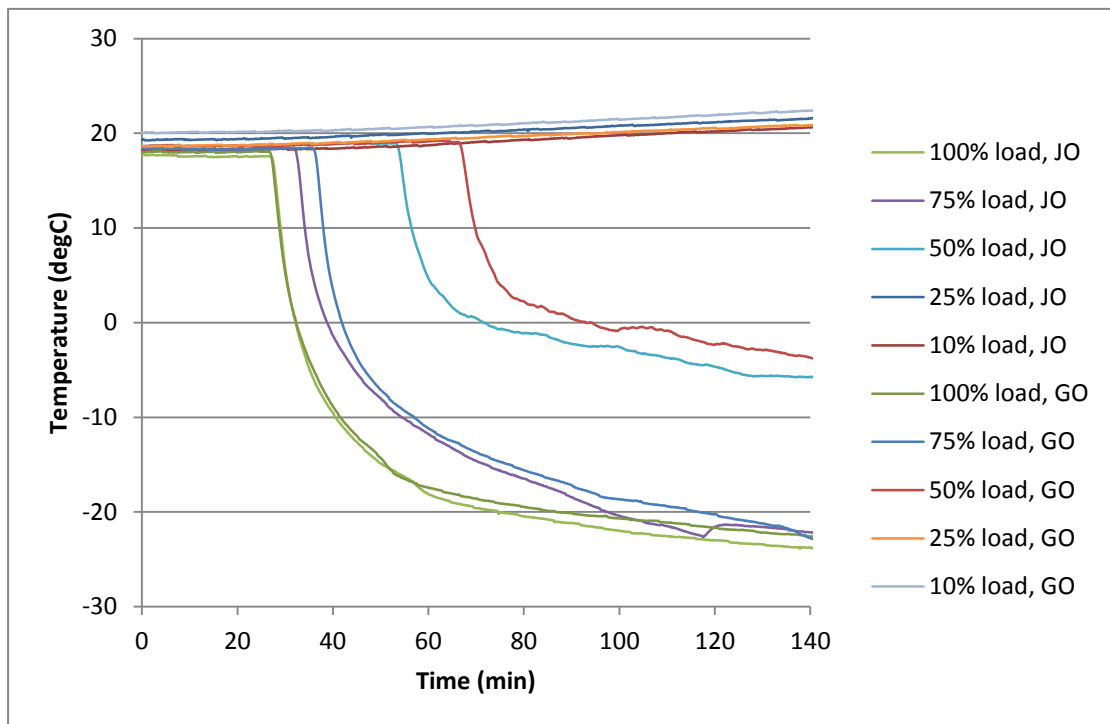


Fig. 4.29 Comparison of evaporator temperatures with different exhaust gases and loads

Fig. 4.30 and Fig. 4.31 illustrate the temperatures of a freezer and food chiller. Compared to the performance running with electricity, higher temperatures were found with the exhaust gases. At 50% and 75% load, no cooling effects were generated in the food chiller after being run for two hours, with the temperatures of the food chiller even higher than ambient temperature. The test data shows that when run with exhaust gases, the temperatures of the condenser were 4-23°C higher than

that with electricity. This indicates that to improve the refrigerator performance, it is necessary to take certain measurements to enhance heat transfer in the rectifier and condenser.

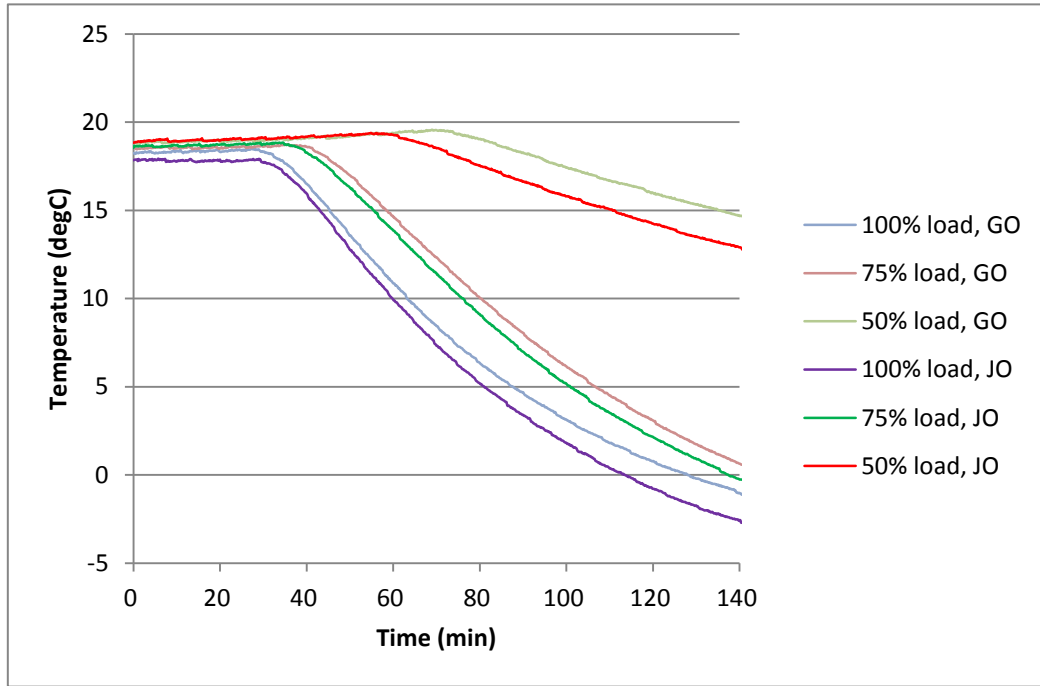


Fig. 4.30 Comparison of freezer temperatures with different exhaust gases and loads

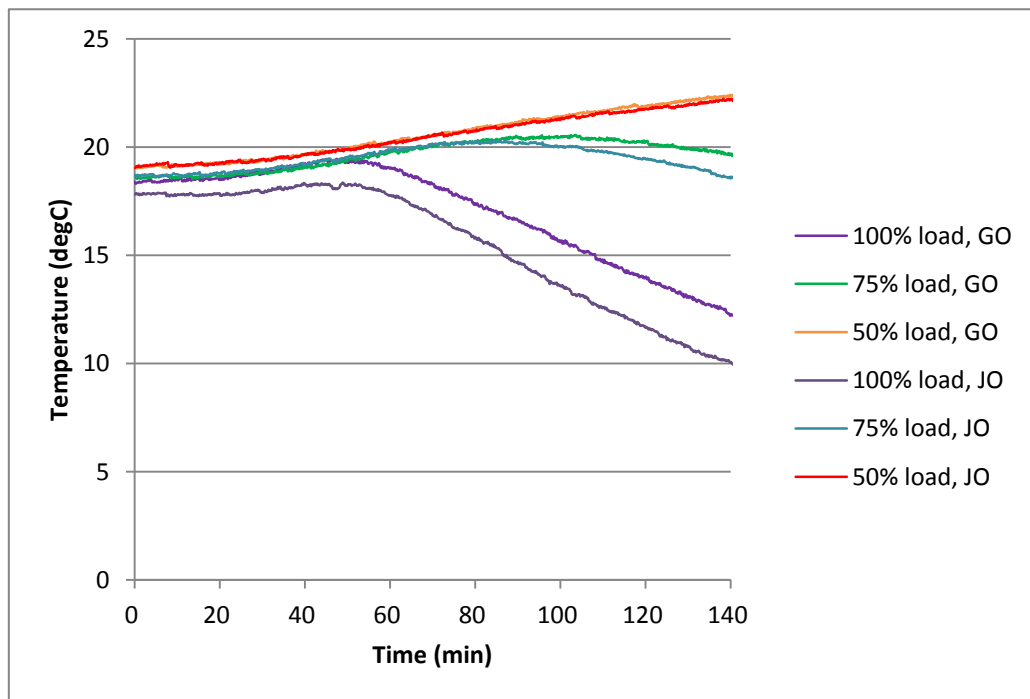


Fig. 4.30 Comparison of food chiller temperatures with different exhaust gases and

loads

The results in Table 4.8 show that when the refrigerator is driven by exhaust gases, the input heats were over two times that when driven by electricity, although less cooling power was produced. Hence, the COPs were lower than 0.03 and approximately one third compared to those using electricity. However, when considering the supply of electricity from the BMT system, it would be more reasonable to evaluate COP from a primary energy consumption point of view, namely, by converting electric power to input fuel energy. Hence, another index of COP' is provided by:

$$\text{COP}' = \text{COP} * \eta_e / 100 \quad (4-7)$$

Where $\eta_e = 26.68\%$ is the average value of the electrical efficiency of the vegetable oils. The input energy Q_h' is hereby given as:

$$Q_h' = Q_h / \eta_e * 100 \quad (4-8)$$

By comparing the calculated results listed in Table 4.10, it can be shown that when powering the refrigerator by electricity, the input fuel energy was much higher than the exhaust gases energy, with a lower COP' of 0.02.

In general, improved cooling effects are observed with the exhaust gas of vegetable oil relative to that of gas oil. By increasing the engine loads and heating power, more cooling power was produced, accompanied by a higher condensing temperature. As a result, the best COP was achieved at 75% load instead of full load.

Heating sources	Electricity			Gas oil			Jatropha oil		
	50	75	100	50	75	100	50	75	100
Load scale or engine loads (%)	50	75	100	50	75	100	50	75	100
Ambient temperature (°C)	20.3	19.8	19.3	18.7	18.2	18.5	18.3	18.2	17.2
Heating temperature (°C)	186.8	186.4	186.2	208.1	241.8	278.1	210.9	243.9	278.6
Time of start cooling (min)	27	25	24	63	33	26	52	31	25
Temperature of evaporator after 2 hours (°C)	-22.4	-24.9	-25.4	-2.3	-20.2	-21.6	-4.6	-22.4	-23.0
Temperature of freezer after 2 hours (°C)	-10.5	-11.3	-11.1	16.0	3.2	0.8	14.3	2.2	-0.7
Temperature of food chiller after 2 hours (°C)	4.9	5.5	-6.3	21.9	20.2	14.0	21.7	19.5	11.7
Temperature of condenser after 2 hours (°C)	28.9	31.0	29.0	33.2	42.7	52.9	33.8	40.5	52.6
Heating power (W)	180.9	181.6	181.4	305.0	364.4	425.3	313.9	372.0	437.0
Input fuel energy (W)	678.0	680.7	679.9	-	-	-	-	-	-
Cooling power (W)	13.8	13.0	15.4	7.1	10.3	10.7	8.9	10.9	11.9
COP	0.076	0.072	0.085	0.023	0.028	0.025	0.028	0.029	0.027
COP'	0.020	0.019	0.023	-	-	-	-	-	-

Table 4.8 Effects of refrigeration with different heating sources and loads

Heating sources	Croton oil			Rapeseed oil			Sunflower oil		
Load scale or engine loads (%)	50	75	100	50	75	100	50	75	100
Ambient temperature (°C)	18.2	20.0	19.3	19.1	19.4	18.6	18.3	18.5	18.8
Heating temperature (°C)	211.5	244.8	282.4	213.6	242.7	284.1	212.3	241.2	281.7
Time of start cooling (min)	56	30	24	55	30	21	53	30	22
Temperature of evaporator after 2 hours (°C)	-4.7	-20.2	-20.8	-2.8	-19.5	-20.2	-4.3	-21.0	-21.5
Temperature of freezer after 2 hours (°C)	11.8	3.0	1.9	14.4	2.8	2.2	13.8	2.4	-0.3
Temperature of food chiller after 2 hours (°C)	20.9	20.2	13.5	22.4	19.7	14.6	21.5	19.1	12.8
Temperature of condenser after 2 hours (°C)	34.8	43.3	54.0	36.0	42.8	54.9	34.2	42.8	53.7
Heating power (W)	319.4	372.6	431.0	317.9	375.4	433.4	316.5	374.3	428.2
Input fuel energy (W)	-	-	-	-	-	-	-	-	-
Cooling power (W)	7.0	9.4	9.7	6.8	9.8	10.4	8.2	10.2	10.8
COP	0.022	0.025	0.022	0.021	0.026	0.024	0.026	0.027	0.025
COP'	-	-	-	-	-	-	-	-	-

Table 4.8 Effects of refrigeration with different heating sources and loads (Renewal)

4.3.4 Cogeneration and trigeneration performance

Fig. 4.32 and Fig. 4.33 show the BSFCs for cogeneration and trigeneration. Due to the recovered heat and cooling energy, the BSFCs for both modes were greatly improved. For trigeneration at full load, the BSFCs were approximately 42% of those for the power generation, while this figure for cogeneration was 40%. Greater improvement rates were found when the load decreased. At 10% load, the BSFCs were only 16-20% of those of the power generation. The BSFCs for the vegetable oils were higher than the gas oil, on average 15% for cogeneration and 16% for trigeneration. This was better than the 18-22% rate for power generation.

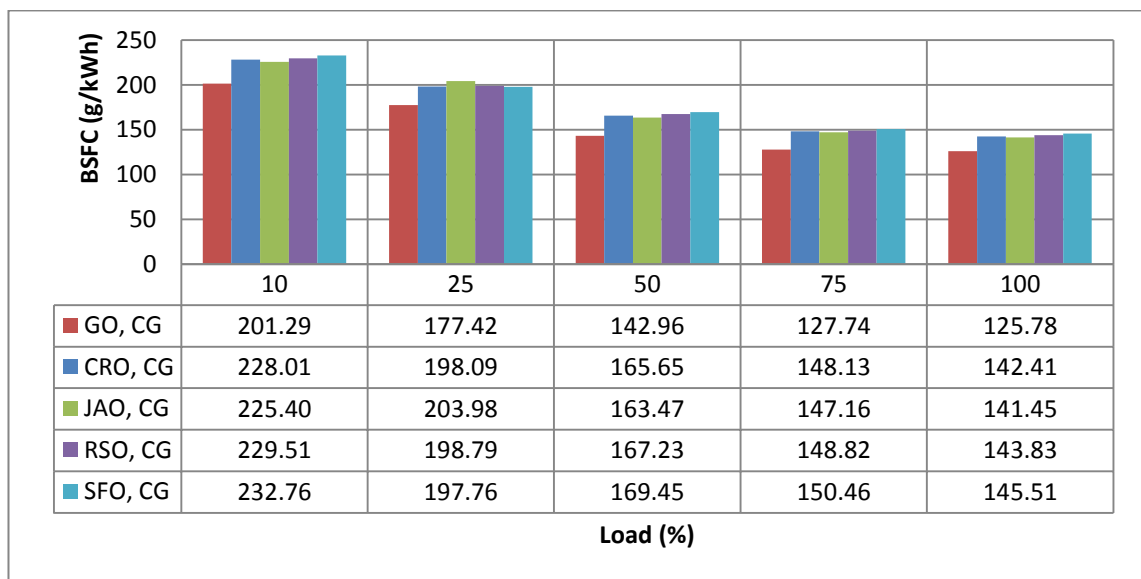


Fig. 4.32 BSFC for cogeneration

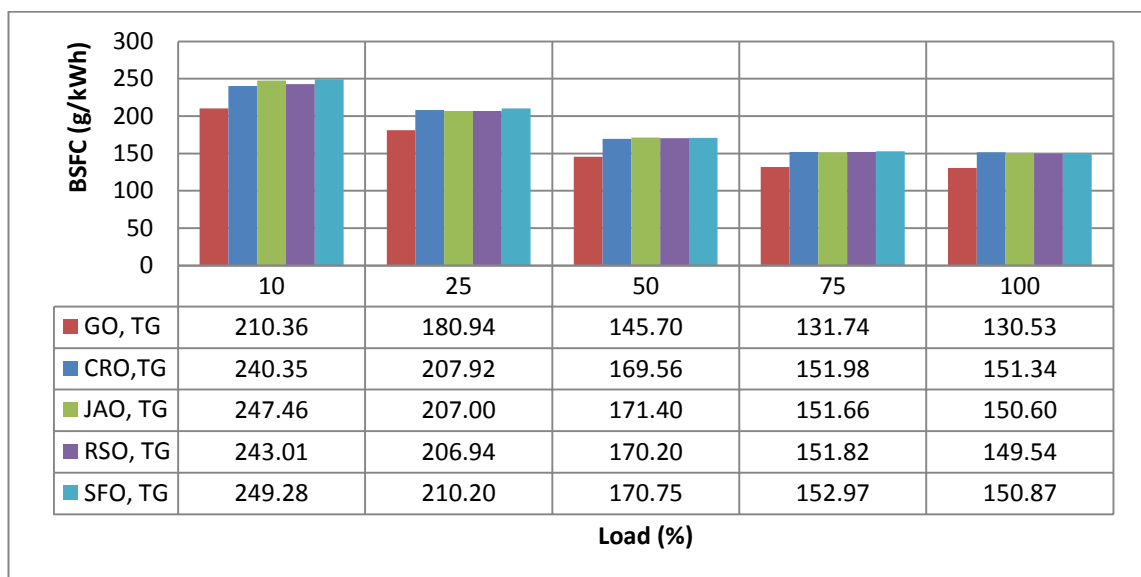


Fig. 4.33 BSFC for trigeneration

Fig. 4.34 and Fig. 4.35 show the BSECs for cogeneration and trigeneration. Improved performance was found in both modes relative to power generation. Due to the similar volumetric energy and additional recovered heating and cooling energy of the vegetable oils, the BSECs of these oils were comparable to those of the gas oil.

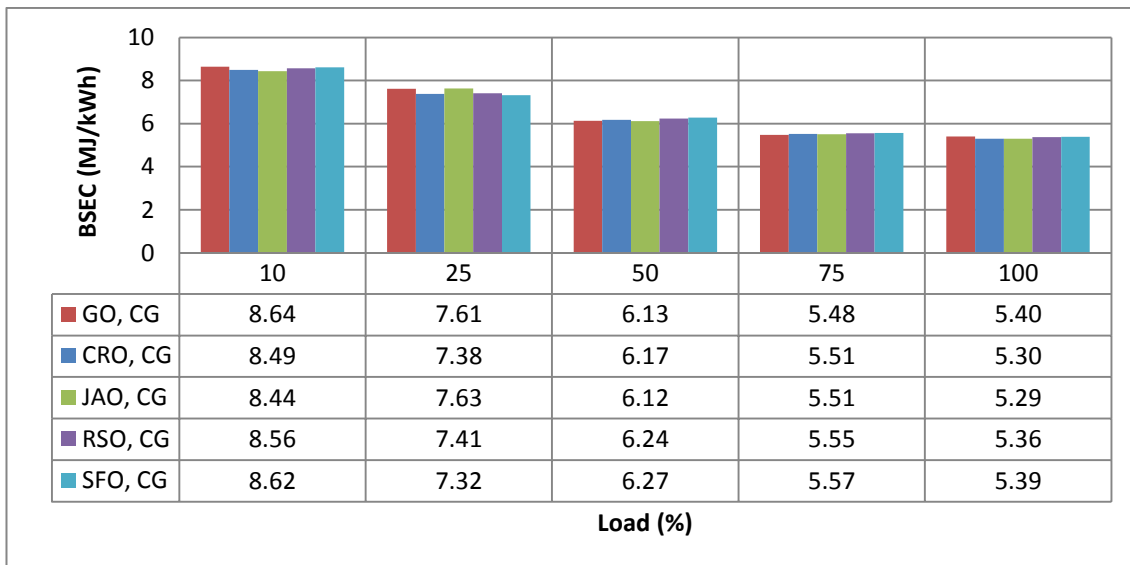


Fig. 4.34 BSEC for cogeneration

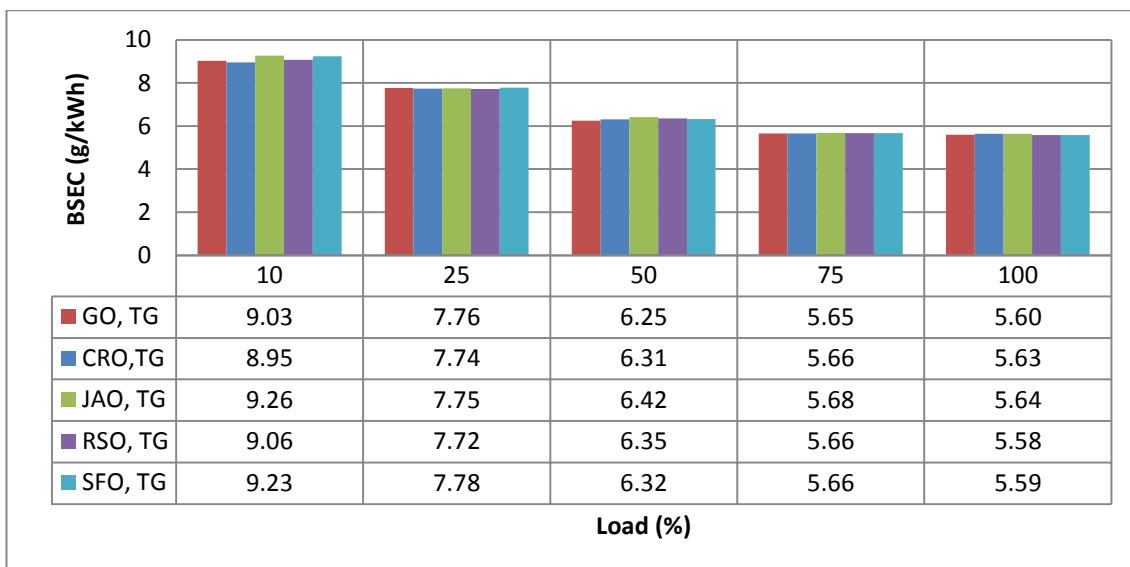


Fig. 4.35 BSEC for trigeneration

Reduced CO₂ emission is one of the great benefits of trigeneration and cogeneration compared to power generation; it forms the basis of a carbon neutral solution using vegetable oil as engine fuel. Fig. 4.36 and Fig. 4.37 show the CO₂ emissions of the oils for cogeneration and trigeneration. The amount of CO₂ emissions were calculated according to the fuel consumption and the mass fraction of carbon in the fuel.

Compared to power generation, the CO₂ emission rate for cogeneration and

trigeneration reduced dramatically. Approximately 58% CO₂ emissions were reduced at full load with trigeneration and this figure increased for cogeneration to around 60%. Due to the higher recovered heating and cooling energy, the CO₂ emissions of the vegetable oils were close to that of the gas oil, only 1-3% higher for cogeneration and 2.5-4% higher for trigeneration.

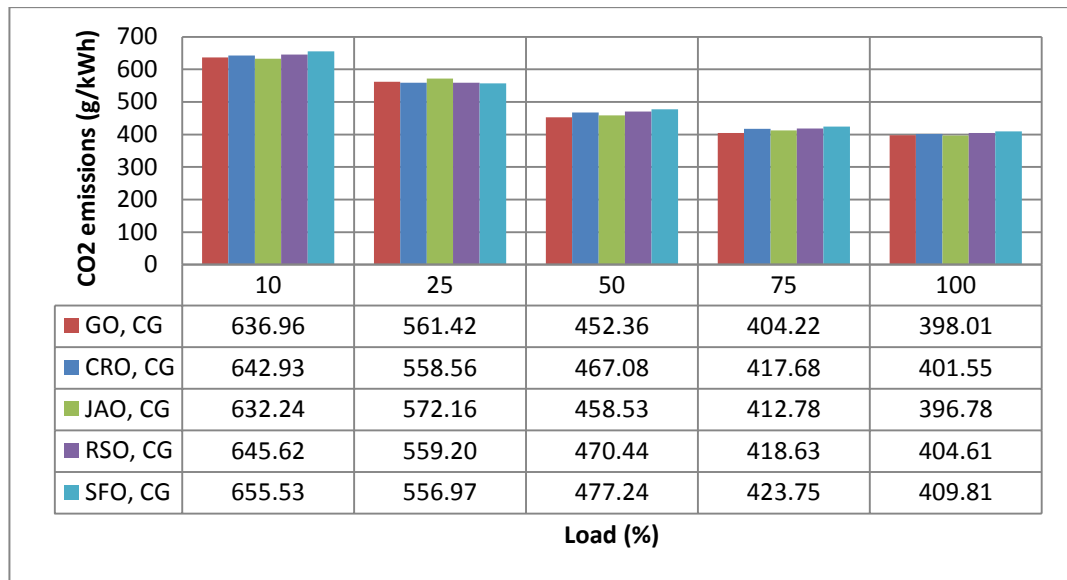


Fig. 4.36 CO₂ emissions for cogeneration

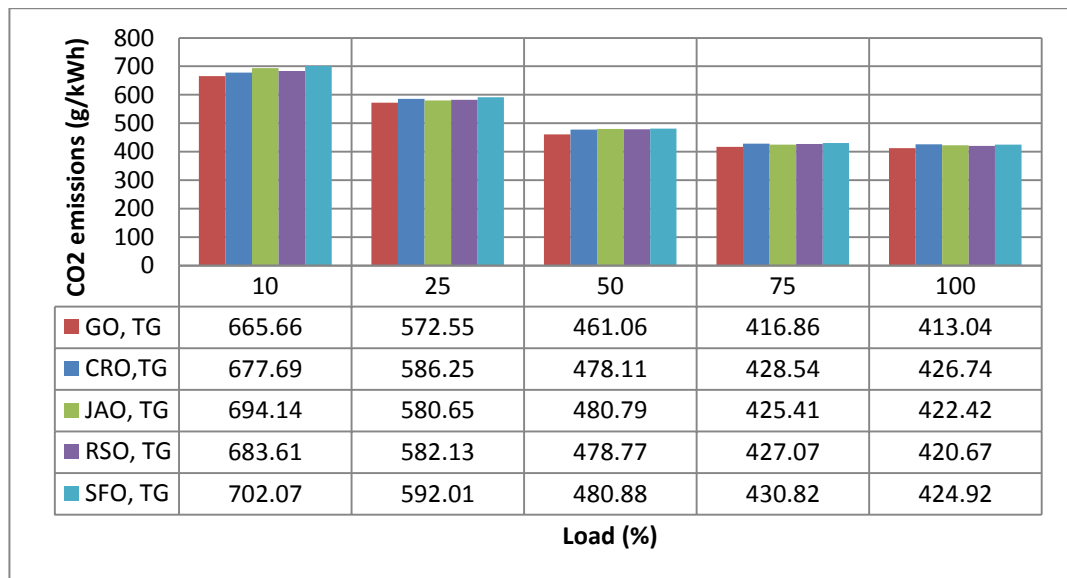


Fig. 4.37 CO₂ emissions for trigeneration

Thermal efficiency is an index used to evaluate the level of fuel energy utilisation. Fig.4.38 and Fig. 4.39 show the overall efficiency of the fuels under CG and TG mode. The overall efficiency of the vegetable oils was comparable to or slightly higher than

that of the gas oil. At full load, the system operated with a maximum efficiency of 68% for cogeneration and 65% for trigeneration. Even at 10% load, the system efficiency was still over 40%. The test results have proved the feasibility of the BMT system running with preheated vegetable oil.

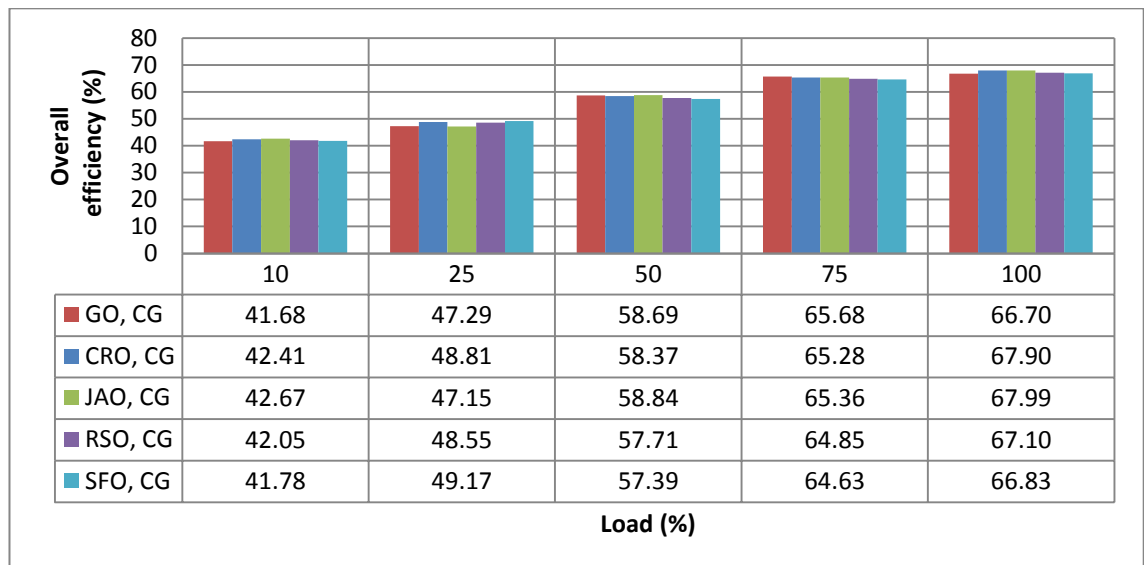


Fig. 4.38 Overall efficiencies for cogeneration

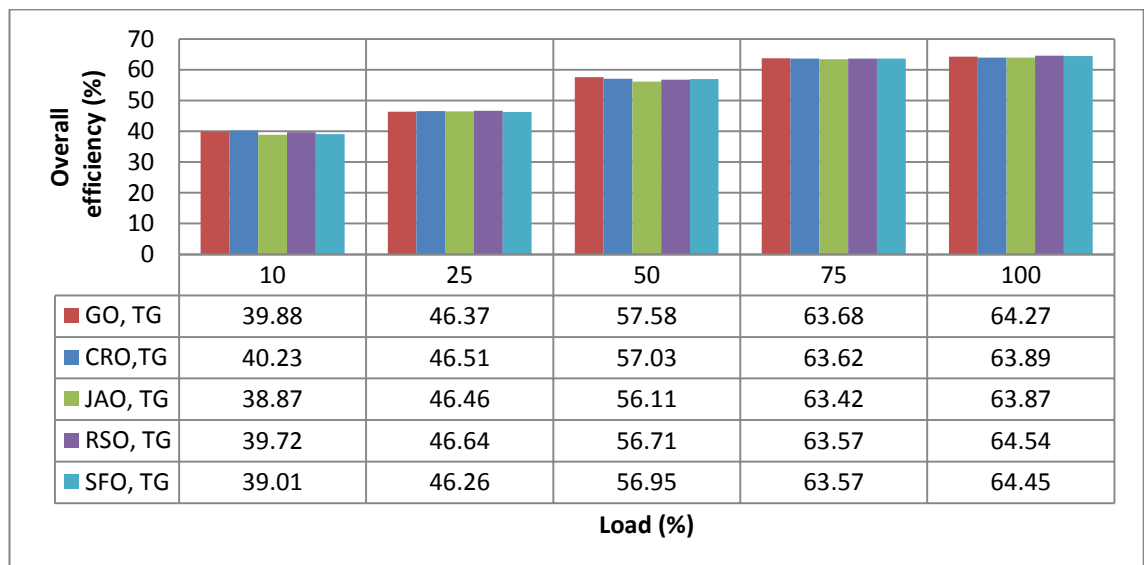


Fig. 4.39 Overall efficiencies for trigeneration

4.3.5 Exergy analysis

The aforementioned thermal efficiency of power generation, cogeneration and trigeneration only provided a quantity point of view of energy consumption and production. To evaluate the value of energy both in terms of quantity and quality, a

parameter of exergy is recommended. Exergy is defined as ‘the maximum useful work of a system during a process that brings the system into equilibrium with a heat reservoir’[144]. When a reference state for the reservoir is chose, the exergy content of a natural material input can be interpreted as a unique quality, such as useful work. In this thesis, all of the recovered heat energy can be transferred into mechanical work by Carnot cycle. The reference temperature is set to 25 °C. For heating cycle, it gives:

$$E_x = Q_{in} \times (1 - T_L / T_H) \quad (4-9)$$

And for cooling cycle:

$$E_x = Q_{in} \times (T_H / T_L - 1) \quad (4-10)$$

Where E_x is exergy, Q_{in} is input energy, T_H is the temperature of hot side and T_L is the temperature of cold side. The calculation of exergy of recovered heat and cooling energy are shown from Fig. 4.40 to Fig. 4.44. They clear show that after conversion, the exergy of the recovered exhaust gas heat, coolant heat were only 10%-13% as those of the heat energy, and this figure increased with the engine loads. This was mainly due to the low water temperatures, only approximately 71 °C for full load and 60 °C for 10% load. The exergy of recovered exhaust gas heat for all of the oils were almost the same, but that of the coolant heat for gas oil was lower than the others. As to the exergy of cooling energy, those figures were so low to be negligible.

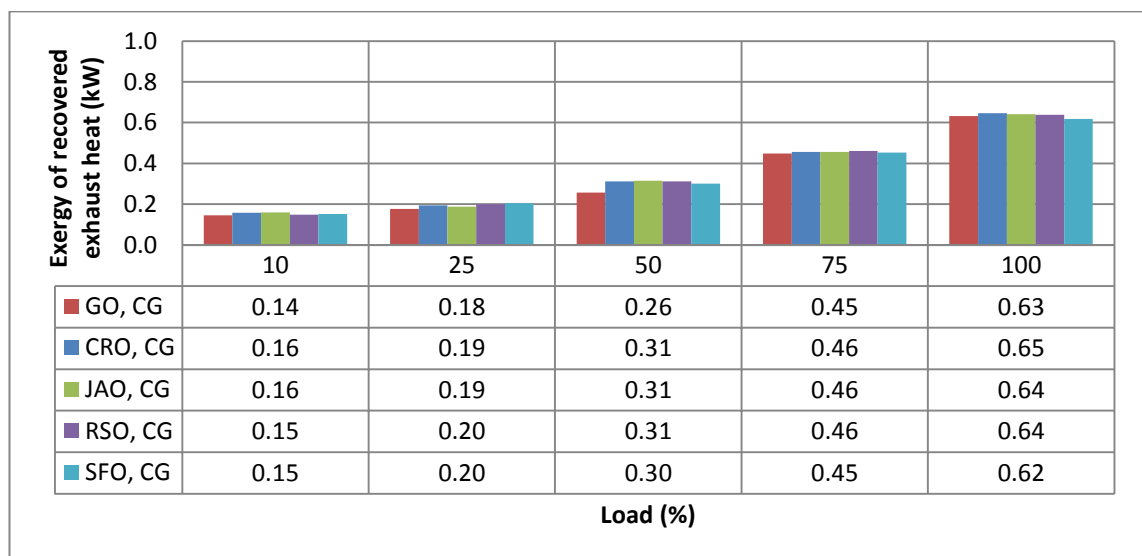


Fig. 4.40 Exergy of recovered exhaust gas heat for cogeneration

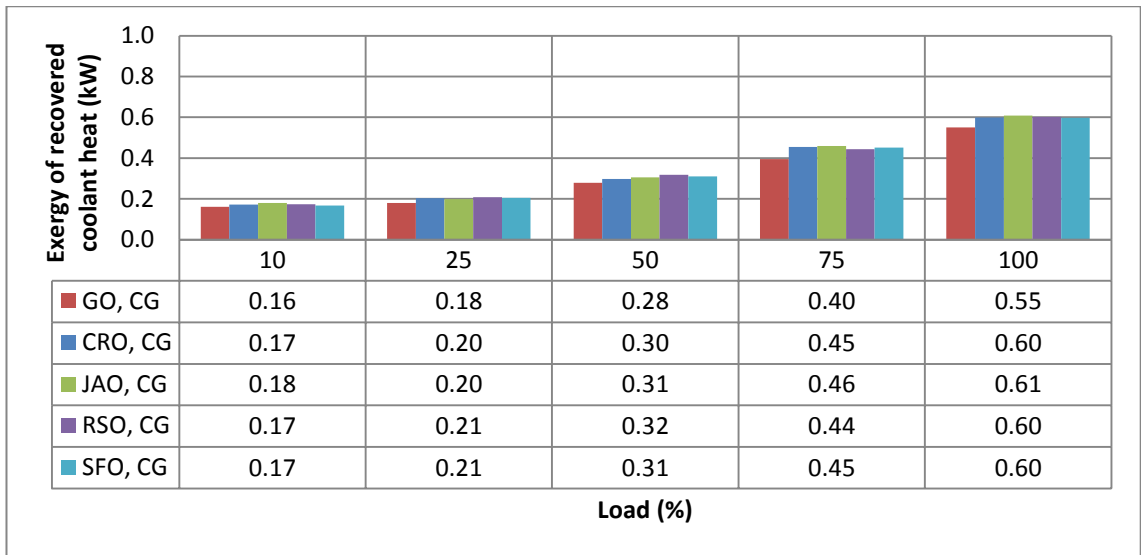


Fig. 4.41 Exergy of recovered coolant heat for cogeneration

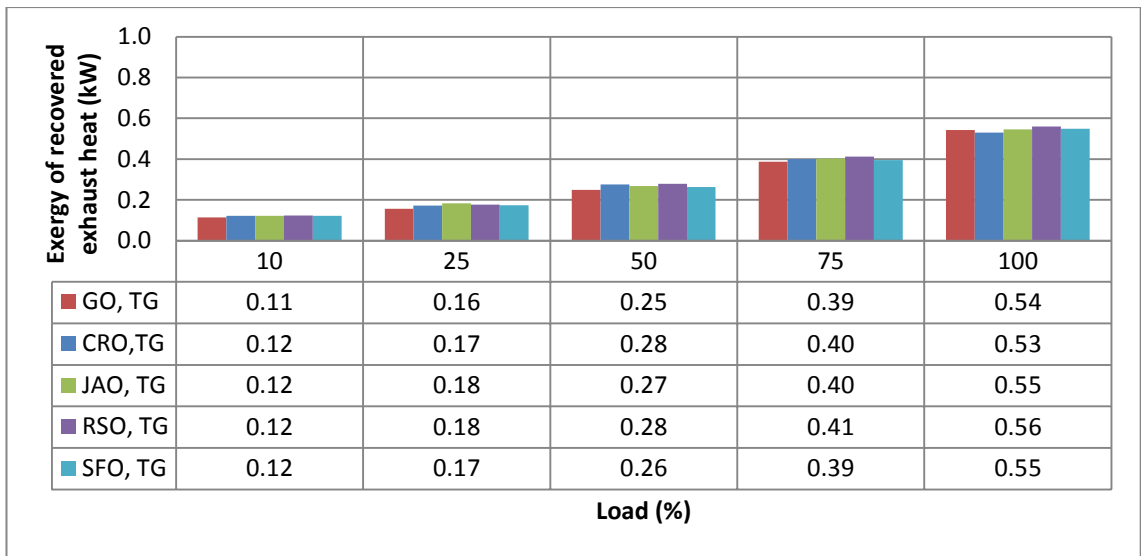


Fig. 4.42 Exergy of recovered exhaust gas heat for trigeneration

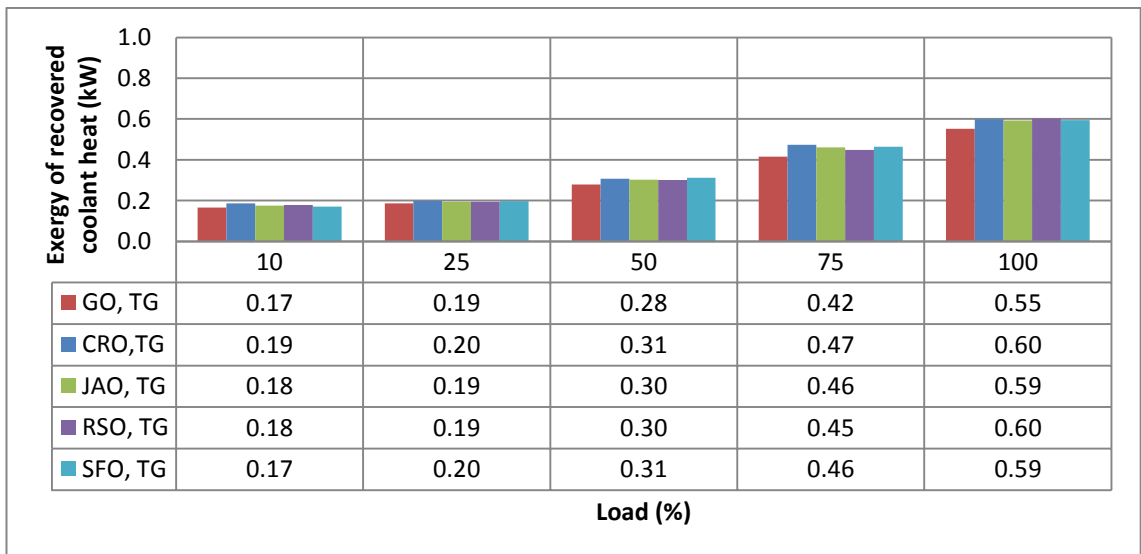


Fig. 4.43 Exergy of recovered coolant heat for trigeneration

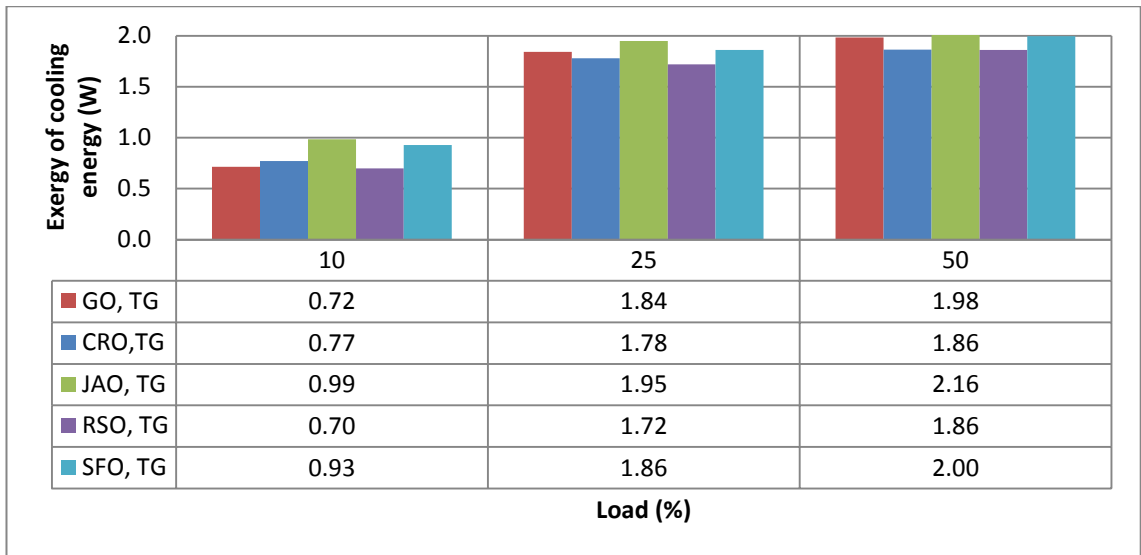


Fig. 4.44 Exergy of cooling energy for trigeneration

As a result, the overall exergy of the trigeneration system can be calculated by summing the electric power and the heating and/or cooling exergy, hence the overall exergy efficiencies of cogeneration and trigeneration are deduced, as shown in Fig 4.45 and Fig. 4.46. Compared to the overall efficiencies shown in Fig. 4.38 and Fig. 4.39, it can be seen that those figures for full load were only as half of the overall efficiencies, and for 10% load, less than 30%. According to Eq. 4-9, the higher the hot side temperature, the much the exergy is. Hence to improve exergy efficiency, one of the important ways is to convert as much high grade heat, i.e., the exhaust gas energy into mechanic energy as possible. For example, by turbocharging, part of the exhaust as energy can be recovered before it goes through the heat exchanger; so that the trigeneration efficiency can be improve both in quantity and quality.

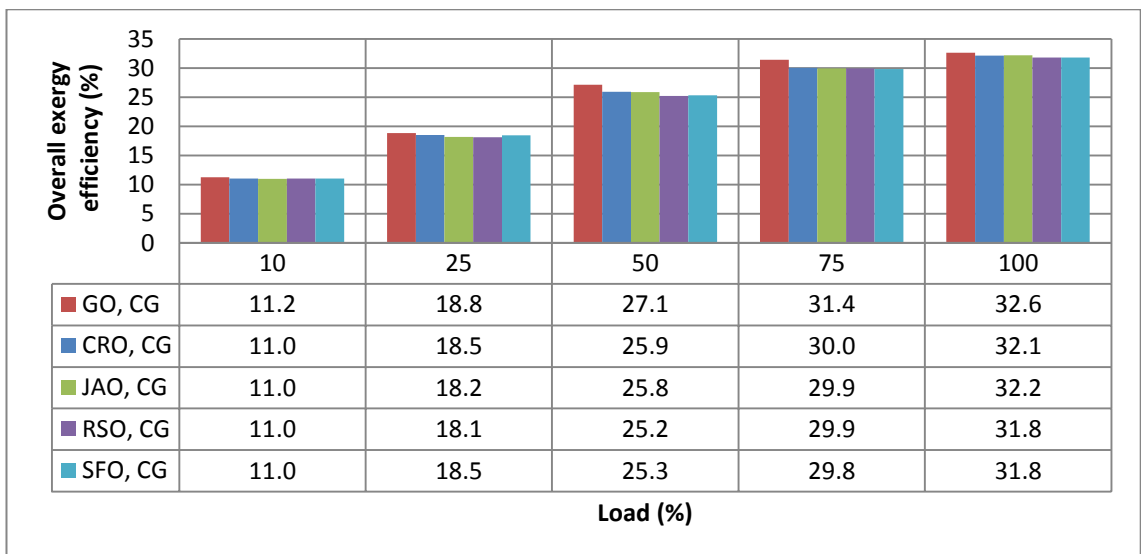


Fig. 4.45 Overall exergy efficiencies for cogeneration

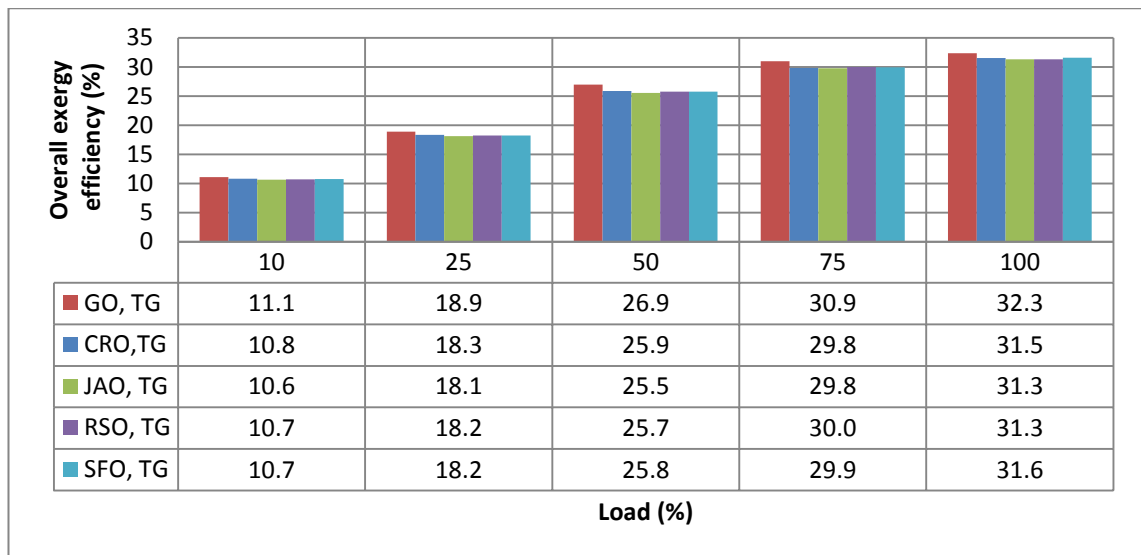


Fig. 4.46 Overall exergy efficiencies for trigeneration

4.4 Conclusions and discussions

This chapter discusses the experimental studies of physicochemical properties and the trigeneration performance of four vegetable oils when compared to that of gas oil. The test results have proved the feasibility of using preheated vegetable oil for driving a micro-trigeneration system. Some conclusions were drawn from the above results and summarised as follows:

- a) Major differences in physicochemical properties were found with the vegetable oils relative to gas oil. Higher viscosity and less HHV are the drawbacks and the major factors which deteriorated their performance in the engine. Nevertheless, higher density and higher oxygen concentration in the oils improve the combustion and made up for their performance.
- b) On average 18-22% higher fuel consumption was observed when the BMT system was operated with the preheated vegetable oils for power generation, with 8-10°C higher exhaust gas temperature. The highest electrical efficiency was around 27% when run with the vegetable oils. When evaluated by BSEC and electrical efficiency, about 5% higher input fuel energy and 0.5-1% less efficiency was discovered, which indicated a comparable performance of the vegetable oils to that of the gas oil.
- c) Due to the higher fuel consumption, higher CO₂ emissions were found. There was and also higher CO emissions except for operating at full load. Less NO_x and HC emissions were observed at part loads, especially for 10% and 25% loads. However, this trend was reversed for 75% and 100% loads.

- d) For cogeneration and trigeneration, the recovered exhaust gas heat and coolant heat with the vegetable oils were both higher than those of the gas oil and also the total recovered heat. The recovered coolant heats were higher than the recovered exhaust gas heat at almost all loads, and it was found that a high exhaust gas temperature occurred at the outlet of the heat exchanger. This indicated that further improvements can be made to recover a greater amount of heat. To drive the absorption refrigerator for trigeneration, about 0.3-0.6kW less exhaust gas heats was recovered compared to those of the cogeneration.
- e) To generate cooling effects when run by electricity, the refrigerator was controlled by an on-off control action. For part load scale operation, shorter heating times and longer heating intervals were applied. The consumed heating power was 181W with around 14W of cooling power produced and a COP of 0.08. However, when evaluating from a primary energy consumption point of view, the input energy was much higher than that of the exhaust gases, and the COP was reduced to 0.02, lower than the value of 0.025 with exhaust gases. Improved cooling effects were observed with exhaust gas of vegetable oil relative to that of gas oil. The best COP was achieved at 75% load instead of full load.
- f) Major improvements were found with cogeneration and trigeneration in terms of BSFCs, CO₂ emission and the overall efficiency. On average only 40% and 42% of that of the power generation figures. The fuel consumptions of the vegetable oils were still higher than that of the gas oil, 15% higher for cogeneration and 17% higher for trigeneration. Concerning the CO₂ emission, only a 1-3% higher rate was found with the vegetable oils for cogeneration, and a 2.5-4% higher rate for trigeneration. Nevertheless, the BSECs and the overall efficiency of the fuels were comparable, with the highest efficiency approximately 68% for cogeneration and 65% for trigeneration.
- g) Exergy analysis shows that the exergy of the recovered heat and cooling energy were poor and the overall exergy efficiencies for full load were only as half of the overall efficiencies. It is recommended to convert high grade heat into mechanic energy rather than directly recovering it in form of hot water.

Chapter 5. Modelling and Simulation

5.1 Introduction

With the development of computer science, computer aided modelling and simulations have been applied in many research fields. This has provided many benefits in the process of design, analysis and optimisation which been proved to be effective, efficient and helped in cost saving.

This chapter describes how an engine model was setup based on the Yanmar diesel engine, using DIESEL-RK software to simulate and predict the engine performance and emissions. Some options were investigated to optimise the engine performance. A further micro-trigeneration model was programmed using Dymola (Dynamic Modelling Laboratory) software that is used for multi-engineering system modelling and simulation. The experimental data of the trigeneration system was used as the input. The dynamic performance of the trigeneration system used two fuels and was simulated over a 24 hour scenario of domestic electrical consumption.

5.2 Engine modelling and investigation strategy

5.2.1 DIESEL-RK software and engine model

The simulation of the working processes involved on the internal combustion engine has significantly progressed since the late 1960s. The simulation of the ICE is used to describe its behaviour and status of the in-cylinder working media with the synthesis application of thermodynamic, fluid mechanics, heat and mass transfer and chemical reaction dynamics, etc. The combustion process is the most important phase for the whole engine cycle.

Various computer models are proposed to help study the transient process of the engine operation. Based on energy conservation and fluid motion, two basic models have been developed for the process governed engine combustion and emission, in terms of thermodynamic and fluid dynamic properties. A thermodynamic energy conservation-based model can be categorised as a zero-dimensional and quasi-dimensional type. While a fluid dynamic based model can be classed as a multidimensional model [145, 146].

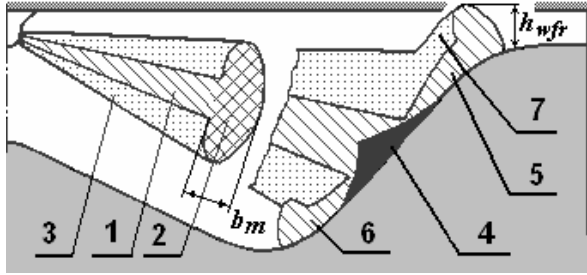
A Zero-dimensional model treats the in-cylinder working media as a uniform measurement and takes no consideration of the flow field dimensions, hence it is 'single zone' and 'zero dimensional'. This model can be applied to a heat release rate calculation based on a foregone indicator diagram or for an engine performance prediction by empirical heat release discipline. However, the accuracy of zero-dimensional models greatly depends on the empirical coefficient and thus cannot reflect in-cylinder fluid flow [145, 147]. A commercial software package used to adopt this type of model is WAVE BUILD by Ricardo Software and GT-Power developed by Gamma Technologies and Inc. (GTI), etc.

A quasi-dimensional model takes geometric features into account and divides in-cylinder space into several areas, thus it can predict the variations of state parameters in each area and simulate emission models. This model cannot fully reveal the mechanism of combustion and substantial empirical parameters must still be used [147, 148]. DIESEL RK and BOOST developed by AVL are two typical software packages to apply this model.

A multidimensional model describes combustion both in time and in two or three dimensions by solving integrated conservation equations within sub-models. Thus, the details of fluid velocity, temperature and fluid compositions distributed in a cylinder can be achieved [149, 150]. Software packages based on this model include WAVE BUILD 3D, AVL FIRE, KIVA by Los Alamos National Laboratory and STAR-CD by CD-adapco.

DIESEL-RK is a software toolkit for thermodynamic engine simulation and optimisation; both for two and four stroke, boosted or naturally aspirated internal combustion engines. It provides a wizard for quickly creating a new engine model with the most common data. Features of the software include: a multi-zone RK-model for the simulation of air-fuel mixture formation and combustion; a multi-parametric and multi-dimensional optimisation tool for simultaneously optimising engine parameters, such as NO_x , soot, SFC, etc.; and a fuel spray evolution visualisation tool which allows researchers to choose the most suitable fuel injection and combustion system parameters [151].

The fuel spray combustion model for diesel engines in DIESEL-RK uses Razleytsev's method, this takes into account free spray and impingement. The free spray model is divided into three zones: the dense conical core, the dense front and the dilute outer sleeve. Near wall flow (NWF) is simulated using four zones: the dense conical nucleus, the dense NWF on piston surface, the dense front and the dilute outer sleeve of the NWF (Fig. 5.1) [152].



1-The dense conical core, 2 –The dense forward front, 3-The dilute outer sleeve. 4-The axial conical core of the NWF, 5-The dense core of the NWF on the piston bowl surface, 6-The dense forward front of the NWF, 7-The dilute outer zone of the NWF.

Fig. 5.1 Characteristic zones of diesel spray

The droplet evaporation rate during injection and combustion progress is calculated by:

$$dc^2 = d_{32}^2 (1 - b_i \times t_e) \quad (5-1)$$

Where d_c is current drop diameter, d_{32} is the Sauter Mean Diameter, t_e is the evaporation time and b_i is the evaporation constants. The ignition delay τ_i is determined by the integration of the Livengood-Wu relation [145, 153]:

$$\int_0^{t_i} \frac{1}{\tau_{id}} dt \geq 1 \quad (5-2)$$

Where τ_{id} is calculated by the CHEMKIN calculation proposed by the developer of the DIESEL-RK, which uses a 4D map of ignition delay calculated with CHEMKIN for varied temperature, pressure, EGR and air/fuel ratio [154].

NO_x consists of NO and NO_2 . Most NO_2 is formed from the NO molecule after combustion, hence the simulation of NO_x formation is often simplified to the formation of NO [145]. The extended Zeldovich mechanism [155, 156] is used to simulate the thermal formation of the nitric oxide by three chemical equations. The reaction below is the main factor for NO formation.



$$k_{i,f} = 7.6 \cdot 10^{13} \exp(-38000/T) \quad (5-$$

4)

Where T is the reaction temperature and $k_{i,f}$ is the forward reaction rate constants in $\text{cm}^3 / (\text{mol} \cdot \text{s})$ [157]. Considering that the rates of reverse reactions are small and usually negligible, the NO change rate can be simplified to:

$$\frac{d[NO]}{dt} = 2k_{i,f} [N_2][O] \quad (5-5)$$

Where [NO], [N₂] and [O] are the equilibrium concentration levels of each chemical composition [158].

The particulate matter (PM) emission consists of many properties, in which soot is the main fraction. Alkidas formula [159] is one of the most popular expressions for predicting the PM emission as a function of the Bosch smoke number:

$$PM = a_{PM} \cdot 565 \left[\ln \left(\frac{10}{10 - Bosch} \right) \right]^{1.206} \quad (5-6)$$

Where a_{PM} is a correction coefficient, by default $a_{PM} = 1$. The Bosch smoke is the function of Hartridge smoke and soot, where the later was modelled by Razleytsev [160].

To the author's best knowledge, limited documentation has been reported on DIESEL-RK, especially relating to raw vegetable oil simulation. Nevertheless, the open literatures have verified that the simulations using DIESEL-RK matched that of the experimental data [161-163]. Hence, it was chosen for predicting the engine performance and emissions on this study.

5.2.2 Estimation of fuel properties

The fuel choice for this study is croton oil. It is one of the inedible vegetable oils which can be easily prepared from the seeds of croton megalocarpus, a tree widely populated

in East Africa. Croton megalocarpus has been reported to be non-competitive to food crops and is usually irrigated and free from fertilisers. Its seeds contain high oil-content and are harvested easily. For these reasons, it is considered as a promising feedstock for biofuel in Africa [135, 164].

The temperatures of the croton oil were set to 30°C (unheated), 60°C and 90°C before it was injected into the cylinder. The major fuel properties required as inputs in DIESEL-RK are listed Table 5.1. Except for the croton oil data taken from Chapter 4 (elementary compositions and dynamic viscosities) and references (sulphur fraction and cetane number), the rest is based on calculations described below:

- a) Lower heating value. According to the equations 4-1 and 4-2, LHV is affected by fuel temperature. Hence, the LHVs of the croton oil listed in Table 5.1 are calculated by these equations
- b) Density ρ . This changes with temperature and is determined by the equation below:

$$\rho = \frac{\sum m_{fai}}{\sum V_{fai}} \quad (5-7)$$

Where m_{fai} and V_{fai} are the masses and volumes of the fatty acids. The mass fractions of the fatty acids are provided in Table 4.3, and the molar volume of each fatty acid V_{Mfai} can be calculated using the equations proposed by Hammond and Lundberg [165]. For saturated and monounsaturated fatty acids, the equation is given as:

$$V_{Mfai} = 16.54 \times C - 6.65 \times D + 26.09 + (0.006 \times C + 0.0085) \times (T - 20) \quad (5-8)$$

And for polyunsaturated fatty acids:

$$V_{Mfai} = 16.54 \times C - 6.87 \times D + 26.09 + (0.006 \times C + 0.0085) \times (T - 20) \quad (5-9)$$

Where C is the carbon atoms number; D is the double bonds number of fatty acid chain; T is the fuel temperature in °C. Hence V_{fai} is given as:

$$V_{fai} = V_{Mfai} \times m_{fai} / M_i \quad (5-10)$$

Where M is the molar mass of fatty acid.

- c) Surface tension γ . This is the outward manifestation of cohesive forces among liquid molecules and is temperature dependent [166]. Generally, it decreases with an increase in temperature. Some empirical equations have been proposed for the relationship [167, 168], among which a Guggenheim-Katayama equation is given by:

$$\gamma = \gamma^0 \times \left(1 - \frac{T}{T_{C0}}\right)^n \quad (5-11)$$

Where γ^0 is a constant for liquid and $n=11/9$ is an empirical factor for organic liquids. T_{C0} is the critical temperature when surface tension reaches zero. A reference figure for the average value of a number of vegetable oils at 20°C [169] is used for the calculation of surface tension of croton oil.

- d) Molar mass of fuel M_f . This can be calculated by dividing the mass of the croton oil by the sum of the molar fraction of the fatty acids, provided by the equation:

$$M_f = \frac{\sum m_{fai}}{\sum (m_{fai}/M_{ai})} \quad (5-12)$$

- e) Critical pressure p_C and critical temperature T_C . The values of these two parameters of fatty acids have been well studied [170-172] and a number shown in Table 5.1. The values of the croton oil are calculated as a molar weight average of the fatty acids:

$$p_C = \sum p_{Ci} \times X_i \quad (5-13)$$

$$T_C = \sum T_{Ci} \times X_i \quad (5-14)$$

Where p_{Ci} and T_{Ci} are the critical pressure and critical temperature of a fatty acid. X_i is the molar fraction of each component.

- f) Saturated vapour pressure. Ndiaye et al. [173] conducted vapour pressure tests on soybean oil, castor oil and biodiesel. They proposed a regression equation to determine the saturated vapour pressure p_s in Pa at a specified temperature T in K, which is shown below.

$$\ln(p_s) = a + b/(c+T)$$

(5-15)

Where a, b and c are the coefficients. For soybean oil: a= 11.4785, b= -708.72 and c= -167.48. It is noted that at a high temperature of 353.2K, the vapour pressure of the two vegetable oils are almost identical. For this reason, the equation and the coefficients are also used to estimate the saturated vapour pressure of the croton oil.

Fuel		Croton oil		
Mass composition (%)	C	76.9		
	H	11.6		
	O	11.5		
Sulphur fraction (%)		0.001[135]		
Lower heating value (MJ/kg)		37.05 @ 303 K	37.13 @ 333 K	37.22 @ 363 K
Cetane number		40.7 [174]		
Density @ 303 K (kg/m ³)		890.6		
Surface tension @ at 323 K (N/m)		0.032		
Dynamic viscosity @ 323 K (Pa.s)		0.0186		
Molar mass (kg/kmol)		279.4		
Saturated vapour pressure @ 480 K (bar)		0.1		
Critical pressure (bar)		13.264		
Critical temperature (K)		819		

Table 5.1 Physicochemical property of croton oil and diesel fuel

Fatty acids	p _c (bar)	T _c (K)
C12	19.22	756.21
C14	16.35	779.07
C16	14.08	799.89
C16:1	14.71	800.34
C18	12.25	819

C18:1	12.76	819.41
C18:2	13.31	819.82
C18:3	13.89	820.23
C20	10.76	836.65
C22	9.52	853.06

Table 5.2 Critical pressures and critical temperatures of fatty acids

5.2.3 Investigation strategy

During the simulation, the engine speed was set to 2400rpm, and the engine loads chosen for the study were the same as those used on the experimental study. For validation purposes, the experimental data of the electrical power was converted to engine power and compared to the experimental results. The electrical efficiency of the generator at full load was 0.78 with power factor value of 1. The diagram illustrates the efficiency of the generator at different loads and is shown in Appendix A.19. The generator was connected to the engine by a belt and the efficiency of the belt transmission was set to 0.945. The comparison of the electrical power and the engine power is listed in Table 5.3.

Load (%)	Electrical power (kW)	Engine power (kW)
10	0.650	0.990
25	1.625	2.397
50	3.250	4.555
75	4.875	6.538
100	6.500	8.818

Table 5.3 Comparison of the electrical power and the engine power

The model was validated against the experimental data of the croton oil preheated to 90°C, by using five loads ranging from 10% to 100%. The engine performance and emissions with the same fuel consumption were simulated at fuel temperatures of 30°C (unheated) and 60°C and compared to those of the oil preheated to 90°C.

5.3 Engine simulation and prediction

5.3.1 Validation of the engine model

The validation was carried out against the test results in terms of engine power, BSFC, CO₂ and NO_x emissions. Due to the conversion of electrical power to engine power, the BSFC and CO₂ emission values displayed in the figures were all re-calculated and were lower than those of the electrical power generation data, except for the NO_x emissions (ppm).

Fig 5-2 and Fig 5-3 illustrate the comparisons of the first two factors and Fig 5-4 depicts the deviations between them. Generally, the simulation results satisfactorily match the engine test bed data. The deviations of engine power increased with the decrease of loads. For loads varying between 50% and 100%, the deviations were within the range of $\pm 1.5\%$. Even for 10% load, this figure was only 4.17%. As a result, this deviation figure was only 4.17%. As a result, the simulated BSFCs were lower than the test data, except at full load when the deviations fell in the range from -3.56% to -0.25%. Both the standard deviations were well within the acceptable range $\pm 5\%$, accurate enough for the performance prediction.

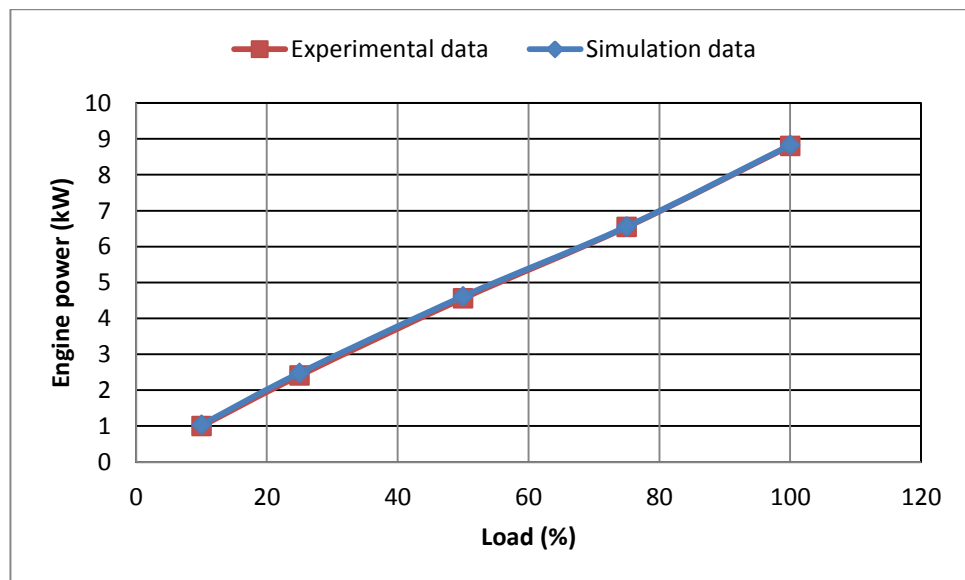


Fig. 5.2 Comparison of tested and simulated engine power

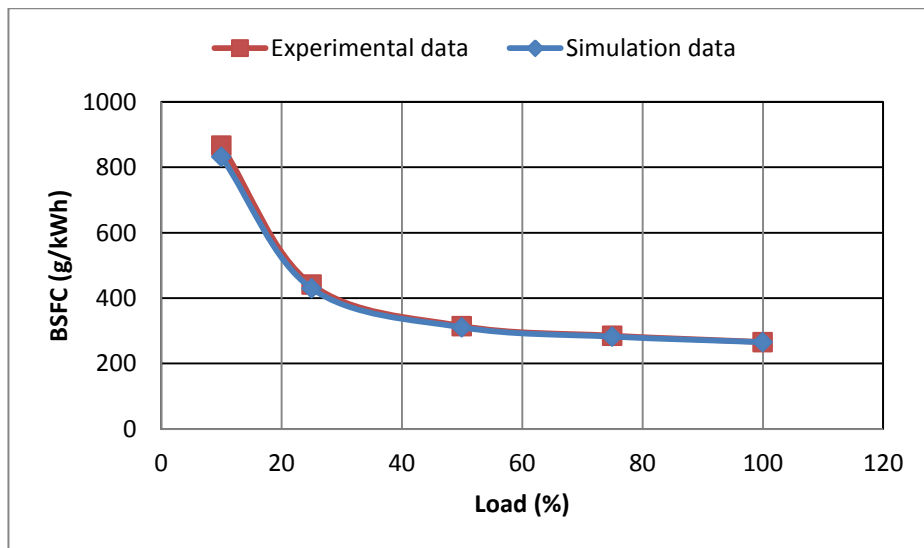


Fig. 5.3 Comparison of tested and simulated BSFC

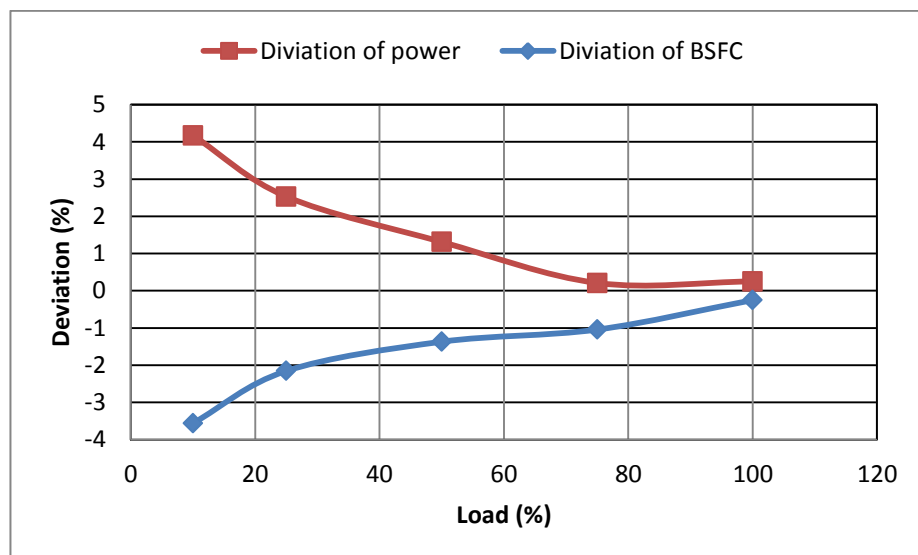


Fig. 5.4 Deviation of engine power and BSFC

Fig 5-5 and Fig 5-6 show the comparison of CO₂ and NO_x emissions and Fig 5-7 depicts the deviations between them. The CO₂ emission was affected by the fuel consumption and engine power output, hence, the deviation of the simulation results reflect the trends of both factors but with less variation at low load. The maximum deviation was found to be -2.08% at 10% load. The simulation results of NO_x emission in DIESEL-RK was mainly affected by the air-fuel equivalence ratio in burning zones. After validation, the minimum deviation value of 2.4% was discovered with 75% load, while the maximum value was found to be 5.83% with 10% load. Considering the complexity of NO_x formation in a real combustion process and the fact that it was hard to predict accurately, this validation result is acceptable.

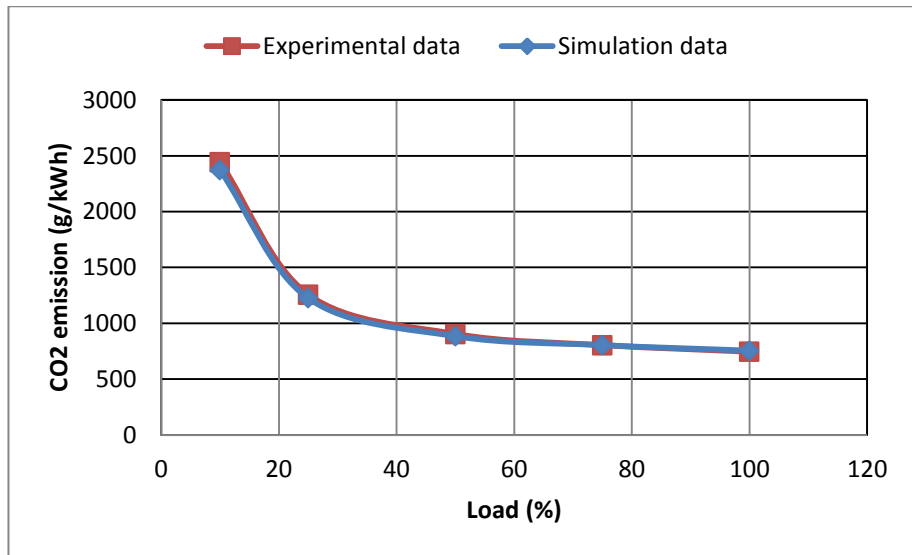


Fig. 5.5 Comparison of tested and simulated CO₂ emissions

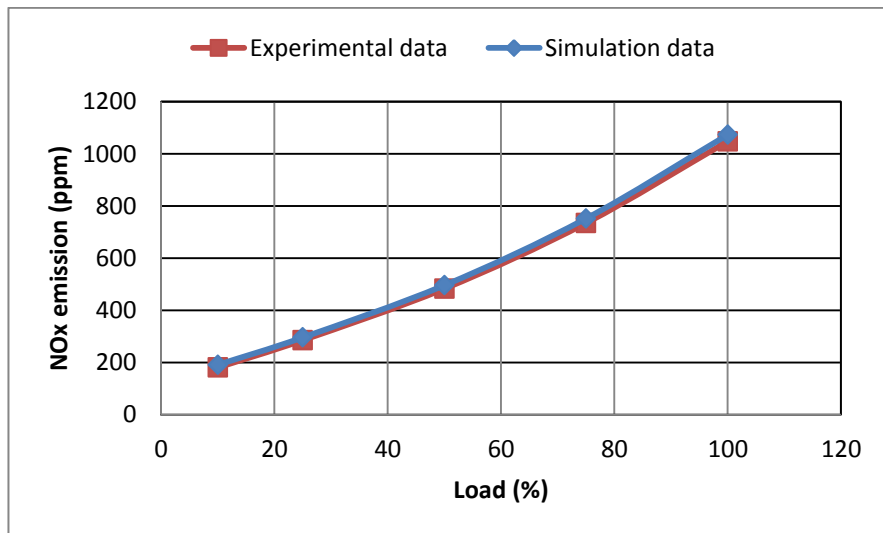


Fig. 5.6 Comparison of tested and simulated NO_x emissions

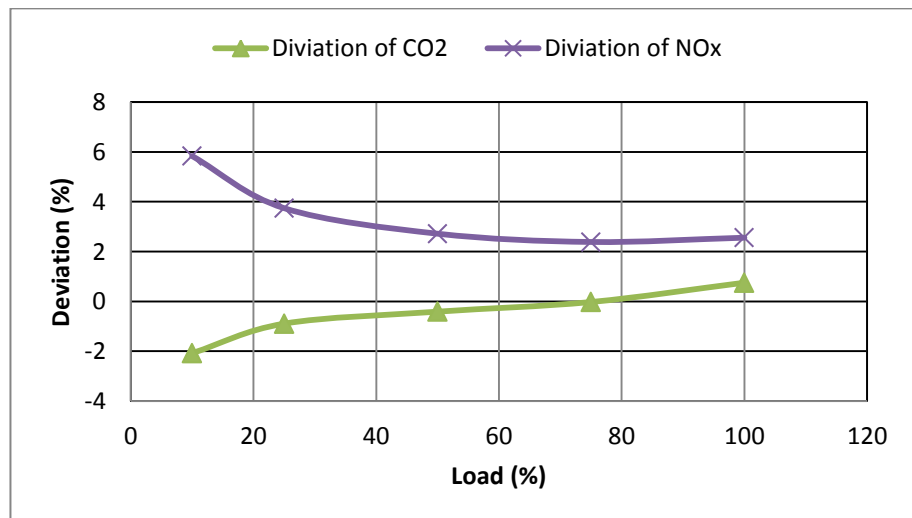


Fig. 5.7 Deviation of CO₂ and NO_x emissions

5.3.2 Engine performance and emissions predictions

5.3.2.1 Engine performance predictions

Fig. 5.8 and Fig. 5.9 compare the engine power and BSFC of the croton oil with different preheating temperatures. The engine power increased with an increase in the preheating temperature. At full load, the engine power with a fuel temperature of 30°C was 8.58kW, and for the fuel temperature of 90°C was 8.83kW, an increase of 2.8%. Accordingly, the BSFC decreased from 272.7 g/kWh to 265.1g/kWh. Analysis of the simulation results highlighted that the ignition delay period was shortened with an increasing preheating temperature. This value at full load for a fuel temperature of 30°C was 10.3 °CA and decreased to 9.0 °CA for a preheating temperature of 90°C. The peak combustion pressure and temperature increased as shown in Fig. 5.10 and Fig. 5.11.

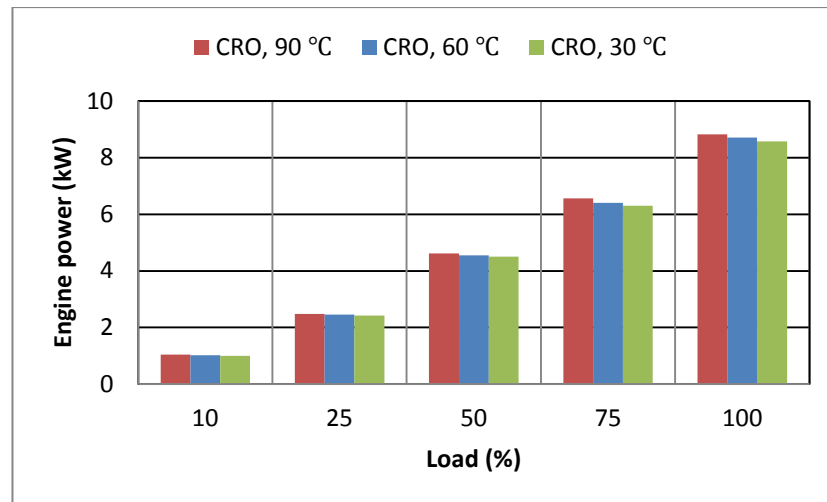


Fig. 5.8 Preheating temperature dependent engine power

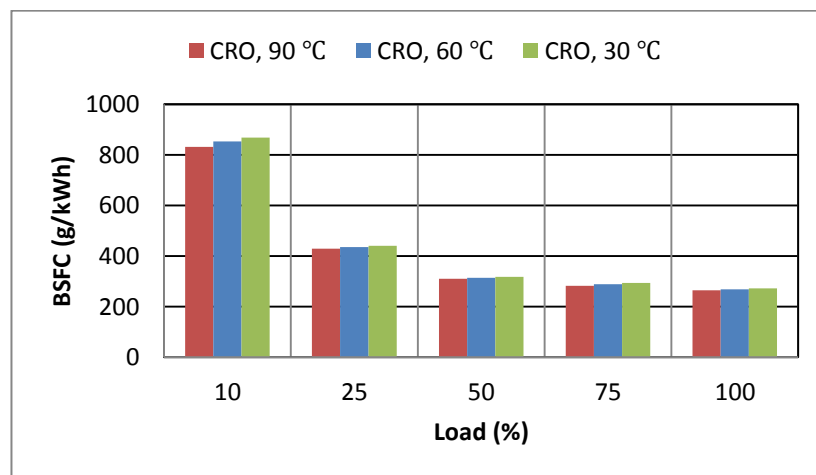


Fig. 5.9 Preheating temperature dependent BSFC

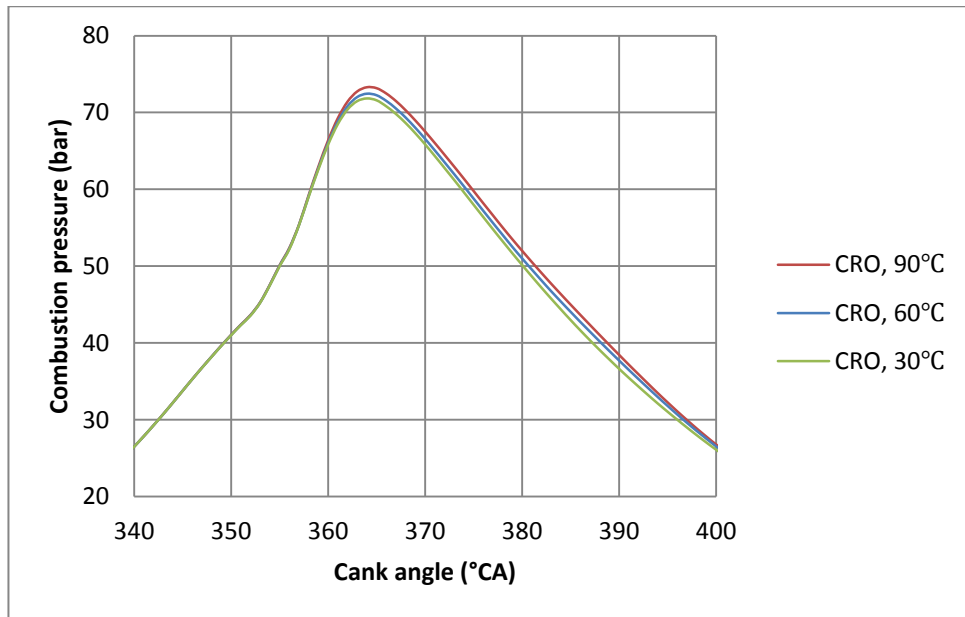


Fig. 5.10 Comparison of combustion pressures at full load with different preheating temperatures

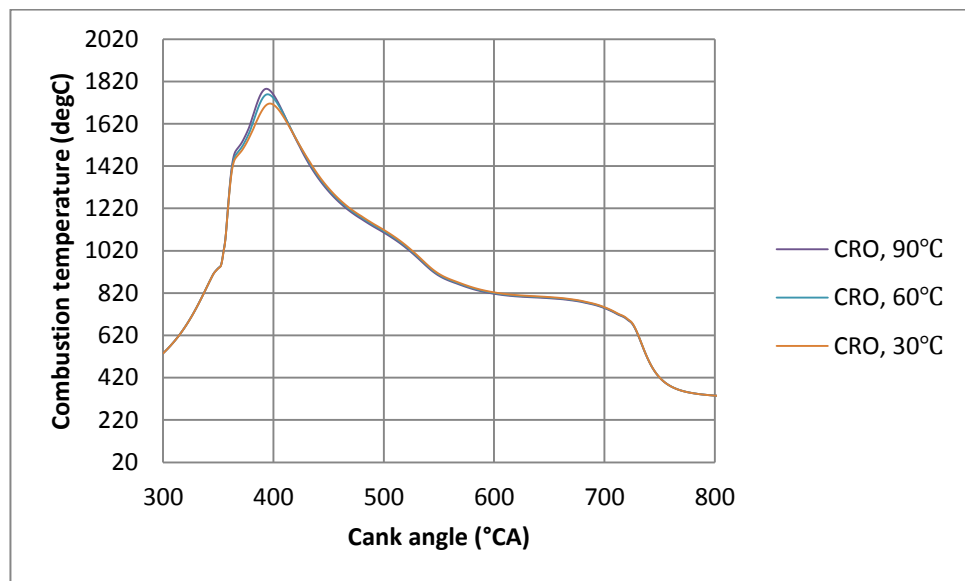


Fig. 5.11 Comparison of combustion temperatures at full load with different preheating temperatures

Fig 5.12 shows the engine power efficiency of the croton oil with different preheating temperatures. Without the conversion loss of mechanical power to electrical power, the engine power efficiency was high, ranging from about 11% to 36%, between 4 to 9 points higher than the electrical efficiency (7%- 27%). The merit of using a higher preheating temperature was shown in terms of the improved engine power efficiency.

Approximately 0.5 to 1 point improvements were found with a preheating temperature of 90 °C relative to those of the temperature at 30 °C.

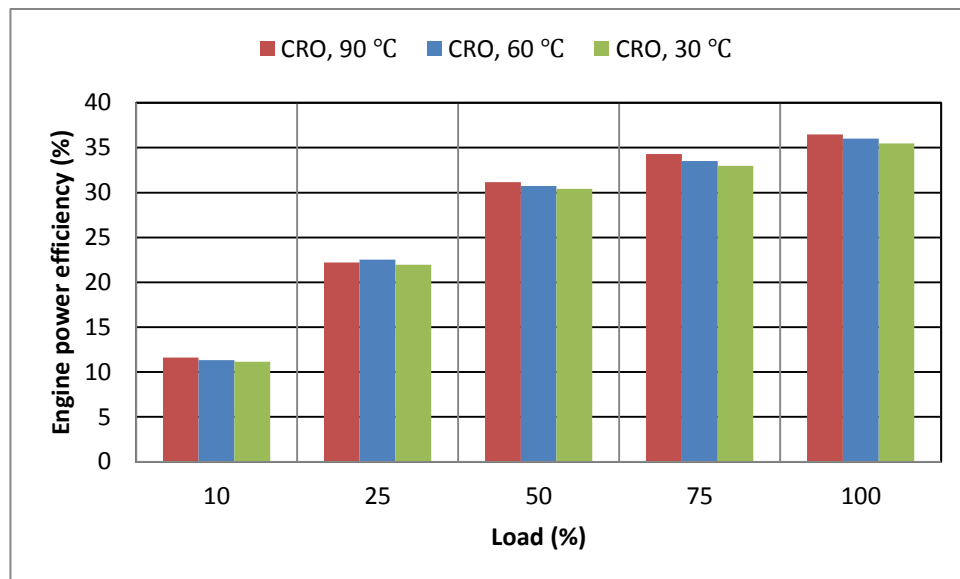


Fig. 5.12 Preheating temperature dependent engine power efficiency

5.3.2.2 Emission predictions

Fig 5-13 shows the CO₂ emissions for the croton oil with different preheating temperatures. Due to the improvement of engine power with fuel preheating, improved CO₂ emission results were possible. The higher the heating temperature, the lower the CO₂ emissions were. Without heating, the average CO₂ emission rates were 2% and 3% higher than the oil heated to 60 °C and 90 °C.

Fig 5-14 shows the NO_x emissions for the croton oil with different preheating temperatures. The NO_x emission of the oil was related to the engine loads and the preheating temperature. A high heating temperature and engine load resulted in severe NO_x emissions, with the latter trend proved by the experimental results. At full load, the NO_x emission of the croton oils was increased by 12.6% from 934ppm to 1052ppm. As previously mentioned, emissions are strongly related to combustion chamber factors such as peak combustion temperature, combustion duration and the oxygen concentration in the burning zone. Low NO_x emissions of unheated croton oil were due to poor combustion and a low heat release rate, thus the peak combustion temperature was reduced. Relating to the heated oils, an improvement in physicochemical

properties and the air-fuel mixture in combustion zones seem to highlight the main factors contributing to the high NO_x emission.

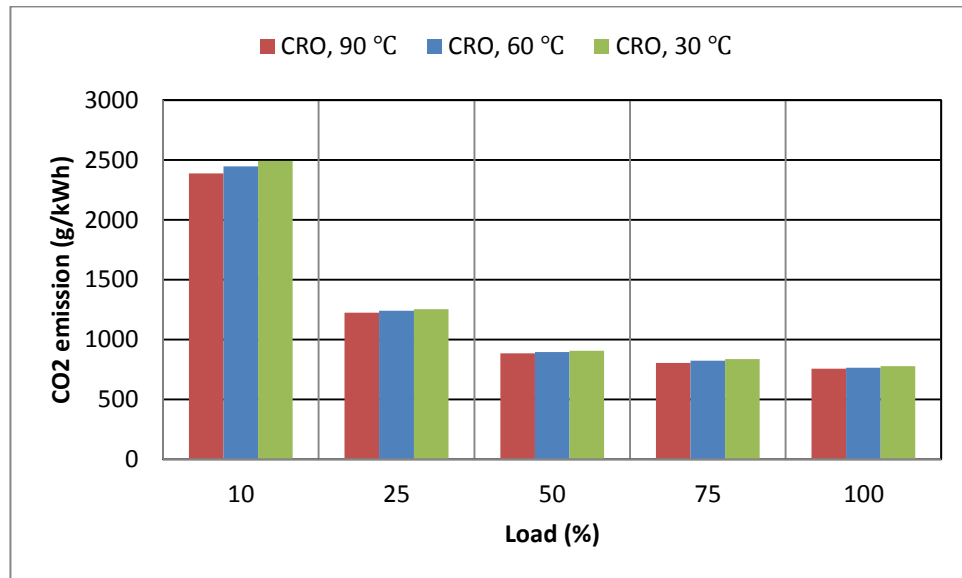


Fig. 5.13 Preheating temperature dependent CO₂ emission

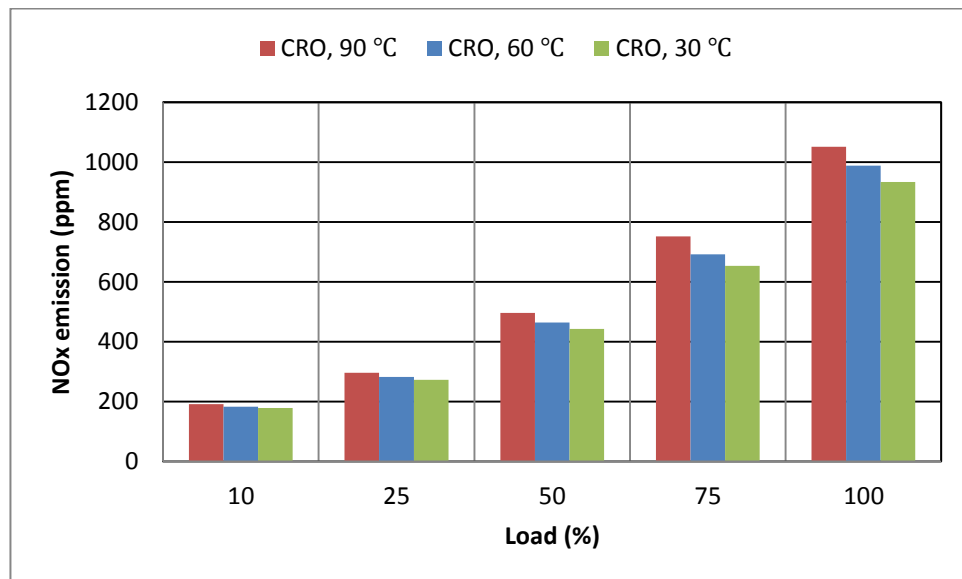


Fig. 5.14 Preheating temperature dependent NO_x emission

Fig.5.15 shows the smoke emission for different preheating temperatures. This is mainly related to engine speed, cylinder pressure before exhaust and soot formation in the combustion chamber; while the latter was in proportion to cycle fuel mass, heat release rate and variable cylinder volume [175]. Due to less fuel being injected and a low heat release rate at low load, an improved smoke emission rate was achieved, but this increased sharply with increasing engine loads. Nevertheless, low combustion

pressure may lead to high smoke emission. For unheated croton oil, the Bosch smoke was significantly higher than those of the preheated oils. When heated to 90°C, on average 14% less smoke emission was produced compared to that of the unheated oil.

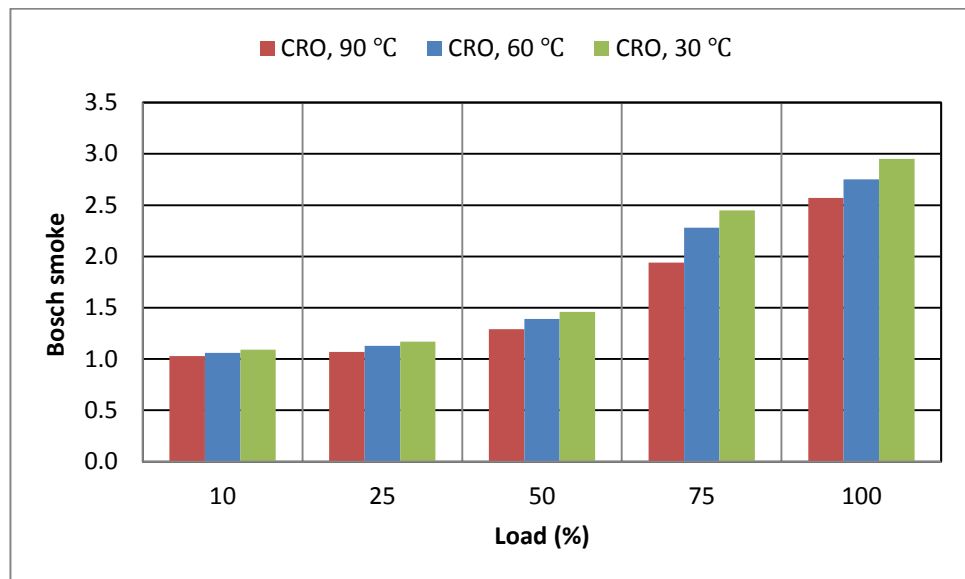


Fig. 5.15 Preheating temperature dependent Bosch smoke

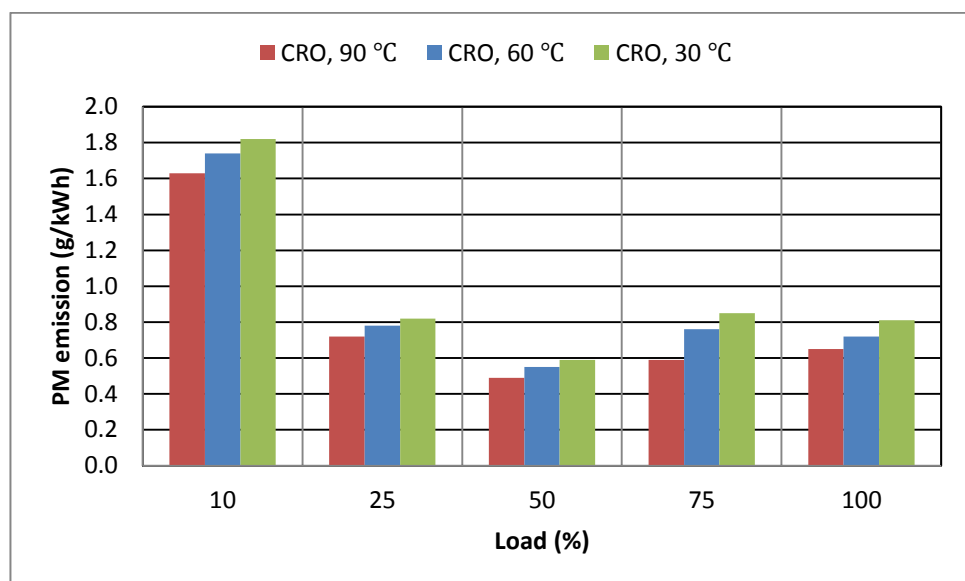


Fig. 5.16 Preheating temperature dependent PM emission

In DIESEL-RK, PM emissions is expressed as a function of the Bosch smoke number hence shows the similar trends of being affected by preheating temperature as that of the smoke emission (Fig. 5.16). Considerable improvement of the PM emission was observed with preheated oil, on average a 23% decrease with the oil preheated to 90°C and a 13% improvement with the oil preheated to 60°C. The PM emission value

decreased with a decreasing load, reaching its minimum value at 50% load. It then increased and reached its maximum value at 10% load. This variation may be due to the improvement of the oxygen concentration in burning zones and a relatively high combustion temperature. A high PM emission value at a low temperature may be caused by the lean mixture and un-burnt hydrocarbons in the combustion chamber.

5.3.3 Engine performance optimisation

Various optimisation options that may be difficult to apply on the engine or for trigeneration could be done theoretically. In this section, optimisation was performed aiming on improving the engine performance at full load. Investigation options including start of injection (SOI), compression ratio (CR), swirl ratio (SR) and intake valve opening (IVO) and injection duration (IDR) were studied. After the potential benefits of each parameter identified, combined multiple optimisation options were applied on to compare the variation of engine performance.

5.3.3.1 Start of injection (SOI)

Injection timing is a major factor influencing the combustion process. The default setting of the Yanmar engine is 18° crank angle (CA) before top dead centre (BTDC) and this figure for the croton oil is set to 15° CA BTDC, which is based on the reality that the injection timing of vegetable oils usually delay 3-5° CA relative to diesel. The optimisation range is set from 10 to 25 °CA BTDC.

Simulation shows that the engine power keep increasing when injection timing increases from 10° CA BTDC to 19° CA BTDC and starts dropping. Delayed injection usually results in the decreasing of maximum cylinder pressure, as combustion happens at the time piston moving down accelerated; and injection too early leads to increasing of combustion pressure before piston reached top dead centre. The brake mean effective pressure will hence drop and will be reflected in lower engine power output. With injection timing of 19° CA BTDC, the power is 8.90kW and SFC is 262.8g/kWh, respectively, both improving by 0.9% compared to that of default injection timing.

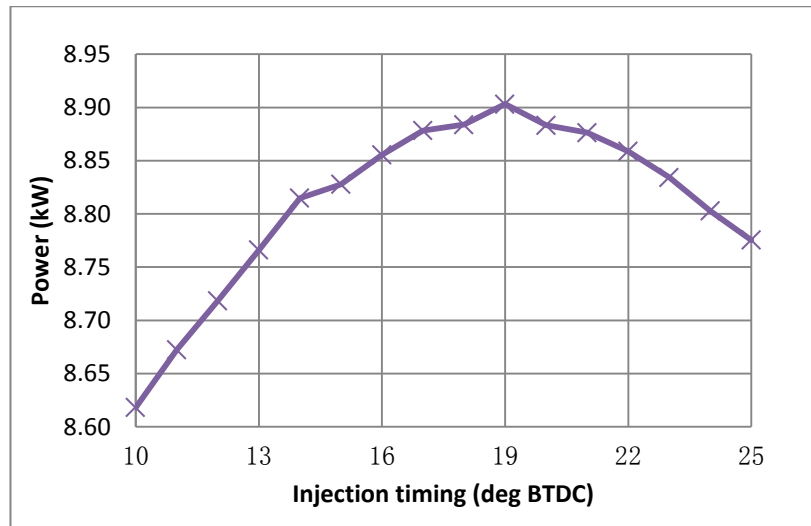


Figure 5.17 Injection timing dependence in engine power optimisation

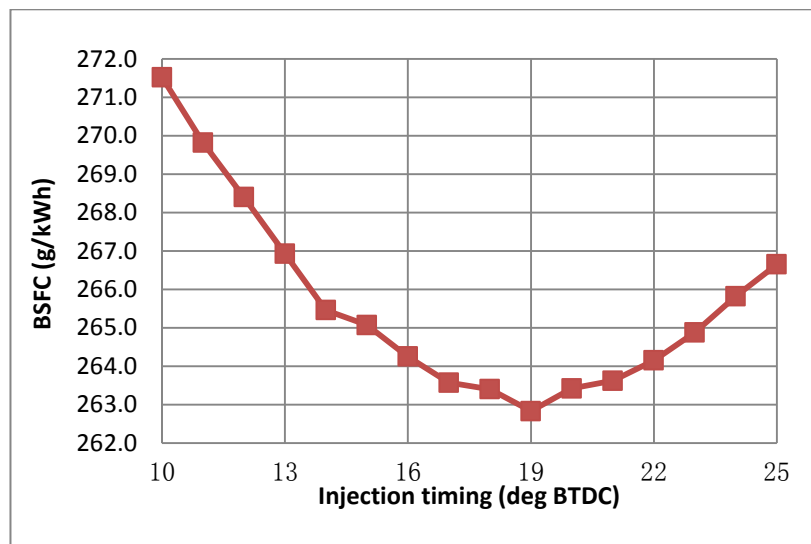


Figure 5.18 Injection timing dependence in SFC optimisation

5.3.3.2 Compression ratio (CR)

Compression ratio is defined as the ratio of the combustion chamber volume before and after compression. High CR gives a higher theoretical cycle efficiency, but leads to higher combustion pressures and combustion temperature. This increases the mechanical and the thermal loads within the engine, and influences heat losses from the combustion chamber and emissions formation. The default setting is 17.7 and the optimization range is 17-20. The range was chosen to enable reasonable and realistic operation of the engine simulation.

The simulation results, as shown in Fig. 5.19 and Fig. 5.20, indicate that as the CR increases from 17 to 20, the engine power increases from 8.81kW to 8.91kW, and the SFC decreases from 265.7g/kWh to 262.8g/kWh. Compared to the default value, the engine performance improved by 0.89% at CR=20. In the Yanmar engine, it is possible to increase CR by reducing the thickness of compression shims or increase the height of piston or the length of connecting rod. The former is easy to realise, but has limited effect on the CR. The latter two solutions rely on the redesign of components of the engine, but can increase CR to a higher level.

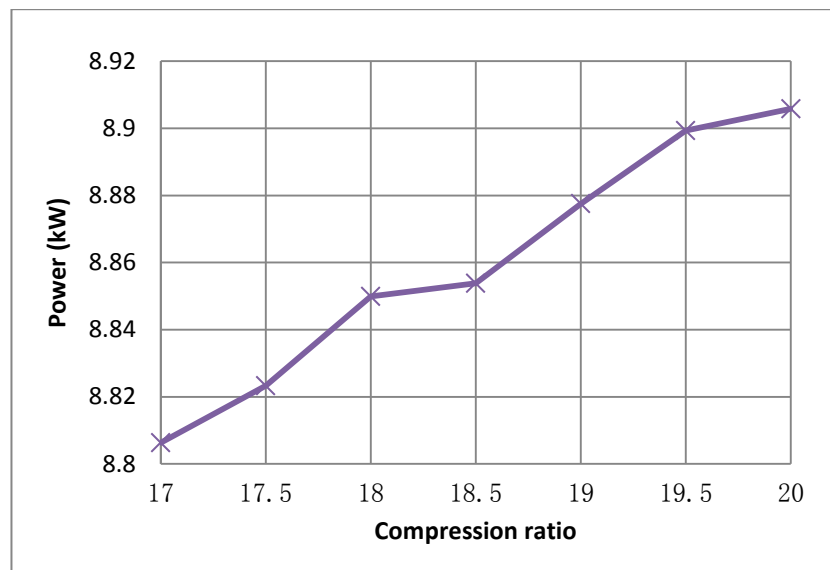


Figure 5.19 Compression ratio dependence in engine power optimisation

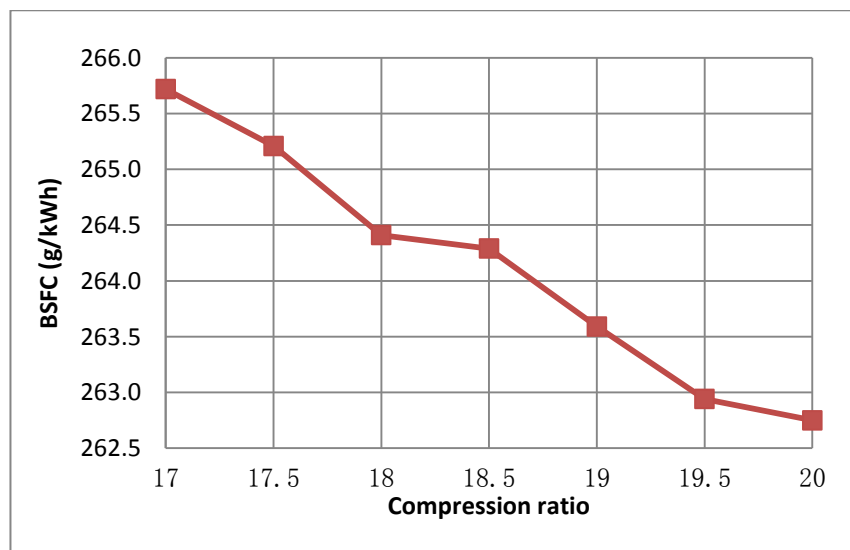


Figure 5.20 Compression ratio dependence in SFC optimisation

5.3.3.3 Swirl ratio (SR)

Swirl ratio is the in-cylinder vortex speed relative to engine revolution. It is mainly affected by the shape of air passage ports and piston bowl. This study set the SR to 3 by default, and defined the optimisation range as 1-5.

Usually, a strong swirl ratio improves fuel atomisation and combustion rates in deep bowl combustion chambers. However, too strong a swirl may lead to the overlap of fuel spray, hence, may deteriorate the combustion process. The simulation results show that mid-swirl ratio (SR=2-3) coupled to a ω -type piston bowl was suitable for the engine, whereas high swirl ratio poses negative effect to the engine performance. Nevertheless, the engine power output with default setting was almost the highest and negligible improvement was observed, which indicating this variable is of less influential on the engine's optimisation.

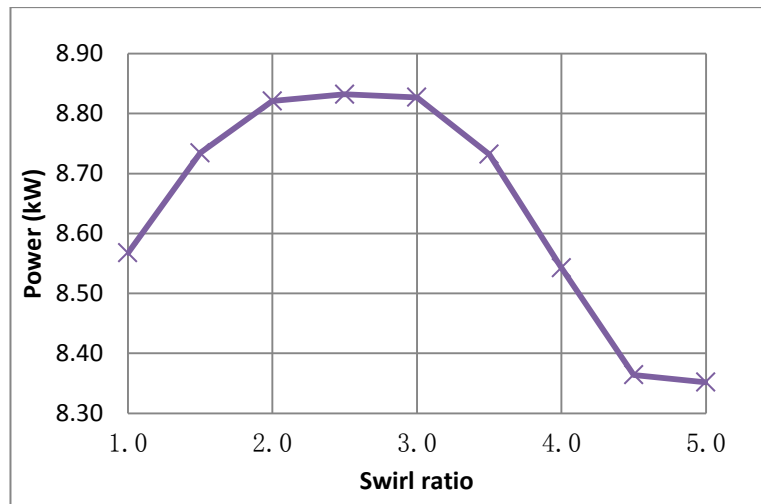


Figure 5.21 Swirl ratio dependence in engine power optimisation

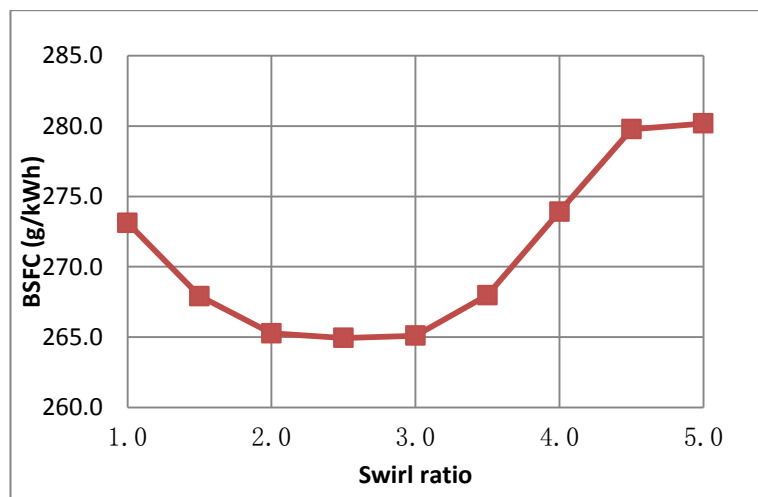


Figure 5.22 Swirl ratio dependence in SFC optimisation

5.3.3.4 Intake valve opening (IVO)

Intake valve opening timing will affect the charge air pressure. Too early Intake valve opened would not help to air charging, as exhaust gas will flow back to the scavenge air cylinder and block the air intake. While the large delay in IPO will result in insufficient air charge, hence will deteriorate combustion. By default, it sets to 19° CA BTDC and the optimization range is $10\text{-}25^{\circ}$ CA BTDC.

Figure 5.23 and Figure 5.24 reveal that the engine performance varies within a narrow range with the increasing of IVO, the best performance was found at 17° CA BBDC, with the engine power and SFC of 8.83kW and 264.9 g/kWh, respectively, only improved by 0.06% compared to the nominal value.

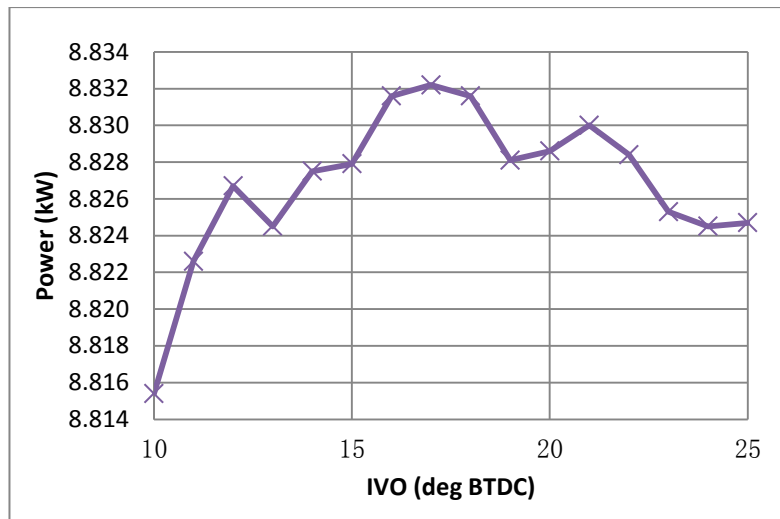


Figure 5.23 Intake valve opening dependence in engine power optimisation

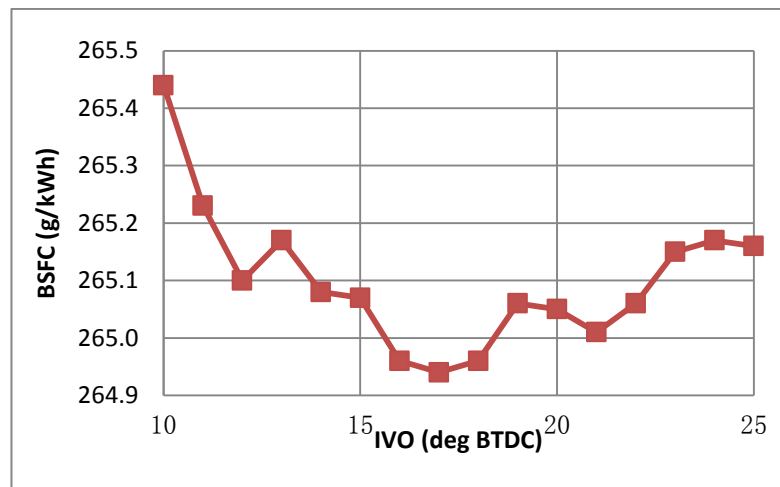


Figure 5.24 Intake valve opening dependence in SFC optimisation

5.3.3.5 Injection duration

Injection duration is relating to maximum injection pressure when injector is chose. Short injection duration indicates more fuel will be injected before combustion began thus enhance premix combustion process and improve engine performance. It sets to 31 ° CA by default and the optimization range is 26-35 ° CA.

Simulations results (Figure 5.25 and Figure 5.26) reveal that with the decreasing of injection duration, the engine performance improves near linearly till reached the top at 26° CA, with the engine power and SFC of 8.83kW and 264.9 g/kWh, respectively, both improved by 3.0%. To achieve that, the maximum fuel injection pressure must be increased from 47.5MPa to 63.4 MPa, or to increase the number or bore of nozzle holes.

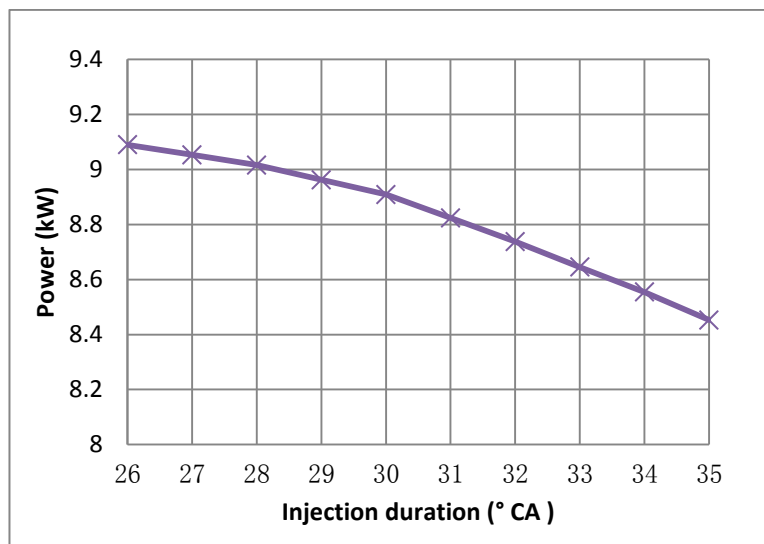


Figure 5.25 Injection duration dependence in engine power optimisation

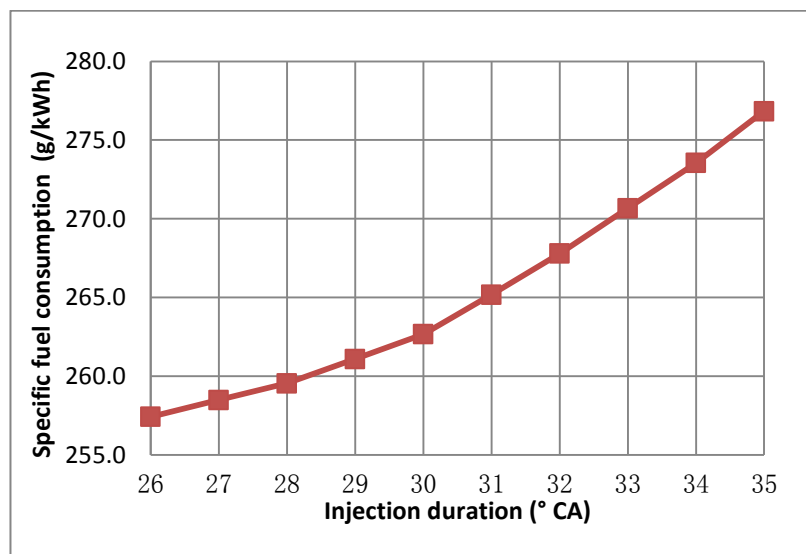


Figure 5.26 Injection duration dependence in SFC optimisation

5.3.3.6 Combined multiple parameters optimisation

Judged from the above optimization results, it can be concluded that SR and IVO produced negligible improvement of less than 0.1%, which is and can be considered as non-significant factors. The factors of SOI (19° CA BTDC), CR (20) and injection duration (26° CA) were applied to study the effect on the engine. The cumulated effects both in terms of engine performance and emissions were shown Table 5.4 for comparison.

Items	Default value	Optimised value	Variation (%)
Engine Power (kW)	8.83	9.07	2.72
BSFC (g/kWh)	265.0	258.1	-2.60
Peak combustion pressure P_{max} (bar)	73.6	84.3	14.54
Peak combustion temperature T_{max} (°C)	1788	1949	9.00
Exhaust gas temperature T_{exh} (°C)	512	467	-8.79
CO ₂ (g/kWh)	755	735	-2.65
NO _x (ppm)	1052	2022	92.21
PM (g/kWh)	0.64	0.24	-62.50
BOSCH Smoke	2.54	1.23	-51.57
Power efficiency (%)	36.50	37.47	2.66

Table 5.4 Engine performance and emissions after optimisation

After optimization, the combustion process was improved, characterised by higher peak combustion pressure and temperature. As a result, the engine performed in higher power and better efficiency, with reduced BSFC and exhaust gas temperature. As to emissions, PM and BOSCH Smoke was reduced drastically. Nevertheless, due to the trade-off relationship, NO_x emissions were doubled.

5.4 Biofuel micro-trigeneration modelling

5.4.1 Introduction to Dymola and Modelica

The software used for the simulation work is called Dymola and it was first introduced by Hilding Elmqvist during his PhD dissertation in 1978. It has benefited greatly by the developments in computer science and the advancements in the Pantelides algorithm for

differential algebraic equations (DAE). Major achievements were made with Dymola in the late 1990s and this led to the development of Modelica, an object and equation-oriented, multi-domain modelling language [176].

Modelica is defined and standardised by the Modelica Association, who also developed the latest version 3.3 of the free Modelica standard library. It contains approximately 780 universal models and 550 functions. Currently, Modelica has been applied in a variety of fields including fluid applications, the automotive sector and mechanical systems, etc. [178-181].

As a powerful tool based on Modelica, Dymola contains the most popular subcomponents and specific libraries such as ThermoFluid and Hydraulic libraries. All of the physical components in Dymola can be expressed in a natural way using ordinary differential equations and algebraic equations, thus releasing the burden of programming and algorithm design. Moreover, this software has no constraints for introducing components from other related software, hence it provides a more open and flexible environment for users [180, 181, 183, 184].

5.4.2 BMT model and mathematic principles

5.4.2.1 BMT model

In this section, a model was setup to simulate the micro-trigeneration performance of gas oil and croton oil. The heat energies in the coolant and exhaust gas were calculated. The recovered heating and cooling energy and the efficiency of the system were simulated and compared.

A case study monitoring the electricity load over 24 hours for a large mid-terrace house with seven bedrooms was chosen [185], as shown in Fig. 5.27. It is generated from the data of electricity consumption in the house during the autumn season, when the electrical load is the highest of the year. It has two peak times, the first from 6:30am to 10am and another from 4:30pm to 7:30pm. During the peak hours, the maximum electricity consumption exceeds 12kW over a short time.

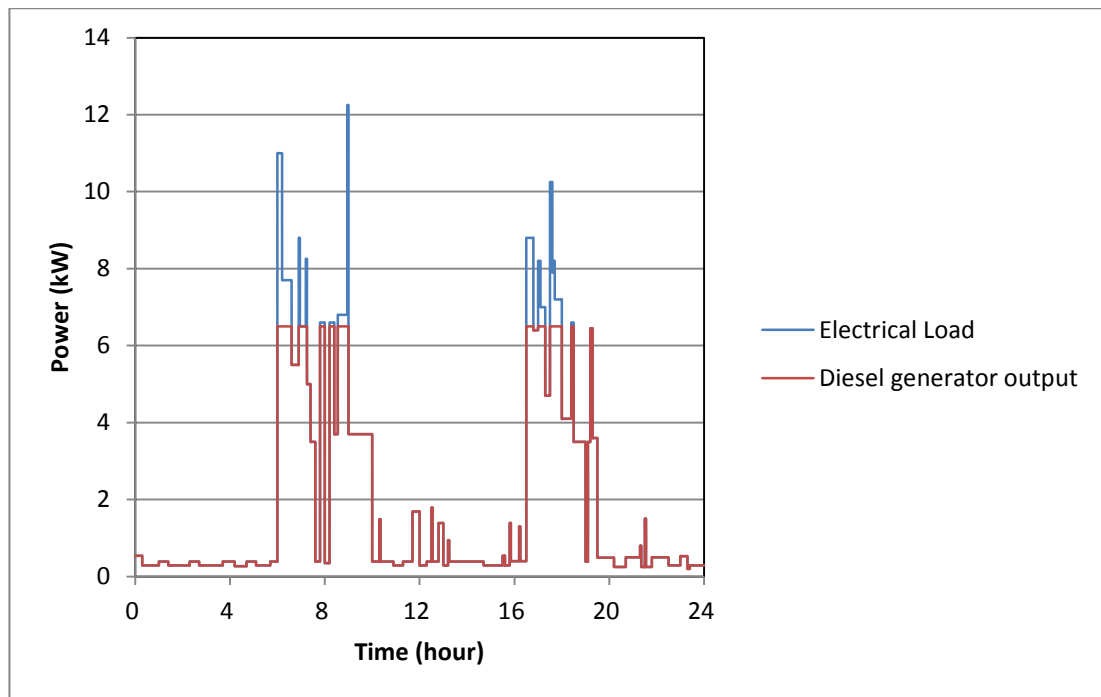


Fig. 5.27 Electrical load

The diagram of the BMT mode is shown in Fig. 5.28, consisting of the following modules:

- a) **electricalLoad.** The electrical load is stored in a lookup table as the input data of the trigeneration system. It is assumed that the BMT system operates throughout the day to supply electrical power up to 6.5kW, with a corresponding engine output of 8.82 kW (Fig. 5.27). Any electricity loads which exceed 6.5kW will be supplied by additional power sources such as a battery and super capacitors; these were not included in the model. The electrical load was output by a suitable connector to supply the other modules.
- b) **fuelSupply.** In this module, the fuel consumption data is stored in a lookup table. It is determined by two parameters: pre-set fuel type and electrical load from the input connector. The fuel type and fuel consumption were then output for use in calculating the energy balance and efficiencies of the system.
- c) **dieselGenerator.** As shown in Fig. 5.29, this module has two input connectors called fuel type and electrical load and three output connectors called air flow rate, exhaust gas temperature and engine power. The air flow rate is stored in a lookup table using the unit kg/h. This was determined by the electrical load and was output in kg/s. The exhaust temperature is determined by both electrical load and fuel type. The engine power is calculated by dividing the efficiencies of the generator and belt transmission.

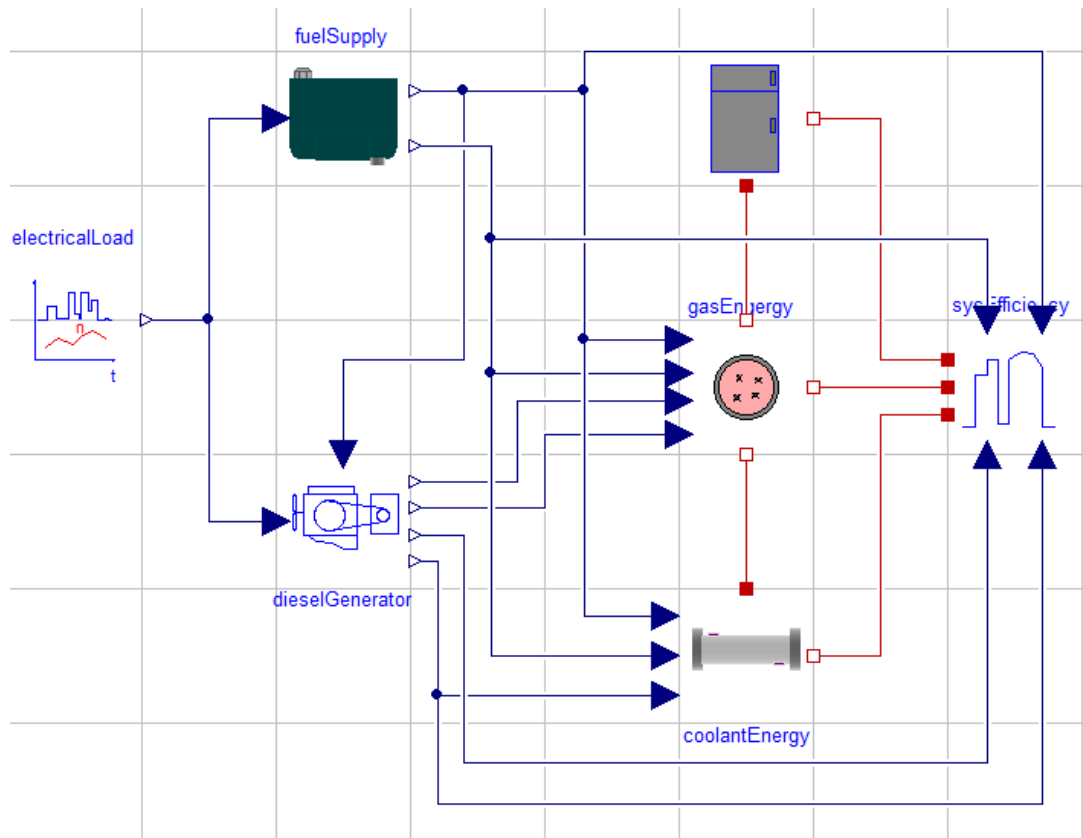


Fig. 5.28 Trigeneration model

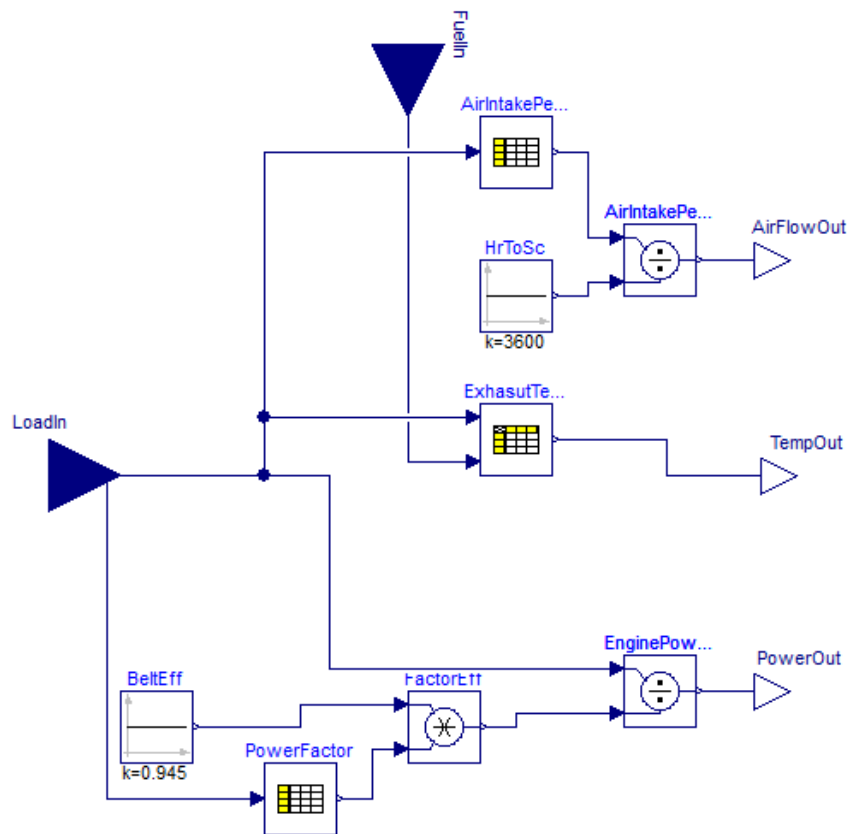


Fig. 5.29 dieselGenerator module

- d) **gasEnergy**. This module deals with the heat energy contained in the exhaust gas. It has four input connectors called fuel type, fuel consumption, air flow rate and exhaust gas temperature. It has three output connectors for the total exhaust gas energy, recovered exhaust gas energy and exhaust gas energy for the absorption refrigeration. The details for the gas energy calculation are presented in Section 5.4.2.
- e) **coolantEnergy**. This module has four input connectors called fuel type, fuel consumption, engine power and exhaust gas energy. It has one output connector for recovered coolant energy (Fig. 5.30). In simple terms, it represents the engine as a lumped mass system consisting of an engine block, coolant in the block, coolant in the radiator and a lube oil system. Each of the lumped masses is assumed to be an independent thermal system represented by two parts: a thermal conductor that transports heat without storage and a heat capacitor for storing heat, as shown in sub-module cHX (Fig. 5.31). The surrounding atmosphere is represented as a heat-sink at constant temperature. Parts of the heat are transferred to the engine block and to the surroundings. The coolant heat is transferred mostly to a radiator and then dissipated to the environment through a fan by convection, only a small portion was transferred to the surroundings by conduction. The third part of the heat is transferred to lube oil by conduction. The lube oil is assumed to be isolated from the surroundings, so when the oil temperature stabilises, the heat flow in it will drop down to zero. The parameter settings of the sub-module cHX are shown in Fig. 5.32. The details for the coolant energy calculation are presented in Section 5.4.3.
- f) **coolingEnergy**. This module simulates the performance of an ammonia-water absorption refrigeration system, with heat energy input to the heater/generator and an output of cooling energy.
- g) **sysEfficiency**. This module calculates the efficiencies of trigeneration. The input connectors include fuel type, fuel consumption, engine power, electrical power, recovered exhaust gas energy, recovered coolant energy and cooling energy. The engine power efficiency η_p , electrical efficiency η_e and trigeneration efficiency is as shown:

$$\eta_p = Pe / Q_f \times 100 \quad (5-16)$$

$$\eta_e = Ee / Q_f \times 100 \quad (5-17)$$

$$\eta_{TG} = (P_e + Q_{RE} + Q_{RC} + Q_E) / Q_f \times 100 \quad (5-18)$$

$$Q_f = H_U \times \dot{m}_f \quad (5-19)$$

Where P_e is engine power, Q_f is the fuel energy, E_e is electric power, Q_{RE} is recovered exhaust gas energy, Q_{RC} is recovered coolant energy, Q_E is cooling energy, H_U is the LHV of fuel and \dot{m}_f is the mass flow rate of fuel.

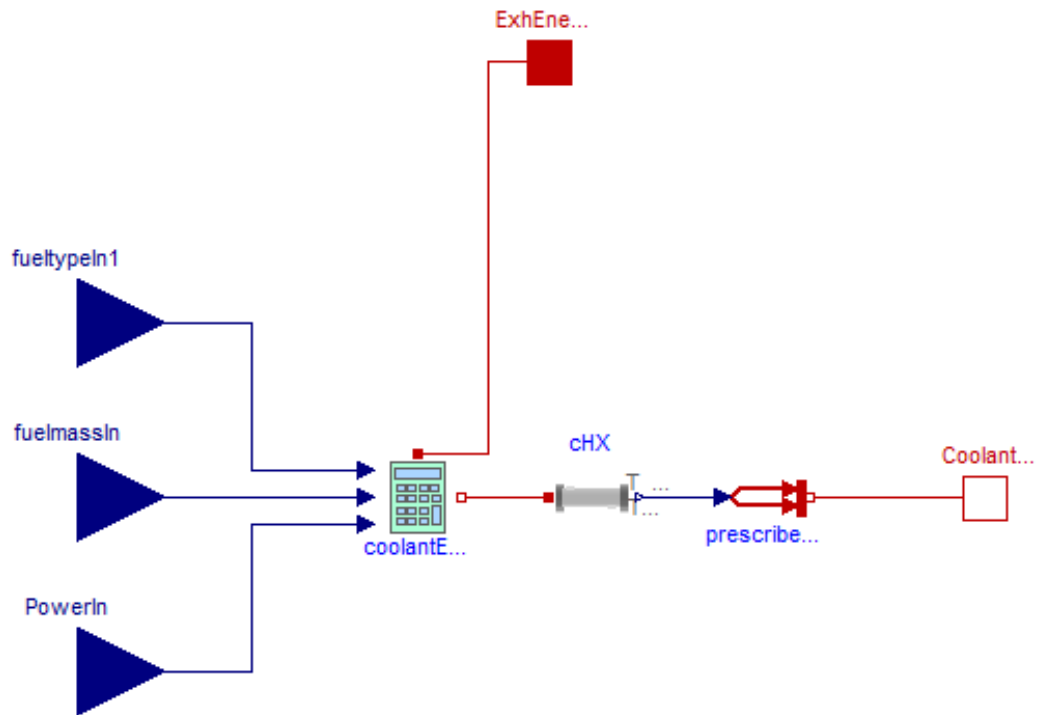


Fig. 5.30 coolantEnergy module

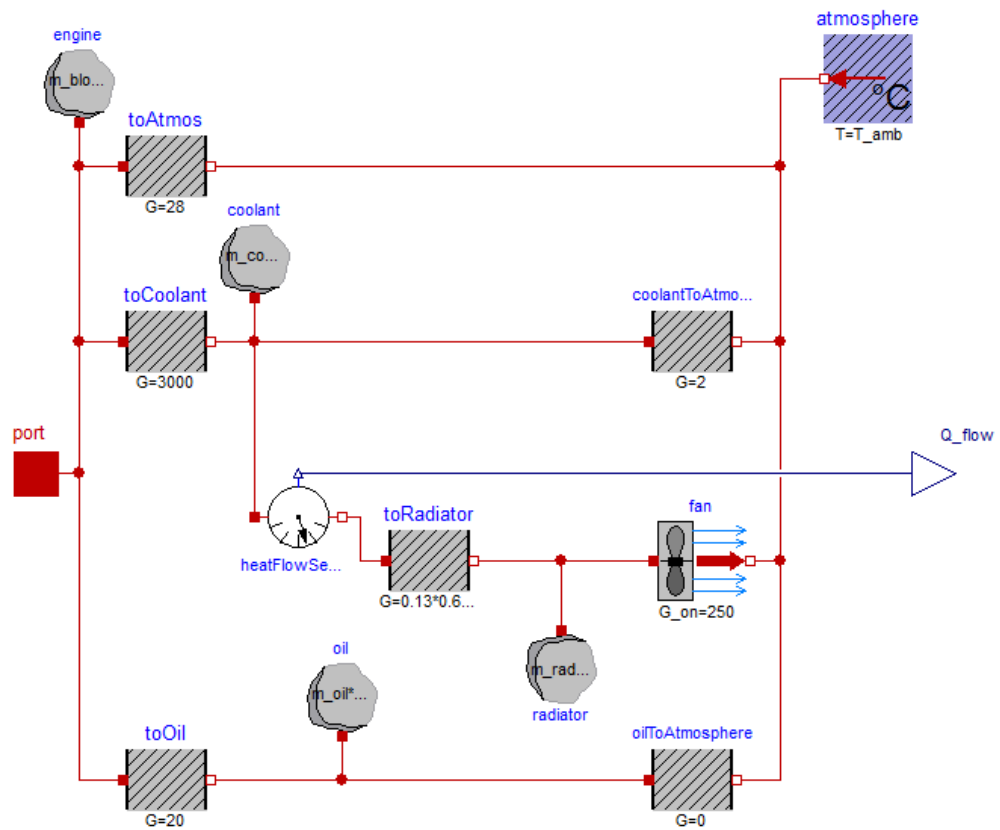


Fig. 5.31 cHX module

Ambient			
T_amb	<input type="text" value="25"/>	degC	Ambient temperature (is used as default initial temperature for all parts)
Engine block			
m_block	<input type="text" value="55"/>	kg	Mass of engine block
c_block	<input type="text" value="470"/>	J/(kg.K)	Specific heat capacity of engine block
Coolant			
m_coolant	<input type="text" value="1"/>	kg	Mass of engine coolant in block
m_radiator	<input type="text" value="1.5"/>	kg	Mass of engine coolant in radiator
c_coolant	<input type="text" value="4200"/>	J/(kg.K)	Specific heat capacity of engine coolant
Oil			
m_oil	<input type="text" value="2"/>	kg	Mass of engine oil
c_oil	<input type="text" value="1870"/>	J/(kg.K)	Specific heat capacity of engine oil
Fan			
T_on	<input type="text" value="40"/>	degC	Temperature at which fan is switched on
T_off	<input type="text" value="30"/>	degC	Temperature at which fan is switched off
G_on	<input type="text" value="250"/>	W/K	Thermal conductance of fan when fan is switched on

Fig. 5.32 Parameter setting of module cHX

5.4.2.2 Mathematic principles for recovered exhaust gas heat

In describing the calculation for the recovered gas energy, the following notations are provided: h = Enthalpy (kJ/kg), \dot{m} = Mass flow rate (kg/s), Q = Thermal energy (kW). The subscripts are: AR = Absorption refrigerator, DAR=Difference of parameters between the inlet and outlet of refrigerator, DEXH= Difference of parameters between the inlet and outlet of exhaust heat exchanger, EG = Exhaust gas, EXH = Exhaust heat exchanger, G = Generator.

Given that the molecular formula of fuel is $C_nH_kO_l$, the theoretical mass of oxygen required for combustion and the combustion products is given as:



The oxygen mass contained in the intake air for combustion is greater than the theoretical value; hence the exhaust gas consists mainly of four major compositions, i.e., CO_2 , H_2O , N_2 and O_2 . Other gases such as SO_2 , CO and HC were ignored due to their low concentration in exhaust gas i.e. usually less than 0.1% total. The mass fraction of oxygen in air is 23.2%. Given the real air-fuel ratio F , the mass of combustion products by combusted m_f kilograms of fuel are given by:

$$\dot{m}_{CO_2} = \dot{m}_f / (12n + k + 16l) \times 44n \quad (5-21)$$

$$\dot{m}_{H_2O} = \dot{m}_f / (12n + k + 16l) \times 9k \quad (5-22)$$

$$\dot{m}_{O_2} = 0.232 \times (\dot{m}_f \times F) - \dot{m}_f / (12n + k + 16l) \times 32(n - k/4 - l/2) \quad (5-23)$$

$$\dot{m}_{N_2} = 0.768 \times (\dot{m}_f \times F) \quad (5-24)$$

The exhaust gas energy was the sum of each energy of its compositions:

$$Q_{EX} = Q_{CO_2} + Q_{H_2O} + Q_{O_2} + Q_{N_2} \quad (5-25)$$

Where Q_{CO_2} , Q_{H_2O} , Q_{O_2} and Q_{N_2} are the heat energies of the subscripted gases. For trigeneration, part of the exhaust gas was used for the absorption refrigeration; hence the exhaust heat energy was divided into two parts. The first passes through the exhaust heat exchanger and the second supplies the refrigerator:

$$Q_{EG} = Q_{EXH} + Q_{AR} \quad (5-26)$$

The energy of each composition in Eq. 5-21 is the product of mass and specific enthalpy and is shown as:

$$Q_i = \Delta h_i \times \dot{m}_i \quad (5-27)$$

Where Δh_i is the difference in the specific enthalpy of each composition between the exhaust gas temperature and ambient temperature. Similarly, the difference in the heat energy of each gas between the inlet and outlet of the exhaust heat exchanger is given by:

$$Q_{DEXHi} = \Delta h_{DEXHi} \times \dot{m}_{DEXHi} \quad (5-28)$$

Where Δh_{DEXHi} is the difference in the specific enthalpy of each composition between the inlet and outlet of the exhaust heat exchanger. The recovered exhaust heat energy is given by:

$$Q_{RE} = \varepsilon_{RE} \times \sum Q_{DEXHi} \quad (5-29)$$

Where ε_{RE} is the effectiveness of heat exchange in the exhaust heat exchanger. The difference in exhaust heat energy between the inlet and outlet of the refrigerator and the heat absorbed by the ammonia water in the generator can be given as follows:

$$Q_{DARi} = \Delta h_{DARi} \times \dot{m}_{DARi} \quad (5-30)$$

$$Q_G = \varepsilon_{AR} \times \sum Q_{DARi} \quad (5-31)$$

Where ε_{AR} is the effectiveness of the heat exchange between the heater and the generator of the refrigerator.

5.4.2.3 Mathematic principles for recovered coolant heat

For calculating the recovered coolant heat, the heat contained in the diesel generator Q_{DG} is determined by the equation:

$$Q_{DG} = (Q_f - Q_{EG} - P_e) \quad (5-32)$$

The heat flow through lumped mass Q_{LM} is given by:

$$Q_{LM} = G_{LM} \times dT_{LM} = c_{pLM} \times m_{LM} \times dT_{LM} \quad (5-33)$$

Where G_{LM} , T_{LM} , c_{pLM} and m_{LM} are the thermal conductance, temperature, specific heat capacity and mass of the lumped mass. In this module, the heat loss of the lube oil is neglected, thus the recovered coolant heat is given by:

$$Q_{RC} = Q_{DG} - Q_{EB} - Q_{LC} \quad (5-34)$$

Where Q_{EB} is the heat flow of the engine block, Q_{LC} is the heat loss of the coolant. The parameter setting of this module is shown in Fig. 5.22.

5.4.2.4 Mathematic principles for cooling energy

The schematic diagram for the diffusion absorption system is illustrated in Fig. 5.33. The refrigeration cycle is mathematically based on the principles of mass continuity, material continuity and energy conservation. The equations are given as:

$$\sum m_i = 0 \quad (5-35)$$

$$\sum m_i x_i = 0 \quad (5-36)$$

$$\sum Q_i + \sum m_i x_i = 0 \quad (5-37)$$

Where x is mass fraction.

When applied to the above equations and to the separate parts, different forms are given and presented in Table 5.4. Except for some notations and subscripts which were inherited from the gasEnergy module, the notations used below are: c_p = Specific heat at constant pressure (kJ/kg K), p = Pressure (kPa), T = temperature (K), ε = Effectiveness. The subscripts are: A = Absorber, C = Condenser, E = Evaporator, GH=Gas heat exchanger, L=Liquid, R=Rectifier, SH=Solution heat exchanger, V=Vapour.

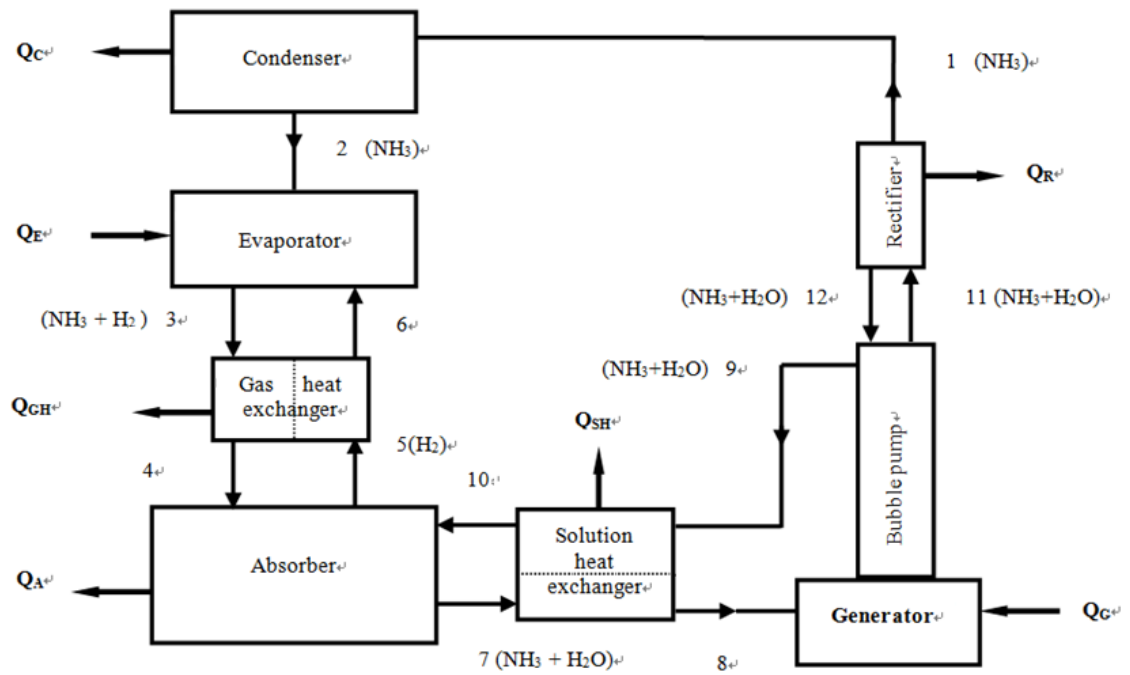


Fig. 5.33 Schematic diagram of diffusion absorption system[186]

No.	Part name	Inlet	Outlet	Equations	Equation number
1	Condenser	m_1	m_2, Q_C	$m_2 = m_1$ $x_2 = x_1$ $Q_C = m_1 (h_1 - h_2)$	(5-38) (5-39) (5-40)
2	Evaporator	m_2, m_6, Q_E	m_3	$m_{3L(NH_3)} = m_2 - m_{3V(NH_3)}$ $m_3 = m_2 + m_6$ $m_3 = m_{3(H_2)} + m_{3V(NH_3)} + m_{3L(NH_3)}$ $\epsilon_{NH_3} = m_{3V(NH_3)} / m_2$ $m_{3V(NH_3)} = \epsilon_{NH_3} m_2$ $Q_E = [m_{3(H_2)} h_{3(H_2)} + m_{3V(NH_3)} h_{3V(NH_3)} + m_{3L(NH_3)} h_{3L(NH_3)}] - m_2 h_2 - m_6 h_{6(H_2)}$	(5-41) (5-42) (5-43) (5-44) (5-45) (5-46)
3	Gas heat exchanger	m_3, m_5	m_4, m_6, Q_{GH}	$(h_4 - h_3) = \epsilon_{GH} (h_5 - h_6)$ $\epsilon_{GH} = (h_4 - h_3) / (h_5 - h_6)$ $Q_{GH} = (h_5 - h_6) - (h_4 - h_3)$ $T_6 = \epsilon_{GH} \times T_E + (1 - \epsilon_{GH}) \times T_A$ $T_4 = \epsilon_{GH} \times (m_5 \times c_{p5} / m_3 c_{p3}) (T_A - T_6) + T_E$	(5-47) (5-48) (5-49) (5-50) (5-51)
4	Absorber	m_4, m_{10}	m_5, m_7	$m_4 + m_{10} = m_5 + m_7$	(5-52)

			Q_A	$m_4 x_4 + m_{10} x_{10} = m_7 x_7$ $Q_A = [m_{3(H_2)} h_{3(H_2)} + m_{3(NH_3)} h_{3(NH_3)}] + m_{10} h_{10} - m_5 h_5 - m_{4(H_2)} h_{4(H_2)}$	(5-53) (5-54)
5	Solution heat exchanger	m_7, m_9	m_8, m_{10}, Q_{SH}	$T_{10} = \epsilon_{SH} T_7 + (1 - \epsilon_{SH}) T_9 = \epsilon_{SH} T_A + (1 - \epsilon_{SH}) T_G$ $T_8 = \epsilon_{SH} (m_9 / m_7) (T_9 - T_{10}) + T_7 = \epsilon_{SH} (m_9 / m_7) (T_G - T_{10}) + T_A (h_8 - h_7) = \epsilon_{SH} (h_9 - h_{10})$ $\epsilon_{SH} = (h_6 - h_5) / (h_9 - h_{10})$ $Q_{SH} = (h_9 - h_{10}) - (h_8 - h_7)$	(5-55) (5-56) (5-57) (5-58)
6	Generator	m_8, m_{12}, Q_G	m_9, m_{11}	$m_8 = m_9 + m_{11} - m_{12}$ $m_8 x_8 = m_9 x_9 + m_{11} x_{11} - m_{12} x_{12}$ $Q_G = m_8 h_8 + m_{12} h_{12} - m_9 h_9 - m_{11} h_{11}$	(5-59) (5-60) (5-61)
7	Rectifier	m_{11}	m_1, m_{12}, Q_R	$m_{11} = m_1 + m_{12}$ $m_{11} x_{11} = m_1 x_1 + m_{12} x_{12}$ $m_1 (x_1 - x_{12}) = m_{11} (x_{11} - x_{12})$ $Q_R = m_{11} h_{11} - m_{12} h_{12} - m_1 h_1$	(5-62) (5-63) (5-64) (5-65)

Table 5.5 Summary of equations for simulating absorption refrigeration

The coefficient of performance of the refrigerator is given by:

$$COP = \epsilon_E \times Q_E / Q_G \quad (5-66)$$

Where $\epsilon_E = 0.7$ is the effectiveness of evaporation.

Some properties of ammonia, hydrogen and ammonia-water mixture still need to be determined. The specific heat of liquid ammonia $c_{pL(NH_3)}$ and ammonia vapour $c_{pV(NH_3)}$ at constant pressure is given as [187, 188]:

$$c_{pL(NH_3)} = 0.00002 \times T^2 + 0.0062 \times T + 4.6176 \quad (5-67)$$

$$c_{pV(NH_3)} = 0.0001 \times T^2 + 0.0163 \times T + 2.6632 \quad (5-68)$$

The specific heat of hydrogen at constant pressure is given as [187, 188]:

$$c_{p(H_2)} = - 0.00004 T^2 + 0.0054 T + 14.198 \quad (5-69)$$

The enthalpy of hydrogen at a pressure of 20bar is:

$$h_{(H_2)} = 14.39 T - 68.991 \quad (5-70)$$

J.Patek and J.Klomfar [189] proposed an equation to calculate the mole fraction of ammonia in gas phase X'' as below:

$$X''(p, X') = 1 - \exp \left[\ln(1 - X') \sum_i a_i \left(\frac{p}{p_0} \right)^{m_i} X'^{n_i/3} \right] \quad (5-71)$$

Where X' is the ammonia mole fraction in the liquid phase, $p_0 = 2000\text{kPa}$ is the reference pressure, a_i, m_i, n_i are the coefficients and their values are stated in Table 5.5.

i	m_i	n_i	a_i	i	m_i	n_i	a_i
1	0	0	19.8022017	8	3	2	-3421.98402
2	0	1	-11.8092669	9	4	3	11940.3127
3	0	6	27.7479980	10	5	4	-24541.3777
4	0	7	-28.8634277	11	6	5	29159.1865
5	1	0	-59.1616608	12	7	6	-18478.2290
6	2	1	578.091305	13	7	7	23.4819434
7	2	2	-6.21736743	14	8	7	4803.10617

Table 5.6 Exponents and coefficients for X''

The specific enthalpy of the ammonia-water solution h_l and ammonia-water vapour h_g are given by [189]:

$$h_l(T, X') = h_0 \sum_i a_i \left(\frac{T}{T_0} - 1 \right)^{m_i} X'^{n_i} \quad (5-72)$$

$$h_g(T, X'') = h_0 \sum_i a_i \left(1 - \frac{T}{T_0} \right)^{m_i} (1 - X'')^{n_i} \quad (5-73)$$

In Eq. 5-72, T is the temperature of the solution (K), and X' is the mole fraction of liquid ammonia, T₀ = 273.16 K is the reference temperature, h₀ = 100 kJ/kg is the reference enthalpy, a_i, m_i, n_i are the coefficients and their values are given in Table 5.6.

i	m _i	n _i	a _i	i	m _i	n _i	a _i
1	0	1	-7.61080	9	2	1	2.84179
2	0	4	25.6905	10	3	3	7.41609
3	0	8	-247.092	11	5	3	891.844
4	0	9	325.952	12	5	4	-1613.09
5	0	12	-158.854	13	5	5	622.106
6	0	14	61.9084	14	6	2	-207.588
7	1	0	11.4314	15	6	4	-6.87393
8	1	1	1.18157	16	8	0	3.50716

Table 5.7 Exponents and coefficients for h_l

In Eq. 5-73, T is the temperature of ammonia-water vapour (K), X'' is the mole fraction of ammonia vapour, T₀ = 324K is the reference temperature, h₀ = 1000 kJ/kg is the reference enthalpy, a_i, m_i, n_i are the coefficients and their values are listed in Table 5.7.

i	m _i	n _i	a _i	i	m _i	n _i	a _i
1	0	0	1.28827	10	1	3	16.4508
2	1	0	0.125247	11	2	3	-9.36849
3	2	0	-2.08748	12	0	4	8.42254
4	3	0	2.17696	13	1	4	-8.58807
5	0	2	2.35687	14	0	5	-2.77049
6	1	2	-8.86987	15	4	6	-0.961248
7	2	2	10.2635	16	2	7	0.988009
8	3	2	-2.37440	17	1	10	0.308482
9	0	3	-6.70515				

Table 5.8 Exponents and coefficients for h_g

The temperature of the ammonia-water solution T(p, X') and ammonia-water vapour T(p, X'') are given by [189]:

$$T(p, X') = T_0 \sum_i a_i (1 - X')^{m_i} \left[\ln\left(\frac{p_0}{p}\right) \right]^{n_i} \quad (5-74)$$

$$T(p, X'') = T_0 \sum_i a_i (1 - X'')^{m_i/4} \left[\ln\left(\frac{p_0}{p}\right) \right]^{n_i} \quad (5-75)$$

Where $P_0 = 2000\text{kPa}$ is the reference pressure, $T_0=100\text{ K}$ is the reference temperature, the values of a_i , m_i , n_i in Eq. 5-74 are given in Table 5.8; the values of a_i , m_i , n_i in Eq. 5-75 are given in Table 5.9.

i	m_i	n_i	a_i	i	m_i	n_i	a_i
1	0	0	3.22302	8	1	2	0.0106154E
2	0	1	-0.384206	9	2	3	-0.000533589
3	0	2	000460965	10	4	0	7.85041
4	0	3	-0.00378945	11	5	0	-11.5941
5	0	4	0.00013561	12	5	1	-0.05.23150
6	1	0	0.487755	13	6	0	4.89596
7	1	1	-0.120108	14	13	1	0.0421059

Table 5.9 Exponents and coefficients for $T(p, X')$

i	m_i	n_i	a_i	i	m_i	n_i	a_i
1	0	0	3.24004	10	3	0	-20.1780
2	0	1	-0.395920	11	3	1	1.10834
3	0	2	0.0435624	12	4	0	14.5399
4	0	3	0.00218943	13	4	2	0.644312
5	1	0	-1.43526	14	5	0	-2.21246
6	1	1	1.05256	15	5	2	-0.756266
7	1	2	-0.0719281	16	6	0	-1.35529
8	2	0	12.2362	17	7	2	0.183541
9	2	1	-2.24368				

Table 5.10 Exponents and coefficients for calculating $T(p, X'')$

To convert ammonia mole fraction to mass fraction, the following equation is used:

$$X' = \frac{x/17.03}{x/17.03 + (1-x)/18.015} \quad (5-76)$$

Where the molecular mass of ammonia is 17.03 and the molecular mass of water is 18.015.

5.5 BMT simulation and prediction

The simulation results of biofuel micro-trigeneration are shown in Fig. 5.34 to Fig. 5.39. Fig. 5.34 shows the energy distributions with the fuels. To retain the same engine output, the input fuel energy of croton oil was always higher than that of the gas oil, and the heat energy in the coolant and exhaust gas with croton oil were also greater. For 24 hours' running time, the generated electrical power was 41.4kWh. The total fuel energy consumed with croton oil was 279.2kWh, only 4% higher than that of the gas value of 268.4 kWh. When running at off-peak time with a load of 0.5kW, the input fuel energy was about 8kW, in which 4kW was in exhaust gas and 2.4kW in coolant. For full load operation at peak time, the input fuel energy was approximately 24kW, in which 8.8kW was in exhaust gas and 4.8kW was in coolant. This means that whatever the load, the heat energy in the exhaust gas was almost 1.5 times greater than in coolant heat.

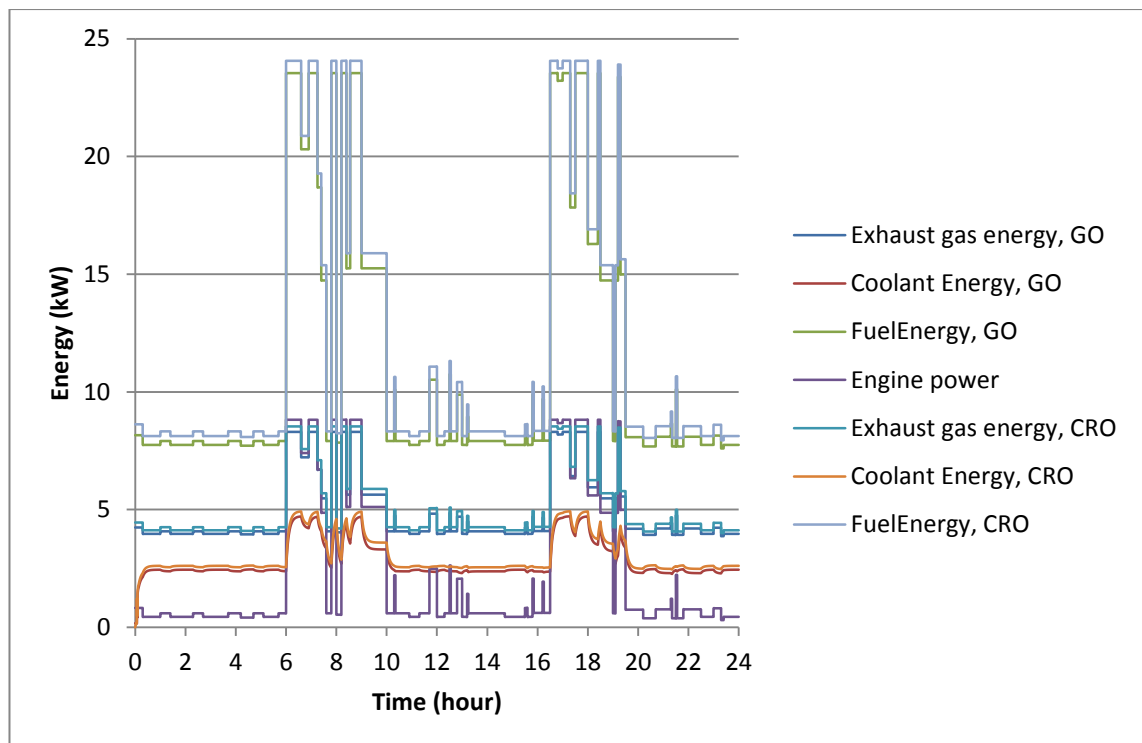


Fig. 5.34 Energy distributions with gas oil and croton oil

The heating and cooling energy generated by trigeneration are shown in Fig. 5.35 and Fig 5.36. Fig. 5.35 reveals that more coolant and exhaust gas heat was recovered when run with croton oil. For peak time operation, around 4.5kW coolant heat and 4.1kW exhaust gas heat were recovered and the generated cooling energy with two fuel fuels were almost identical (approximately 13W). When running at off-peak time, less heat was recovered, around 1.2kW from the coolant and 0.9kW from the exhaust. Since no

cooling energy was produced at low loads, the refrigerator must be run by electricity during the off-peak time. It should be noted that Fig. 5.26 is not the ‘real’ operational curve of the cooling energy generation. It only presents the cooling energy that could be generated for each load after running for at least half an hour. Fig. 5.37 shows the comparison of COP values with the two fuels. Due to the difference in input heat for the generator, the maximum COP with croton oil was about 0.034, slightly higher than that with gas oil. For 24 hours’ running time with croton oil, 88.9kWh heat energy was recovered, in which 50.0kWh was from coolant and 38.9kWh was from exhaust gas; while 68Wh of cooling energy was produced. When running with gas oil, a total of 83.5 kWh heat was recovered, including 46.0kWh of coolant heat and 37.5kWh of exhaust gas heat; while the cooling energy was 67.6Wh. This indicated that the heat to power ratio of the BMT was roughly 2:1. Compared to the reference data of the heat to power ratio of 4:1 in Chapter 2, it also illustrates that when the system runs during winter, additional heating equipment may be required to meet the overall heating demand.

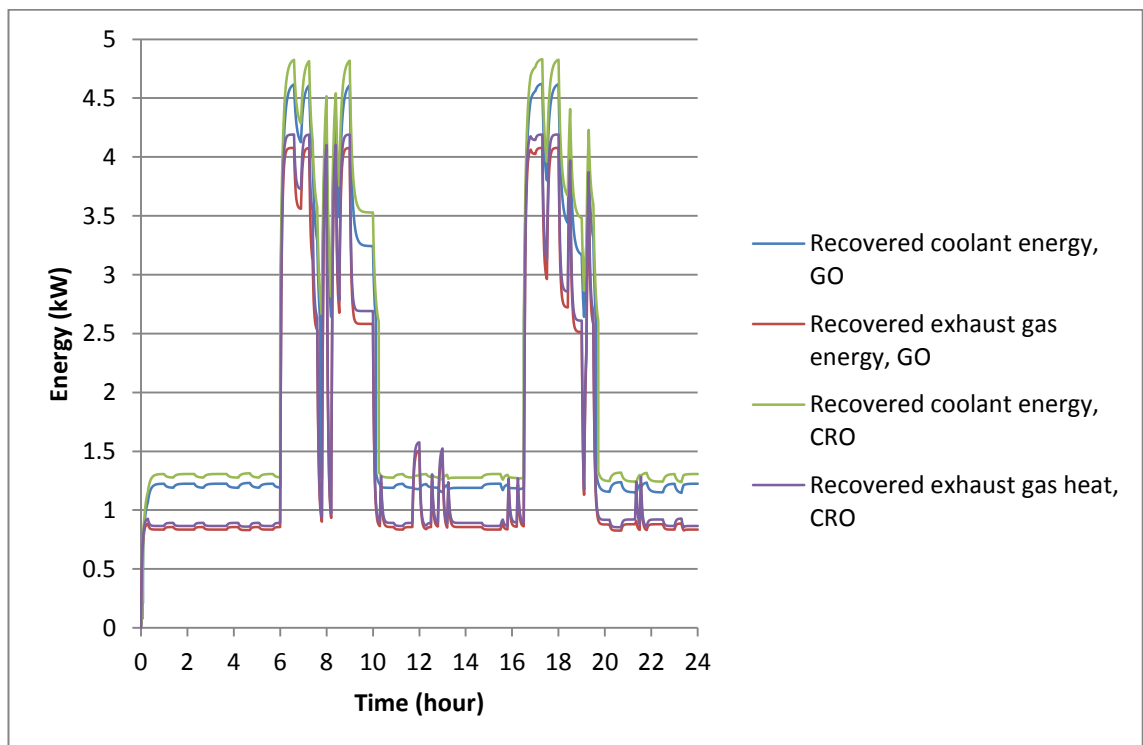


Fig. 5.35 Recovered heat energy with gas oil and croton oil

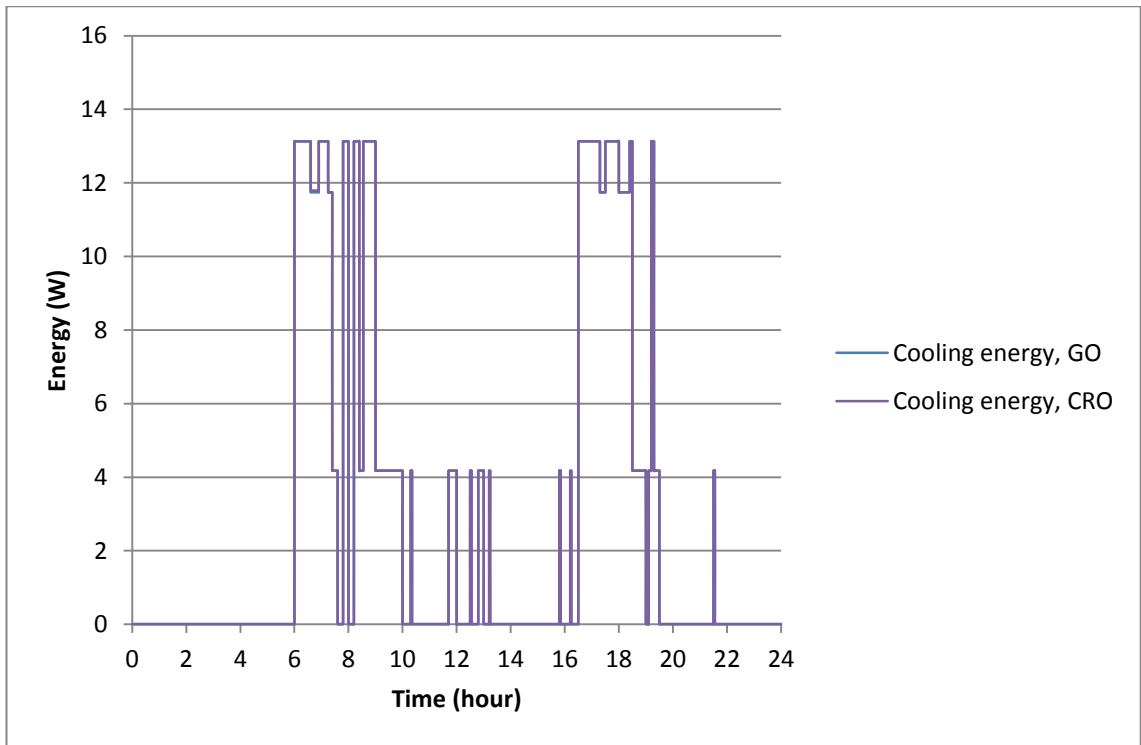


Fig. 5.36 Cooling energy with gas oil and croton oil

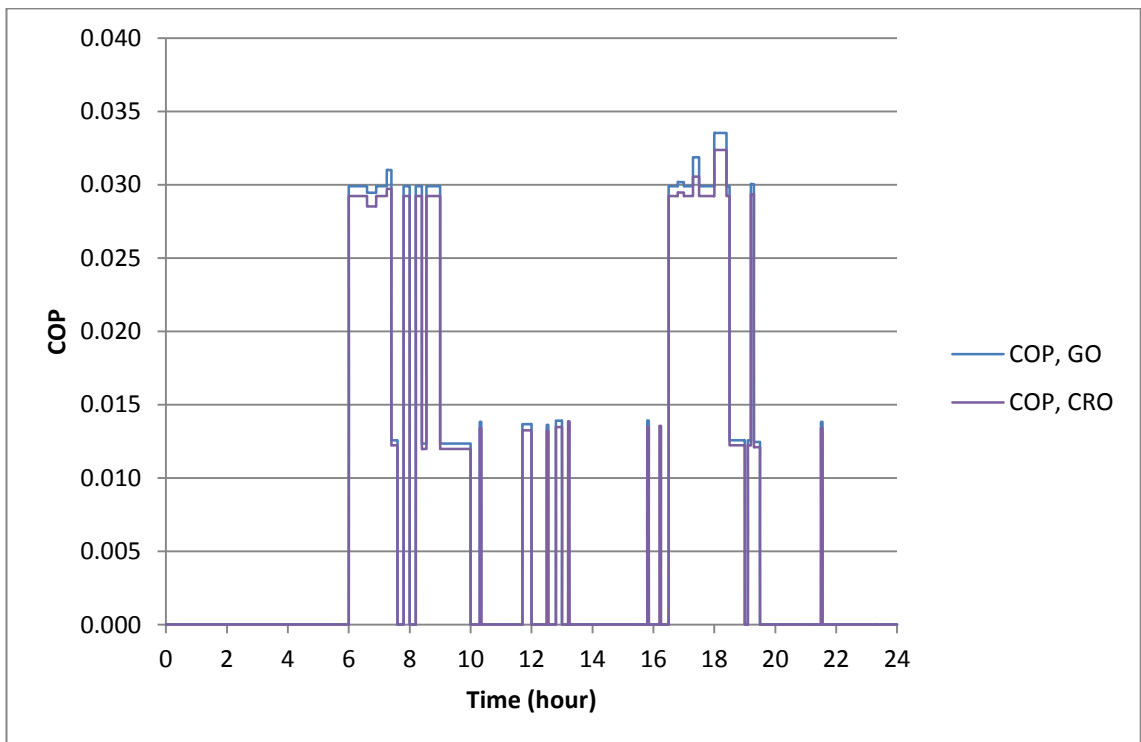


Fig. 5.37 COP with gas oil and croton oil

Fig. 5.38 and Fig.5.39 show the simulated efficiencies of the trigeneration system. When running with croton oil, due to a higher fuel consumption, the engine power efficiency and electrical efficiency were slightly lower than those with gas oil. The low

electrical efficiency compared to the engine efficiency was caused by the loss of belt transmission and the conversion losses in mechanical power to electricity. For peak time operation, the maximum engine efficiency and electrical efficiency were about 37% and 27%. However, when running at off peak time, these figures dropped sharply to around 5% and 3%. For the trigeneration efficiency, the figures for the two fuels were comparable, with the highest figure of 65% for peak load and lowest figure of 30% for off-peak load. It is noted that some sharp peaks appear and are shown in Fig. 5.39. The reason was that when the engine load changed from high to low, the input fuel energy reduced quickly. But due to the high thermal capacities of the coolant and heat exchangers, the recovered heat energy changed slowly, hence the calculated thermal efficiency increased. In extreme cases, the simulated trigeneration efficiency may exceed 100%. To avoid this situation the diagram value was smoothed out by taking the dynamic average of the nearest three values.

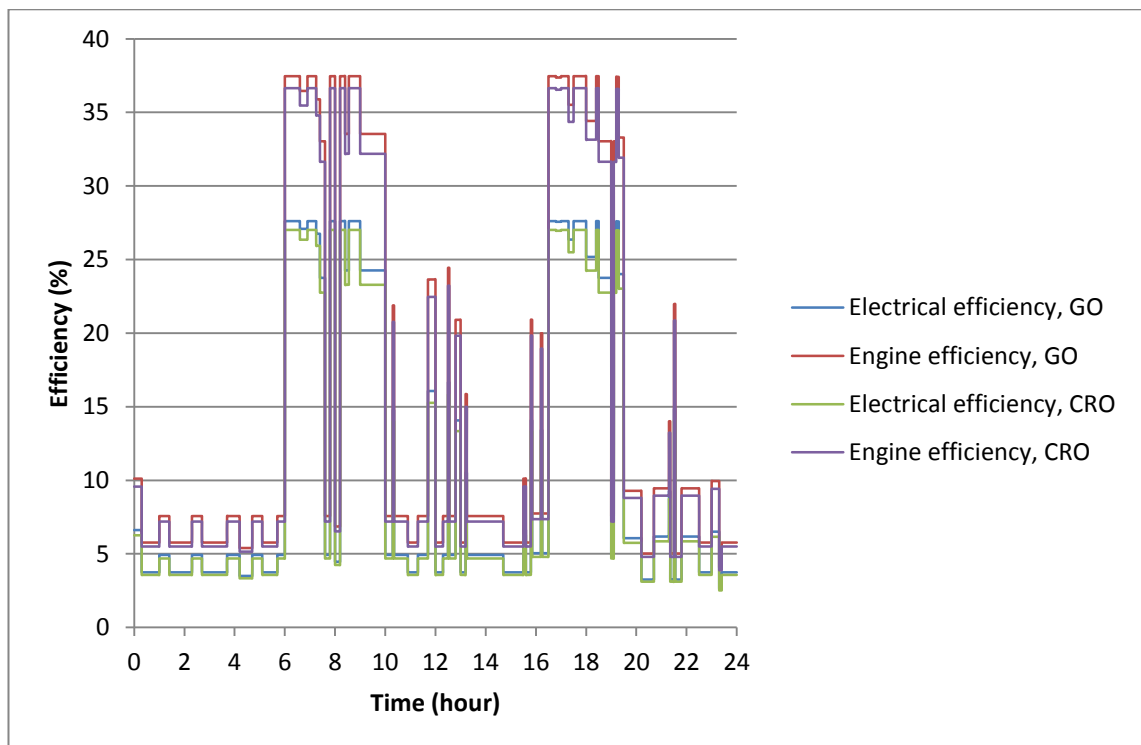


Fig. 5.38 Power and electrical efficiencies with gas oil and croton oil

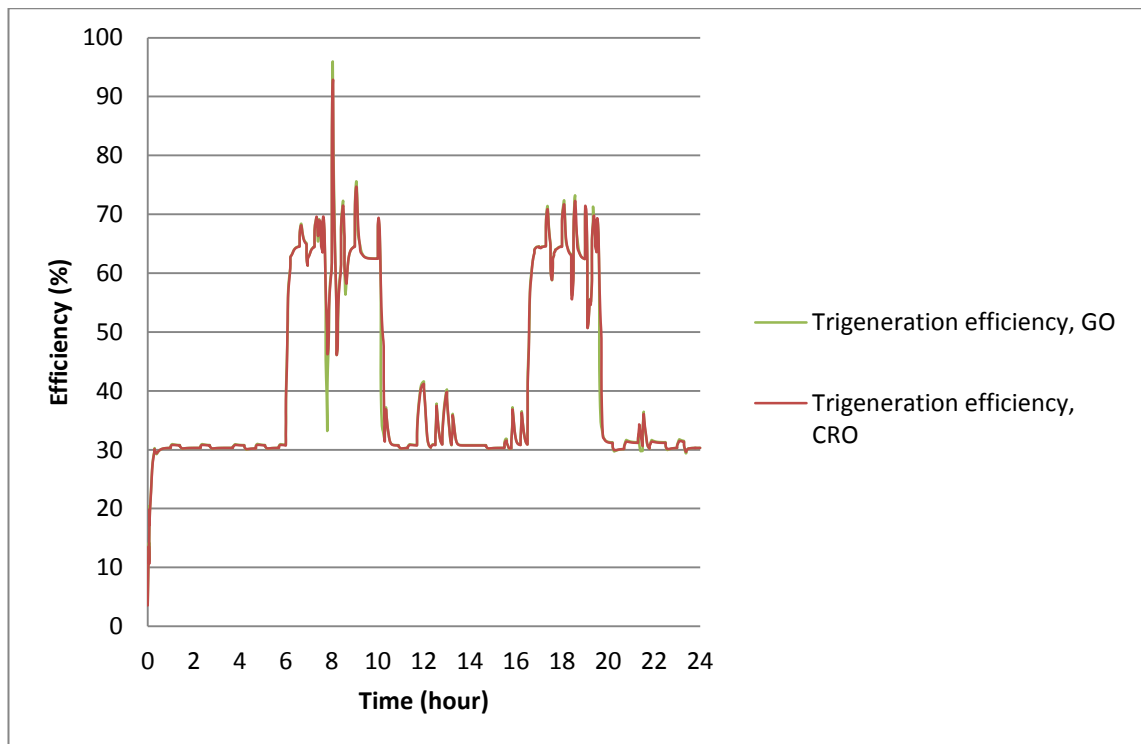


Fig. 5.39 Trigeration efficiencies with gas oil and croton oil

Based on the simulation results above, it can be seen that the BMT system performed at a low efficiency with an off-peak load. Considering the peak time only accounted for approximately a quarter of a day, it would require a high cost to run the system all day. Hence, energy storage systems (including electricity and heat storage) are necessary to meet the energy gap during the off peak time. The BMT system is suggested to run at peak time or slightly longer to charge up the energy storage system.

5.6 Conclusions and discussions

In this chapter, two models were setup and the performance of the engine and BMT system running with croton oil were theoretically investigated. Experimental data was used as the input for the models validation and proved accurate enough for simulation and prediction purposes. A number of conclusions were drawn from the engine simulation and summarised as follows:

- a) Preheating temperature posed great effects on both engine performance and emissions. Combustion was improved when the preheating temperature was increased from 30°C to 90°C, represented by a shorter ignition delay and increased peak combustion pressure and combustion temperature. As a result, improved engine power, BSFC and engine power efficiencies were observed.

- b) Improved CO₂ and PM emissions were found by increasing the preheating temperature. However, NO_x emission levels deteriorated and increased by 12.6% at full loads.
- c) Optimisation shows that SOI (19° CA BTDC), CR (20) and injection duration (26° CA) posed positive effect on the engine performance. When combined these parameters on optimization, the engine performed better both in performance and emissions, except NO_x emissions were doubled.

Conclusions drawn from the BMT simulation were:

- a) When run with croton oil, more fuel energy was needed in order to keep the same engine output relative to gas oil; and also the heat energy in coolant and exhaust gas with croton oil, as well as the recovered heat energy was greater.
- b) For trigeneration, more heat was recovered from coolant than exhaust gas. The heat to power ratio was roughly 2:1, this indicated that other heating equipment may be required to meet the heat demand during winter time. When running at peak times, approximately 13W of cooling energy was generated with a maximum COP of 0.034. During the off-peak time, no cooling energy was produced and the refrigerator had to be run by electricity.
- c) The engine power efficiency and electrical efficiency with croton oil were slightly lower than those with gas oil. Nevertheless, the trigeneration efficiencies running with the two fuels were almost the same.
- d) The BMT system performed with a low efficiency rate at off-peak loads, while the costs are high to run the system all day from a power supply. Hence, it is necessary to meet the energy demand by the use of energy storage systems (including electricity and heat storage). The BMT system is suggested to run during peak time or slightly longer to charge up the energy storage system.

Chapter 6. Conclusions and Recommendations

The BMT system performed with a low efficiency rate at off-peak loads, while the costs are high to run the system all day from a power supply. Hence, it is necessary to meet the energy demand by the use of energy storage systems (including electricity and heat storage). The BMT system is suggested to run during peak time or slightly longer to charge up the energy storage system.

6.1 Conclusions

Chapter 2 presented a literature study covering three aspects: a) Domestic energy demand and consumption, b) Micro-trigeneration and c) Vegetable oil research. It was discovered that the peak electricity consumption of most households was lower than 8 kW, and the heat to electricity ratio was roughly 4:1. For micro-trigeneration, an ICE with a power output lower than 10kW seems to be the favourable prime mover for micro-trigeneration relative to alternative competitive power sources. These usually cope with an absorption and adsorption refrigerator driven by waste heat. For vegetable oil research on the engine, directly combusting vegetable oils may lead to higher fuel consumption, lower thermal efficiency and reduced durability to the engine. Hence, methods such as blending, preheating and micro-emulsification are necessary to overcome these drawbacks. Based on a background study, a biofuel micro-trigeneration system was designed and constructed. The experimental apparatus, instrumentation, test plan and procedures as well as error analysis are presented in Chapter 3.

Chapter 4 discusses the experimental studies of physicochemical properties and the trigeneration performance of preheated vegetable oils compared to those with gas oil. The four raw vegetable oils chosen for the studies were sunflower oil, rapeseed oil, jatropha oil and croton oil. Test results have proven the feasibility of using preheated vegetable oil for driving a micro-trigeneration system. The following conclusions drawn from the test results are as follows:

- a) The vegetable oils contained a higher viscosity, higher density, richer oxygen concentration and lower HHV relative to gas oil.
- b) Comparable performances were discovered when using vegetable oils on the engine for power generation compared to that of the gas oil, except for

observations relating to higher fuel consumption and higher exhaust gas temperature.

- c) Higher CO₂, CO emissions and a lower O₂ content in the exhaust were found when using the vegetable oils. At the same time improved NO_x and HC emissions were observed for part loads.
- d) The recovered exhaust gas heat and coolant heat using the vegetable oils were higher than those of the gas oil for both cogeneration and trigeneration. The recovered coolant heat was higher than the recovered exhaust gas heat.
- e) When driven by exhaust gases, the input heating energy for the refrigerator was much greater than that when operated by electricity, while less cooling power was produced and the COP was significantly lower. However, this trend was reversed when it was evaluated from the input primary energy point of view. Improved cooling effects were observed with vegetable oil compared to gas oil. No cooling effects were noted when the engine load was lower than 50%.
- f) Significant improvements were discovered with cogeneration and trigeneration in terms of overall efficiency, BSFCs and CO₂ emission relative to power generation. Nevertheless, the fuel consumptions and CO₂ emission of the vegetable oils were still higher than that of the gas oil, while the BSECs and the overall efficiency of the fuels were comparable. Exergy analysis shows that the maximum exergy efficiency of trigeneration was only as half of the trigeneration efficiency, which indicates further measures can be made to improve the trigeneration efficiency both in quality and quantity.

In Chapter 5, a model was setup using the DIESEL-RK software to simulate and predict the engine performance. The model was run using croton oil and operated over a number of different preheating temperatures. A further BMT model was programmed using Dymola software to simulate the trigeneration performance for a case study lasting 24 hours using an electricity load. Both model's results closely matched the experimental results, highlighting a high accuracy representation for the theoretical study.

The engine simulation results show that the method of fuel preheating greatly affected both the engine performance and emissions. An increased preheating temperature resulted in improved engine combustion and hence improved engine power, BSFC and

efficiency. Less CO₂ and PM emissions were found with fuel preheating, while NO_x emission was reduced at high loads.

The BMT simulation results show that when run with croton oil, more fuel energy was needed in order to keep the same engine output relative to gas oil. This corresponds to more recovered heat energy and a slightly improved cooling effect. During the off-peak period, no cooling energy was produced and the refrigerator must be run by the use of electricity. The heat to power ratio of the BMT system was approximately 2:1.

Although the engine power efficiency and electrical efficiency using croton oil was slightly lower than that using gas oil, the trigeneration efficiency using both fuels was almost identical. Due to the low efficiency at off-peak load, it was necessary to use energy storage systems (including electricity and heat storage) to meet the energy demand. The BMT system was recommended to run during peak time or slightly longer to charge up the energy storage system.

6.2 Recommendations for future work

At this stage, intensive research has been carried out on biofuel micro-trigeneration. Theoretical and experimental study results have proved the feasibility of the system running with raw vegetable oils. Based on the current research outcomes, further investigation can be performed but not limited to the following aspects.

6.2.1 Diesel generator

As mentioned above, current experimental studies have only verified the possibility of applying vegetable oils in a trigeneration system. Looking to the future, further work is recommended in order to improve the performance of the diesel generator:

- a) Combustion investigation. Detailed investigation on the combustion of vegetable oil in the cylinder will help to better understand and explain the engine performance. This work could be achieved by using a constant volume combustion bomb for observing the air-fuel mixture formation and fuel combustion, or by installing sensors on the engine to measure cylinder pressure and temperature. In addition, work in optimisation techniques such as adjusting the injection timing and injection pressure could be adopted.
- b) Emission study. This thesis has investigated the regulated gas emissions of the engine. Other emissions such as PM and PAHs are also a restriction to the diesel

engine, while both pose harmful effects to human health. Further studies could focus on this aspect to identify the compositions of PM and exhaust gas of vegetable oil.

6.2.2 Heat exchanger and refrigerator

For the current experimental study, the heat exchangers were connected in series; hence the water flow of each heat exchanger cannot be adjusted independently. Besides, during the test, the water flow rate was fixed and no adjustment was made according to the engine load. It was found that at high loads, the exhaust gas temperature at the outlet of the exhaust gas heat exchanger was still high. This indicates that more exhaust gas could be recovered but is currently lost. For future studies, a different scheme of heat exchanger connections and water flow rates could be explored and tested to help improve the heat exchange efficiency. Concerning the refrigerator, the main problem was the low cooling effect when driven by exhaust gas. This was due to a large amount of exhaust gas heat being absorbed by the ammonia-water vapour in the siphon pump and rectifier. Further studies are recommended to enhance the heat exchange properties of the rectifier, water separator and condenser. This will enable the ammonia temperature to be dropped down to the same level as that driven by electricity.

6.2.3 BMT system

This stage was limited in the study of the static output energy of the BMT system. A recommendation would be to try and integrate the system with an energy storage system, i.e. a heat storage system and electricity storage system. This would allow the dynamic performance of the systems to be investigated under different electrical and heat loads. Based on this setup, the system operation and control strategy could be explored in more detail.

6.2.4 Simulation and optimisation

Recommendations for future work related to simulation and optimisation are:

- a) Engine modelling. As previously shown in Chapter 5, simulation studies on the engine and BMT system were based on the models setup using two different software platforms. When setting up an engine model in Dymola, the engine and BMT system performance can be simulated as a whole while the engine parameters can be transferred to other modules both directly and dynamically.

- b) Optimisation. Various optimisation options that may be difficult to apply on the engine or for trigeneration could be done theoretically. This could involve investigations on the shape of the combustion chamber, dual-fuel, schematic layout of heat exchanger connections, etc. Further study may focus on reducing NO_x emissions by trying more multiple parameter optimizations.
- c) Improvement of the refrigeration model. Due to the complexity of heat transfer and two-phase flow, it was not possible to simulate the dynamic performance of the absorption refrigeration with a high accuracy. Further efforts are still required in this area.

References

1. EIA, *International Energy Outlook 2011*, 2011:
[http://205.254.135.7/forecasts/ieo/pdf/0484\(2011\).pdf](http://205.254.135.7/forecasts/ieo/pdf/0484(2011).pdf).
2. IEA. *Key World Energy Statistics 2011*. 2011; Available from:
http://www.iea.org/textbase/nppdf/free/2011/key_world_energy_stats.pdf.
3. BP, *BP Statistical Review of World Energy 2011*, 2011: BP Statistical Review of World Energy. p. 48.
4. Klass, D.L., *A critical assessment of renewable energy usage in the USA*. Energy Policy, 2003. **31**(4): p. 353-367.
5. Carson, R., *Silent Spring* 1962, Boston: Houghton Mifflin.
6. Deffeyes, K.S., *Hubbert's Peak, The Impending World Oil Shortage* 2001, Princeton, NJ: Princeton University Press.
7. Klass, D.L., *Biomass for Renewable Energy, Fuels, and Chemicals* 1998, San Diego, CA: Academic Press.
8. EIA. *World Carbon Dioxide Emissions from the Consumption and Flaring of Fossil Fuels (Million Metric Tons of Carbon Dioxide), 1980-2006*. 2008; Available from: <http://www.eia.doe.gov/pub/international/iealf/tableh1co2.xls>.
9. UN. *Agenda 21 and the Rio Principles*. 1992; Available from:
<http://www.un.org/esa/desa/aboutus/dsd.html>.
10. UN. *Kyoto Protocol*. 1997; Available from:
http://unfccc.int/kyoto_protocol/items/2830.php.
11. EWEA. *EU Energy Policy to 2050*. 2011; Available from:
http://www.ewea.org/fileadmin/ewea_documents/documents/publications/reports/EWEA_EU_Energy_Policy_to_2050.pdf.
12. DTI, *Meeting the energy challenge – a white paper on energy*, 2007, The Stationary Office Limited: London.
13. OFGEM, *A review of the first year of the Energy Efficiency Commitment 2005–2008*, 2006: London.
14. DTI, *Wicks gives a helping hand to green householders – Press Release P/2006/231*, 2006, Department of Trade and Industry,
: London.
15. DTI, *Our energy challenge – power from the people – microgeneration strategy*, 2006, Department of Trade and Industry: London.

16. DTI. *Low Carbon Buildings Programme [online]*. 2006; Available from:
Available from: <http://www.lowcarbonbuildings.co.uk/>.
17. BERR, *Digest of United Kingdom energy statistics: 2007*, 2007.
18. Huangfu, Y., et al., *Evaluation and analysis of novel micro-scale combined cooling, heating and power (MCCHP) system*. Energy Conversion and Management, 2007. **48**(5): p. 1703-1709.
19. Hui_Li, et al., *Energy utilization evaluation of CCHP systems*. Energy and Buildings, 2006. **38**(2006): p. 253-257.
20. Wu, D.W. and R.Z. Wang, *Combined cooling, heating and power: A review*. Progress in Energy and Combustion Science, 2006. **32**(5-6): p. 459-495.
21. Gluesenkamp, K., Y. Hwang, and R. Radermacher, *High efficiency micro trigeneration systems*. Applied Thermal Engineering, (0).
22. Chicco, G. and P. Mancarella, *Distributed multi-generation: A comprehensive view*. Renewable and Sustainable Energy Reviews, 2009. **13**(3): p. 535-551.
23. Demirbas, A., *Biofuels sources, biofuel policy, biofuel economy and global biofuel projections*. Energy Conversion and Management, 2008. **49**: p. 10.
24. Sims, R., et al. *from 1st - to 2nd - generation biofuel technologies*. 2008; Available from:
http://www.iea.org/textbase/papers/2008/2nd_Biofuel_Gen_Exec_Sum.pdf.
25. UN. *Sustainable Bioenergy: A Framework for Decision Makers*. 2008; Available from: <http://esa.un.org/un-energy/pdf/susdev.Biofuels.FAO.pdf>.
26. Wikipedia. *Biofuel in the European Union*. 2008; Available from:
http://en.wikipedia.org/wiki/Biofuel_in_the_European_Union#cite_note-BaroBiofuels2007-1.
27. Eriksson, G. and B. Kjellström, *Assessment of combined heat and power (CHP) integrated with wood-based ethanol production*. Applied Energy, 2010. **87**(12): p. 3632-3641.
28. rahimi, H., et al., *Diesterol: An environment-friendly IC engine fuel*. Renewable Energy, 2009. **34**(1): p. 335-342.
29. Kerr, T. *Near-term Solutions: CHP and DHC*. in *IDEA 99th Annual Conference & Trade Show*. 2008. Orlando, Florida USA.
30. Nitske, W.R. and C.M. Wilson, *Rudolf Diesel Pioneer of the Age of Power* 1965: University of Oklahoma Press, Norman, OK

31. Rocha, M.S., R. Andreos, and J.R. Simões-Moreira, *Performance tests of two small trigeneration pilot plants*. Applied Thermal Engineering, 2012. **41**(0): p. 84-91.
32. Angrisani, G., C. Roselli, and M. Sasso, *Distributed microtrigeneration systems*. Progress in Energy and Combustion Science, 2012. **38**(4): p. 502-521.
33. DECC, *Energy consumption in the United Kingdom: 2011*, 2011: Available from: <http://www.decc.gov.uk/assets/decc/11/stats/publications/energy-consumption/2323-domestic-energy-consumption-factsheet.pdf>.
34. DECC, *Energy consumption in the UK: domestic data tables*, 2011: Available from: <http://www.decc.gov.uk/media/viewfile.ashx?filetype=4&filepath=Statistics/publications/ecuk/4186-ecuk-domestic-2010.xls>.
35. Firth, S., et al., *Identifying trends in the use of domestic appliances from household electricity consumption measurements*. Energy and Buildings, 2008. **40**(5): p. 926-936.
36. Allen, S.R., G.P. Hammond, and M.C. McManus, *Prospects for and barriers to domestic micro-generation: A United Kingdom perspective*. Applied Energy, 2008. **85**(6): p. 528-544.
37. Newborough, M., *Assessing the benefits of implementing micro-CHP systems in the UK* Proceedings of the Institution of Mechanical Engineers, Part A: Journal of Power and Energy, 2004. **218**(4): p. 203-218.
38. Peacock, A.D. and M. Newborough, *Impact of micro-combined heat-and-power systems on energy flows in the UK electricity supply industry*. Energy, 2006. **31**(12): p. 1804-1818.
39. M.Newborough and P.Augood, *Demand-side management opportunities for the UK domestic sector*. IEEE Proceedings of Generation Transmission and Distribution, 1999. **146**(3): p. 283-293.
40. Wood, G. and M. Newborough, *Dynamic energy-consumption indicators for domestic appliances: environment, behaviour and design*. Energy and Buildings, 2003. **35**(8): p. 821-841.
41. G.Wood and M.Newborough, *Dynamic energy-consumption indicators for domestic appliances:environment, behaviour and design*. Energy and Buildings, 2003. **35**(2003): p. 821-841.
42. COGENEurope, *A Guide to Cogeneration*, 2001.

43. *DIRECTIVE 2004/8/EC OF THE EUROPEAN PARLIAMENT AND OF THE COUNCIL of 11 February 2004 on the promotion of cogeneration based on a useful heat demand in the internal energy market and amending Directive 92/42/EEC*, Official Journal of the European Union.
44. Overend, R.P. and E.H.S. Ralph, *Heat, Power and Combined Heat and Power*, in *Bioenergy Options for a Cleaner Environment* 2004, Elsevier: Oxford. p. 63-102.
45. Aspen, *Combined Heat and Power: A Federal Manager's Resource Guide*, 2000: http://www1.eere.energy.gov/manufacturing/distributedenergy/pdfs/chp_femp.pdf.
46. Hawkes, A.D. and M.A. Leach, *Cost-effective operating strategy for residential micro-combined heat and power*. *Energy*, 2007. **32**(5): p. 711-723.
47. Dong, L., H. Liu, and S. Riffat, *Development of small-scale and micro-scale biomass-fuelled CHP systems - A literature review*. *Applied Thermal Engineering*. **In Press, Corrected Proof**.
48. Martin, P., et al., *Micro Cogeneration Towards Decentralized Energy Systems* 2006, Berlin: Springer.
49. J.Godefroy, R.Boukhanouf, and S.Riffat, *Design, testing and mathematical modelling of a small-scale CHP and cooling system (small CHP-ejector trigeneration)*. *Applied Thermal Engineering*, 2007. **27**(2007): p. 68-77.
50. João, C. *The Lisbon DHC: a Model for Southern Europe-Climate talks, climate action*. in *Euroheat & Power 34th Congress*. 26 May 2009. Venice, Italy.
51. John, C., F. Ron, and S. Richard. *Cooling, Heating, and Power Facility in University of Illinois at Chicago*. 2001; Available from: http://www.esmagazine.com/Articles/Feature_Article/72c6fca6a4ca8010VgnVCM100000f932a8c0.
52. Monty, G. *City of Austin dedicates new "super-efficient" 4.5MW tri-generation plant*. . 2004; Available from: <http://www.cogeneration.net/Trigeneration%20Advantages.htm>.
53. A.Marantan, *Optimization of integrated micro-turbine and absorption chiller systems in CHP for buildings applications*, in *Department of Mechanical Engineering* 2002, University of Maryland: Maryland, College Park.
54. Alanne, K. and A. Saari, *Sustainable small-scale CHP technologies for buildings: the basis for multi-perspective decision-making*. *Renewable and Sustainable Energy Reviews*, 2004. **8**(5): p. 401-431.

55. Kuhn, V., J. Klemes, and I. Bulatov, *MicroCHP: Overview of selected technologies, products and field test results*. Applied Thermal Engineering, 2008. **28**(16): p. 2039-2048.
56. Cockroft, J. and N. Kelly, *A comparative assessment of future heat and power sources for the UK domestic sector*. Energy Conversion and Management, 2006. **47**(15-16): p. 2349-2360.
57. Kong, X.Q., R.Z. Wang, and X.H. Huang, *Energy efficiency and economic feasibility of CCHP driven by stirling engine*. Energy Conversion and Management, 2004. **45**(9-10): p. 1433-1442.
58. Thombare, D.G. and S.K. Verma, *Technological development in the Stirling cycle engines*. Renewable and Sustainable Energy Reviews, 2008. **12**(1): p. 1-38.
59. Sternlicht, B., *The stirling engine: prime mover of the 21st century*. Endeavour, 1984. **8**(1): p. 21-28.
60. Kongtragool, B. and S. Wongwises, *A review of solar-powered Stirling engines and low temperature differential Stirling engines*. Renewable and Sustainable Energy Reviews, 2003. **7**(2): p. 131-154.
61. Pilavachi, P.A., *Mini- and micro-gas turbines for combined heat and power*. Applied Thermal Engineering, 2002. **22**(18): p. 2003-2014.
62. El-Khattam, W. and M.M.A. Salama, *Distributed generation technologies, definitions and benefits*. Electric Power Systems Research, 2004. **71**(2): p. 119-128.
63. Suter, M., *Active filter for a microturbine*, in *INTELEC 2001: international telecommunications energy conference* IEE, London, ROYAUME-UNI (2001): Edinburgh, 14-18 October 2001 p. 162-165.
64. Lasseter, B. and Microgrids. *distributed power generation*. in *Proceedings of the Power Engineering Society Winter Meeting IEEE*. 2001.
65. Piet, I. and W. Peter, et al., *Biofuels for Fuel Cells* 2005, London: IWA Publishing.
66. Kerry-Ann, A., *Stationary fuel cells: an overview*. First edition ed2007, London: Elsevier.
67. Susai, T., et al., *Development of a 1 kW PEM fuel cell power source*. Fuel Cells Bulletin, 2001. **3**(29): p. 7-11.
68. EERE. *Comparison of Fuel Cell Technologies*. 2008; Available from: http://www1.eere.energy.gov/hydrogenandfuelcells/fuelcells/pdfs/fc_comparison_chart.pdf.

69. *Worldwide Fuel Cell Installations 2000*; Available from:
<http://www.fuelcells.org/info/charts/FCInstallationChart.pdf>.
70. Onovwiona, H.I. and V.I. Ugursal, *Residential cogeneration systems: review of the current technology*. Renewable and Sustainable Energy Reviews, 2006. **10**(5): p. 389-431.
71. Staffell, I., *Review of PEM fuel cell performance 2007*.
72. Srikihrin, P., S. Aphornratana, and S. Chungpaibulpatana, *A review of absorption refrigeration technologies*. Renewable and Sustainable Energy Reviews, 2001. **5**(4): p. 343-372.
73. Marcriss, R., J. Gutraj, and T. Zawacki, *Absorption fluid data survey: final report on worldwide data*, 1988, ORLN/sub/8447989/3, Inst. Gas Tech.
74. Hwang, Y., *Potential energy benefits of integrated refrigeration system with microturbine and absorption chiller*. International Journal of Refrigeration, 2004. **27**(8): p. 816-829.
75. Corporation, R.D., *Integrated Energy Systems (IES) for Buildings: A Market Assessment*, August, 2002.
76. Wang, J.-J., et al., *Performance comparison of combined cooling heating and power system in different operation modes*. Applied Energy, 2011. **88**(12): p. 4621-4631.
77. Wang, L.W., R.Z. Wang, and R.G. Oliveira, *A review on adsorption working pairs for refrigeration*. Renewable and Sustainable Energy Reviews, 2009. **13**(3): p. 518-534.
78. Critoph, R.E. and S.J. Metcalf, *Specific cooling power intensification limits in ammonia-carbon adsorption refrigeration systems*. Applied Thermal Engineering, 2004. **24**(5-6): p. 661-678.
79. Srivastava, N.C. and I.W. Eames, *A review of adsorbents and adsorbates in solid-vapour adsorption heat pump systems*. Applied Thermal Engineering, 1998. **18**(9-10): p. 707-714.
80. Anyanwu, E.E., *Review of solid adsorption solar refrigerator I: an overview of the refrigeration cycle*. Energy Conversion and Management, 2003. **44**(2): p. 301-312.
81. Qun, C., *Studies on Adsorption Refrigeration Working Pairs and Refrigeration Process*, 2002, Nanjing University of Technology: Nanjing.
82. Wang, R.Z., *Adsorption refrigeration research in Shanghai Jiao Tong University*. Renewable and Sustainable Energy Reviews, 2001. **5**(1): p. 1-37.

83. Cui, X., *Alternate fuels for automobiles and biomass energy* 2007: China Petrochemical Press. 561.
84. Deng, J., et al., *Exergy cost analysis of a micro-trigeneration system based on the structural theory of thermoeconomics*. Energy, 2008. **33**(9): p. 1417-1426.
85. Lin, L., et al., *An experimental investigation of a household size trigeneration*. Applied Thermal Engineering, 2007. **27**(2-3): p. 576-585.
86. Wang, Y.D., D. McIlveen-Wright, and Y. Huang, *An Investigation of a Sustainable Biomass Fuelled Household Size Trigeneration*, in *REMIC2 Conference* 26-28 April 2006: Dublin, Germany.
87. Miguez, J.L., et al., *Feasibility of a new domestic CHP trigeneration with heat pump: I. Design and development*. Applied Thermal Engineering, 2004. **24**(10): p. 1409-1419.
88. Wang, R., et al. *Performance research of a micro CCHP system with adsorption chiller*. in *Proceedings of the international sorption heat pump conference*. 2005. Denver, CO, USA.
89. Angrisani, G., et al., *Experimental results of a micro-trigeneration installation*. Applied Thermal Engineering, 2012. **38**(0): p. 78-90.
90. Porteiro, J., et al., *Feasibility of a new domestic CHP trigeneration with heat pump: II. Availability analysis*. Applied Thermal Engineering, 2004. **24**(10): p. 1421-1429.
91. Moya, M., et al., *Performance analysis of a trigeneration system based on a micro gas turbine and an air-cooled, indirect fired, ammonia–water absorption chiller*. Applied Energy, 2011. **88**(12): p. 4424-4440.
92. Arosio, S., M. Guilizzoni, and F. Pravettoni, *A model for micro-trigeneration systems based on linear optimization and the Italian tariff policy*. Applied Thermal Engineering, 2011. **31**(14–15): p. 2292-2300.
93. Wang, Y., et al., *An investigation of a household size trigeneration running with hydrogen*. Applied Energy, 2011. **88**(6): p. 2176-2182.
94. QIAN_Ye-jian and ZUO_Cheng-ji, *Review of Researches on Biofuel as Fuels for Diesel Engines*. Tractor & Farm Transport, 2006. **33**: p. 12-16.
95. Sharma, Y.C., B. Singh, and S.N. Upadhyay, *Advancements in development and characterization of biodiesel: A review*. Fuel, 2008. **87**(12): p. 2355-2373.
96. Demirbas, A., *Relationships derived from physical properties of vegetable oil and biodiesel fuels*. Fuel, 2008. **87**: p. 1743-1748.

97. Kaul, S., et al., *Corrosion behavior of biodiesel from seed oils of Indian origin on diesel engine parts*. Fuel Processing Technology, 2007. **88**(3): p. 303-307.
98. Bossel, U., *Well-to-Wheel Studies, Heating Values, and the Energy Conservation Principle in Proceedings of Fuel Cell Forum 2003* 2003.
99. Mohibbe Azam, M., A. Waris, and N.M. Nahar, *Prospects and potential of fatty acid methyl esters of some non-traditional seed oils for use as biodiesel in India*. Biomass and Bioenergy, 2005. **29**(4): p. 293-302.
100. Cetin, M. and F. Yuksel, *The use of hazelnut oil as a fuel in pre-chamber diesel engine*. Applied Thermal Engineering, 2007. **27**(1): p. 63-67.
101. Srivastava, P.K. and M. Verma, *Methyl ester of karanja oil as an alternative renewable source energy*. Fuel, 2008. **87**(8-9): p. 1673-1677.
102. Agarwal, A.K. and K. Rajamanoharan, *Experimental investigations of performance and emissions of Karanja oil and its blends in a single cylinder agricultural diesel engine*. Applied Energy, 2009. **86**(1): p. 106-112.
103. Baiju, B., M.K. Naik, and L.M. Das, *A comparative evaluation of compression ignition engine characteristics using methyl and ethyl esters of Karanja oil*. Renewable Energy, 2009. **34**(6): p. 1616-1621.
104. FAO. *The State of Food And Agriculture 2008* Available from: <ftp://ftp.fao.org/docrep/fao/011/i0100e/i0100e.pdf>.
105. van Eijck, J. and H. Romijn, *Prospects for Jatropha biofuels in Tanzania: An analysis with Strategic Niche Management*. Energy Policy, 2008. **36**(1): p. 311-325.
106. Wood, P., *Out of Africa: Could Jatropha vegetable oil be Europe's biodiesel feedstock?* Refocus. **6**(4): p. 40-44.
107. Vinay, B.J. and T.C. Sindhu Kanya, *Effect of detoxification on the functional and nutritional quality of proteins of karanja seed meal*. Food Chemistry, 2008. **106**(1): p. 77-84.
108. Singh, A. and I.S. Singh, *Chemical evaluation of mahua (Madhuca indica) seed*. Food Chemistry, 1991. **40**(2): p. 221-228.
109. Rijssenbeek, W., *Report:Expert Meeting Jatropha, Brussels 07/12/07*, 2007.
110. Sharma, Y.C. and B. Singh, *Development of biodiesel from karanja, a tree found in rural India*. Fuel, 2008. **87**(8-9): p. 1740-1742.
111. Chakraborty, N. and L. Mandal, *Histopathological changes in liver and kidney of mice fed pure Karanja oil and its different fractions*. Indian Veterinary Journal 1992. **69**: p. 1082–1084.

112. Menon, K.K.G., *Nutritional and toxicological aspects of uncommon edible oils. The Role of Fats in Human Nutrition*, ed. M.J. Mulky and V.V.S. Mani 1989, New York: Academic Press. 407–440.
113. Natanam, R., R. Kadirvel, and R. Ravi, *The toxic effects of karanja (Pongamia glabra Vent) oil and cake on growth and feed efficiency in broiler chicks. Animal Feed Science and Technology*, 1989. **27**(1-2): p. 95-100.
114. Gandhi, V.M. and K.M. Cherian, *Red cell haemolysis test as an in vitro approach for the assessment of toxicity of karanja oil. Toxicology in Vitro*, 2000. **14**(6): p. 513-516.
115. Adam, S.E.I., *Toxic effects of Jatropha curcas in mice. Toxicology*, 1974. **2**(1): p. 67-76.
116. Adam, S.E.I. and M. Magzoub, *Toxicity of Jatropha curcas for goats. Toxicology*, 1975. **4**(3): p. 388-389.
117. Goonasekera, M.M., et al., *Pregnancy terminating effect of Jatropha curcas in rats. Journal of Ethnopharmacology*, 1995. **47**(3): p. 117-123.
118. Hemmerlein, N., V. Korte, and I. Richter, *Performance Exhaust Emissions and Durability of Modern Diesel Engines Running on Rapeseed Oil. SAE 910848*, 1991.
119. Labeckas, G. and S. Slavinskas, *Performance of direct-injection off-road diesel engine on rapeseed oil. Renewable Energy*, 2006. **31**(6): p. 849-863.
120. Bari, S., W. Yu, and T. Lim, *Performance deterioration and durability issues while running a diesel engine with crude palm oil. Automob Eng*, 2002. **216**(D1): p. 785-792.
121. Haldar, S.K., B.B. Ghosh, and A. Nag, *Studies on the comparison of performance and emission characteristics of a diesel engine using three degummed non-edible vegetable oils. Biomass and Bioenergy*, 2008. **In Press, Corrected Proof**.
122. Masjuki, H., et al., *Performance, emissions and wear characteristics of an indirect injection diesel engine using coconut oil blended fuel. Proceedings of the Institution of Mechanical Engineers, Part D: Journal of Automobile Engineering*, 2001. **215**(3): p. 393-404.
123. Wang, Y.D., et al., *An experimental investigation of the performance and gaseous exhaust emissions of a diesel engine using blends of a vegetable oil. Applied Thermal Engineering*, 2006. **26**(14-15): p. 1684-1691.

124. Hazar, H. and H. Aydin, *Performance and emission evaluation of a CI engine fueled with preheated raw rapeseed oil (RRO)–diesel blends*. Applied Energy, 2010. **87**(3): p. 786-790.
125. Kalam, M.A. and H.H. Masjuki, *Emissions and deposit characteristics of a small diesel engine when operated on preheated crude palm oil*. Biomass and Bioenergy, 2004. **27**(3): p. 289-297.
126. de Almeida, S.C.A., et al., *Performance of a diesel generator fuelled with palm oil*. Fuel, 2002. **81**(16): p. 2097-2102.
127. Canakci, M., A.N. Ozsezen, and A. Turkcan, *Combustion analysis of preheated crude sunflower oil in an IDI diesel engine*. Biomass and Bioenergy, 2009. **33**(5): p. 760-767.
128. Agarwal, D. and A.K. Agarwal, *Performance and emissions characteristics of Jatropha oil (preheated and blends) in a direct injection compression ignition engine*. Applied Thermal Engineering, 2007. **27**(13): p. 2314-2323.
129. Chauhan, B.S., et al., *Performance and emission study of preheated Jatropha oil on medium capacity diesel engine*. Energy, 2010. **35**(6): p. 2484-2492.
130. Yilmaz, N. and B. Morton, *Effects of preheating vegetable oils on performance and emission characteristics of two diesel engines*. Biomass and Bioenergy, 2011. **35**(5): p. 2028-2033.
131. Pugazhvadivu, M. and K. Jeyachandran, *Investigations on the performance and exhaust emissions of a diesel engine using preheated waste frying oil as fuel*. Renewable Energy, 2005. **30**(14): p. 2189-2202.
132. Rakopoulos, C.D., K.A. Antonopoulos, and D.C. Rakopoulos, *Multi-zone modeling of Diesel engine fuel spray development with vegetable oil, bio-diesel or Diesel fuels*. Energy Conversion and Management, 2006. **47**(11–12): p. 1550-1573.
133. Rakopoulos, C.D., K.A. Antonopoulos, and D.C. Rakopoulos, *Development and application of multi-zone model for combustion and pollutants formation in direct injection diesel engine running with vegetable oil or its bio-diesel*. Energy Conversion and Management, 2007. **48**(7): p. 1881-1901.
134. Aliyu, B., *Biodiesel Production and Analysis: Non Food Source*, in *School of Mechanical and Systems Engineering* March 2009, Newcastle University.
135. Aliyu, B., B. Agnew, and S. Douglas, *Croton megalocarpus (Musine) seeds as a potential source of bio-diesel*. Biomass and Bioenergy, 2010. **34**(10): p. 1495-1499.

136. Lujaji, F., et al., *Cetane Number and Thermal Properties of Croton Oil, Biodiesel, 1-Butanol, and Diesel Blends*. Journal of Thermal Analysis and Calorimetry, 2010. **102**(3): p. 1175-1181.
137. Haldar, S.K., B.B. Ghosh, and A. Nag, *Studies on the comparison of performance and emission characteristics of a diesel engine using three degummed non-edible vegetable oils*. Biomass and Bioenergy, 2009. **33**(8): p. 1013-1018.
138. Misra, R.D. and M.S. Murthy, *Straight vegetable oils usage in a compression ignition engine—A review*. Renewable and Sustainable Energy Reviews, 2010. **14**(9): p. 3005-3013.
139. Deng, J., R.Z. Wang, and G.Y. Han, *A review of thermally activated cooling technologies for combined cooling, heating and power systems*. Progress in Energy and Combustion Science, 2011. **37**(2): p. 172-203.
140. Knothe, G., *Historical Perspectives on Vegetable Oil-Based Diesel Fuels*. Industrial Oils, 2001. **12**: p. 1103-1107.
141. Spiers, H.M., *Technical Data on Fuel (Fourth Edition)*1937, London: British National Committee, World Power Conference. p.261.
142. *Properties of HIPS*. 2012; Available from: <http://www.makeitfrom.com/compare-materials/?A=High-Impact-Polystyrene-HIPS&B=Rigid-Thermoset-Polyurethane-RPU>.
143. *Common properties for air*. 2012; Available from: http://www.engineeringtoolbox.com/air-properties-d_156.html.
144. Perrot, P., *A to Z of Thermodynamics* 1998: Oxford University Press.
145. Heywood JB, *Internal Combustion Engine Fundamentals* 1998, Sydney: McGraw-Hill.
146. Launder, B.E. and D.B. Spalding, *Lectures in mathematical models of turbulence*1972: Academic Press.
147. Zhu FJ, *Numerical computation and optimization on the working process of internal Combustion Engine*1997.7, Beijing: National Defence Industry Press (Chinese only).
148. Hiroyasu H. Kadota T and Arai M, *Development and Use of a Spray Combustion Model to Predict Diesel Engine Efficiency and Pollutant Emissions. Part I: Combustion Modeling*. Bull JSME, 1983a. **26**(214): p. 569-575.
149. Hiroyasu, H. *Diesel Engine Combustion and Its Modelling*. in *COMODIA 85, Proceeding of Symposium*. 1985. Tokyo

150. Weaving, J.H., *Internal Combustion Engineering Science and Technology* 1990, London: Elsevier Applied Science.
151. *Home page of DIESEL-RK*. 2012; Available from: <http://www.diesel-rk.bmstu.ru/Eng/index.php>.
152. Kuleshov, A.S., A.V. Kozlov, and K. Mahkamov. *Self-Ignition delay Prediction in PCCI direct injection diesel engines using multi-zone spray combustion model and detailed chemistry*. 2010; Available from: <http://www.diesel-rk.bmstu.ru/Eng/downloads/10CV-0019.pdf>.
153. Livengood, J.C. and P.C. Wu, *Correlation of Autoignition Phenomena in Internal Combustion Engines and Rapid Compression Machines*, in *5th International Symposium on Combustion* 1955: Pittsburgh, Pennsylvania. p. 347-356.
154. Isaev, A.V. *Fuel Autoignition Processes Simulation (In Russian)*. 2009; Available from: <http://dieselexpert.narod.ru/Autoignition.pdf>.
155. Zeldovich YB, *The Oxidation of Nitrogen in Combustion and Explosions*. Acta Physicochimica, USSR, 1946. **vol 21**: p. 577-628.
156. Lavoie GA, Heywood JB, and K. JC, *Experimental and Theoretical Investigation of Nitric Oxide Formation in Internal Combustion Engines*. Combust Sci Tech, 1970. **vol 1**: p. 313-326.
157. Bowman CT, *Kinetics of Pollutant Formation and Destruction in Combustion*. Prog Energy Combust Sci, 1975. **vol 1**: p. 33-45.
158. G.stiesch, *Modeling Engine Spray and Combustion Processes* 2003, Berlin: Springer.
159. Alkidas, A.C., *Relationship between smoke measurements and particulate measurements*. SAE Technical Paper 1984. **No. 840412**.
160. N.F., R., *Combustion simulation and optimization in diesels (In Russian)*. Kharkov: Vischa shkola, 1980: p. 169.
161. Al-Dawody, M.F. and S.K. Bhatti, *Effect of soybean oil biofuel blending on the performance and emissions of diesel engine using DIESEL-RK software*. International Journal of Engineering Science and Technology, 2011. **3(6)**: p. 4539-4555.
162. Hamdan, M.A. and R.H. Khalil, *Simulation of compression engine powered by Biofuels*. Energy Conversion and Management, 2010. **51**: p. 1714-1718.

163. Kuleshov, A.S., *Multi-Zone DI Diesel Spray Combustion Model for Thermodynamic Simulation of Engine with PCCI and High EGR Level*. SAE Paper 2009. No **2001-01-1255**.
164. Kafuku, G. and M. Mbarawa, *Biodiesel production from Croton megalocarpus oil and its process optimization*. Fuel, 2010. **89**(9): p. 2556-2560.
165. Hammond, E.G. and L. W.O., *Ibid.* 1954. **31**: p. 247
166. Lee, B.-B., P. Ravindra, and E.-S. Chan, *New drop weight analysis for surface tension determination of liquids*. Colloids and Surfaces A: Physicochemical and Engineering Aspects, 2009. **332**(2–3): p. 112-120.
167. MOORE, W.J., *Physical Chemistry (3rd Edition)*1962: Prentice Hall.
168. Adam, N.K., *The Physics and Chemistry of Surfaces (3rd Edition)*. ed1941: Oxford University Press.
169. Esteban, B., et al., *Characterization of the surface tension of vegetable oils to be used as fuel in diesel engines*. Fuel, (0).
170. Rakett, H.G., *Equation of state for saturated liquids*. J. Chem. Eng. Data, 1970. **15**: p. 514-517.
171. Reid, R.C., J.M. Prausnitz, and B.E. Poling, *The properties of gases and liquids (4th Edition)*. 4th ed1987, New York: McGraw-Hill.
172. Marsh, K.N., *TRC thermodynamic tables: non-hydrocarbons*1991: Thermodynamics Research Center, Texas A&M University System, College Station, TX.
173. Ndiaye, P.M., et al., *Vapor Pressure Data of Soybean Oil, Castor Oil, and Their Fatty Acid Ethyl Ester Derivatives*. J. Chem. Eng. Data, 2005(2): p. 330–333.
174. Lujaji, F., et al., *Cetane Number and Thermal Properties of Croton Oil, Biodiesel, 1-Butanol, and Diesel Blends*. Journal of Thermal Analysis and Calorimetry, 2010. **102**(3): p. 1175-1181.
175. N.F., R., *Combustion simulation and optimization in diesels (In Russian)*. Kharkov: Vischa shkola, 1980: p. 169.
176. Cellier, F. *Dymola: Environment for Object-oriented Modeling of Physical Systems*. Available from:
http://www.inf.ethz.ch/personal/fcellier/Res/Soft/Dymola_engl.html.
177. *Dymola: Multi-Engineering Modeling and Simulation*. Available from:
<http://www.3ds.com/products/catia/portfolio/dymola>.
178. *Modelica*. Available from: <http://en.wikipedia.org/wiki/Modelica>.

179. *Introduction to Modelica*. Available from:
<http://www.dynasim.se/update/Dymola70/releasenotes.pdf>.
180. Ren, Z., *Modelling and Simulation for Aircraft Gas Turbine Based on MODELICA and DYMOLA*, in *School of Mechanical Engineering*2006, Shanghai Jiaotong University: Shanghai, China.
181. He, J., *Modelling and Simulation of Steam Turbine System Based on Modelica*, in *School of Automation*2007, North China Electric Power University Beijing, China.
182. *Getting started with Dymola*.
183. Xu, Z., *Modular Modelling and Simulation in Turbocharging Diesel Engine*, in *School of Mechanical Engineering*2004, Shanghai Jiaotong University: Shanghai, China.
184. Li, J., *Object-oriented Modeling and Simulation for Engine System Dynamic Studies*, in *School of Mechanical Engineering*2004, North China Polytechnic Institute: Taiyuan, China.
185. Lawson, R., *A study of the energy usage in domestic UK dwellings to aid the development of domestic combined heat and power(CHP) and micro renewable technologies*, in *School of Mechanical and System Engineering*2010, Newcastle University: Newcastle. p. 131.
186. Wang, Y., *An experimental and analytical investigation of the use of a diesel engine in trigeneration*, in *School of Engineering and Advanced Technology*2004, Staffordshire University: Staffordshire. p. 102.
187. Owen, M.S. and H.E. Kennedy, *2009 Ashrae Handbook: Fundamentals 2009*: American Society of Heating, Refrigerating and Air-Conditioning Engineers, Inc.
188. Green, D.W. and R.H. Perry, *Perry's Chemical Engineers' Handbook, Eighth Edition* 2007: McGraw-Hill.
189. Patek, J. and J. Klomfar, *Simple functions for fast calculations of selected thermodynamic properties of the ammonia-water system*. *International Journal of Refrigeration*, 1995. **18**(4): p. 228-234.

Appendices

A. Specifications of Apparatus and Instruments

A.1 specification of Visco 88 viscometer

Measuring system	DIN 53019		C14, C25, C30		
	“Infinite sea”		C14, C25, C30		
	“Wide gap”		C14, C25		
	Cones		1° , 2.5° or 5.4° angle; 15mm, 30mm diameter		
	Parallel plates		15mm, 30mm		
	Accumulator capacity		1.5 to 8 hours	Serial interface	RS232
	Analog output (BNC) (V)		0-1	Power consumption (W)	≤4
Measuring mode ranges	Display	Mode	Units	Measured range	
	η	Viscosity	Pas	0.006 – 350	
	γ	Shear rate	1/s, s-1	4 – 1,200	
	τ	Shear stress	Pa	8 – 1,500	
	T	Temperature	°C	0 – 100	
	M	Torque	mN.m	0 – 10	
	f	Frequency	Hz	0.33 – 16.7 (rotational speed/60)	
Dimensions (including stand)	Height (mm)		560	Length (mm) 245	
	Width (mm)		230	Weight (kg) 5	

A.2 Specification of Julabo SE-6 thermostatic bath/circulator

Working temperature range	20 to 300 °C
Temperature control	ICC
Temperature stability	±0.01 °C
Display	VFD
Display resolution	0.01 °C
Integrated programmer	available

Heater capacity	3000 W
Pump capacity	Pressure: 0.7 bar Suction: 0.4 bar Flow rate: 22-26 l/min
Digital interfaces	RS232, optional Profibus
External Pt100 sensor connection	available
Bath opening / bath depth (W x L / D)	13 x 15 / 20 cm
Filling volume	6 Litres
Dimensions (W x L x H)	21 x 43 x 44 cm
Weight	13,5 kg
Ambient temperature	5 to 40 °C
Classification according to DIN 12876-1	3 (FL)

A.3 Specification of CAL2k-ECO calorimeter

Technical specification	Type	CAL2k-ECO	Power	90 – 260 VAC 50/60Hz
	Ambient temperature	0~60°C	Repeatability	0.1 (% RSD)
	Resolution:	0.01 (MJ/kg)	Temperature Resolution:	0.000006°C
Dimension	Height	240 mm	Length	330 mm
	Width	240 mm	Weight(dry)	5 kg

A.4 Specification of A&D HR-200 analytical balance

Capacity	210 g
Resolution	0.0001 g
Percentage Min Div	0.01%, 0.1% or 1% (auto prompt)
Counting Min Weight	0.1 mg
Linearity	±0.0002 g
Repeatability / Std Dev	0.0001 g
Stabilization Time	3 seconds (typically)
Sensitivity Drift	±2 ppm / °C (when automatic self – calibration was not used)
Display Refresh	5 times per second / 10 times per second

Pan Size	Ø 85 mm / 3.3 inches
Physical Dimensions	213(W) x 319(D) x 301(H) mm
Breeze Break Dimensions	180(W) x 192(D) x 200 (H) mm
Operating Temperature	5 °C to 40 °C (41 °F to 104 °F), 85% RH or less (no condensation)
Weight	Approximately 5.7 kg / 12.5 lb
Power	100, 120, 220, 240 VAC (AC Adaptor) 50 Hz / 60 Hz. 10 hours continuous operation with rechargeable battery pack

A.5 specification of Henry Troemner magnetic stirrer hotplate

Type	HB502	Power	AC240V 50Hz 550W
Maximum plate temperature	450°C	Speed range	0 to 2000 rpm
Plate dimensions	210 x 210 mm	Heated area	120 x 120 mm
Overall height	105 mm	Overall length	285 mm
Overall width	220 mm	Weight	3.2 kg

A.6 specification of Yanmar engine and generator

Engine	Type	Yanmar TF120M	Bore	92mm
	Number of cylinders	1	Stroke	96mm
	Displacement	0.638 litres	Fuel consumption	2.8 litres per hour
	Fuel type	Diesel	Continuous power output	10.5 hp/7.72 kW
	Revolutions	2400 rev./min	Rated output	12 hp / 8.82 kW
	Starting system	Electrical start	Combustion system	Direct injection
	Cooling system	radiator	Fuel tank capacity	11 litres
	Lubricating system	Fully sealed forced lubrication with trochold pump & hydraulic regulator valve		
Alternator	Model	YTG6.5S	Alternator	50 kg

			weight	
	Alternator model	MR2-160/2	Insulation class	H
	Operation condition	Ambient temperature not exceeding 50 °C; Attitude not exceeding 1000m		
Generator set	Capacity	6.5 kVA/6.5 kW	Drive system	V-belt drive
	Frequency	50 Hz	Voltage Output	220 V
	Revolutions	3000 rev./min	Current Output	29.5 A
	No. of phase	Single phase(2 wire)	Recommend cable dia.	6-16 mm
	Power Factor	1	Recommend earth cable	Equal to the conductor size
	Excitation system	Brushless, self-excitation system		
Dimension	Height	1360 mm	Length	800 mm
	Width	690 mm	Weight(dry)	227 kg

A.7 Specification of PowerLink fuel flow meter

Technical specification	Type	FC2210	Power	AC220V±22V 50HZ±1HZ
	Ambient temperature	0~40°C	RH	≤85%RH
	Measuring range	0~40kg	accuracy	0.4%F.S
	time range of measurement		1~99s handpick	
Dimension	Height	445 mm	Length	350 mm
	Width	274 mm	Weight(dry)	18 kg

A.8 Specification of KERN PCB 1000-1 Precision balance

Mode	PCB 1000-1	Weighing plate (Ø/WxD)	130x130 mm
Readout (d)	0.1 g	Measuring range (Max)	10000 g
Min. piece weight at counting	200 mg	Reproducibility	0.1 g
linearity	±0.2g	Net weight	1.4 kg

A.9 Specification of Omega rope heater

Type	FGR-030	Standard diameter	5mm(3/16 inch)
Maximum temperature	482°C (900° F), Teflon sleeves at ends rated to 500° F		
Suitable for use on conductive surface	Yes		
Resists moisture, vapour or chemicals	No		
voltage	120 Volt ac or dc, 240V optional		
Linear wattage	1.8watts/inch	Heater length	0.9m (3 feet)
Lead length	609mm (24 inch)	termination	Stripped leads

A.10 Specification of Omega CN79000 temperature/process controller

Input:	Thermocouple	Input Impedance	Thermocouple = 3 mega ohms minimum
Sensor Break Protection	De-energizes control output to protect system after customer set time		
Set Point Range:	Selectable	Display:	Two 4 digit, 7 segment 6.35 mm (0.25") high LEDs
Control Action	Reverse (usually heating), Direct (usually cooling) selectable		
Proportional Band	1 to 9999 °F, °C, or counts	Reset Time (Integral)	Off or 0.1 to 99.9 minutes
Rate Time (Derivative)	Off or 0.01 to 99.99 minutes	Cycle Rate	1 to 80 seconds.
On – Off Differential:	Adjustable 1° F, 1° C, or 1 count to full scale in 1° F, 1° C, or 1 count steps		
Fuzzy Percent	0 to 100%.	Fuzzy Rate	Off or 0.01 to 99.99 minutes
Fuzzy Band	Off or 1 to 4000 °F, °C, or counts	Accuracy	±0.25% of span, ±1 least significant digit
Resolution	1 degree or 0.1 degree, selectable	Line Voltage Stability	±0.05% over the supply voltage range
Temperature Stability	100 ppm /°C typical, 200 ppm /°C maximum	Common Mode Rejection	140 dB minimum at 60 Hz
Normal Mode Rejection	65 dB typical, 60 dB at 60 Hz	Power Consumption	5VA maximum

Isolation	Relay outputs: 1500 Vac to all other inputs and outputs		
Supply Voltage	100 to 240 Vac, nominal, +10 -15%, 50 to 400 Hz. Single phase; 132 to 240 Vdc, nominal, +10 -20%		
Operating Temperature	-10 to +55 °C (+14 to 131 °F)	Storage Temperature	-40 to +80 °C (-40 to 176 °F)
Humidity Conditions	0 to 90% up to 40 °C non-condensing, 10 to 50% at 55 °C non-condensing		
Memory Backup	Non-volatile memory, no batteries required		
Control Output Ratings	Relay (Output A, Output B):	SPST, 3 A @ 240 Vac resistive; 1.5A @240 Vac inductive; 1/10 HP @ 120 Vac	
	Switched Voltage (non-isolated, Output A, Output B):	5 V dc @ 20 mA	
Depth Behind Mounting Surface	111.6 mm (4.395")		
Panel Cut-out	45.0 mm x 22.2 mm (1.772" x 0.874")	Weight	114 g (4 oz)

A.11 Specification of Bowman coolant heat exchanger

type	Plate heat exchanger 10-17	Weight (kg)	1.3
Volume per side (litre)	0.21	dimensions l/w/d (mm)	106106/90
shell	Flow (Litre/min)	13	Pressure drop (kPa)
	Temperature (°C)	85(in)/ 77.6 (out)	
Tube	Flow (Litres/min)	10	Pressure drop (kPa)
	Temperature (°C)	70(in)/ 79.5 (out)	
	Heat (kW)	6.49	

A.12 Specification of icenta turbine flow meter

Type	IC-LT 1/2 "
Flow Range (Linear)	2-20 l/min
Output	4-20 mA
Connections	1/2 inch BSP Male
Linearity	±0.5% (better than ±0.2% when used with "101" totalizer)
Repeatability	± 0.1%

Temperature:	-30°C to +120°C
Pressure Drop	250 mbar at maximum quoted Flow rate

A.13 Specification of Bowman exhaust heat exchanger

type	Plate heat exchanger 10-17		Weight (kg)	1.3
Volume per side (litre)	0.21	dimensions l/w/d (mm)		106106/90
shell	Flow (Litre/min)	13	Pressure drop (kPa)	28
	Temperature (°C)	85(in)/ 77.6 (out)		
Tube	Flow (Litres/min)	10	Pressure drop (kPa)	18
	Temperature (°C)	70(in)/ 79.5 (out)		
	Heat (kW)	6.49		

A.14 Specification of Flowline DF10MFG Pitot flow meter

Differential Pressure Measurement				
Span Limits ΔP		0.12 and 2.5 kPa (0.5 and 10 inH ₂ O)	Range Limits ΔP	-2.5 and +2.5 kPa (-10 and +10 inH ₂ O)
Absolute Pressure Measurement				
Span Limits ΔP		0.02 and 2.1 Mpa (3 and 300 psia)	Range Limits ΔP	0 and 2.1 Mpa (0 and 300 psia)
Maximum Static, Working, and Over range Pressure				
Sensor URL		Maximum Static (Mpa)	Max Working (Mpa)	Maximum Over range (Mpa)
Differential Pressure	Absolute Pressure			
10 inH ₂ O	500 psia	3.4	3.4	5.2
Process Temperature Measurement				
Measurement Element		DIN/IEC, 2-, 3-, or 4-wire, 100 ohm platinum RTD		
Range Limits		-200 and +850°C (-328 and +1562°F)		
Operative Limits				
Influence Normal		Normal Operating Conditions		Operative Limits
Sensor Body Temperature		-29 and +82°C (-20 and +180°F)		-46 and +121°C (-50 and +250°F)

Silicone Fill Fluid Fluorinert Fill Fluid	-29 and +82°C (-20 and +180°F)	-29 and +121°C (-20 and +250°F)
Electronics Temperature With LCD Display	-29 and +82°C (-20 and +180°F) -20 and +82°C (-4 and +180°F)	-40 and +85°C (-40 and +185°F) -29 and +85°C (-20 and +185°F)
Relative Humidity	0 and 100%	0 and 100%
Supply Voltage	11.5 and 42 V dc	11.5 and 42 V dc
Output Load	0 and 1450 ohms	0 and 1450 ohms
Supply Voltage and output		
Minimum Supply Voltage	16 V with HART Communication	11.5 V without HART Communication
Minimum Resistance	250 Ω with HART Communication	0 Ω without HART Communication
Output	4-20 mA	
Approximate Mass		
Without Process Connectors	3.5 kg (7.8 lb)	
With Process Connectors	4.2 kg (9.2 lb)	
With Optional 316ss Housing	Add 1.1 kg (2.4 lb)	

A.15 Specification of Dometic absorption refrigerator

Model	RM 7655 L	Energy Sources	12v/230v/LPG
Door type	Double curved door	Total gross volume (l)	150
Refrigerator volume (litres)	124	Height (mm)	1245
Freezer volume (litres)	26	Depth (mm)	570
Built-in dimensions (HxWxD) (mm)	1248 x 530 x 510	Weight (kg)	43
Energy consumption @ amb. Temp. +25°C (kWh/24h)	3.2	Energy consumption gas (g/24h)	380
Max input 12V (W)	170	Max input 230V (W)	200

Max input Gas (g/h)	22.5		
---------------------	------	--	--

A.16 Specification of Omega HHT13 tachometer

Display	5-digit alphanumeric LCD
Range	Optical: 5 to 200,000 rpm Contact*: 0.5 to 20,000 rpm
Accuracy	Optical: $\pm 0.01\%$ of reading Contact*: $\pm 0.05\%$ of reading (rpm)
Resolution	0.001 to 10 rpm (speed range dependent)
Operating Range	50 mm to 7.6 m (2" to 25')
Power	2 "AA" 1.5 V DC batteries
Environmental	5 to 40°C (41 to 104°F), 80% RH up to 30°C (86°F)
Dimensions	176 x 61 x 41 mm (6.9 x 2.4 x 1.6")
Weight	210 g (7 oz)

* With optional remote contact assembly.

A.17 Specification of Fluke 435 power quality analyser

Technical Data			
Inputs	Number: 4 voltage and current (3 phases + neutral)		um voltage: 1000 Vrms (6 kV peak)
	Maximum sampling 200 kS/s on each channel		speed simultaneously
Volt/Amps/Hertz	Items	Measurement range:	Accuracy:
	Vrms (AC + DC)	1000 V	0.1% of Vnom
	Vpeak	1 ... 1400 V	5% of Vnom
	Crest factor, voltage	1.0 ... > 2.8	$\pm 5\%$
	Arms (AC + DC)	0 ... 20 kA	$\pm 0.5\% \pm 5$ counts
	Apeak	0 ... 5.5 kA	0.5%
	Crest factor, A	1 ... 10	$\pm 0.5\%$
	Hz 50 Hz nominal	40 ... 70 Hz	± 0.01 H
Dips and swells	Vrms (AC+DC) ²	0.0% ... 100% of	$\pm 0.2\%$ of nominal

		Vnom	voltage
	Arms (AC+DC) ²	0 ... 20 kA	±1% ± 5 counts
Harmonics	Harmonic (interharmonic) (n)	DC, 1..50; (Off, 1..49) measured according to IEC 61000-4-7	-
	Vrms	0.0 ... 1000 V	±0.05% of nominal voltage
	Arms	0.0 ... 4000 mV x clamp scaling	±5% ± 5 counts
	Watts	Depends on clamp scaling and voltage	±5% ± n x 2% or reading, ± 10 counts
	DC voltage	0.0 ... 1000 V	±0.2% of nominal voltage
	THD	0.0 ... 100.0%	±2.5% V and A (± 5% Watt)
	Hz	0 ... 3500 Hz	± 1 Hz
	Phase angle	-360° ... +360°	± n × 1.5°
Power and energy	Watt, VA, VAR	1.0 ... 20.00 MVA	±1% ± counts
	kWh, kVAh, kVARh	00.00 ... 200.0 GVAh	± 1.5% ± 10 counts
	Power Factor/ Cos Φ / DPF	0...1	± 0.03
Flicker	Pst (1 min), Pst, Plt, PF5	0.00 ... 20.00	±5%
Unbalance	Volts	0.0 ... 5.0%	±0.5%
	Current	0.0 ... 20%	± 1%
Transient Capture	Volts	±6000 V	±2.5% of Vrms
Inrush mode	Arms (AC+DC)	0.000 ... 20.00 kA	±1% of meas ± 5 counts
	Inrush duration	7.5 s ... 30 min	±20 ms (Fnom = 50

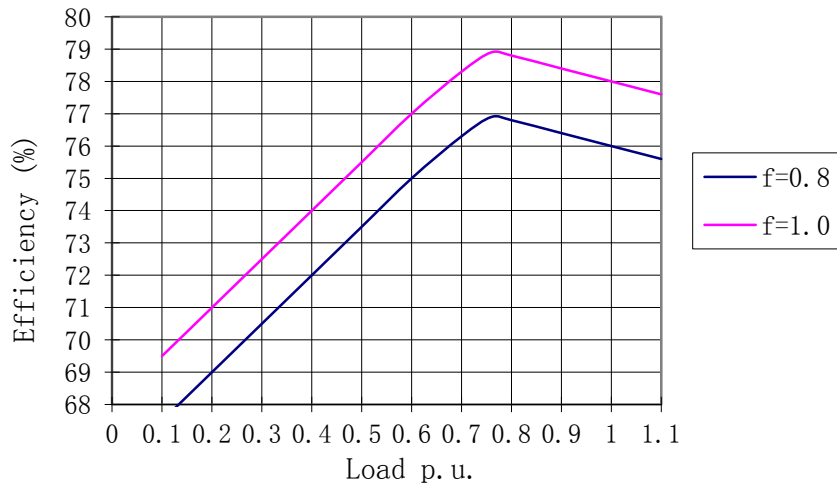
	(selectable)		Hz)
Autotrend recording	Sampling:	5 readings/sec continuous sampling per channel	
	Memory:	1800 min, max and avg points for each reading	
	Recording time:	Up to 450 days	
	Zoom:	Up to 12x horizontal zoom	
Memory	Screens & data:	50, shared memory divided between logging, screens and data sets	
Environmental Specifications			
Operating Temperature	0 °C to +50 °C		
Safety Specifications			
Safety	EN61010-1 (2nd edition) pollution degree 2; 1000 V CAT III / 600 V CAT IV ANSI/ISA S82.01		
Mechanical & General Specifications			
Size	256 x 169 x 64 mm		
Weight	2 kg		
Battery Life	Rechargeable NiMH pack (installed): >7 hours Battery charging time: 4 hours typical		
Shock & Vibration	Shock: 30 g Vibration: 3 g according to MIL-PRF-28800F Class 2		
Case	Rugged, shock proof with integrated protective holster, IP51 (drip and dust proof)		

A.18 Specification of HORIBA MEXA-1600D exhaust gas analyser

Component Specifications					
Model	Component	Method	Range	T90	Noise
AIA-260	NDIR (250-mm cell)	100-3K ppm	3.5 s	±1.0 FS	
	CO-H	NDIR (10-mm cell)	1-10 vol%	2.0 s	±1.0 FS%
	CO ₂	NDIR (10-mm cell)	1-16 vol%	2.0 s	±1.0 FS%

FCA-266	THC	Hot-FID	100-20K ppmC	2.0 s	±1.0 FS%
	NO _x	CLD (atmospheric)	100-5K ppm	3.5 s	±1.0 FS%
IMA-262	O ₂	MPD	10-25 vol%	2.5 s	±1.0 FS%
System Specifications					
Response Time		Td + T90 within 9 s			
Ambient Conditions		Temperature: 5-35°C Humidity: under 80% RH			
Dimensions and Weight (W x H x D)		570 x 1970 x 850 mm 22.44 x 77.56 x 33.46 in Approx. 250 kg / 551.2 lb			
Power		AC 100V, 120V, 200V, 220V, 230V, 240V - 50/60 Hz			

A.19 Diagrammatic efficiency of the MR2-160/2 generator



B. Details of experimental results

B.1 Viscosity of the vegetable oils

Vegetable oils	Croton oil	Jatropha oil	Rapeseed oil	Sunflower oil	Gas oil
Temperature (°C)	Viscosity (mPa.s)				
20	52.6	63.1	64.6	55.0	3.7
30	36.3	42.9	43.5	37.9	3.0
40	25.7	30.3	31.0	27.1	2.4
50	18.6	21.5	22.0	19.5	1.9
60	13.8	16.1	16.5	14.7	1.5
70	10.5	12.3	12.6	11.2	
80	8.3	9.4	9.6	9.1	
90	6.5	7.9	7.9	7.4	
100	4.3	6.0	5.9	5.9	
110	3.2	4.5	4.7	4.2	
120	2.1	3.3	3.7	3.5	

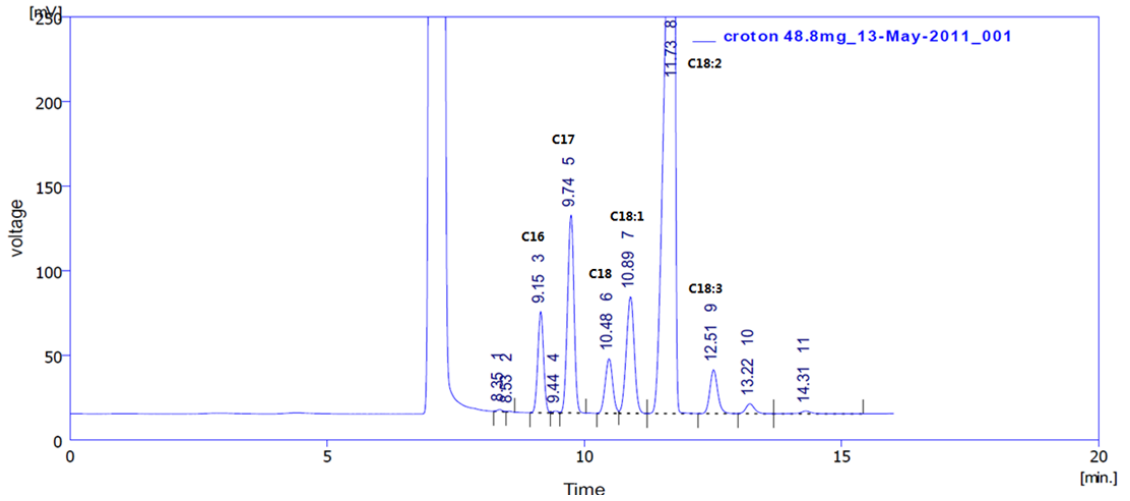
B.2 Density of the vegetable oils

Sample volume	10ml	Temperature	20°C	Average density (kg/m ³)
Fuels	Density (kg/m ³)			
Croton oil	918.6	916.3	917.0	917.3
Jatropha oil	905.4	901.1	903.1	903.2
Rapeseed oil	907.0	908.2	906.0	907.1
Sunflower oil	915.3	913.8	914.4	914.5
Gas oil	828.9	827.8	827.6	828.1

B.3 Higher heating value of the vegetable oils

Fuels	HHV (MJ/kg/)			Average HHV (MJ/kg)
Croton oil	39.62	39.57	39.60	39.60
Jatropha oil	39.86	39.87	39.82	39.85
Rapeseed oil	39.71	39.71	39.71	39.71
Sunflower oil	39.37	39.37	39.45	39.40
Gas oil	45.72	45.77	45.73	45.74

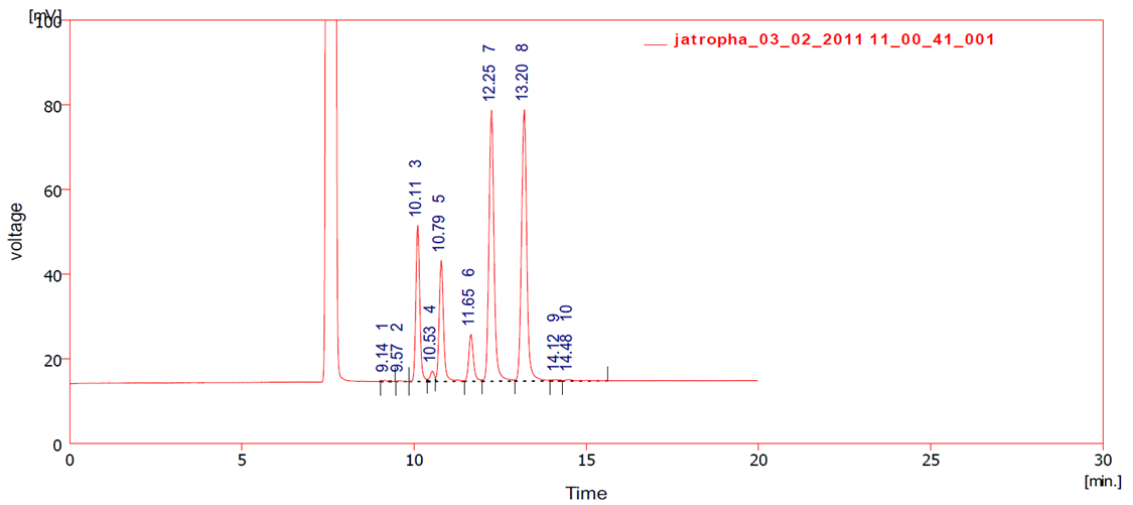
B.4 GC trace of croton biodiesel



Result Table (croton 48.8mg_13-May-2011_001)

	Reten. Time [min]	Area [mV.s]	Height [mV]	Area [%]	Height [%]	W05 [min]
1	8.353	8.391	1.184	0.1	0.2	0.11
2	8.525	2.887	0.424	0.0	0.1	0.11
3	9.150	468.940	59.877	5.5	7.9	0.12
4	9.442	8.023	1.077	0.1	0.1	0.13
5	9.742	1029.507	117.129	12.0	15.4	0.14
6	10.477	329.087	32.341	3.8	4.2	0.16
7	10.893	748.761	68.997	8.8	9.1	0.17
8	11.730	5591.704	447.809	65.4	58.7	0.20
9	12.508	272.373	25.947	3.2	3.4	0.16
10	13.220	69.594	5.858	0.8	0.8	0.18
11	14.308	25.117	1.599	0.3	0.2	0.19
	Total	8554.382	762.243	100.0	100.0	

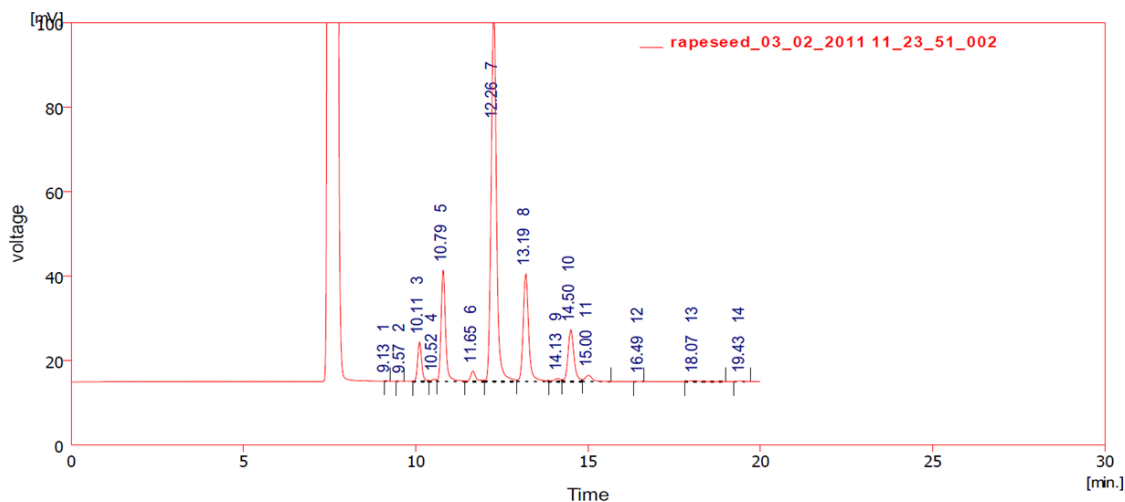
B.5 GC trace of jatropha biodiesel



Result Table (jatropa_03_02_2011 11_00_41_001)

	Reten. Time [min]	Area [mV.s]	Height [mV]	Area [%]	Height [%]	W05 [min]
1	9.143	2.504	0.307	0.1	0.1	0.10
2	9.572	1.922	0.194	0.1	0.1	0.13
3	10.105	296.732	36.818	14.5	17.7	0.12
4	10.527	21.044	2.445	1.0	1.2	0.14
5	10.785	254.781	28.562	12.4	13.7	0.13
6	11.648	105.956	11.066	5.2	5.3	0.14
7	12.248	664.351	64.038	32.5	30.7	0.15
8	13.200	687.358	64.154	33.6	30.8	0.16
9	14.115	4.380	0.351	0.2	0.2	0.21
10	14.483	8.270	0.370	0.4	0.2	0.20
	Total	2047.300	208.303	100.0	100.0	

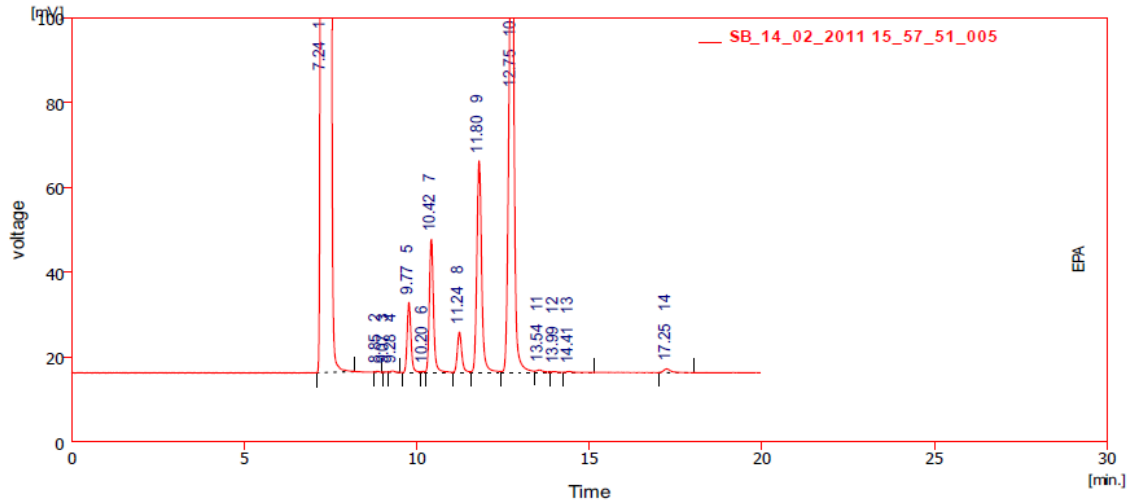
B.6 GC trace of the Rapeseed biodiesel



Result Table (rapeseed_03_02_2011 11_23_51_002)

	Reten. Time [min]	Area [mV.s]	Height [mV]	Area [%]	Height [%]	W05 [min]
1	9.128	0.619	0.104	0.0	0.1	0.08
2	9.575	0.594	0.074	0.0	0.0	0.10
3	10.108	75.776	9.331	4.3	5.5	0.13
4	10.518	4.850	0.525	0.3	0.3	0.15
5	10.792	238.323	26.427	13.5	15.6	0.13
6	11.655	26.380	2.499	1.5	1.5	0.14
7	12.263	948.313	89.753	53.7	53.0	0.16
8	13.193	283.165	25.606	16.0	15.1	0.16
9	14.127	9.600	0.733	0.5	0.4	0.20
10	14.497	147.069	12.296	8.3	7.3	0.18
11	15.003	22.714	1.505	1.3	0.9	0.21
12	16.488	0.781	0.079	0.0	0.0	0.10
13	18.075	5.645	0.257	0.3	0.2	0.26
14	19.432	2.407	0.169	0.1	0.1	0.22
	Total	1766.236	169.357	100.0	100.0	

B.7 GC trace of sunflower biodiesel



Result Table (Uncal - SB_14_02_2011 15_57_51_005)

	Reten. Time [min]	Area [mV.s]	Height [mV]	Area [%]	Height [%]	W05 [min]
1	7.240	21000.639	1233.701	90.4	84.2	0.27
2	8.845	1.394	0.208	0.0	0.0	0.11
3	9.073	0.750	0.123	0.0	0.0	0.10
4	9.282	3.136	0.338	0.0	0.0	0.13
5	9.770	127.472	16.520	0.5	1.1	0.12
6	10.195	2.020	0.300	0.0	0.0	0.14
7	10.422	264.213	31.420	1.1	2.1	0.13
8	11.237	85.542	9.510	0.4	0.6	0.14
9	11.802	484.385	49.835	2.1	3.4	0.14
10	12.752	1234.898	121.785	5.3	8.3	0.15
11	13.538	8.699	0.625	0.0	0.0	0.23
12	13.988	3.370	0.215	0.0	0.0	0.23
13	14.413	4.433	0.250	0.0	0.0	0.21
14	17.248	14.044	0.904	0.1	0.1	0.21
	Total	23234.994	1465.734	100.0	100.0	